# A Molecular Hydrodynamic Study of Marine Based Non-Digestible Fibre Polysaccharides Considered for Use in Health Products

**Fahad Mohammed Almutairi**
BSc., MSc.

Thesis submitted for the degree of Doctor of Philosophy

University of Nottingham
National Centre for Macromolecular Hydrodynamics
School of Biosciences, Sutton Bonington,
Loughborough, Leicestershire,
LE12 5RD, United Kingdom

March, 2015

*In The Name of Allah, The Most Beneficent, The Most Merciful*

*"Thinking is the key to science, the process of researching and investigating, a call for challenge and honourable competition, its absence means the lack of creativity, innovation, production and ambition"*

*Lieutenant Colonel*

***Mansour M. Almutairi***

*To whom this thesis is dedicated*

# ABSTRACT

Marine polysaccharides have been widely used as a source of nutritional supplement for various therapeutic applications. Uncertainties and significant gaps in our knowledge about the macromolecular properties of these substances have limited their use particularly in the pharmaceutical industries where a detailed understanding of materials used for therapies are essential. Therefore, in order to increase our awareness so as to develop better healthcare and therapies against common diseases it is important to establish a better understanding of molecular properties and interactions. The focus of this thesis has been on carrageenans – materials which have arguably been the greatest source of controversy and disagreement in the past in terms of properties – chitosan and alginate and their relations with other substances (mucins, DNA and other polysaccharides).

Firstly the main classes of carrageenan - lambda, kappa and iota - have been characterised in terms of their conformation, size and structural integrity utilizing a variety of hydrodynamic techniques including analytical ultracentrifugation based on sedimentation velocity and equilibrium, size exclusion chromatography coupled to multi angle light scattering (SEC-MALS) and viscometry. Studies have suggested that these marine polysaccharides adopt in general semi-flexible structures in solution in contrast to, for example, mucin glycoproteins which adopt a linear random coil conformation. Such conformation analyses are significant in relation to macromolecular structure–function relationships. In addition, the effect of a wide range of solvent conditions was investigated to provide any evidence of dimerization/double helix formation for the main classes of carrageenan (kappa, iota and lambda) using the principal tools of hydrodynamics supported by micro-differential scanning calorimetry. The study showed that, kappa carrageenan adopted a dimeric form under appropriate experimental conditions whereas iota and lambda carrageenan did not.

Then, chitosans of different degrees of acetylation were studied, and these too adopted a semi-flexible conformation, but, as with iota and lambda carrageenan, with no evidence of self-association behaviour.

A selected group of interactions involving marine polysaccharides or mucin were then investigated. Strong evidence is provided for a clear interaction was observed between chitosan and two polyanions (DNA and xanthan) using the principle of co-sedimentation, and the relevance of this for DNA condensation phenomena is indicated. The use of lambda carrageenan as a possible replacement for alginate in ternary complexes with konjac glucomannan and xanthan for use in the anti-obesity product PolyGlycopleX®, revealed no improvement compared with the use of alginate. Finally, the interaction between the mucin and PolyGlycopleX® was investigated showing that mucin appeared to reinforce interactions between the components of PolyGlycopleX® at higher ionic strengths than seen previously.

# ACKNOWLEDGMENTS

The author wishes to acknowledge several people and organizations. First and foremost, I would like to express my extreme gratitude and sincere appreciation to the leader of the renaissance of the education in the kingdom of Saudi Arabia the custodian of the two holy mosques king Abdullah bin Abdul-Aziz (God bless his soul), for sponsoring this project through the University of Tabuk.

A special gratitude to my principal supervisor Professor Dr. Steve Harding for the guidance, support, supervision, and encouragement I received over these past four years. Without his assistance and dedicated involvement in every step throughout the process this thesis would have never been accomplished.

I would similarly like to express my thanks to my co-supervisor Dr. Gary Adams for his support and guidance during the PhD. Deep thanks go to Professor Dr. Arthur Rowe and Professor Dr. Tim Foster for advice and support for this project. I wish also to gratitude the assistance and support I received from Dr. Samil Kok, Dr. Ali Abdelhameed and Dr. David Besong whose advice and ideas provided a positive contribution towards the realisation of this project.

A special thanks to my family (mother, brothers and sisters) for their invaluable support and encouragement to complete this PhD. And at last, I would like to pass my appreciation and gratitude to my wife and son for emotional support throughout my PhD.

# LIST OF CONTENTS

ABSTRACT ..... i
ACKNOWLEDGMENTS ..... iii
LIST OF CONTENTS ..... iv
LIST OF FIGURS ..... viii
LIST OF TABLES ..... xviii
LIST OF ABBREVIATIONS ..... xx
**CHAPTER 1** ..... 1
MARINE BASED NON-DIGESTIBLE FIBRE POLYSACCHARIDES ..... 1
1.1 INTRODUCTION ..... 2
1.2 MARINE POLYSACCHARIDES ..... 5
1.2.1 Polysaccharides from Seaweed ..... 6
1.2.2 Polysaccharides from Shellfish ..... 15
1.3 MARINE BASED DIETARY FIBRE ..... 21
1.4 HEALTH BENEFITS OF MARINE POLYSACCHARIDES ..... 24
1.5 INTERACTION WITH OTHER BIOPOLYMERS ..... 28
1.6 HYDRODYNAMIC METHODS ..... 29
1.7 THE AIM OF THIS INVESTIGATION ..... 30
**CHAPTER 2** ..... 32
METHODS FOR CHARACTERISING THE BIOPHYSICAL PROPERTIES OF MACROMOLECULES IN SOLUTION ..... 32
2.1 INTRODUCTION ..... 32
2.2 ANALYTCAL ULTRACENTRFUGATION (AUC) ..... 34
2.2.1 Ultracentrifuge Instrumentation ..... 35
2.2.2 Sedimentation Velocity ..... 40
2.2.3 Sedimentation Equilibrium ..... 47
2.3 SIZE EXCLUSION CHROMATOGRAPHY COUPLED TO MULTIANGLE LIGHT SCATTERING (SEC-MALS) ..... 51
2.3.1 Size Exclusion Chromatography (SEC) ..... 52
2.3.2 MultiAngle Light Scattering (MALS) ..... 54
2.4 VISCOMETRY ..... 57
2.4.1 Capillary Viscometry ..... 59
2.4.2 Pressure Imbalance Differential Viscometry ..... 62
2.5 MICRO-DIFFERENTIAL SCANNING CALORIMETRY (micro-DSC) ..... 64

2.6 COMBINED HYDRODYNAMIC APPROACHES ..... 66
2.6.1 Wales-van Holde Ratio (R) ..... 66
2.6.2 Mark-Houwink-Kuhn-Sakurada (MHKS) or Power Law Relations ..... 67
2.6.3 Conformation Zoning ..... 69
2.6.4 Estimation of the Persistence Length ($L_p$) and Mass Per Unit Length ($M_L$) 71
**CHAPTER 3** ..... 76
MOLECULAR CONFORMATION STUDY OF LAMBDA CARRAGEENAN IN AQUEOUS SOLUTION ..... 76
3.1 INTRODUCTION ..... 76
3.2 MATERIALS ..... 80
3.3 METHODS ..... 81
3.3.1 Sedimentation Velocity (SV) ..... 81
3.3.2 Sedimentation Equilibrium (SE) ..... 82
3.3.3 Size Exclusion Chromatography Coupled to Multi Angle Light Scattering (SEC-MALS) ..... 84
3.3.4 Capillary and Differential Pressure Viscometry ..... 85
3.4 RESULTS ..... 86
3.4.1 Sedimentation Coefficient and Sedimentation Coefficient Distribution .... 86
3.4.2 Estimation of Molecular Weight ..... 89
3.4.3 Intrinsic Viscosity ..... 93
3.4.4 Conformational Analysis ..... 96
3.5 DISCUSSION ..... 108
**CHAPTER 4** ..... 112
HYDRODYNAMIC INVESTIGATION OF THE OLIGOMERIC STATE OF THE MAIN CLASSES OF CARRAGEENAN (KAPPA, IOTA AND LAMBDA) IN SOLUTION ..... 112
4.1 INTRODUCTION ..... 112
4.2 MATERIALS ..... 117
4.3 METHODS ..... 118
4.3.1 Micro-Differential Scanning Calorimetry (micro-DSC) ..... 118
4.3.2 Sedimentation Velocity (SV) ..... 118
4.3.3 Sedimentation Equilibrium (SE) ..... 120
4.3.4 Size Exclusion Chromatography Coupled to Multi Angle Light Scattering (SEC-MALS) ..... 121
4.3.5 Capillary and Differential Pressure Viscometry ..... 122
4.4 RESULTS ..... 123
4.4.1 Thermal Behavior of Carrageenans ..... 123

4.4.2 Sedimentation Coefficient and Sedimentation Coefficient Distribution .. 126
4.4.3 Estimation of Molecular Weight ..... 132
4.4.4 Intrinsic Viscosity ..... 138
4.5 DISCUSSION ..... 141
**CHAPTER 5** ..... 147
HYDRODYNAMIC CHARACTERISATION OF CHITOSAN AND ITS INTERACTION WITH TWO POLYANIONS: DNA AND XANTHAN ..... 147
5.1 INTRODUCTION ..... 147
5.2 MATERIALS ..... 151
5.3 METHODS ..... 152
5.3.1 Sedimentation Velocity (SV) ..... 152
5.3.2 Sedimentation Equilibrium (SE) ..... 153
5.3.3 Size Exclusion Chromatography Coupled to Multi Angle Light Scattering (SEC-MALS) ..... 153
5.3.4 Capillary and Differential Pressure Viscometry ..... 154
5.4 RESULTS ..... 155
5.4.1 Sedimentation Coefficient and Sedimentation Coefficient Distribution .. 155
5.4.2 Estimation of Molecular Weight ..... 158
5.4.3 Intrinsic Viscosity ..... 163
5.4.4 Conformational Analysis ..... 165
5.4.5 Interaction with Two Polyanions: DNA and Xanthan ..... 176
5.5 DISCUSSION ..... 180
**CHAPTER 6** ..... 184
HYDRODYNAMIC STUDIES ON A MIXTURE OF NON-DIGESTIBLE CARBOHYDRATES ..... 184
6.1 INTRODUCTION ..... 184
6.1.1 Konjac Glucomannan ..... 188
6.1.2 Xanthan ..... 190
6.1.3 Sodium Alginate ..... 192
6.2 MATERIALS ..... 193
6.3 METHODS ..... 194
6.3.1 Sedimentation Velocity (SV) ..... 194
6.3.2 Sedimentation Equilibrium (SE) ..... 194
6.3.3 Size Exclusion Chromatography Coupled to Multi Angle Light Scattering (SEC-MALS) ..... 195
6.3.4 Capillary Viscometry ..... 195
6.4 RESULTS ..... 196

6.4.1 Individual Polysaccharides ..... 196
6.4.2 Binary Mixture of Polysaccharides ..... 205
6.4.3 Ternary Mixture of Polysaccharides ..... 210
6.5 DISCUSSION ..... 218
**CHAPTER 7** ..... 221
APPLICATION OF NEW HYDRODYNAMIC METHODOLOGY TO THE STUDY OF MUCIN AND ITS INTERACTION WITH BIOPOLYMERS IN SOLUTION ..... 221
7.1 INTRODUCTION ..... 221
7.2 MATERIALS ..... 226
7.3 METHODS ..... 227
7.3.1 Sedimentation Velocity (SV) ..... 227
7.3.2 Sedimentation Equilibrium (SE) ..... 227
7.3.3 Size Exclusion Chromatography Coupled to Multi Angle Light Scattering (SEC-MALS) ..... 228
7.3.4 Differential Pressure Viscometry ..... 228
7.4 RESULTS ..... 229
7.4.1 Sedimentation Coefficient and Sedimentation Coefficient Distribution ..... 229
7.4.2 Estimation of Molecular Weight ..... 232
7.4.3 Intrinsic Viscosity ..... 237
7.4.4 Conformational Analysis ..... 239
7.4.5 Interaction with Biopolymer Mixtures: PolyGlycopleX (PGX) ..... 248
7.5 DISCUSSION ..... 252
**CHAPTER 8** ..... 256
CONCLUDING REMARKS AND SUGGESTIONS FOR FUTURE WORK ..... 256
8.1 CONCLUDING REMARKS ..... 256
8.2 SUGGESTION FOR FUTURE WORK ..... 263
REFERENCES ..... 264
APPENDIX ..... 293

# LIST OF FIGURS


| | | |
|---|---|---|
| **Figure 1.1** | Examples of three classes of seaweed, collected from the south-east coast of Ireland. | 7 |
| **Figure 1.2** | Chemical structure of iota (ι), kappa (κ) and lambda (λ) commercial carrageenans. | 10 |
| **Figure 1.3** | A source of carrageenan from different type of seaweeds: (a) *Eucheuma denticulatum* (spinosum) – iota carrageenan, (b) *Kappaphycus alvarezi* (cottonii) – kappa carrageenan, (c) *Gigartina radula* and (d) *Chondrus crispus* kappa/lambda carrageenan. | 11 |
| **Figure 1.4** | Thallus, cell types and tissues of *Laminaria saccharina* an example of alginate source. | 12 |
| **Figure 1.5** | Chemical structure of alginate. | 13 |
| **Figure 1.6** | Chemical structure of chitosan. | 18 |
| **Figure 1.7** | The major classes of marine polysaccharides with health benefits and potential industrial applications. | 27 |
| **Figure 2.1** | Schematic of cell assembly, where (A) window assembly components, (B) showing centerpiece and window assemblies, and (C) cell hosing, screw ring and screw ring gaskets. | 37 |
| **Figure 2.2** | Interference optics detector of the Beckman XL-I ultracentrifuge. | 39 |
| **Figure 2.3** | Diagram of a macromolecule in the sedimentation process. | 42 |
| **Figure 2.4** | Movement of the boundary in sedimentation velocity experiment for lambda carrageenan 0.25 mg $mL^{-1}$. | 43 |
| **Figure 2.5** | Profile of sedimentation equilibrium process for kappa carrageenan at NaI 0.1M and concentration 0.3 mg $mL^{-1}$. | 48 |
| **Figure 2.6** | Separation of two different samples by size exclusion chromatography. | 53 |
| **Figure 2.7** | The schematic setup of chromatography with on-line light scattering detection. | 56 |
| **Figure 2.8** | Schematic diagram representing the movement of a Newtonian liquid between parallel plates. | 58 |
| **Figure 2.9** | Schematic of the Ostwald capillary viscometer, which the flow solution is measured between A and B. | 60 |
| **Figure 2.10** | Schematic diagram of four capillary bridge design of pressure imbalance viscometer. | 63 |
| **Figure 2.11** | Example of a Mark–Houwink–Kuhn–Sakurada (MHKS) power law double logarithmic plot for chitosan CHIT1 (see *Chapter 5*) from an on-line differential pressure viscometer ViscoStar coupled to SEC-MALS. The plot is of intrinsic viscosity [η] as a function of elution volume (ordinate) versus molecular weight $M_w$ as a function of elution volume. | 68 |
| **Figure 2.12** | Example of Mark–Houwink–Kuhn–Sakurada (MHKS) power law double logarithmic plot of $s^o_{20,w}$ *vs* $M_w$ for chitosan samples (see *Chapter 5*). | 69 |

| | | |
|---|---|---|
| **Figure 2.13** | The sedimentation conformation zoning plot, which helps to define zones: A: extra rigid rod, B: rigid rod, C: semi-flexible coil, D: random coil, E: globular/heavily branched structure. | 70 |
| **Figure 2.14** | Contour plots of the mucin Nov13. The target function, $\Delta$ calculated based on variables values of $L_p$ and $M_L$, and are represented on the full colour spectrum from blue ($\Delta$ = 0.005) to red ($\Delta \geq 0.65$) (see *Chapter 7*). | 75 |
| **Figure 3.1** | Lambda carrageenan repeat unit. | 78 |
| **Figure 3.2** | Sedimentation coefficient distribution profiles using least squares g*(s) method of SEDFIT obtained from sedimentation velocity experiment for lambda carrageenan samples (a) GM-λ690 (b) GM-λ850 (c) GM-λ460 (d) TF-λ730 (e) TF-λ870 (f) TF-λ340. | 87 |
| **Figure 3.3** | Concentration dependence (reciprocal) of the sedimentation coefficient plot (after correction to standard solvent conditions) for lambda carrageenan samples (a) GM-λ690 (b) GM-λ850 (c) GM-λ460 (d) TF-λ730 (e) TF-λ870 (f) TF-λ340. | 89 |
| **Figure 3.4** | Molecular weight plots for lambda carrageenan samples GM-λ690, GM-λ850, GM-λ460 (a, b and c, respectively), TF-λ730, TF-λ870 and TF-λ340 (d, e and f, respectively) using SEDFIT-MSTAR: $M^*$ versus $r$ plot (open squares) and fit based on the $M^*$ transformation of the $c(M)$ fit of the raw data (red line): the value of $M^*$ extrapolated to the cell base = $M_{w,app}$ the apparent weight average molecular weight for whole distribution. | 91 |
| **Figure 3.5a** | Elution profiles of the lambda carrageenan samples GM-λ690 (black line), GM-λ850 (red line) and GM-λ460 (green line) examined by SEC-MALS at concentration 0.5 mg $mL^{-1}$. The horizontal black (open square), red (open circle) and green (up triangle) lines correspond to SEC-MALS calculated molecular weights for lambda carrageenan samples GM-λ690, GM-λ850 and GM-λ460, respectively. | 92 |
| **Figure 3.5b** | As (Figure 3.5a) but the analysis of lambda carrageenan samples TF-λ730 (black), TF-λ870 (red) and TF-λ340 (green) at concentration 0.5 mg $mL^{-1}$. | 93 |
| **Figure 3.6** | The intrinsic viscosity plot from capillary viscometry: Huggins, Kraemer and Solomon-Ciuta extrapolations for (a) GM-λ690, (b) GM-λ850, (c) GM-λ460, (d) TF-λ730, (e) TF-λ870 and (f) TF-λ340. | 94 |
| **Figure 3.7a** | Intrinsic viscosity (mL $g^{-1}$) plot (red line) versus retention time (min) for GM-λ460 from the differential pressure viscometer (Viscostar coupled to SEC-MALS). The red squares correspond to SEC-MALS calculated intrinsic viscosity. | 95 |
| **Figure 3.7b** | Intrinsic viscosity (mL $g^{-1}$) plot (red line) versus retention time (min) for TF-λ340 from the differential pressure | 96 |

| | | |
|---|---|---|
| | viscometer (Viscostar coupled to SEC-MALS). The red squares correspond to SEC-MALS calculated intrinsic viscosity | |
| **Figure 3.8** | The Mark-Houwink-Kuhn-Sakurada (MHKS) plots for lambda carrageenan samples (GM-λ and TF-λ): (a) and (c) plots of $s^{o}_{20,w}$ *vs* $M_w$ for both lambda carrageenan samples GM-λ and TF-λ respectively, whereas (b) and (d) plots of [η] *vs* $M_w$ again for GM-λ and TF-λ respectively. | 99 |
| **Figure 3.9a** | The conformation zoning plot for lambda carrageenan samples GM-λ690, GM-λ850 and GM-λ460, are adopted semi-flexible coil structures (zone C), whereas zone A: Extra-rigid rod; zone B: Rigid rod; zone C: Semi-flexible coil; zone D: Random coil and zone E: Branched. | 101 |
| **Figure 3.9b** | The conformation zoning plot for lambda carrageenan samples TF-λ730, TF-λ870 and TF-λ340, are adopted semi-flexible coil structures (zone C). | 101 |
| **Figure 3.10** | Show Bushin-Bohdanecky plots for lambda carrageenan (a) GM-λ and (b) TF-λ. Also the plots of Yamakawa-Fujii for lambda carrageenan (c) GM-λ and (d) TF-λ. | 105 |
| **Figure 3.11** | Global flexibility analysis (Multi-HYDFIT) for lambda carrageenan samples. (**a** & **b**) Contour plots of GM-λ and TF-λ, respectively. The target function, $\Delta$ calculated based on variables values of $L_p$ and $M_L$, and are represented on the full colour spectrum from blue to red. (**c** & **d**) Plots of target function ($\Delta$) vs. Persistence length ($L_p$) for GM-λ and TF-λ, respectively. | 107 |
| **Figure 3.12** | Multi-Gaussian fit of the highest concentration g(s) vs *s* profiles for lambda carrageenan samples GM-λ690, GM-λ850, GM-λ460 (a, c and e respectively), TF-λ730, TF-λ870 and TF-λ340 (b, d and f respectively). In each case two components are resolved, with the sedimentation coefficient of the faster component being approximately 1.1x greater than that of the slower component. | 110 |
| **Figure 4.1** | Chemical structure of iota (ι), kappa (κ) and lambda (λ) commercial carrageenans. | 114 |
| **Figure 4.2** | Micro-DSC trace of carrageenans (0.15%) in aqueous solution (0.1M NaCl, PBS and NaI); (a) kappa, (b) iota and (c) lambda, whereas (d) gives a comparison of micro-DSC traces of kappa in DMSO (100% and 80%). | 125 |
| **Figure 4.3** | Sedimentation coefficient distribution profiles using least squares g*(s) method of SEDFIT obtained from sedimentation velocity experiment for **kappa carrageenan** samples at different conditions (a) NaCl (b) NaI (c) PBS 20.0$^{o}$C (d) PBS 30.0$^{o}$C (e) DMSO 100% (f) DMSO 80%. | 128 |
| **Figure 4.4** | Sedimentation coefficient distribution profiles using least squares g*(s) method of SEDFIT obtained from | 129 |

| | | |
|---|---|---|
| | sedimentation velocity experiment for **iota carrageenan** samples at different conditions (a) NaI (b) NaCl (c) PBS 20.0$^{o}$C (d) PBS 30.0$^{o}$C. | |
| **Figure 4.5** | Sedimentation coefficient distribution profiles using least squares g*(s) method of SEDFIT obtained from sedimentation velocity experiment for **lambda carrageen** samples at different conditions (a) NaI (b) NaCl (c) PBS 20.0 $^{o}$C (d) PBS 30.0$^{o}$C. | 129 |
| **Figure 4.6** | Concentration dependence (reciprocal) of the sedimentation coefficient plot (after correction to standard solvent conditions) for **kappa carrageenan** samples at different conditions (a) NaCl (b) NaI (c) PBS 20.0$^{o}$C (d) PBS 30.0$^{o}$C (e) DMSO 100% (f) DMSO 80%. | 130 |
| **Figure 4.7** | Concentration dependence (reciprocal) of the sedimentation coefficient plot (after correction to standard solvent conditions) for **iota carrageenan** samples at different conditions (a) NaCl (b) NaI (c) PBS 20.0$^{o}$C (d) PBS 30.0$^{o}$C. | 131 |
| **Figure 4.8** | Concentration dependence (reciprocal) of the sedimentation coefficient plot (after correction to standard solvent conditions) for **lambda carrageenan** samples at different conditions (a) NaCl (b) NaI (c) PBS 20.0$^{o}$C (d) PBS 30.0 $^{o}$C. | 131 |
| **Figure 4.9** | SEDFIT-MSTAR output for analysis of **kappa carrageenan** in 0.1 M NaCl at a loading concentration of 0.3 mg mL$^{-1}$ sedimentation equilibrium experiment | 133 |
| **Figure 4.10** | As (Figure 4.9) but the analysis of **iota carrageenan** in PBS 0.1M at a loading concentration (0.3 mg mL$^{-1}$). $M_{w, app}$ from extrapolation of $M^*$ to cell base = 550 kDa, and the fitted lines are defined in the legend Figure 4.9. | 134 |
| **Figure 4.11** | As (Figure 4.9) but for the analysis of **lambda carrageenan** in PBS 0.1M at a loading concentration (0.3 mg mL$^{-1}$). $M_{w, app}$ from extrapolation of $M^*$ to cell base = 540 kDa, and the fitted lines are defined in the legend Figure 4.9. | 134 |
| **Figure 4.12** | Molecular weight distribution for carrageenan samples at different solvents obtained from transformation of the g(s) versus *s* distribution at concentration (0.2 mg mL$^{-1}$), using the Extended Fujita method of Harding et al., (2011) (a) kappa (b) iota (c) lambda. | 135 |
| **Figure 4.13** | Example of elution profile of carrageenan samples and PBS 0.1M buffer (a) kappa, (b) iota and (c) lambda (black line) examined by SEC-MALS at concentration 0.8 mg mL$^{-1}$. The horizontal black lines (open square) correspond to SEC-MALS calculated molecular weights. | 137 |
| **Figure 4.14** | Intrinsic viscosity plots from capillary viscometry: Huggins, Kraemer and Solomon-Ciuta extrapolations for **kappa carrageenan** (a) NaCl (b) NaI (c) PBS 20.0$^{o}$C (d) DMSO 100% and (e) DMSO 80%. | 139 |
| **Figure 4.15** | The intrinsic viscosity plot from capillary viscometry: | 140 |

| | | |
|---|---|---|
| | Huggins, Kraemer and Solomon-Ciuta extrapolations for **iota carrageenan** (a, b and c) and **lambda carrageenan** (d, e and f) at different solvents NaCl, NaI and PBS 20.0$^{o}$C, respectively. | |
| **Figure 5.1** | Chemical structure of chitosan. | 148 |
| **Figure 5.2** | Sedimentation coefficient distribution profiles using least squares g*(s) method of SEDFIT obtained from sedimentation velocity experiment for chitosan samples (a) CHIT1 (b) CHIT2 (c) CHIT3 (d) CHIT4 (e) CHIT5 (f) CHIT6. | 156 |
| **Figure 5.3** | Concentration dependence (reciprocal) of the sedimentation coefficient plot (after correction to standard solvent conditions) for chitosan samples (a) CHIT1 (b) CHIT2 (c) CHIT3 (d) CHIT4 (e) CHIT5 (f) CHIT6. | 157 |
| **Figure 5.4** | As (Figure 4.9) but the analysis of **CHIT4** at a loading concentration of (0.5 mg mL$^{-1}$). $M_{w,\,app}$ from extrapolation of $M$* to cell base = 80 kDa, and the meaning of the fitted lines in "c" and "d" are explained in the legend Figure 4.9. | 159 |
| **Figure 5.5** | Plots of the apparent weight average molecular weight ($M_{w,app}$) against concentration c (g mL$^{-1}$). | 160 |
| **Figure 5.6** | Elution profile of commercial and laboratory prepared chitosan samples in 0.2 M, pH 4.3, acetate buffer, (a) CHIT1 (b) CHIT2 (c) CHIT3 (d) CHIT4 (e) CHIT5 (f) CHIT6 (black line) examined by SEC-MALS at concentration 0.5 mg mL$^{-1}$. The open squares correspond to SEC-MALS calculated molecular weights. | 161 |
| **Figure 5.7** | Molecular weight distribution for all chitosan samples in 0.2 M, pH 4.3, acetate buffer obtained from transformation of the g(s) versus *s* distribution at concentration (0.2 mg mL$^{-1}$), using the Extended Fujita method of Harding et al., (2011) (a) CHIT1 (b) CHIT2 (c) CHIT3 (d) CHIT4 (e) CHIT5 (f) CHIT6. | 163 |
| **Figure 5.8** | The intrinsic viscosity plots from capillary viscometry: Huggins, Kraemer and Solomon-Ciuta extrapolations for chitosan samples (a) CHIT1 (b) CHIT2 (c) CHIT3 (d) CHIT4 (e) CHIT5 (f) CHIT6. | 165 |
| **Figure 5.9** | Mark–Houwink–Kuhn–Sakurada (MHKS) power law double logarithmic plot of $s^{o}_{20,w}$ *vs* $M_w$ for all chitosan samples. | 166 |
| **Figure 5.10** | Mark–Houwink–Kuhn–Sakurada (MHKS) power law double logarithmic plot from on-line differential pressure viscometery coupled to SEC-MALS. The plot is of intrinsic viscosity [η] as a function of elution volume (ordinate) versus molecular weight $M_w$ as a function of elution volume. For chitosan samples (a) CHIT1 (b) CHIT2 (c) CHIT3 (d) CHIT4 (e) CHIT5 (f) CHIT6. | 168 |
| **Figure 5.11** | The conformation zoning plot for chitosan samples, commercial (CHIT1 to CHIT4) and in house laboratory- | 170 |

| | | |
|---|---|---|
| | prepared (CHIT5 and CHIT6) adopted rigid rod structures at (zone B) and semi-flexible coil structures (zone C), respectively. | |
| **Figure 5.12** | Bushin-Bohdanecky plot for commercial (CHIT1 to CHIT4) and in-house laboratory-prepared (CHIT5 and CHIT6) chitosan samples, where $L_p$ = (10 ± 1) nm from the slope. | 172 |
| **Figure 5.13** | Yamakawa-Fujii plot for commercial (CHIT1 to CHIT4) and in-house laboratory-prepared (CHIT5 and CHIT6) chitosan samples, where $L_p$ = (18 ± 1) nm from the slope. | 173 |
| **Figure 5.14** | Contour plots of chitosan samples (a) CHIT1 (b) CHIT2 (c) CHIT3 (d) CHIT4 (e) CHIT5 and (f) CHIT6. The target function, $\Delta$ calculated based on variables values of $L_p$ and $M_L$, and are represented on the full colour spectrum from blue ($\Delta$ = 0) to red ($\Delta \geq 0.95$). | 174 |
| **Figure 5.15** | Plots of target function ($\Delta$) vs. persistence length ($L_p$) for chitosan samples (a) CHIT1 (b) CHIT2 (c) CHIT3 (d) CHIT4 (e) CHIT5 and (f) CHIT6. | 176 |
| **Figure 5.16** | Normalized sedimentation coefficient distribution profiles obtained from sedimentation velocity experiment for unmixed controls and mixture for chitosan samples (CHIT5 and CHIT6) with DNA. | 179 |
| **Figure 5.17** | Normalized sedimentation coefficient distribution profiles obtained from sedimentation velocity experiment for unmixed controls and mixture for chitosan samples (CHIT5 and CHIT6) with xanthan-STD. | 180 |
| **Figure 5.18** | Multi-Gaussian fit using MULTIG (locally written software, run under pro Fit™, Quansoft, Zurich) (a) Multi-Gaussian fit to the CHIT5-DNA mixture and (b) Multi-Gaussian fit to the CHIT6-DNA mixture. With the routine MULTIG fitting was initially performed manually via the interactive *Preview Window*, floating the position (*s* value), area and standard deviation of each peak. | 182 |
| **Figure 6.1** | Chemical structure of konjac glucomannan. | 189 |
| **Figure 6.2** | Chemical structure of xanthan repeat unit indicating a trisaccharide side chain with pyruvalated end mannose unit. | 191 |
| **Figure 6.3** | Chemical structure of alginate. | 193 |
| **Figure 6.4** | Sedimentation coefficient distribution profiles using least squares g*(s) method of SEDFIT obtained from sedimentation velocity experiment for all individual polysaccharides at different ionic strengths (0.1M and 0.001M) konjac glucomannan (a and b), lambda carrageenan (c and d) and xanthan (e and f) respectively. | 197 |
| **Figure 6.5** | Concentration dependence (reciprocal) of the sedimentation coefficient plot (after correction to standard solvent conditions) for all individual polysaccharides at different ionic strengths (0.1M and 0.001M) konjac glucomannan (a and b), lambda | 198 |

carrageenan (c and d) and xanthan (e and f), respectively.
**Figure 6.6** Molecular weight plots for konjac glucomnannan (a and b), lambda carrageenan (c and d) and xanthan (e and f) using SEDFIT-MSTAR. 200
**Figure 6.7** Elution profile (black line) for (a) xanthan and (b) lambda carrageenan in 0.1M PBS examined by SEC-MALS at concentration of 0.5 mg $mL^{-1}$. The open squares correspond to SEC-MALS calculated molecular weights. 201
**Figure 6.8** Molecular weight distribution for individual polysaccharides (a) konjac glucomannan, (b) lambda carrageenan and (c) xanthan in 0.1M PBS buffer obtained from transformation of the g(s) versus *s* distribution at concentration (0.2 mg $mL^{-1}$), using the *Extended Fujita* method of Harding et al., (2011b). 202
**Figure 6.9** The intrinsic viscosity plot from capillary viscometry: Huggins, Kraemer and Solomon-Ciuta extrapolations for konjac glucomannan (a and b) lambda carrageenan (c and d) xanthan (e and f). 204
**Figure 6.10** Concentration dependence (reciprocal) of the sedimentation coefficient plot – main free peak (after correction to standard solvent conditions) for the binary mixture of konjac glucomannan and xanthan: (a) 0.1M ionic strength and (b) 0.001M ionic strength. 206
**Figure 6.11** Sedimentation coefficient distribution profiles using least squares g*(s) method of SEDFIT obtained from sedimentation velocity experiment for the binary mixture of konjac glucomannan and xanthan with individual component controls at 0.1M ionic strength: (a) 2.00 mg $mL^{-1}$, (b) 1.00 mg $mL^{-1}$, (c) 0.50 mg $mL^{-1}$ and (d) 0.25 mg $mL^{-1}$. 207
**Figure 6.12** Sedimentation coefficient distribution profiles using least squares g*(s) method of SEDFIT obtained from sedimentation velocity experiment for the binary mixture of konjac glucomannan and xanthan with individual component controls at 0.001M ionic strength and concentration (2.0 mg $mL^{-1}$). 208
**Figure 6.13** Sedimentation coefficient distribution profiles using least squares g*(s) method of SEDFIT obtained from sedimentation velocity experiment for (a) the binary mixture of konjac glucomannan and xanthan at 0.001M ionic strength, (b) the normalized data. 209
**Figure 6.14** The intrinsic viscosity plot from capillary viscometry: Huggins, Kraemer and Solomon-Ciuta extrapolations for the binary mixture of konjac glucomannan and xanthan at tow ionic strengths (a) 0.1M and (b) 0.001M. 210
**Figure 6.15** Sedimentation coefficient distribution profiles using least squares g*(s) method of SEDFIT for the ternary mixture of lambda carrageenan, konjac glucomannan and xanthan at 0.1M ionic strength: (a) 2.00 mg $mL^{-1}$, (b) 1.00 mg 212

| | | |
|---|---|---|
| | $mL^{-1}$, (c) 0.50 mg $mL^{-1}$ and (d) 0.25 mg $mL^{-1}$. | |
| **Figure 6.16** | Sedimentation coefficient distribution profiles using least squares g*(s) method of SEDFIT for the ternary mixture of lambda carrageenan, konjac glucomannan and xanthan at 0.001M ionic strength: (a) 2.00 mg $mL^{-1}$, (b) 1.00 mg $mL^{-1}$, (c) 0.50 mg $mL^{-1}$ and (d) 0.25 mg $mL^{-1}$. | 212 |
| **Figure 6.17** | Concentration dependence (reciprocal) of the sedimentation coefficient plot for the ternary mixture of lambda carrageenan, konjac glucomannan and xanthan at ionic strength 0.1M: (a) C30, (b) C25, (c) C20, (d) C15, (e) C10 and (f) C05. | 213 |
| **Figure 6.18** | Sedimentation coefficient distribution profiles using the least squares g*(s) method of SEDFIT for the ternary mixture of lambda carrageenan, konjac glucomannan and xanthan at all mixing ratio (C30 – C05) companied with non-interacting species at 0.001M ionic strength and 0.25 mg $mL^{-1}$. | 214 |
| **Figure 6.19** | Concentration dependence (reciprocal) of the sedimentation coefficient plots for the ternary mixture of lambda carrageenan, konjac glucomannan and xanthan at ionic strength 0.1M: (a) C30, (b) C25, (c) C20, (d) C15, (e) C10 and (f) C05. | 215 |
| **Figure 6.20** | Intrinsic viscosity plots from capillary viscometry: Huggins, Kraemer and Solomon-Ciuta extrapolations for the ternary mixtures of lambda carrageenan, konjac glucomannan and xanthan at 0.1M ionic strength: (a) C30, (b) C25, (c) C20, (d) C15, (e) C10, and (f) C05. | 217 |
| **Figure 6.21** | Intrinsic viscosity plots from capillary viscometry: Huggins, Kraemer and Solomon-Ciuta extrapolations for the ternary mixture of lambda carrageenan, konjac glucomannan and xanthan at 0.001M ionic strength: (a) C30, (b) C25, (c) C20, (d) C15, (e) C10, and (f) C05. | 218 |
| **Figure 7.1** | The principle sugars of gastrointcstinal mucins. | 223 |
| **Figure 7.2** | Sedimentation coefficient distribution profiles using least squares g*(s) method of SEDFIT obtained from sedimentation velocity experiment for all mucin Sep 13, Oct 13 and Nov 13 (a, c and e), and normalised plots (b, d and f) respectively. | 230 |
| **Figure 7.3** | Concentration dependence (reciprocal) of the sedimentation coefficient plot (after correction to standard solvent conditions) for all mucin samples (a) Sep 13, (b) Oct 13 and (c) Nov 13. | 231 |
| **Figure 7.4** | Elution profile for the three mucin samples at a loading concentration of 1.0 mg $mL^{-1}$. The red dot indicates light scattering at a scattering angle of $90^0$ (nb the full scattering envelope was used) and the black indicates specific viscosity. | 233 |
| **Figure 7.5** | Elution profiles for the three mucin samples (Sep 13, Oct 13 and Nov 13) at concentration 1.0 mg $mL^{-1}$. | 234 |
| **Figure 7.6** | Elution profiles for the three mucin samples Sep 13 | 234 |

(black line), Oct 13 (red line) and Nov 13 (green line) examined by SEC-MALS at concentration 1.0 mg $mL^{-1}$. The horizontal black (open square), red (open circle) and green (up triangle) lines correspond to SEC-MALS calculated molecular weights for mucin samples Sep 13, Oct 13 and Nov 13, respectively.

**Figure 7.7** As (Figure 4.9) but the analysis of **Sep 13 mucin** at a loading concentration of (0.5 mg $mL^{-1}$). $M_{w,\,app}$ from extrapolation of $M^*$ to cell base = 2000 kDa, and the meaning of the fitted lines in "c" and "d" are explained in the legend Figure 4.9. 235

**Figure 7.8** The reciprocal plots of the apparent weight average molecular weight ($M_{w,app}$) against concentration $c$ (g $mL^{-1}$) for mucin samples (a) Sep 13, (b) Oct 13 and (c) Nov 13. 236

**Figure 7.9** Molecular weight distribution for all mucin samples obtained from transformation of the g(s) versus $s$ distribution at concentration (0.25 mg $mL^{-1}$), using the Extended Fujita method of Harding et al., (2011) (a) Sep 13 (b) Oct 13 and (c) Nov 13. 237

**Figure 7.10** Elution profiles for the three mucin samples: Sep 13 (black line), Oct 13 (red line) and Nov 13 (green line) examined by SEC-MALS at concentration 1.0 mg $mL^{-1}$. The horizontal black (open square), red (open circle) and green (up triangle) lines correspond to SEC-MALS calculated intrinsic viscosity for mucin samples Sep 13, Oct 13 and Nov 13, respectively. 238

**Figure 7.11** Mark–Houwink–Kuhn–Sakurada (MHKS) power law double logarithmic plot for mucin samples (a) Sep 13, (b) Oct 13 and (c) Nov 13 from on-line differential pressure viscometery coupled to SEC-MALS. The plot is of intrinsic viscosity [η] as a function of elution volume (ordinate) versus molecular weight $M_w$ as a function of elution volume. 240

**Figure 7.12** Bushin-Bohdanecky plots for mucin samples (a) Sep 13, (b) Oct 13 and (c) Nov 13, where $L_p$ (17±1) nm, (15±1) nm and (14±1) nm, respectively. 243

**Figure 7.13** Schematic view for a linear random coil model of mucin, showing the influence of the oligosaccharide on the macromolecule flexibility. 245

**Figure 7.14** Contour plots of the mucin samples (a) Sep13, (b) Oct13 and (c) Nov13. The target function, $\Delta$ calculated based on variables values of $L_p$ and $M_L$, and are represented on the full colour spectrum from blue ($\Delta$ = 0.005) to red ($\Delta \geq 0.65$). 246

**Figure 7.15** Plots of target function ($\Delta$) vs. Persistence length ($L_p$) for the mucin samples (a, b and c) Sep13 (2.0±0.1), Oct13 (7.5±0.5) and Nov13 (11±1), respectively. 247

**Figure 7.16** Plots of the experimental and calculated values for the intrinsic viscosity of the mucin samples (a, b and c) 247

Sep13, Oct13 and Nov13, respectively.
**Figure 7.17** Apparent sedimentation coefficient distribution profile using least squares g*(s) methods for PGX and its individual components at loading concentration 0.5 mg $mL^{-1}$ and high ionic strength 0.1M. 248
**Figure 7.18** Apparent sedimentation coefficient distribution profile using the least squares g*(s) methods for the mixture of mucin with (a) PGX, (b) KGM, (c) xanthan and (d) alginate at a loading concentration 0.5 mg $mL^{-1}$ and high ionic strength 0.1 M. 249
**Figure 7.19** Apparent sedimentation coefficient distribution profile using least squares g*(s) methods for the mixture of mucin with PGX at different loading concentrations and ionic strength 0.1M; (a) Interference and (b) Absorbance. 251
**Figure 7.20** Apparent sedimentation coefficient distribution profile using least squares g*(s) methods for the mixture of mucin with PGX at loading concentration 0.5 mg $mL^{-1}$ and different ratios (1:1 to 5:1). 251

# LIST OF TABLES


| | | |
|---|---|---|
| **Table 1.1** | Some nutraceutical and functional compounds yielded from marine sources. | 4 |
| **Table 1.2** | Hydrocolloid polysaccharides obtained from seaweed sources. | 8 |
| **Table 1.3** | Summary of seaweed authorised in France for human consumption. | 15 |
| **Table 1.4** | Sources of chitin and the percentage content obtained from crustacean and molluscan organisms. | 17 |
| **Table 1.5** | Summary the principal applications of chitin and its derivative chitosan. | 20 |
| **Table 3.1** | Summary of $s^{\circ}_{20,w}$ and $k_s$ results for all lambda carrageenan unheated and heated samples. | 88 |
| **Table 3.2** | Summary of molecular weights $(M_w)$ results for lambda carrageenan unheated and heated samples from sedimentation equilibrium and SEC-MALS. | 90 |
| **Table 3.3** | Intrinsic viscosity values for lambda carrageenan unheated and heated samples from capillary viscometry and differential pressure viscometry (Viscostar in SEC-MALS). | 94 |
| **Table 3.4** | Wales-van Holde ration for lambda carrageenan unheated and heated samples. | 97 |
| **Table 3.5** | Mark-Houwink-Kuhn-Sakurada Power Low exponents. | 99 |
| **Table 4.1** | Summary of $s^{\circ}_{20,w}$ and $k_s$ results for kappa, iota and lambda carrageenans in different solvents. | 127 |
| **Table 4.2** | Summary of weight average molecular weight $(M_w)$ results for kappa, iota and lambda carrageenans in different solvents. | 132 |
| **Table 4.3** | Summary of intrinsic viscosity [η] results for kappa, iota and lambda carrageenans in different solvents obtained from capillary viscometry and on line ViscoStar. | 138 |
| **Table 4.4** | Predicted sedimentation coefficient values obtained based on experimental data for carrageenans. | 144 |
| **Table 5.1** | Summary of $s^{\circ}_{20,w}$ and $k_s$ results for all chitosan Commercial (“C”) and in-house laboratory (“L”) prepared samples. | 157 |
| **Table 5.2** | Summary of weight average molecular weights $(M_w)$ results for chitosan samples from sedimentation velocity, equilibrium and SEC-MALS. | 159 |
| **Table 5.3** | Intrinsic viscosity values of (“C”) and (“L”) chitosan samples obtained from capillary viscometry and differential pressure viscometry (Viscostar in SEC-MALS). | 164 |
| **Table 5.4** | Mark-Houwink-Kuhn-Sakurada (MHKS) power law exponent $a$, from SEC-MALS and Wales-van Holde ration, $R$ for chitosan samples. | 168 |
| **Table 5.5** | Summary of the persistence length $L_p$ and the mass per unit length $M_L$ values for chitosan samples. | 175 |

| | | |
|---|---|---|
| **Table 5.6** | Sedimentation coefficients at $s_{20,w}$ at a total concentration of 1 mg $mL^{-1}$, for chitosan, DNA, xanthan and chitosan-DNA and chitosan-xanthan complexes. | 178 |
| **Table 6.1** | Summary of $s^{\circ}_{20,w}$ and $k_s$ results for all individual polysaccharides samples. | 197 |
| **Table 6.2** | Summary of molecular weights $(M_w)$ results for individual polysaccharides from sedimentation velocity, equilibrium and SEC-MALS. | 201 |
| **Table 6.3** | Intrinsic viscosity values for individual polysaccharides konjac glucomannan, lambda carrageenan and xanthan yielded from capillary viscometry. | 203 |
| **Table 6.4** | Summary of sedimentation velocity and capillary viscometry results for the binary mixture of konjac glucomannan and xanthan samples at 0.1M and 0.001M. | 206 |
| **Table 6.5** | Summary of $s^{\circ}_{20,w}$ results for ternary mixture samples at different ionic strengths. | 211 |
| **Table 6.6** | Intrinsic viscosity values (mL $g^{-1}$) for ternary mixtures of lambda carrageenan, konjac glucomannan and xanthan (mixing ratios C30 to C05) at 0.1M and 0.001M ionic strengths yielded from capillary viscometry. | 216 |
| **Table 7.1** | Summary of $s^{o}_{20,w}$ and $k_s$ results for all mucin samples. | 229 |
| **Table 7.2** | Summary of weight average molecular weight $(M_w)$ results for mucin samples from sedimentation velocity, equilibrium and SEC-MALS. | 232 |
| **Table 7.3** | Intrinsic viscosity and MHKS power law exponent *a*, values for mucin samples yielded using the Viscostar in SEC-MALS. | 239 |
| **Table 7.4** | Summary of the results obtained from Multi-HYDFIT for mucin samples. | 244 |

# LIST OF ABBREVIATIONS

| | |
|---|---|
| Ac | Acetyl |
| $a$ | Mark-Houwink exponent of viscosity |
| $A$ | Absorbance |
| $A_2$ —or $B$ | Second virial coefficient |
| $A_3$ —or C | Third virial coefficient |
| AFM | Atomic Force Microscopy |
| AUC | Analytical ultracentrifugation |
| $b$ | Mark-Houwink-Sakurada power law exponent of sedimentation |
| $c$ | Concentration |
| $c(r)$ | Concentration at radius $r$ |
| $c(a)$ | Concentration at meniscus |
| $c(b)$ | Concentration at cell base |
| DSC | Differential scanning calorimetry |
| $d$ | Diameter |
| $dc$ | Change of solute concentration |
| $dn$ | Change of refractive index |
| $dx/dy$ | The shear strain |
| $D^o$ | Diffusion coefficient (extrapolated to infinite dilution) |
| $F_c$ | Centrifugal force |
| $F_b$ | Buoyant force |
| $F_f$ | Viscous ―frictional‖ drag force |
| $f/f_0$ | Frictional ratio |
| FDA | Food and Drug Administration |
| $IP$ | Inlet pressure |
| $I_o$ | Intensity of the incident beam |
| $I$ | Ionic strength |
| $I\theta$ | Intensity of scattered beam |
| $j(r)$ | Fringe concentration subjected to the meniscus |
| $J(a)$ | Absolute meniscus concentration |
| $J(r)$ | Absolute fringe concentration |
| $K$ | Polymer constant |
| $K_\eta$ | Mark-Houwink constant of viscosity |
| $K_s$ | Mark-Houwink constant of sedimentation |
| $K_H$ | Huggins coefficient |
| $K_K$ | Kraemer coefficient |
| $kDa$ | kilo Daltons |
| KGM | Konjac glucomannan |
| $k_S$ | Gralén concentration dependence parameter |
| $k_S/\eta$ —or $R$ | Wales-van Holde ratio |
| $\lambda$ | Wavelength |
| $L_p$ | Persistence length |
| $ls\text{-}g^*(s)$ | Least-square $g^*(s)$ |
| MALS | Multi-angle light scattering detector |
| MHKS | Mark-Houwink-Kuhn-Sakurada |
| $M_L$ | Mass per unit length |
| $m$ | Mass of particle |
| $M_w$ | Weight average molecular weight |

| | |
|---|---|
| $M_z$ | z-average molecular weight |
| $M_{w,app}$ | Apparent molecular weight |
| $m_0$ | Mass of fluid displaced by a particle |
| M | Molar mass |
| $M^*$ | M-star function of molecular weight |
| $M^*(r)$ | M-star function of molecular weight at a certain radius |
| M:G | Mannose: Glucose ratio |
| $\eta$ | Viscosity of the solution |
| $\eta_0$ | Viscosity of the solvent |
| $\eta_{inh}$ | Inherent viscosity |
| $\eta_{red}$ | Reduced viscosity |
| $\eta_{rel}$ | Relative viscosity |
| $\eta_{sp}$ | Specific viscosity |
| $n$ | Refractive index |
| $[\eta]$ | Intrinsic viscosity |
| $N$ | Avogadro's constant |
| $\phi$ | Flory-Fox constant |
| $\Delta P$ | Differential pressure |
| $\rho$ | Density of solution |
| $\rho_o$ | Density of solvent |
| $P(\theta)$ | The form factor |
| PBS | Phosphate buffer saline |
| $R\theta$ | Rayleigh factor |
| $r$ | Radial displacement |
| $R_g$ | Radius of gyration |
| rpm | Revolution per minute |
| $R$ | Universal gas constant |
| RI | Refractive index |
| $R\theta$ | Rayleigh ratio |
| SEM | Scanning electron microscopy |
| SDS-PAGE | Sodium Dodecyl Sulfate Polyacrylamide Gel Electrophoresis |
| $s$ | Sedimentation coefficient |
| S | Svedberg units |
| $s_{T,b}$ | Sedimentation coefficient achieved during experimental conditions |
| $s_{20,w}$ | Sedimentation coefficient corrected from $s_{T,b}$ in the form of standard solvent of water at 20 $^0$C |
| $s^0_{20,w}$ | $s_{20,w}$ extrapolated to zero concentration and elimination of non-ideality |
| [s] | Intrinsic sedimentation coefficient |
| SE | Sedimentation equilibrium |
| SEC | Size exclusion chromatography |
| SEC-MALS | size exclusion chromatography coupled with multi angle light scattering |
| SV | Sedimentation velocity |
| SA | Sodium alginate |
| T | Absolute temperature |
| $V_M$ | The volume of mobile phase and inside and outside the pores |
| $V$ | Scattering volume |

| | |
|---|---|
| $V_i$ | Internal pore volume |
| $V_o$ | Void volume |
| $\nu$ | Velocity |
| $v$ | Partial specific volume |
| WFI | Water for injection |
| $\omega^2 r$ | Centrifugal field |
| $\theta$ | Angle of scattering light |
| $\Delta$ | Target (error) function |

# CHAPTER 1

## MARINE BASED NON-DIGESTIBLE FIBRE POLYSACCHARIDES

The demand for carbohydrate based therapeutics and nutritional supplements of medicinal value have increased in recent times. Natural biopolymers – and in particular marine polysaccharides – have been considered for therapeutic development and these materials form the cornerstone of this thesis.

Polysaccharides obtained from different sources of marine organisms such as seaweeds and shellfish present a large variety of structures, many of which possess interesting nutraceutical and pharmaceutical behaviour for use in different applications (see, for example Jiao et al., 2011; Senni et al., 2011). Unfortunately, marine polysaccharide based formulations for potential therapeutic use have not been completely investigated, resulting in a deficiency of scientific or clinical data to support their use. Consequently, an understanding of the molecular properties and interactions of these substances is important in order to address this gap in our knowledge so as to facilitate their use as medication against many diseases.

Before we introduce the main body of this thesis, I will first review the main marine polysaccharides in terms of their properties and their impact or possible impact on human healthcare. The ability of marine polysaccharides to further interact with other biopolymers has been mentioned and these interactions might provide new materials that can be utilized for further applications.

# 1.1 INTRODUCTION

The life style of the world's population changed significantly in the twentieth century, particularly because of the increased well-being and reduced physical activity together with the rise of purchasing power (Venugopal, 2009). In general, this has led to a shift in the consumption patterns by the public, food rich in energy with high levels of sugar and saturated fats being consumed at increasing level. This has resulted in harmful effects on health, manifested for example by an increase in chronic diseases such as obesity, diabetes, cancer and cardiovascular disease (Jackson and Paliyath, 2011). In 2001, approximately 59% of the 56.5 million total deaths in the world were a result of chronic diseases with the above mentioned contributing to nearly 46% of global diseases. In particular cardiovascular diseases were responsible for a third of the global deaths in 1999, and by 2010 became the major cause of death in developing countries (Mayakrishnan et al., 2013). The majority of cardiovascular diseases can be controlled and prevented, since the protective role of a diet rich in fruits and vegetables against these diseases has been well reported and supported by many studies (see, for example Hu and Willett, 2002).

However, parallel to these developments has been an increasing awareness of the protective role of diet for resisting these diseases. The old tenet of Hippocrates "*Let food be your medicine and medicine be your food*" has brought back to the attention of the public the strong relationship between diet and health (see, Szarc vel Szic et al., 2010). The consumption of food with a low content of sugar, sodium and saturated fats has become preferred, along

with regular check for the biomarker profile (e.g. blood pressure and glucose tolerance) to prevent or treat these diseases earlier. This has affected the strategy for the food industry which has been steadily refocusing to meet the needs of consumer health (Arvanitoyannis and Van Houwelingen-Koukaliaroglou, 2005). Although, the food industry worldwide has been developing high-value nutrition and wellness products, or nutracetical and functional foods, by reformulation of existing products, the development cost is still high. Consequently, the high preparation cost of these products together with the ever increasing population of the world has attracted scientists to the goal of identifying new materials with useful health properties for the improvement of functional foods: and foods from marine sources have become a particular focus (Abu-Ghannam and Cox, 2013).

The oceans cover more than 70% of the world's surface, offering a rich source from the wide diversity of marine organisms that include seaweed, shellfish, corals and microorganisms. For centuries marine organisms have been used as a source of food however, it is now recognised that they also have a role in promoting health, supported by the fact that many contain bioactive compounds (Tombs and Harding, 1998). Recently, they have been highlighted as good sources for nutrients providing more than 3000 different compounds - some of which are shown in Table 1.1. These compounds contain antimicrobial, anti-inflammatory and antioxidant properties, which have numerous beneficial health effects and play a role in the treatment and/or prevention of human diseases such as cancer and cardiovascular disease (Noda et al., 1990; Faulkner, 2000).

Marine organisms provide numerous sources of natural products with functional materials including polyunsaturated fatty acids (PUFA), polysaccharides, minerals and vitamins, antioxidants, enzymes and bioactive peptides (Pomponi, 1999; Wijeskara et al., 2011). Many possess good nutritional and medicinal benefits and provide sources of dietary fibre (Venugopal, 2011; Mayakrishnan et al., 2013). Unfortunately, marine polysaccharide-based medicines have been poorly investigated, resulting in a lack of scientific or clinical data supporting their therapeutic use. Consequently interest in the utilization and exploitation of their unique properties and bioactive compounds – and underpinning data – is increasing.

**Table 1.1**: Some nutraceutical and functional compounds yielded from marine sources. Adapted from Venugopal (2009).

| **Marine Sources** | **Products** |
|---|---|
| Seaweeds | Mineral sources |
| | Proteins |
| | Hydrocolloids (food additives, fibers and bioactive functions) |
| Shellfish | Chitin, chitosan and related compounds |
| | Glucosamine |
| | Glue from mussel |
| | Enzymes |
| | Antioxidants |
| | Antimicrobials |
| Corals | Drugs and other bioactive compounds |
| | Enzymes |
| | Biochemicals |
| | Calcium |
| Microorganisms (Microalgae) | Carotenoids |
| | Fine chemicals |

## 1.2 MARINE POLYSACCHARIDES

Recently demand has increased for the nutritional supplements that provide additional medicinal benefits. Natural sources, in particular marine polysaccharides are a promising and largely unexplored source for development of such therapeutic agents. Polysaccharides obtained from different source of marine organisms such as seaweeds and shellfish present a huge variety of structures which possess interesting nutraceutical and pharmaceutical behaviour for use in a wide range of applications (Jiao et al., 2011; Senni et al., 2011). Moreover, marine polysaccharides are an exciting area for biotechnological exploitation due to their potential in the development of cell therapies and regenerative medicine. This is especially true in the case of seaweed polysaccharides: for instance the carrageenans present a real potential for cell delivery and tissue engineering along with therapeutics. Alginate has also been a key component in the development of microencapsulation technology and its use for the treatment of diabetics through the encapsulation of insulin producing cells. Another group of marine polysaccharides, the chitosans – derived from marine shellfish – have been considered for use as bioadhesive polymers for drug delivery and increasing epithelial uptake (Tombs and Harding, 1998; Venugopal, 2011; Li et al., 2014). In summary, although there are large numbers of marine polysaccharides obtained from various marine organisms, only polysaccharides from marine seaweed (e.g. carrageenan and alginate) and from marine shellfish (e.g. chitosan) appear to have been considered the most in terms of their use or potential use in treatment or control of disease.

### 1.2.1 Polysaccharides from Seaweed

Seaweed is a common term for the plants of sea or "marine algae" including both macroalgae and microalgae. Seaweeds are classified into three main groups namely: *Rhodophyta* (red algae), *Phaeophyta* (brown algae) or *Chlorophyta* (green algae) based on their nutrient, pigments and chemical composition (Figure 1.1). They have been used as dietary components for humans for the last three thousand years. In Asia, the consumption of seaweeds has been traditionally as sea vegetables, whereas they are more commonly used as food gelling and thickening agents in western countries (Tombs and Harding, 1998; Venugopal, 2011). In Asia, people use seaweed directly for different culinary purposes, but such use has been limited in the West. Consequently the average quantity of seaweed consumption per person in Asia is much higher, particularly Japan at about 1.4 kg a year, while consumption is low in western countries (Burtin, 2003).

Worldwide, seaweeds have increasingly come to be recognised as a healthy renewable resource; because of they provide a low calorie food, rich in vitamins, minerals and dietary fibre. Seaweeds are nutritionally important since they contain protein, lipids, polysaccharides, vitamins and minerals, all of which have a number of biological activities for example antimicrobial, antifungal, antiviral and antioxidant behaviour. Therefore, they have potential benefits for the control of tumours, obesity, thrombosis and hyperlipidemia (Duan et al., 2006; Venugopal, 2009; Cox et al., 2010). Seaweeds can be exposed to a combination of light and high oxygen concentrations. This environment can lead to the formation of free radicals and other strong

oxidizing agents, but during metabolism seaweeds do not suffer any serious photodynamic damage. These results support the view that seaweed cells have some intrinsic protective mechanisms and compounds (Matsukawa et al., 1997; Abu-Ghannam and Cox, 2013).

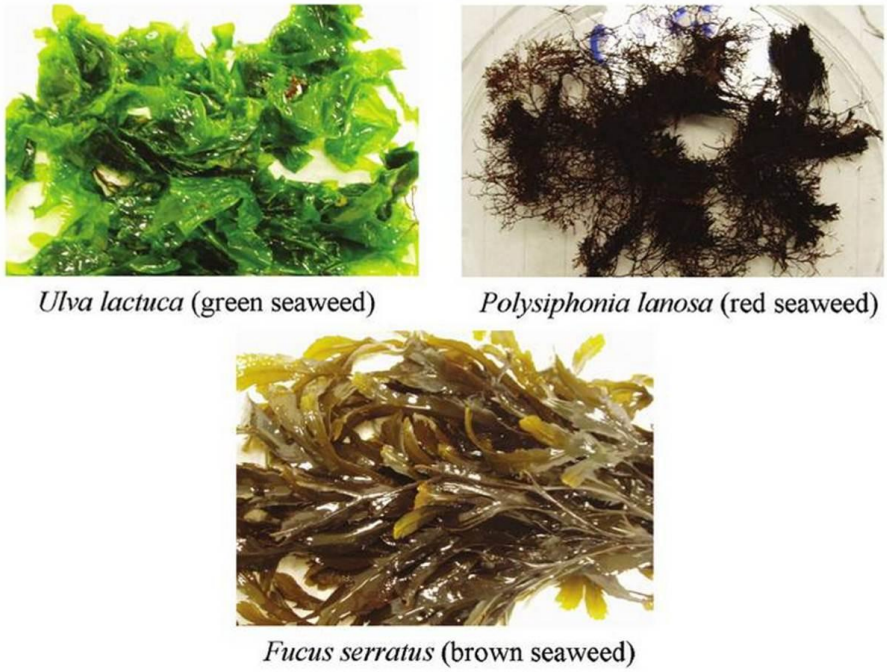


**Figure 1.1**: Examples of three classes of seaweed, collected from the south-east coast of Ireland. Adapted from Tan *et al.* (2013).

Polysaccharides are the major component of the different seaweed elements and can be extracted in large amounts from the cell walls and intercellular spaces of the red and brown species. Most of these polysaccharides are considered as dietary fibre since they are not digested by the human endogenous digestive enzymes. Thus, the high content of insoluble dietary fibre (50 – 80% of the total) make seaweed a rich source of healthy food for nutrition (Vaugelade et al., 2000; Ortiz et al., 2006). The main components of seaweed polysaccharides are galactose, mannose and glucose (or derivatives of

these). For example galactose and 3,6-anhydro-D-galactose are the main elements of carrageenan and agar. The three major groups of seaweed polysaccharides namely alginate, carrageenan and agar extracted from brown and red seaweed species, respectively, in which also has known as phycocolloids, hydrocolloids or gums (Table 1.2). They are extensively used in various industrial applications including as thickeners, gelling agents and stabilizers (Venugopal, 2011; Bixler and Porse, 2011).

**Table 1.2:** Hydrocolloid polysaccharides obtained from seaweed sources. Adapted from Venugopal (2009).

| **Hydrocolloids** | **Seaweed source** |
|---|---|
| Agar, agarose | Rhodophyta *(Gracilaria, Gelidium, Pterocladia)* |
| Carrageenans | Rhodophyta *(Eucheuma, Chondrus, Hypnea, Gigartina)* |
| Alginic acid (Alginate) | Phaeophyta *(Macrocystis, Laminaria, Ascophyllum)* |

The polysaccharides from seaweed have three principal groups of functions depending on their types, namely biological, physiological and technological. The biological functions play a role in the seaweed cells structure by providing components for the cell wall architecture, cell-cell recognition, hydration of intracellular fluid and stimulation of host defence. Physiological functions are generally linked to physicochemical properties; solubility, viscosity, hydration and ion exchange capacities in the digestive tract (Venugopal, 2011). Seaweed

polysaccharides have a higher capacity for binding to water, as high as twenty times their volume, depending on their length and thickness compared to other fibres with a high water-holding capacity such as cellulose. This is consistent with these polysaccharides being referred to as hydrocolloids. In this respect, they have become commercially and technologically important as texturizers, stabilizer, emulsifiers, fat reducers, film formers, shelf-life extenders and viscosity modifiers in food applications (Holdt and Kraan, 2011).

Seaweed polysaccharides however have enormous potential not only for food application, but also for health benefits due to their biologically actives compounds. Marine algae particularly seaweed polysaccharides are rich sources of biologically active compounds such as antioxidants, antithrombin activity, antitumor, cell recognition and cell adhesion and regulation of receptor functions. For example, these compounds are used as inhibitors against various viruses including herpes simplex virus (HSV), and human immunodeficiency virus (HIV) (Laurienzo, 2010; Wijesekara et al., 2011; Jiao et al., 2011). The mechanism of inhibition against virus for carrageenan in particular was demonstrated, suggestion that carrageenan acts initially by preventing the binding or entry of virions into cells (Buck et al., 2006; Grassauer et al., 2008). Additionally, carrageenan and alginate have been exploited as pharmacological agents or biomaterials for cell therapy and tissue engineering (Senni et al., 2011).

Before describing the regulatory status of using seaweed polysaccharides in both food and health products the favourable properties of carrageenan and alginate, will be briefly addressed.

### 1.2.1.1 Carrageenan

Carrageenan is a generic term for a number of polysaccharides with repeating galactose units along with different sulphate groups and anhydro-bridges (Figure 1.2), which are combined alternately by α-(1,3) and β-(1,4) glycosidic bonds (Imeson, 2009). These sulphated polysaccharides are derived from a certain species of "red" seaweeds (*Rhodophyceaea*) and classified into various types such as kappa (κ), lambda (λ), iota (ι), Mu (μ), Nu (ν) and Theta (θ). These types of carrageenan are found in the particular types of seaweed, for instant kappa and lambda were extracted from *Gigartina radula* and *Chondrus crispus* whilst *Eucheuma denticulatum* (*spinosum*) and *Kappaphycus alvarezi* (*cottonii*) are mainly provided iota and kappa, respectively as shown in Figure 1.3 (Campo et al., 2009).

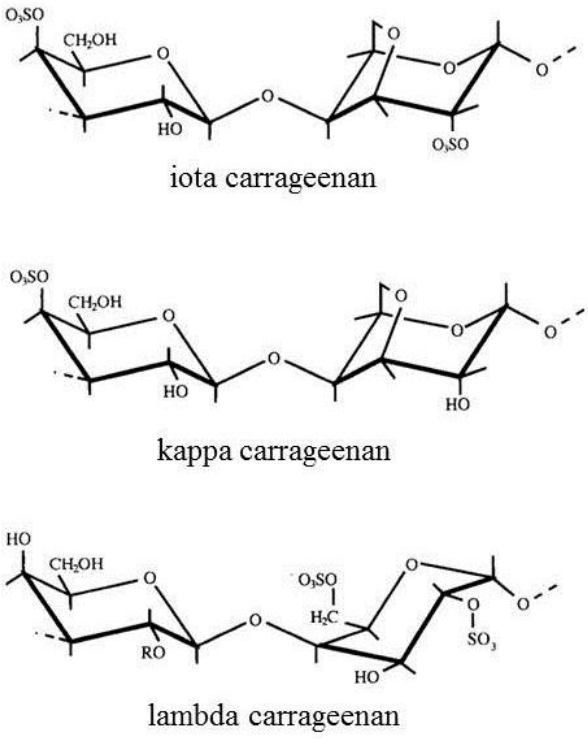


**Figure 1.2:** Chemical structure of iota (ι), kappa (κ) and lambda (λ) commercial carrageenans. Adapted from Perez et al., (1996).

Variation in the chemical structures of the carrageenan types is achieved by different content of 3,6-anhydrogalactose and ester sulphate groups, which provides unique characteristics for each type, including gel strength, viscosity, temperature stability, synergism and solubility. A greater number of sulphate groups cause the carrageenan molecule to be more water soluble, whereas anhydro-bridges produce a hydrophobic behaviour (Tombs and Harding, 1998; Hoefler, 2001).

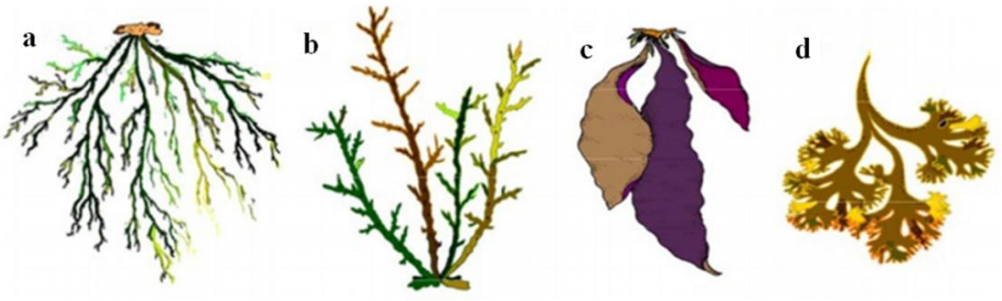


**Figure 1.3:** A source of carrageenan from different type of seaweeds: (a) *Eucheuma denticulatum* (spinosum) – iota carrageenan, (b) *Kappaphycus alvarezi* (cottonii) – kappa carrageenan, (c) *Gigartina radula* and (d) *Chondrus crispus* kappa/lambda carrageenan. Adapted from Prajapati *et al.* (2014).

Seaweed sulphated polysacchardies are utilized in several applications for food, oil recovery, pharmaceutical and healthcare industries as either gelling agents, natural thickeners or formulation stabilizers (Bonferoni et al., 1994 and Therkelsen, 1995; Iglauer et al., 2011; Zhou et al., 2004; Farias et al., 2000; Carlucci et al., 1999). The most soluble carrageenan is lambda with three sulphate groups per disaccharide repeat and as it contains no 3,6 anhydrogalactose residues it cannot form gels. The high viscosities of its solutions and its inability to form gels have made lambda carrageenan a

popular thickening agent, whereas kappa and iota are known as gelling agents due to their formation of thermoreversible gels in aqueous solution (Therkelsen, 1995; Bonferoni et al., 1994).

### 1.2.1.2 Alginate

Alginate is a generic term used for the salts of alginic acid such as sodium, potassium, calcium, and propylene glycol alginates. They have a long history, indeed were first described by the English chemist Edward Stanford in the 1880s. Their commercial production started in 1929 in California (Tombs and Harding, 1998).

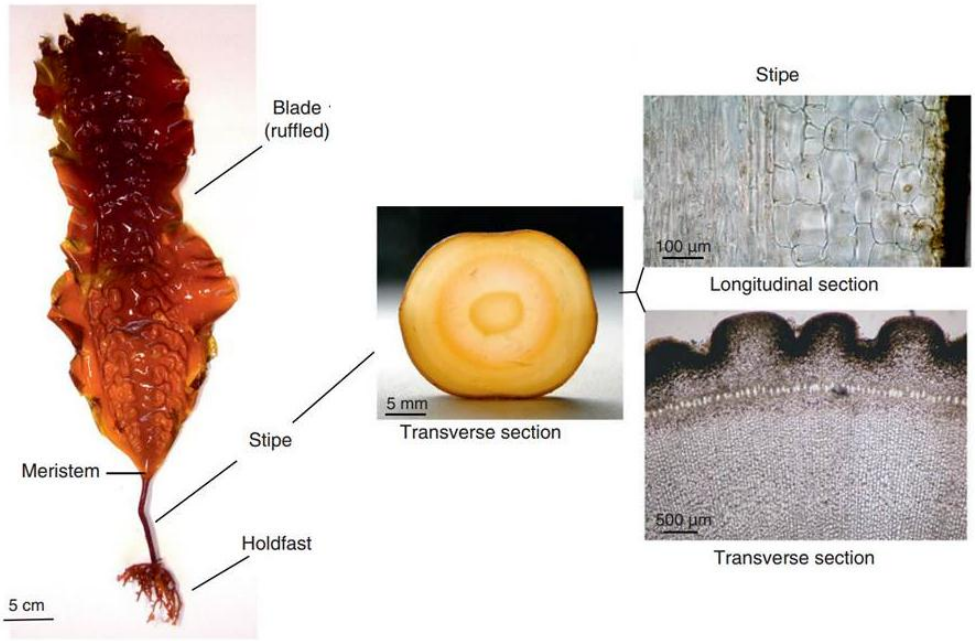


**Figure 1.4:** Thallus, cell types and tissues of *Laminaria saccharina* an example of alginate source. Adapted from Charrier *et al.(*2012).

Alginate is present in the cell walls of all brown seaweeds, where it is concentrated in the intracellular space, in the form of insoluble mixed salts with high amounts of calcium and lesser amounts of magnesium, sodium and potassium (Figure 1.4). *Macrocystis pyrifera*, *Laminaria* and *Ascophyllum nodosum* are the main sources of alginate (Tombs and Harding, 1998; Venugopal, 2011). Alginate is a linear anionic polysaccharide composed of (1,4) linked β-D-mannuronic (M) and α-L-gluronic acids (G), and arranged in homopolymeric and heteropolymeric sequences of MM or GG and MG blocks (Figure 1.5).

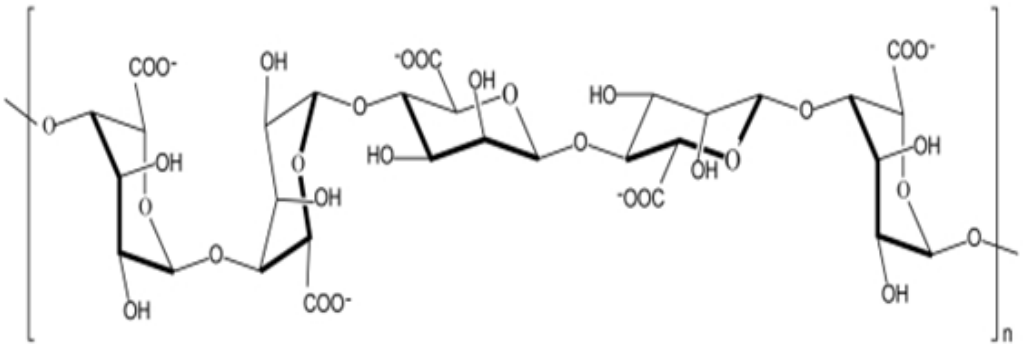


**Figure 1.5:** Chemical structure of alginate. Adapted from Tombs and Harding (1998).

The diversity of the M and G residues depend on the biological source and state of plant maturation (Haug et al., 1967; King, 1983). The main properties of alginate are forming gels with calcium ions and the ability to retain significant amount of water, which has led to extensive use in both the food and pharmaceutical industries (Pongjanyakul and Puttipipatkhachorn, 2007). The zones rich in GG block play an important role in the formation of these gels. The alginate physiological and rheological properties as well as their

application for example in stabilizing, thickening and gelling, would be affected through the variety in the arrangement of blocks along the chain and also the total uronic acid composition (M and G residues ratio) (Tønnesen and Karlsen, 2002).

#### 1.2.1.3 Safety and Regulation of Seaweeds

Consumption of seaweeds and their components must satisfy certain safety regulations. In fact, all edible seaweeds have a high guarantee of food safety; since the maximum permitted levels of toxic minerals (lead, cadmium, tin, mercury, mineral arsenic and iodine) have been clearly defined. Moreover, the maximum allowed levels of bacteria have been defined from the dried seaweed only (Mabeau and Fleurence, 1993; Holdt and Kraan, 2011). France (in 1990) was the first European country to establish specific regulations concerning the use of seaweeds for human consumption as vegetables or condiments. The number of species authorised are thirteen, which are obtained from macroalgae and microalgae, and reported in Table 1.3 (Mabeau and Fleurence, 1993; Vaugelade et al., 2000; Burtin, 2003; Venugopal, 2009). In several European countries (for example Ireland, Denmark and The Netherlands) seaweed uses are regulated by general food regulations, whereas in other countries (e.g. Greece) seaweeds are not considered as food. Therefore, in the European Union seaweed species are legally considered as food only for those that have been available in the market as food or food ingredients, and have been consumed to significant degree before May 15 1997 (Holdt and Kraan, 2011). On the other hand the Food and Drug Administration (FDA) has allowed the

use of seaweeds as condiments in the United States. Thus, algal products consumed have to be within the following upper-level limits on the dry-weight basis: 45% of ash; 3 ppm of inorganic arsenic; 40 ppm of heavy metals; 10 ppm of lead; 5000 ppm of iodine (Mabeau and Fleurence, 1993).

**Table 1.3**: Summary of seaweed authorised in France for human consumption. Adapted from Burtin (2003).

| Phyllum | Name |
|---|---|
| Red seaweeds | *Porphyra umbilicalis* |
| | *Palmaria palmate* |
| | *Cracilaria verrucosa* |
| | *Chondrus crispus* |
| Brown seaweeds | *Ascophyllum nodosum* |
| | *Fucus vesiculosus* |
| | *Fucus serratus* |
| | *Himanthalia elongate* |
| | *Undaria pinnatifida* |
| Green seaweeds | *Ulva spp.* |
| | *Enteromorpha spp.* |
| Microalgae | *Spirulina sp.* |
| | *Odontella aurita* |

## 1.2.2 Polysaccharides from Shellfish

Crustaceans and molluscs are species of the shellfish family including crabs, shrimps, lobsters, squids and cuttlefish, which are utilized as food or human consumption. Marine crustaceans and molluscs in 2012 were harvested to a level of about 21.6 million tonnes according to *The State of World Fisheries and Aquaculture*, as published by the Food and Agriculture Organization (FAO, 2014). There is a massive amount of marine waste generated from the processing of seafood consisting of heads, exoskeleton, cephalothorax and

carapace of crab, shrimp and lobster. Recent estimates suggest that processing wastes from crab can be high as 51% based on wet weight, whereas krill and shrimp results in 40% shell waste (Venugopal, 2011). The high demand for processed seafood has produced a huge proportion of marine waste which is considered to be an environmental problem. Utilisation of seafood waste has become the best solution for the environmental pollution issue, since it has long been known that these wastes are rich sources of biological compounds and minerals providing additional economic benefits for the marine industry (De Holanda and Netto, 2006; Gortari and Hours, 2013).

Crustaceans and molluscs wastes are rich sources of three major compounds extensively used in the marine industry namely the polysaccharide chitin, protein and carotenoid. Shrimp, krill and crab wastes contain about 25% of polysaccharide chitin on a dry weight basis, whereas the high values from the squid pen roughly 40%. On average the head waste comprises a lower level of chitin rather than the shell. For example shrimp head was reported to contain 17% chitin, 41% protein, and 148 μg carotene per gram on a weight basis in Table 1.4 (Heu et al., 2003; Synowiecki and Al-Khateeb, 2003; Sagheer et al., 2009). The most abundant sources of chitin are *Pandalus borealis*, *Crangon crangon* and *Penaeus monodon* from the shrimp species, and *Callinectes sapidus* and *Chionoecetes opilio* from crabs (Rødde et al., 2008; Beaulieu et al., 2009). Thus, the polysaccharide chitin is known as the second most commonly used natural biopolymer in food and medicine applications. Generally chitin and its derivative chitosan exhibit several properties such as biocompatibility, biodegradability, nontoxic, fungistatic, spermicidal, antitumor, anticholesteremic, wound-healing, antimicrobial, antioxidative, and

hemostatic qualities (Aranaz et al., 2009; Zhang et al., 2010). These polysaccharides have been extensively utilized for various applications in areas such as biotechnology, cosmetics, water treatment, the paper industry, textile products, biomedical products and food processing (Hirano, 1996; Ravi Kumar, 2000; Jayakumar et al., 2010; Cheba, 2011).

**Table 1.4**: Sources of chitin and the percentage content obtained from crustacean and molluscan organisms. Adapted from Venugopal (2011).

| Organism | Chitin Content (%) |
|---|---|
| Shrimp head | 11 |
| Shrimp shell | 27 |
| Commercial shrimp waste | 12-18 |
| Atlantic crab | 26.6 |
| Blue crab | 14 |
| Crangan (shrimp) | 69 |
| Alaska shrimp | 28 |
| Clam shell | 6.0 |
| Squid, skeleton pen | 41 |
| Krill | 24 |

### 1.2.2.1 Chitin and its Derivative Chitosan

Chitin is the most abundant amino polysaccharide, and can be extracted from the exoskeletons of crustaceans or the cell walls of fungi. The first identification of chitin was in mushrooms in 1811 by Henri Braconnot in France, whilst it was isolated from insects and named chitin in the 1830s (Venugopal, 2009). Marine organisms including crab, shrimp and prawn are the main sources of commercially available chitin; however, it is also found in terrestrial organisms such as insects and fungi. The structure of the chitin polymer consists of 2-acetamido-2-deoxy-β-D-glucose through a β-(1,4)

linkage (Figure 1.6). In addition three different polymorphic forms of chitin have been found namely α, β and γ: the structure of α and β only differ in the arrangement of the stacking of chains which are alternately antiparallel in α-chain and parallel in β-chain. However the complete picture of γ-chain structure has not yet been obtained, but it has been proposed as an arrangement of two parallel and one antiparallel sheet (Jang et al., 2004; Rinaudo, 2006; Sagheer et al., 2009).

In general chitin is extracted using three steps; first a demineralization (acid treatment) to dissolve calcium carbonate followed by deproteinization to solubilize proteins, then eventually a decolorization step to remove leftover pigments yielding a colourless material. For use in products chitin then has to be classified in terms of purity and colour especially for biomedical application due to the effect of protein and pigment residuals (Tombs and Harding, 1998; Synowiecki and Al-Khateeb, 2003; Rinaudo, 2006). Under alkaline condition partial deacetylation of chitin occurs to generate, the most important derivative in terms of applications chitosan.

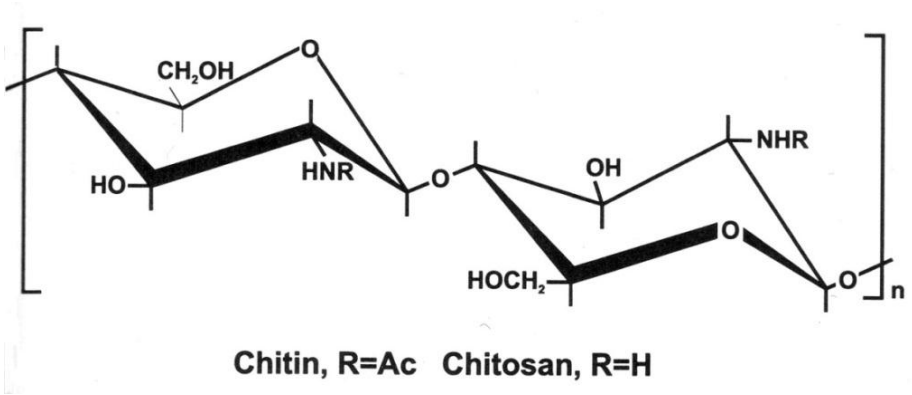


**Figure 1.6:** Chemical structure of chitosan. Adapted from Tombs and Harding, (1998). Ac=acetyl.

Chitosan is one of the most important copolymeric polysaccharide derivatives from chitin. The basic structure of chitosan is similar to cellulose – consists of 2-amino-2-deoxy-β-D-glucopyranose units linked through a β-(1,4) linkage, with a high degree of N-acetylation – except the acetylamino group is replaced by a hydroxyl group at the C-2 position (Tombs and Harding, 1998). It is much easier to protonate the primary amine groups in an acidic medium, providing a positively charged polysaccharide with a high charge density. This characteristic is important, as it makes chitosan water soluble and a bioadhesive, facilitating the binding of negatively charge macromolecules (Hejazi and Amiji, 2003). The variation of chitosans in solution depends on three degrees of freedom, namely their molecular weight, degree of acetylation (DA) and also the distribution of acetyl group along the main chain (Venugopal, 2011).

The natural chitin and its derivative chitosan have many unique properties including biocompatibility, biodegradability, hemocompatiblity, antibacterial activity, nontoxic, antitumor, fungistatic and anticholesteremic (Rinaudo, 2006). As a consequence of these properties they have received a considerable deal of interest for utilisation (Table 1.5) in agriculture, biotechnology (Venugopal, 2009), and also in the food (No et al., 2007), cosmetic (Ravi Kumar, 2000), and pharmaceutical industries (Morris et al., 2010).

In particular chitosan offers the greatest promise for pharmaceutical and biomedical applications. For instance, specific complexes of chitosan with an oppositely charged polyelectrolyte, yield three-dimensional networks or "hydrogels" and these have potential for controlled drug release from drug

delivery systems as well as protecting the drug from degradation in the gastrointestinal tract (Il'ina and Varlamov, 2005; Jayakumar et al., 2010).

**Table 1.5**: Summary the principal applications of chitin and its derivative chitosan. Adapted from Rinaudo (2006).

| Fields | Examples |
|---|---|
| Agriculture | Work as defence system for plants,<br>Improve the growth of plants<br>Use as coating to protect seeds<br>Control the release time of fertilizers and nutrients into the soil |
| Water and waste treatment | Use as clarifying agent for water such as Flocculant (drinking water, pools)<br>Used to remove metal ions<br>Biodegradable polymer (known as Ecological polymer) to eliminate synthetic polymers<br>Reduce odors |
| Food and beverages | Dietary fiber (Not digestible by human)<br>Help to reduce cholesterol by binding to lipids<br>Preservative materials<br>Utilise as the thickener and stabilizer for sauces<br>For fruit used as protective agent, fungistatic, antibacterial coating |
| Cosmetics and toiletries | For the skin used to maintain moisture, treat acne and tone.<br>In the case of the hair applied as improvement of suppleness and reducing static electricity<br>Toothpaste and chewing gum for the oral use |
| Biopharmaceutics | Immunologic, antitumoral<br>Hemostatic and anticoagulant<br>Healing, bacteriostatic |

### 1.2.2.2 Safety and Regulation of Chitin and Chitosan

Generally chitin, chitosan and their derivatives are described as safe, since they are naturally extracted from the living organisms. The human gastrointestinal

tract is not able to digest or absorb chitin and chitosan similar to several natural origin food additives of high molecular weight polymers such as cellulose, carrageenan and guar gum (Venugopal, 2009). The Food and Drug Administration (FDA) in the United States in 1983 clearly defined the status of chitin and chitosan to be "Generally Recognized as Safe (GRAS)". Following this, commercial chitosan has been approved to be used in waste water treatment up to a maximum level of 10 mg $L^{-1}$ by the Environmental Protection Agency in the U.S. (Shepherd et al., 1997). Additionally, chitin and its derivatives chitosan have been approved as functional food ingredients in Japan 1992. Chitin and chitosans provided more features in healthcare for instance enhancement of immunity, prevention of illness and recovery from illness (Shahidi and Abuzaytoun, 2005).

## 1.3 MARINE BASED DIETARY FIBRE

Although over the past two hundred years dietary fibre has been known as a substantial part of the human diet which provides many health benefits, however up to now there has been a gradual reduction in overall intake by consumers. A lack of dietary fibre intake is significantly associated with being overweight, diabetes, heart disease and gastrointestinal disorders (Smith et al., 2014). Dietary fibre is a term for plant material that is resistant to digestion and absorption in the human small intestine, whilst they can be fermented partially or even completely in the large intestine. In particular dietary fibre substances have been classified as non-digestible carbohydrates or "NDC's". Along with lignin in plants, NDC's have been shown to have beneficial physiological

effects in humans (Champ et al., 2003; Slavin, 2005). Nowadays, the definition of dietary fibre has become wider to cover fibres of animal origin such as chitosans, and also modified or synthetic non-digestible carbohydrate polymers for instance polydextrose and fructo-oligosaccharides (Borderías, Sánchez-Alonso and Pérez-Mateos, 2005).

Simplistically dietary fibre is classified into two types, soluble and insoluble based on solution form when mixed with water. Insoluble dietary fibres include substances such as cellulose, manna and xylan, while carrageenan, galactomannan, pectins and agars are considered as soluble dietary fibre or "SDF". The differences observed between the soluble and insoluble dietary fibres are referred to their technological functionality and physiological effects (Jiménez-Escrig and Sánchez-Muniz, 2000). For instance viscous soluble fibres can be distinguished based on the ability of reduce the hypocholesterolemic and hypoglycemic effects, whereas insoluble fibres are associated with increase stool weight and decreased intestinal transit (Abdul-Hamid and Luan, 2000; Elleuch et al., 2011).

In general the consumption of dietary fibre has been shown to improve human health by increasing faecal bulk, decreasing digestive tract transit time, regulating activity of the colonic microflora, absorbing toxins, affecting appetite and trapping absorption of fats, sugars, minerals and bile acids (Blackwood et al., 2000). These physiological properties are associated with lowering the risk factors for several diseases such as coronary heart disease (CHD), stroke, hypertension, diabetes, obesity, and dyslipidemia. For example high levels of dietary fibre intake assist people with obesity and/or diabetes by reducing absorption of food containing high-fat as well as reducing the amount

of starch digestion and glucose uptake (Champ et al., 2003; Anderson et al., 2009; Venugopal, 2009). In addition, excess of bile acids are excreted in the digestive system as result of its interaction with dietary fibre components particularly β-glucans (Asp, 2004). However, the physiological effects of dietary fibre depend on a complex mixture of structure, chemical and physical properties. In the case of dietary fibre structure, the fermentation of polysaccharides chains is likely to be affected by their composition and degree of stiffness. The physicochemical properties consist of water-holding capacity, faecal bulking capacity, fermentation, viscosity, and binding capacity, for instance high viscosity is associated with reducing the rate of glucose and lipid absorbance (Jiménez-Escrig and Sánchez-Muniz, 2000; Blackwood et al., 2000).

Since seaweed is comprised of massive amounts of soluble polysaccharides – including SDFs, they form an important source of dietary fibre. A significant number of dietary fibres are obtained from seaweed (mainly agar, carrageenan, alginate etc.), which have been used as part of the human diet for at least three thousand years (Lahaye, 1991; Tombs and Harding, 1998). To illustrate this, the market for seaweeds – an important source of dietary fibre – have been growing continuously 1-3 % per year linked to their high consumption in food and pharmaceutical industries (Bixler and Porse, 2011). The impact of seaweed on human healthcare (e.g. obesity and diabetes) is referred to its physicochemical properties in the alimentary tract such as dispersibility in water, viscosity, binding ability, absorptive capacity and fermentability (Kendall et al., 2010). For example, the dispersibility in water for seaweed polysaccharides cause retention of cholesterol and inhibit lipid absorbance in

the gut tract, which leads to a decrease in serum cholesterol levels (Jiménez-Escrig and Sánchez-Muniz, 2000). Further, scientists have recently developed an anti-obesity diet based on seaweed or seaweed hydrocolloids for overweight people (see, Venugopal, 2009).

## 1.4 HEALTH BENEFITS OF MARINE POLYSACCHARIDES

The marine environment offers great biodiversity, of which marine polysaccharides form one of the most important group of organic compounds that can be extracted from this environment particularly marine plant or animal organisms. Marine polysaccharides are being extensively used for health benefits, including control of hyperlipidaemia, thrombosis, tumour and obesity among others. Marine polysaccharides are biodegradable, biocompatible, water soluble, non-toxic and have a highl swelling ability. These properties make them more suited for functional food, nutraceuticals, cosmeceuticals, pharmaceutical and biomedical applications (Figure1.7) (MacArtain et al., 2007; Wijesekara et al., 2011; Wijesinghe and Jeon, 2012). During the last decade, great attention has been paid to the biomedical applications such as controlled drug delivery, tissue regeneration, wound dressing, dental implants, blood plasma expanders, vaccines and gene delivery (Venugopal, 2011). For example, in the delivery system marine polysaccharides (e.g. alginate or chitosan) have been utilized for microencapsulation for oral delivery of proteins or peptides. Consequently, these polysaccharides have potential for controlling the release rate of protein or peptide as well as protecting them

from denaturation and degradation in the gastrointestinal tract (Laurienzo, 2010; Borgogna et al., 2011). The real potential of using marine polysaccharides for therapeutic application (e.g. natural product drug discovery) has attracted a special interest, due to differences in the structures of their bioactive components resulting in various biological activities (Senni et al., 2011; Wijesekara et al., 2011).

Bioactive compounds are active macromolecules occurring in nature, and they also a part of the food chain referred to as "nutraceuticals" that have a potentially positive effect on human health (Biesalski et al., 2009). The earliest biologically active substance extracted from a marine environment was holothurin which exhibited some antitumor activities in mice. Since then, extraction of bioactive compounds from marine resources has received a great deal of interest to yield drugs and natural products (Nigrelli et al., 1966; Laurienzo, 2010). Marine organisms provide a wide range of natural products including polyunsaturated fatty acids, polysaccharides, proteins, essential minerals and vitamins. Among marine organism contents, marine polysaccharides are the best sources of bioactive compounds used in biomedical applications (Kim and Wijesekara, 2010). Therefore, anticoagulant, antiviral, antioxidative, anticancer, and immunomodulation are the biological activities provided by marine polysaccharides which depend on molecular weight, chemical structure and conformation properties (Ye et al., 2008; Ahmed et al., 2014).

The carrageenan polysaccharides from red algae have been reported to have good anticoagulant activity arising from their sulphated groups and large molecular weights (Shanmugam and Mody, 2000). Carrageenan offers

antioxidant activity that also depends on the amount of sulphate content (Rocha de Souza et al., 2007). In addition, earlier studies *in vitro* have suggested that carrageenan may exhibit antiviral activity particularly inhibiting the replication of herpes and hepatitis A viruses (Girond et al., 1991; Marchetti et al., 1995; Carlucci et al., 1999). The effect of carrageenan as an immunomodulator has been linked to their ability to act as an anti-inflammatory agent by removing pathogens and cell debris after inflammation. However, alginate extracted from brown seaweed has been reported to have antilipidemic activity because of its capability to reduce the total cholesterol and triglyceride content along with increasing the levels of high-density lipoprotein (Ahmed et al., 2014). The biological activity properties of alginate (e.g. nontoxic, biocompatible and biodegradable) generally have provided beneficial effects in biomedical applications such as controlled drug delivery (Laurienzo, 2010; Hickey, 2012).

Marine polysaccharides extracted from shellfish particularly chitosan and its derivatives also contribute in several medical and health applications. Chitosan and its derivatives have attracted massive attention from the biomedical, food and chemical industries due to their biological activities such as, antitumor, anticholesteremic, antimicrobial, antioxidative, and drug delivery properties (Aranaz et al., 2009; Zhang, et al., 2010; Xia et al., 2011). The hypocholesterolemic effect of chitosan has been observed to reduce total cholesterol levels and triacylglycerol without side effects. Moreover, one of the most important properties of chitosan and its derivatives are antimicrobial activity that have been claimed to act against bacteria, yeasts and fungi. Chitosan has been claimed to inhibit the growth of microorganisms by

damaging the barrier properties of the microbial cell membrane (Helander et al., 2001; Sagoo et al., 2002).

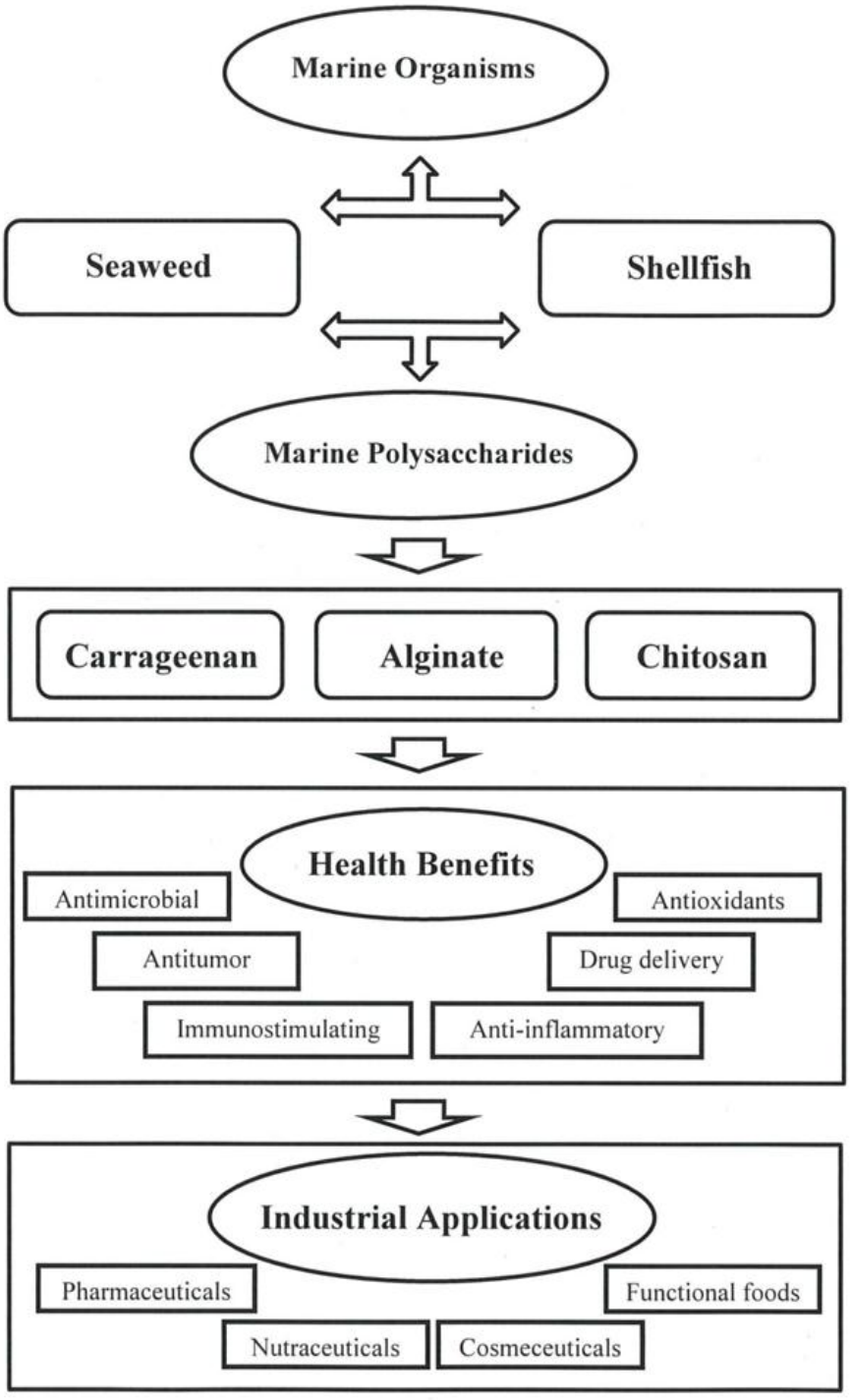


**Figure 1.7**: The major classes of marine polysaccharides with health benefits and potential industrial applications. Adapted from Prajapati *et al.* (2014).

Additionally chitosan and its derivatives have been claimed to have the ability to be used as drug carriers in cancer chemotherapy. For example conjugates of N-succinyl-chitosan with one of the anticancer agent Mitomycin C have been reported to improve the efficacy of the anticancer effect along with lowering the side effects because of their predominant distribution into cancer tissue and slowing the release of drugs (Kato et al., 2005; Xia et al., 2011).

## 1.5 INTERACTION WITH OTHER BIOPOLYMERS

Marine polysaccharides exhibit many molecular interactions with (1) other biopolymers such as proteins and glycoproteins, (2) other polysaccharides, (3) smaller molecules such as water and other ionic solvents. Knowledge and understanding of the behaviour of these interactions is required in order to develop new materials for food, cosmetic and medical applications. Thus, the interactions involving marine polysaccharides might also extend to include weak reversible interactions to very strong and irreversible interaction complexes (Harding, 2013). It has been reported that seaweed polysaccharides (e.g. alginate) show favourable interaction with proteins (e.g. bovine serum albumin) leading to complex formation because of attractive forces (Kelly et al., 1994). A more spectacular example of the formation of large irreversible micron size particles is the interaction of polycationic chitosan with a mucin glycoprotein. Chitosan has thus been considered as a potential mucoadhesive for pharmaceutical application, due to its potential ability of increasing the residence time thus enhancing the absorption rate of the drug (Harding, 2003, 2006).

The second important group of interactions involves electrostatic and synergistic interactions of marine polysaccharides with other polysaccharides. For example, carrageenan can interact with an oppositely charged polyelectrolyte (e.g. chitosan) forming hydrogels that have potential for controlled drug release from drug delivery systems (Il'ina and Varlamov, 2005). Moreover, synergistic interactions have been observed for alginate with a mixture of konjac glucomannan and xanthan, which are ionic strength dependent, offering beneficial properties for therapeutic purposes (Abdelhameed et al., 2010; Harding et al., 2011a; Harding et al., 2012). However, a better understanding of these interactions using advances in hydrodynamic techniques might prove useful.

## 1.6 HYDRODYNAMIC METHODS

Characterisation of marine polysaccharides is by no means easy due to their polydispersity, variety of conformation and different polyelectrolyte behaviour in solution. Although these features can make interpretation of solution data complicated, it nonetheless provides a fascinating challenge to biophysical chemist scientists and has encouraged them to develop improved and new tools (Harding, 2005). The new advances of modern hydrodynamic methodology have provided such progress for investigating the properties of polysaccharides (e. g. molar mass, polydispersities, conformation, and their interactions) in solution. The recent advances in analytical ultracentrifugation (AUC) - specifically sedimentation velocity and sedimentation equilibrium - have impacted on the determination of the physical homogeneity, conformation and

flexibility of polysaccharides materials without the need for separation columns or membranes. Furthermore, AUC has enhanced estimation of the molar mass (molecular weight) and molar mass distribution using both sedimentation equilibrium (Schuck et al., 2014) or velocity (Harding et al., 2011b), and also size exclusion chromatography coupled to multi angle light scattering (SEC-MALS). Moreover, the ability of combining a viscometer to SEC-MALS can give information not only on intrinsic viscosity but also the conformation (Wyatt, 1993; 2013). Therefore, the combination of hydrodynamic methods (e.g. AUC based on sedimentation velocity and equilibrium, SEC-MALS and viscometry) has enabled significant advances in terms of characterisation of the shape and flexibility for linear polymers in solution using a combination of different approaches.

## 1.7 THE AIM OF THIS INVESTIGATION

The aim of this study is firstly to investigate marine polysaccharides (e.g. carrageenan and chitosan) in solution for assessment of their structural integrity, size and conformation in terms of sedimentation coefficient, molecular weight, distribution of molecular weight and intrinsic viscosity. Sedimentation velocity along with sedimentation equilibrium in the AUC were used with SEC-MALS and viscometry in order to provide those fundamental biophysical information, which will support any strategy planned to investigate whether interaction occurs between one of these marine polysaccharides and other biopolymers including glycoproteins (e.g. mucin) and other polysaccharides (e.g. konjac glucomannan and xanthan). Thus, understanding

the behaviour of these marine polysaccharides alone and in mixture with other biopolymers can help increase our knowledge to develop better healthcare and therapies for common diseases.

After a brief description of the hydrodynamic methods (*Chapter 2*) used for the series of studies described in this thesis we will sequentially highlight the determination of hydrodynamic properties for marine polysaccharides and their interaction with other biopolymers along the following lines:

- Molecular conformation study of lambda carrageenan in aqueous solution (*Chapter 3*)
- Hydrodynamic investigation of the oligomeric state of the main classes of carrageenan (kappa, iota and lambda) in solution (*Chapter 4*)
- Hydrodynamic characterization of chitosan and its interaction with two polyanions: DNA and xanthan (*Chapter 5*)
- Hydrodynamic studies on a mixture of non-digestible carbohydrates (*Chapter 6*)
- Application of new hydrodynamic methods to study the mucin and its interaction with obter biopolymers in solution (*Chapter 7*)

# CHAPTER 2

# METHODS FOR CHARACTERISING THE BIOPHYSICAL PROPERTIES OF MACROMOLECULES IN SOLUTION

This chapter describes the principles and theory of the methodologies employed for characterising the macromolecular solutions used in this study, particularly polysaccharides and glycoprotein "mucin". These methods would establish the basis of determining the biophysical properties of these molecules, including molecular weight, sedimentation coefficient, intrinsic viscosity, and conformational flexibility.

## 2.1 INTRODUCTION

Knowledge of the biophysical properties of macromolecules in dilute and concentrated solutions is crucial for understanding their function and structure on a macroscopic scale in nature. A wide range of analytical methods have been developed for the characterisation of macromolecules – such as proteins and polysaccharides – under solution conditions (Harding, 2013). In particular polysaccharides along with glycoproteins – for example mucin – show a different challenge to proteins in terms of estimation of their biophysical properties. As is well known polysaccharides are by no means easy to characterise, not only due to their polydispersity in nature, but also because of their great variety of conformation and – for many – high charge in solution

(Harding, 2005). Taking advantage of the new advances of modern hydrodynamic methodology provide us powerful techniques for investigating the properties of polysaccharides (e. g. molar mass, conformation) in solution. Such advances include enhanced estimation of the molar mass (molecular weight) and molar mass distribution using analytical ultracentrifugation based on sedimentation equilibrium (Schuck et al., 2014) or velocity (Harding et al., 2011), and size exclusion chromatography coupled to multi angle light scattering (Wyatt, 1993; 2013). Therefore, a combination of hydrodynamic methods has significant advantages in terms of characterisation the shape and flexibility of linear polymers in solution. Flexibility is also represented quantitatively by the persistence length, $L_p$ and the mass per unit length, $M_L$ and can be estimated using different approaches for example Bushin-Bohdanecky, Yamakawa-Fujii and Multi-HYDFIT.

In this study all samples (mainly polysaccharides and glycoproteins) have been characterised using several techniques, based on hydrodynamic and thermodynamic analytical methods. The analytical ultracentrifuge, size exclusion chromatography coupled to multi angle light scattering and viscometry were the main techniques used to evaluation the hydrodynamic properties such as molar mass, sedimentation coefficient, distribution of molar mass and intrinsic viscosity, whilst the thermally induced transitions – referred to conformation transitions – was examined using the micro-differential scanning calorimetry (see *chapter 4*). In this chapter, we will outline the principles and properties of these techniques, as has already been mentioned.

# 2.2 ANALYTCAL ULTRACENTRFUGATION (AUC)

Analytical ultracentrifugation (AUC) is a very powerful separation technique employed for characterising the hydrodynamic and thermodynamic properties of biological and non-biological macromolecules in a wide range of solvents and concentrations (Cole et al., 2008). AUC was developed by Svedberg and co-workers in the 1920s. Later on, Edward Pickels redesigned it into a commercial instrument (see, e.g. Scott and Schuck, 2005). The boom period for this technique was between 1950 and 1970, with the focus in obtaining the molecular weight and sedimentation coefficient parameters. It declined with the advent of the much simpler techniques (e.g. electrophoresis and chromatographic) that became more popular for estimation of the molecular weight for macromolecules. However, such techniques have limitations to determine the molecular weight in case of polydisperse and interacting systems due to calibration requirements and reliance on a series of assumptions that are frequently invalid (Ralston, 1993). In the 1980's and 1990's AUC has re-emerged as a popular method for analysing the properties of macromolecules in solution, thanks to advancement in the new instrumentation with automatic computer on-line data capture and simple computer analysis systems (Harding, 2005).

The free-solution method of AUC has great advantages compared to other methods as it has an intrinsic separation ability (unlike light scattering) and without the need for columns, membrane materials, other separation media or immobilisation materials (unlike electrophoresis and chromatography), which might otherwise disrupt or interfere with interaction phenomena because of

anomalous binding. Conceptually, AUC involves the application of a centrifugal force with a detection system observing the distribution of macromolecules in real time (Scott and Schuck, 2005). Thus, absolute molar mass (weight, number and z-average) and molar mass distribution can be obtained using sedimentation equilibrium, and used alongside other methods such as the sister technique of sedimentation velocity in the analytical ultracentrifuge – which gives a direct record of sample heterogeneity – it is a very powerful probe (Harding, 2005; Harding, 2012). The next section will consider the most important components of AUC, followed by a short description of the two experimental modes – sedimentation velocity and sedimentation equilibrium.

### 2.2.1 Ultracentrifuge Instrumentation

The renaissance of analytical ultracentrifugation has been induced by the modern Optima XL-A and XL-I series (Beckman-Coulter instrument) following their release in 1990 and 1996, respectively (Schuster and Toedt, 1996). These instruments provided two different detection (optics) systems, UV/Vis absorbance and Rayleigh interference with real-time observation, which allowed rapid data acquisition and analysis for macromolecules across a wide range of concentrations (Furst, 1997). An analytical ultracentrifuge is made up of a number of components, and its most important components will be briefly described.

#### 2.2.1.1 Rotor

Nowadays the analytical rotors are constructed with either four or eight holes from one piece of titanium. Usually one of the holes is used for the counterbalance, which provides the radial calibration at given centrifugal speed. Commercially available rotors for eight and four holes are namely the Beckman-Coulter An-50Ti and An-60Ti, respectively. The remaining holes of the rotors therefore, are employed for sample cells, which in case of eight holes rotors (if multi-channel cells are used) can be used for different measurements under several conditions. The maximum speeds allowed for the 8-hole and 4-hole analytical rotors are in the range of 50 000 and 60 000 rpm, respectively.

#### 2.2.1.2 Cells

The ultracentrifuge cells are composed of a number of components designed to resist the extreme stresses that are often generated at high speed, without distortion or leaking. In addition, the cells should allow the passage of light through, to allow for samples to be examined. Figure 2.1 shows an example of a cell assembly for the typical analytical ultracentrifugation cell. There are many types of cell available based on the different type of centerpieces and windows, depending on the experiment. Generally the most common windows used are sapphire and quartz, while three types of centerpieces are available (mono-sector, double-sector and multi-channel) are made of aluminum, titanium, Kel-F (polychlorotriflouroethylene or PCTFE) or Teflon filled epon. The cells normally have double-sector shaped channels a designed that allows

the molecules to sediment without convective disturbances arising from the interaction with walls of the centerpieces. Another advantage of having two separate chambers over one is to allow the detection systems to measure the difference in signal between the sample and reference sectors (Ralston, 1993).

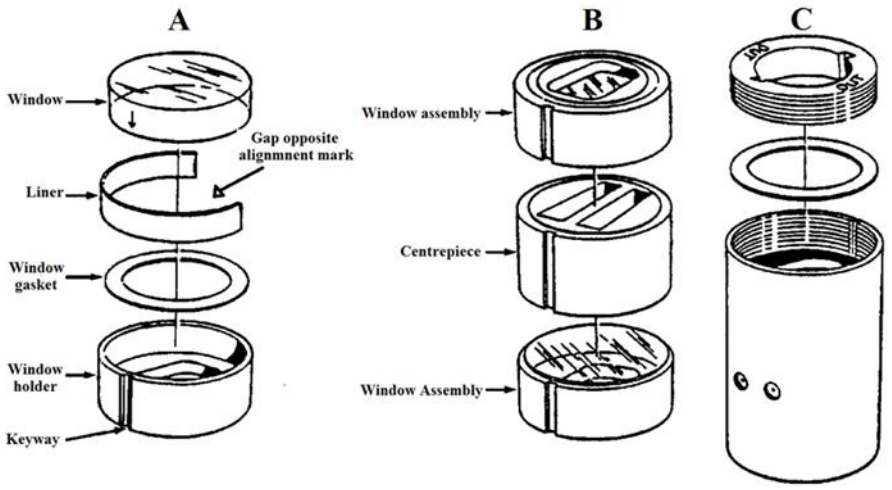


**Figure 2.1:** Schematic of cell assembly, where (A) window assembly components, (B) showing centerpiece and window assemblies, and (C) cell housing, screw ring and screw ring gaskets. Adapted from Ralston (1993).

However, a centerpiece is the heart of the cell between two windows, and each one of these is placed in a window holder including a gasket and a window liner. All these pieces are assembled together inside a metal housing, after which the cell has to be tightened using a torque wrench. In this study, a standard thickness for centerpieces of 12.0 mm is mostly used for both sedimentation velocity and equilibrium experiments, whereas 20.0 mm can be applied for some cases of sedimentation equilibrium experiments. Using such long path length centrepieces cells (20.0 mm) has allowed us to work at relatively low concentration (0.3 mg $mL^{-1}$), producing a greater signal to noise ratio (Harding, 2005).

### 2.2.1.3 Detection System

The data obtained essentially from the analytical ultracentrifugation experiment are the radial concentration distributions at given times. The passage of light yield by the optical detectors allows the measurement of the concentration distribution of the samples and its redistribution with time in the cell. There are three main detectors mostly used in modern analytical ultracentrifugation namely, interference optics, absorbance optics and fluorescence optics. The recent addition to Optima XL-A/I ultracentrifuges is fluorescence. This system is used for detecting trace quantities of materials, and is extremely sensitive for detecting concentrations as low as (10 ng $mL^{-1}$). It can also be applied for the mixture components and analysing the interaction, but samples has to be pre-labeled with an appropriate fluorescence label (Laue, 2004).

In absorbance optics, detection of the concentration in terms of absorbance utilizes the Lambert-Beer law ($A = \varepsilon . c . a$); where the signal of absorbance ($A$) is proportional to concentration ($c$) of the solute, and optical path length of the cell ($a$ = 1.2 cm for standard centerpieces), with the absorption coefficient ($\varepsilon$), being the constant of proportionality. The optics is applicable over a wavelength range from 190 to 800 nm (Ralston, 1993). The main disadvantage of the absorbance system is the relatively long time required to complete the measurement, which is usually not a problem for a sedimentation equilibrium experiment. However, in the case of sedimentation velocity longer duration of measurement may affect the amount of data collected particularly at high speed 60000 rpm (Mächtle and Börger, 2006; Cole et al., 2008). Therefore,

absorbance optics are mostly applicable to macromolecules that can absorb UV light.

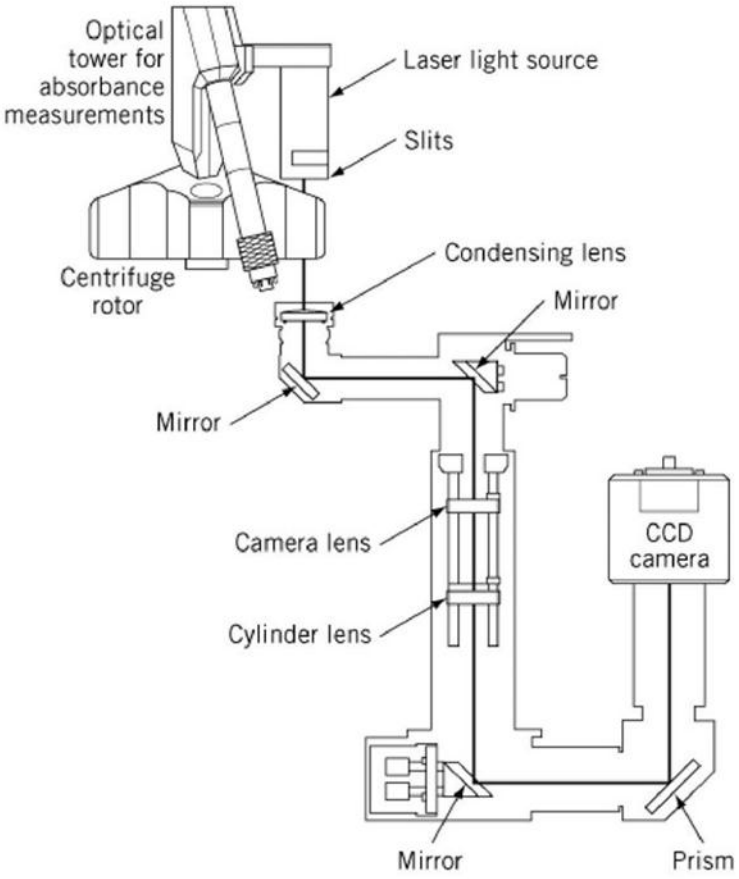


**Figure 2.2:** Interference optics detector of the Beckman XL-I ultracentrifuge. Adapted from Ralston (1993).

The interference optical system is designed on the principle of a Rayleigh interferometer, whose measurement depends on the different refractive index of solution to solvent. In these optics, the laser (wavelength 670 nm) on Optima XL-I ultracentrifuge is directed through the solution sector and reference solvent sector to create an interference pattern of parallel bright and dark fringes, and captured by a charge-coupled device (CCD) camera (Figure 2.2). The change of the sample concentration at the boundary region while it

sediments leads to the difference of the refractive index, which results in the displacement of the fringe pattern, obtained. In contrast to absorbance optics, this system recorded more scans with a higher frequency, making it particularly useful for the detection of fast moving large macromolecules (e.g. polysaccharides and glycoproteins). Further, this optical system can be used to monitor a wide range of macromolecules in different solvents; due to the ability of all macromolecular to change the refractive index of solvents and this can be recorded.

In general, the different optical systems can be combined yielding a system called multiple detections. For instance, combination of interference optics and absorbance optics can acquire useful information about the mixture, where absorbance optic used to detect the absorbing component, and interference optics monitored all components together. This method (also refer to co-sedimentation) is particularly useful for assaying the interaction, and previously successfully employed (see, e.g. Cölfen et al., 1996; Deacon et al., 1999).

### 2.2.2 Sedimentation Velocity

Sedimentation velocity, one of the basic types of experiment carried out by analytical ultracentrifugation provides a quantitative assessment for the heterogeneity of samples and also analysis of the purity and degree of aggregation of the native structure (Stafford III, 1992; Ralston, 1993). Sedimentation velocity experiments are performed with a Beckman Optima XL-I analytical ultracentrifugation at controlled speed and temperature, where

the change in solute distribution across the solution in a cell is measured as a function of time. The fact that sedimentation velocity experiments employ, relatively high speeds and a long solution column helps to maximise the resolution of the solution components (Harding, 2005).

The principle of sedimentation velocity will now be briefly described. Basically a macromolecular solute is affected by three forces when suspended of dissolved in a solvent on a rotor spinning at high speed. Under the influence of these forces, the macromolecules quickly accelerate and reach terminal velocity. Figure 2.3 shows an example of these phenomena (three forces) in an ultracentrifuge cell. Centrifugal force, $F_c$ is the first force experienced by the moleculer, which is depended on the molecule mass ($m$), the distance of the molecule from the axis of rotation ($r$) and the angular velocity ($\omega$). From Archimedes Principle the second is the buoyant force, $F_b$ which equal to the weight of the solution displaced. Finally, frictional force, $F_d$ will also be exerted on the macromolecule as result of movement the molecule through a viscous solution with the velocity ($v$). At terminal velocity the three forces come into balance:

$$F_c + F_b + F_d = 0 \tag{2.1}$$

where,$F_c = \omega^2 rm$, $F_b = -\omega^2 r m_0$ and $F_d = -fv$. The frictional coefficient $f$ is dependent on the molecule size and shape. The negative signs in the last two forces indicted that these act in the opposite direction to centrifugal force. Therefore, the mass of solution displaced, $m_0$ may replace to the molecule mass times its partial specific volume ($\bar{\upsilon}$), multiplied density ($\rho$) of the solution:

$$\omega^2 rm\,(1 - \bar{\upsilon}\rho) - fv = 0 \qquad (2.2)$$

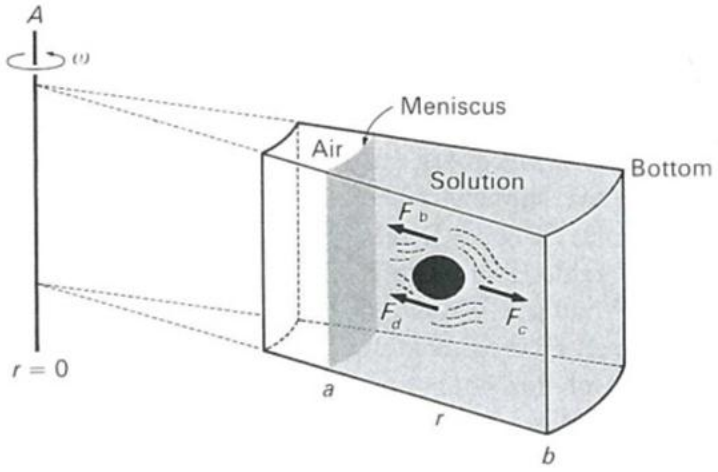


**Figure 2.3:** Diagram of a macromolecule in the sedimentation process. Adapted from van Holde (1985).

Rearranging, and replacing the molecular mass m (g) by *M/N*, where *M* is the molar mass or molecular weight (g mol$^{-1}$ or Da) and *N* is Avogadro's number 6.02 x 10$^{23}$ mol$^{-1}$ we get an equation for the sedimentation coefficient:

$$\frac{M(1-\bar{\upsilon}\rho)}{Nf} = \frac{v}{\omega^2 r} = s \qquad (2.3)$$

The sedimentation coefficient (*s*) is defined as the velocity of the sedimentation molecule per unit gravitational acceleration. It has unit of Svedberg, S where 1 S = 10$^{-13}$ second.

In a centrifugal field the molecules will sediment towards the cell bottom, therefore the region near the meniscus will become completely cleared of the solute, and a moving boundary is formed between the solute and solvent. From the rate of this boundary (see, Figure 2.4), it is possible to calculate the sedimentation coefficient and distribution of sedimentation coefficient (see e.g.

van Holde, 1985; Dam and Schuck, 2004). Since the sedimentation velocity has been expressed as a differential in radial position of the boundary ($dr_b$) over time ($dt$) from equation:

$$s = \frac{v}{\omega^2 r} = \frac{dr_b/dt}{\omega^2 r} \tag{2.4}$$

Integration of (2.4) with the radial position of the meniscus ($r_m$):

$$\ln(r_b/r_m) = s\omega^2 t = s \int_0^t \omega^2 dt \tag{2.5}$$

Plotting $\ln(r_b/r_m)$ versus time $t$, yielded a slope of straight line $\omega^2 s$, this leads to determine the sedimentation coefficient ($s$).

The moving boundary on Figure (2.4) shows a good example of diffusion of the sample in solution since its concentration increases with time towards cell base; sharp boundary presents less diffusion whereas significant diffusion spreads the boundary out.

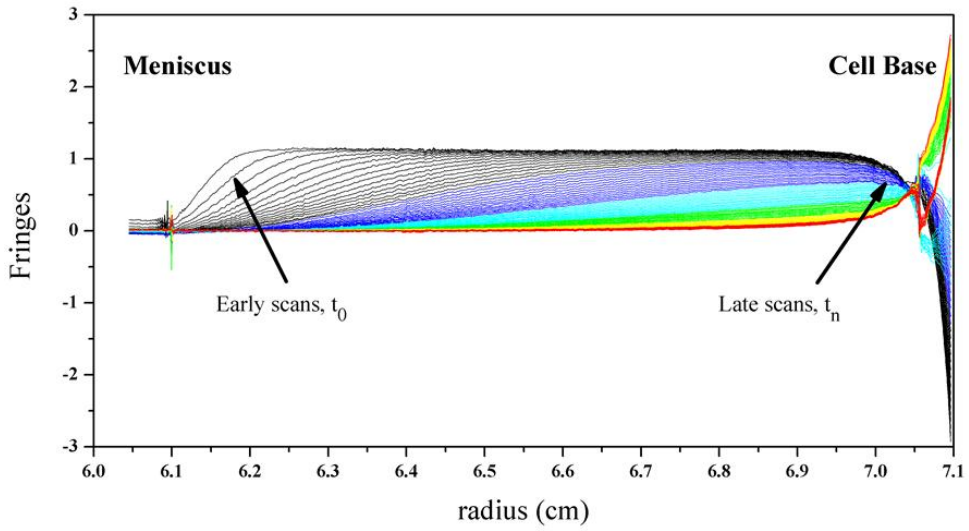


**Figure 2.4:** Movement of the boundary in sedimentation velocity experiment for lambda carrageenan 0.25 mg $mL^{-1}$.

In the sedimentation velocity experiment, the value of the sedimentation coefficient is influenced by temperature as well as the density and the viscosity of the solvent. Thus, in order to normalize these contributions the collected data can easily be transformed to standard conditions (the density, $\rho$ and viscosity, $\eta$ of water at 20.0 $^0$C):

$$s_{20,w} = s_{T,b} \left(\frac{1-\bar{\upsilon}\, \rho_{20,w}}{1-\bar{\upsilon}\, \rho_{T,b}}\right) . \left(\frac{\eta_{T,b}}{\eta_{20,w}}\right) \quad (2.6)$$

$\rho_{T,b}$ and $\eta_{T,b}$ are the density and viscosity of the solvent, $\rho_{20,w}$ and $\eta_{20,w}$ the corresponding values for water at temperature 20.0 $^0$C, whereas $\bar{\upsilon}$ is the partial specific volume.

It is known that the sedimentation coefficient $s_{20,w}$ is concentration dependent, which normally decreases with increasing the concentration. Thus the value of $s_{20,w}$ measured at a given concentration will be an *apparent* one, due to non-ideality effects arising from co-exclusion and charge effects. Such effects can be corrected using the conventional way – namely, measurement performed at a series loading concentration and then extrapolated to zero concentration (Harding, 2005). This is usually applied by plotting 1/ $s_{20,w}$ versus *c* using the following equation:

$$1/s_{20,w} = \left(1/s^o_{20,w}\right) . (1 + k_s\, c) \quad (2.7)$$

where, $k_s$ (mL g$^{-1}$) is the concentration dependence coefficient. This relation is valid however only over a limited range of concentrations (Harding, 2005). For a system with strict concentration dependence other relations can be used such as that proposed by Rowe (Rowe, 1977, 1992).

Taking advantage of new advances in the software for recording the whole radial concentration with time has allowed us to measure the distribution of sedimentation coefficient; where the differential distribution is described as the population – weight fraction – of species with sedimentation coefficient between *s* and *s+ds* (Dam and Schuck, 2004). A recent approach based on modeling of the Lamm equation (2.8) – now popularly referred to as the SEDFIT algorithm – is used to calculate the distribution and the weight average sedimentation coefficient of the sedimenting species. This is achieved by integration the peak or resolved peaks from the plotting of g*(s) versus *s* (Harding, 2005; Dam and Schuck, 2004). The distribution yielded here is influenced by diffusion effects (usually small for polysaccharides) that can be corrected in the method of c(s) using the approximation of a single, weight average frictional coefficient (see, e.g. Dam and Schuck, 2004). The calculation of g*(s) from the radial derivative *dc/dr* is always presents a noise due to the nature of interference optical system. This noise is eliminated using least squares boundary modeling – ls-g*(s) – introduced by Schuck (1998) and Dam & Schuck (2004), where the star indicates the apparent sedimentation coefficient distribution is not corrected to diffusion.

$$\left(\frac{dc}{dt}\right)_r = -\frac{1}{r}\left\{\frac{d}{dr}\left[s\omega^2 r^2 c - D\, r \left(\frac{dc}{dr}\right)_t\right]\right\} \tag{2.8}$$

The molecular weight can be obtained from the information of sedimentation coefficient combined with another measurement parameter namely the diffusion coefficient in the Svedberg equation (see, e.g. Harding, 2005):

$$M = \frac{s^0 RT}{D^0(1-\bar{\upsilon}\,\rho_0)} \tag{2.9}$$

where, $\rho_0$ is solvent density, $s^o$ and $D^o$ are the sedimentation and diffusion coefficients, respectively.

It is also possible to estimate the molecular weight by transforming a distribution of sedimentation coefficient g(s) versus *s* into a distribution of molecular weight *f (M)* versus *M* using the Extended Fujita method of Harding, Schuck and co-workers (Harding et al., 2011). The transformation is as follows:

$$f(M) = (ds/dM) \, . \, g(s) \tag{2.10}$$

The linking is applied with manipulation of the power law relation (similar to Mark-Houwink-Kuhn-Sakurada relation linking the intrinsic viscosity with molecular weight) (see, e.g. Harding et al., 1991; Tombs and Harding, 1998):

$$s = K_s \, M^b \tag{2.11}$$

Shape is taken care of by the power law coefficient *b* and manipulation of the equations yields the following relation (Harding et al., 2011):

$$f(M) = b.\left(K_s^{1/b}\right) . \left(s^{b-1/b}\right) . g(s) \tag{2.12}$$

*b* the conformation parameter, has limits of 0.4-0.5 for a flexible coil, 0.67 for a compact sphere and 0.15 for a rigid rod (see, e.g. Tombs and Harding, 1998), and $K_s$ can be found from equation (2.11) provided that at least one value of *M* is known for one value of *s* (from analytical ultracentrifugation). Furthermore, working at low concentration (0.2 mg $mL^{-1}$) and high ionic strength (e.g. 0.1M) minimizes the non-ideality arising from co-exclusion and polyelectrolyte effects, which could have led to significant underestimate for molecular weight (Harding, 2005).

This method has been popularly used for monodisperse system by transformation of c(s) into *c(M)* distribution if the frictional coefficient is known (see, e.g. Schuck, 2000). The methods, known as the "Extended Fujita" method has recently been implemented into the SEDFIT platform algorithms for estimation the heterogeneous systems including polysaccharides and mucins (Harding, et al., 2011; Gillis et al., 2013).

### 2.2.3 Sedimentation Equilibrium

The sedimentation equilibrium experiment is another type of experiment that can be carried out in the AUC. It is different from sedimentation velocity in that relatively lower angular velocities are required and it usually takes a longer duration depending on the size and shape of the macromolecule (van Holde, 2002; Cole et al., 2008). An important factor for the sedimentation equilibrium experiment is the selected rotor speed, where needs to be high enough to ensure the sedimentation of the macromolecule from the meniscus, but not too high to sediment a significant proportion of macromolecule to the cell base. Therefore, the speed and duration of sedimentation equilibrium is affected by a number of experiment factors such as the mass range of the molecule, the solvent viscosity and the solution column length. In particular the time to attain equilibrium is approximately proportional to the square of solution column length – the shorter the solution column used the faster the time to reach equilibrium (Ralston, 1993; Laue and Stafford, 1999).

As the macromolecule begins to sediment to the cell base, the concentration is increased at the base and the diffusion force become increasingly significant

opposes that of sedimentation. After a period of time, the forces of the sedimentation and diffusion become comparable so that a steady state pattern of macromolecule concentration is established (Figure 2.5). Since there is no net transport or frictional effect, the final pattern is only a functional of molecular weight and polydispersity. This method is an absolute way of estimating the molecular weight of macromolecule, whereby sample fractionation is achieved without the need for a separation column or membranes (Harding, 2005). In addition, it is applicable for a wide range of molecular weights from hundred up to several millions, due to the varied rotor speed from 500 rpm (for high $M_w$) to 60000 rpm (for small $M_w$) (Mächtle and Börger, 2006).

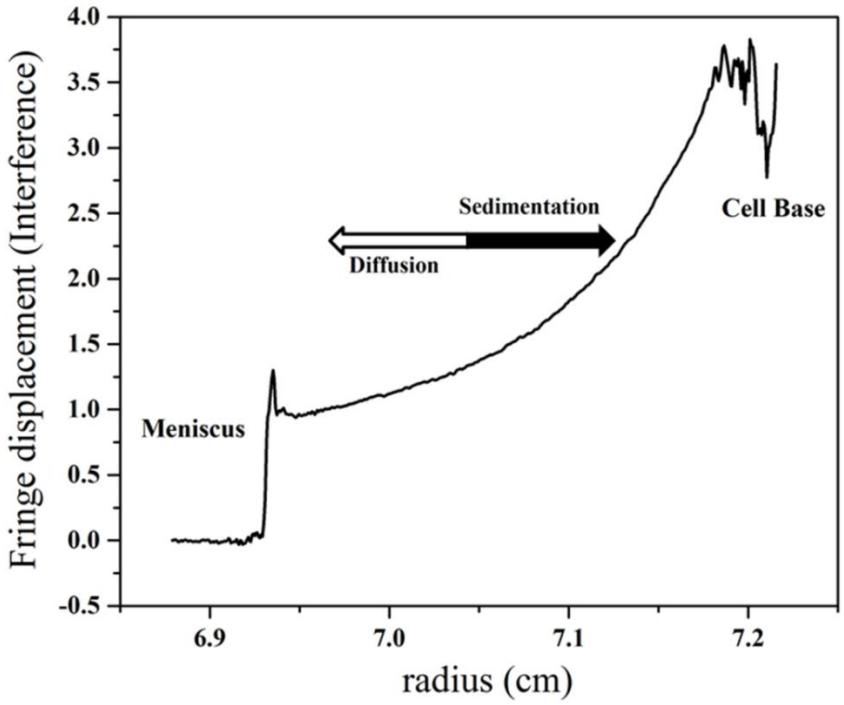


**Figure 2.5:** Profile of sedimentation equilibrium process for kappa carrageenan at NaI 0.1M and concentration 0.3 mg $mL^{-1}$.

Under ideal conditions the concentration distribution between selected radial positions $r$ and $r_0$ can be explained for a single macromolecule using the following equation:

$$c(r) = c_0 \exp\left[\frac{M_{w,app}\,(1-\bar{\upsilon}\rho_0)\omega^2\,(r^2-r_0^2)}{2RT}\right] \tag{2.13}$$

where $c(r)$ is concentration of the sample at radial position $r$, $c_0$ concentration of the sample at a reference radial position $r_0$ whereas $R$ is the gas constant and the $T$ is temperature (see, e.g. Cole et al., 2008). This equation also provides the molecular weight in the form of an *apparent* weight average molecular weight ($M_{w,app}$) as it is affected by thermodynamic non-ideality. To obtain $M_{w,app}$ for a heterogeneous or non-ideal distribution of molecules from this equation requires extrapolation of the *c(r)* to meniscus or base since the data near both positions are not measurable due to interface distortion effects of the optical signal. However, the extrapolation of *c(r)* to the cell base for heterogeneous systems can provide unreliable results due to strong curvature of the optical signal in the region approaching the cell base. A further difficulty is that in terms of the meniscus region, interference optics records not *c(r)* directly but *c(r) – c(a)* versus radial displacement *r*, and in terms of the corresponding fringe displacement units *J(r) – J(a)*; thus *c(a)* or *J(a)* has to be found by some other way since information of molecular weight depends upon both.

To address these problems, the MSTAR algorithm can be used by applying the *M** function (see, e.g. Creeth and Harding, 1982; Harding et al., 1992; Cölfen and Harding, 1997). Recently, it has been incorporated into the SEDFIT platform as SEDFIT-MSTAR (Schuck et al., 2014). The *M** function is defined

by the integral transformation for sector shaped solution columns with the radial position *r*:

$$M^*(r) = \frac{c(r) - c_m}{kc_m(r^2 - r_m^2) + 2k\int_{r_m}^{r}[c(r) - c_m]\, r dr} \tag{2.14}$$

where, the meniscus concentration is $c_m = c(r = r_m)$, and $k$ is obtained from the following equation:

$$k = \frac{(1 - \bar{\upsilon}\rho)\omega^2}{2RT} \tag{2.15}$$

Then the extrapolation towards cell base of *M*(r)* yields the apparent weight average molecular weight for the whole distribution:

$$M^*(r = r_b) = M_{w,app} \tag{2.16}$$

The extrapolation is much easier to do than the corresponding extrapolation of *c(r)* to the base required by eqn. (2.13). It is also possible to evaluate the point apparent weight average molecular weights as function of radial position, $M_{w,app}$ and at the hinge point ($r = r_{hinge}$):

$$M_{w,app}(r_{hinge}) = M_{w,app} \tag{2.17}$$

where hinge point is given as the radial position at which the local concentration, $c(r)$ is equal to the loading concentration, $c^0$.

Working at low concentration (0.3 mg $mL^{-1}$) and a reasonable ionic strength (0.1M) helps to minimize the non-ideality arising from co-exclusion and polyelectrolyte effect, and the apparent molecular weight at this loading concentration $M_{w,app}$ is approximately ~ $M_w$ the true or ideal weight average molecular weight. However, for some polysaccharides (for example chitosan)

these effects can still be significant and the assumption is made is sometimes not valid (Harding, 2005; Schuck et al., 2014). Consequently, such effects can normally be vanished by performing a series of measurements at different loading concentration and extrapolating back to zero concentration. There is a simple relation relating $M_{w,app}$ and $M_w$ at dilution (Tanford, 1961):

$$M_{w,app} = M_w \,.\, [1/(1 + 2BM_w c)] \tag{2.18}$$

where $B$ is the second thermodynamic virial coefficient (mL mol g $^{-2}$).

## 2.3 SIZE EXCLUSION CHROMATOGRAPHY COUPLED TO MULTI ANGLE LIGHT SCATTERING (SEC-MALS)

One of the most important parameters describing a macromolecule is its molecular weight and its molecular weight distribution. The size exclusion chromatography (SEC) combined with a photometer, such as a classical multi-angle light scattering (MALS) detection has revolutionised the measurement of absolute molecular weight – like sedimentation equilibrium in analytical ultracentrifugation – and molecular weight distribution for polymers (Wyatt, 1993; 2013; Harding, 2012). In the case of a polydisperse systems, the SEC separates macromolecules and the elution fractions (on-line) pass through a flow cell in the MALS, thus the total intensity of light scattered can be measured for each elution volume. As the system is also coupled to on-line to a refractive index (concentration) detector the weight average molecular weight can be specified as well the distribution of molecular weights. The method has become a popular choice for polydisperse systems since the first determination

of polysaccharides – alginate – by *Horton et al.* and glycoprotein – such as mucin – by *Jumel et al.* (Horton et al., 1991; Jumel et al., 1996).

### 2.3.1 Size Exclusion Chromatography (SEC)

Size exclusion chromatography (SEC) has become one of the popular fractionation technique combined with light scattering, which separates molecules upon their size in solution (hydrodynamic volume). The SEC column is packed with a matrix of porous particles beads of selected size and porosity. The solute molecules will penetrate through this matrix based on phases moving, where solvent is known as the mobile phase and the matrix beads as stationary phase. The basis of separation for mixtures of molecules in solution is shown in Figure (2.6); the large molecules are not able to penetrate the matrix beads and and eluted out faster, whereas a small molecules will pass through the column taking a relatively longer time to elute. Therefore, the separation process can be affected by several factors including temperature, mobile phase, type of material of the column, flow rate of mobile phase and column packing pore size (Kostanski et al., 2004). Thus, separation on this method depends on the size of a macromolecule, and with some major assumptions has become a direct and simple measure for the molar mass or molecular weight of a macromolecule (Wen, et al., 1996).

However, molecular weight measurement can be affected by the shape of molecule - since separation also depends on shape - and self-association (e.g. protein) or interaction with the column in case of polysaccharides. Thus, the SEC technique is not an absolute method by itself for estimating the molecular

weight, which calibration and assumption have to be made (see, e.g. Harding et al., 1991). Combination of SEC with the appropriate detection systems (e.g. MALS) provides the absolute estimation of hydrodynamic properties such as molecular weight.

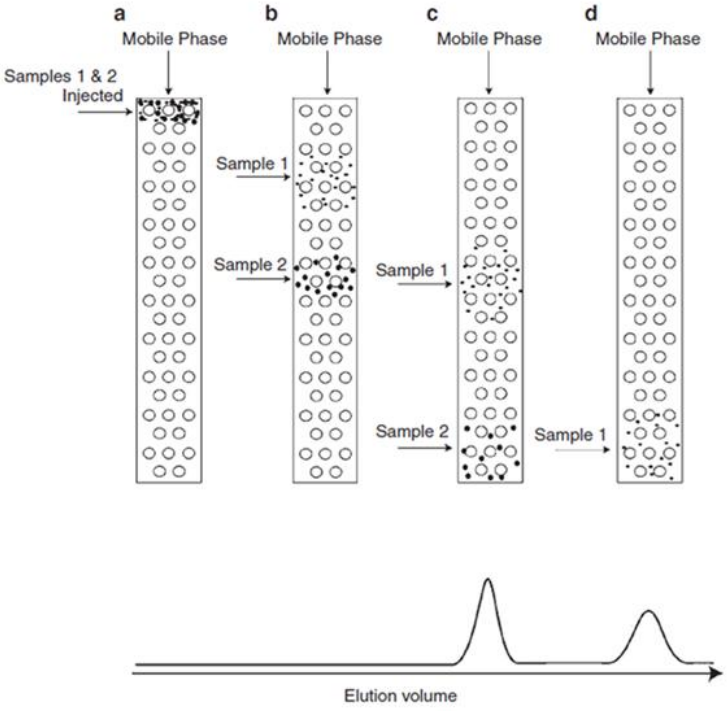


**Figure 2.6:** Separation of two different samples by size exclusion chromatography. Adapted from Wyatt (2013).

In this study SEC was performed using several conditions to ensure a high quality of separation. A filtered mobile phase – using 0.2 μM nylon membrane filter – was run overnight for equilibration at flow rate of 0.8 mL $min^{-1}$. The SEC columns consist of a guard column and a series of two columns for separation of sample components, which are equilibrated at 20.0 $^{o}$C using a chromatographic temperature regulator cabinet (Anachem Ltd, UK).

### 2.3.2 Multi Angle Light Scattering (MALS)

Light scattering is one of the absolute methods for determine the molecular weight and radius of gyration of macromolecules, which can be performed in batch or chromatographic modes (see, e.g. van Holde, 1985; Jumel et al., 1992; Wyatt, 1992, 1993). Theoretically the light scattering phenomena take places after electromagnetic radiation strikes a macromolecule. The macromolecule emits scattered light that is induced by interaction of the electrons from the molecule with the oscillating electric field component from light (Wyatt, 1993). The angular dependence of the intensity of scattered light is recorded in classical light scattering (van Holde, 1985). As single macromolecule can have many scattering points due to intramolecular interference. Therefore, the scattering intensity is reduced with increasing the scattering angles. In general there are two principle physical parameters of a macromolecule associated with the phenomenon of light scattering: Firstly the intensity of the scattered light scattering is directly proportional to the weight average molecular weight multiplied by concentration. Secondly the variation of the scattering intensity with angle is related directly to the radius of gyration of molecule.

The molecular weight is measured as a function of the intensity impinging on the scattering volume, $V$ using the intensity of light scattered at some angle, $\theta$ and can be arranged as follow (Jumel et al., 1992):

$$R_\theta = J_\theta / I_0 V \tag{2.19}$$

where $R_\theta$ is known as the Rayleigh factor, and the intensity of scattered beam $J_\theta$ whereas $I_0$ is the intensity of the incident beam. Light scattering results from

the random fluctuations in solute concentration: information of solute concentration and refractive index is therefore required. Consequently, the relation of the Rayleigh excess factor with the physical characteristics of the scattering molecule is described by the following expression (see, e.g. Jumel et al., 1992; Wyatt, 1992, 1993):

$$\frac{Kc}{R_\theta} = \frac{1}{M_w P(\theta)} + 2A_2c + 3A_3c^2 \ldots \quad (2.20)$$

where $c$ is the concentration of solution, $P(\theta)$ the form factor describes the angular dependence of scattered light which depends on shape and size of molecules, the $A$ thermodynamic term called 2nd, 3rd, … and subsequent virial coefficients which is equal to zero for ideal solution, and $K$ an optical constant which includes the wavelength $(\lambda)$ and refractive index increment *dn/dc* as in the following:

$$K = 4\pi^2 n^2 (dn/dc)^2 / N_A \lambda_0^4 \quad (2.21)$$

However, at low angles where $\theta$ approaches zero and $P_\theta$ = 1, the third and higher virial coefficients can be eliminated and equation (2.20) becomes (see, e.g. Wyatt, 2013):

$$\frac{Kc}{R_\theta} = \frac{1}{M_w} + 2A_2c \quad (2.22)$$

whereas at low concentration with low angle the following equation is adequate:

$$\frac{Kc}{R_\theta} = \frac{1}{M_w} \quad (2.23)$$

Taking advantage of measuring the scattering intensity at different angles and concentration using multi-angle light scattering allows us to determine the value of weight average molecule weight $M_w$, second virial coefficient, $A_2$ and radius of gyration, $R_g$ utilizing a Zimm plot. In the case of MALS combined to SEC however, the working concentration is too low, thus Zimm plot cannot be performed which depends on different concentrations. Therefore, the Debye plot is adopted as it depends on different angle – as Zimm plot – but at one single low concentration (Wyatt, 1993, 2013).

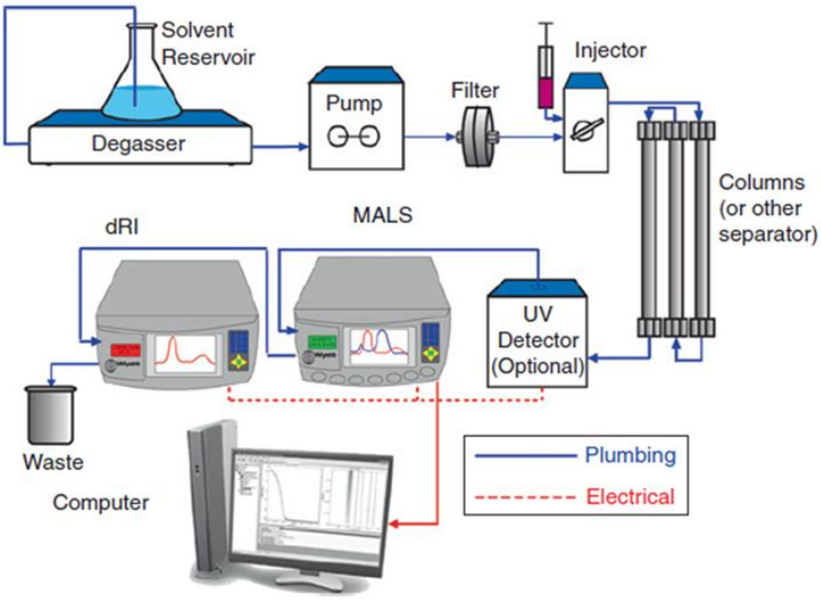


**Figure 2.7:** The schematic setup of chromatography with on-line light scattering detection. Adapted from Wyatt (2013).

In these studies described in this thesis, the SEC-MALS system used is a combination of different components as shown in (Figure 2.7); namely size exclusion chromatography (SEC), a photometer (MALS) and on-line refractometer (concentration detector) to measure the different average molecular weight and other parameters utilizing the Debye equation (2.22).

Thus, although the angular extrapolation plot can be done using different procedures, only two have been considered on this chapter and they are based on the ASTRA package of software (Wyatt Technology, Santa Barbara, CA). The first is a Debye fit where $R_\theta/Kc$ is plotted versus $\sin^2(\theta/2)$ and extrapolated to zero angle, thereby $M_w$ is obtained from the intercept and from the slope the z-average $R_g$. The second methods is a Zimm fit in which $Kc/R_\theta$ is plotted as a function of $\sin^2(\theta/2)$, to yield 1/ $M_w$ and the z-average $R_g$ from intercept and slope, respectively.

## 2.4 VISCOMETRY

Viscometry is one of the simplest methods used in the hydrodynamic analysis of a polymer in solution, which can provide basic information about shape, conformation flexibility and the state of aggregation or degradation (Harding, 2012). In general, the fluid viscosity is a measurement of fluid resistance to flow and depends on the volume occupied by macromolecules as well as their shape and size (see, e.g. Harding, 1997). For understanding the theory behind the viscosity Figure (2.8) should be considered: a liquid is held between two infinite parallel plates, of which one is moving in the *x* direction with a constant velocity *v*, whereas the other is stationary. The degree of resistance is measured by viscosity, where deformation that is experienced thereby liquid is known as shear strain and can be referred to as *d/dt* (*dx/dy*) or *dv/dy* at any point. Therefore, the liquid will shear at a constant rate when is subjected to a constant shear strain (van Holde, 1985).

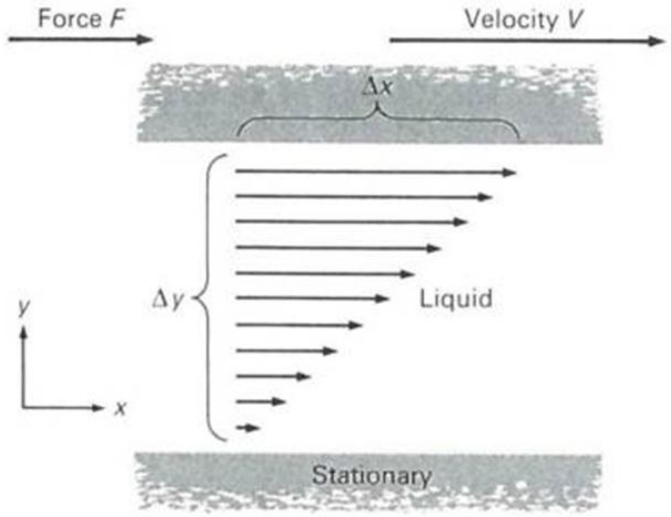


**Figure 2.8:** Schematic diagram representing the movement of a Newtonian liquid between parallel plates. Adapted from van Holde (1985).

The relation between shear stress $\sigma$ and the rate of shear strain for the most liquids (Newtonian liquids) can be presented as follows (van Holde, 1985):

$$\sigma = \eta \frac{d}{dt}\left(\frac{dx}{dy}\right) \tag{2.24}$$

where $\eta$ is the viscosity of the liquid and has the dimensions of g $cm^{-1}$ $s^{-1}$, these units are called Poise. From the expression of equation (2.24) a definition of viscosity can be yielded as well. Therefore, the measurement of the rate energy dissipation of the flow and shear rate has been used as another definition of viscosity, which was developed by Einstein (1906) as shown in equations (2.25 and 2.26), respectively:

$$\frac{F}{A\Delta y} \cdot \frac{dx}{dt} = \eta \left(\frac{v}{\Delta y}\right)^2 \tag{2.25}$$

in deforming the sample of fluid the energy expended $F\,dx$ ($=dE$) in time $dt$ and $A\Delta y$ is the volume of the fluid, hence.

$$\frac{dE}{dt} = \eta \left(\frac{v}{\Delta y}\right)^2 \tag{2.26}$$

For estimation of the viscosity of macromolecules in solution, the solvent viscosity should be first measured after that the solute measurement performed at an appropriate concentration showing more viscosity compared to solvent. The concentration and macromolecular interactions both affect solution viscosity relative to the pure solvent (Harding, 1997: Harding 2012). In this study there are two principle types of viscometry used to measure viscosity namely: capillary viscometry and pressure imbalance differential viscometry.

## 2.4.1 Capillary Viscometry

The most common viscometer is still the capillary (or Ostwald), and is a precision piece of glassware suspended in a constant temperature environment (Figure 2.9). It is simply used by determining electronically the time for a volume of liquid to flow through the capillary in the vertically aligned viscometer. The solvent flow time is measured followed by the macromolecule solution at a series of concentration typically 0.2 – 1.0 mg $mL^{-1}$ for polysaccharides (Harding, 1997). Dilution can sometimes be made directly in the viscometry taking advantage of a modified form called an *Ubbelohde* viscometer which the amount of liquid at the time of flow measurement is independent from the amount of solution in viscometry. This type of

measurement however, should not be used if the molecule degrades or denatures during the measurement (Harding, 1997).

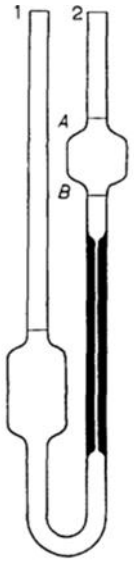


**Figure 2.9:** Schematic of the Ostwald capillary viscometer, which the flow of a solution is measured between A and B. Adapted from Harding (1997).

The relative viscosity is the ratio of the viscosity of solution containing macromolecule to that of pure solvent. It can be given simply under the appropriate experimental conditions by the following equation:

$$\eta_{rel} = \left({}^{t}/_{t_0}\right) \tag{2.27}$$

where the $t$ and $t_0$ are the flow times for the macromolecule solution and solvent respectively at specific concentration. An adjustment for solution and solvent density is also required, but in the case of polysaccharides this correction is usually negligible at the low concentration used. The relative viscosity depends on the macromolecule concentration, shape and the volume it occupies (van Holde, 1985; Harding, 1997).

For estimation of the effect of shape and volume of macromolecule from the viscosity measurement, the concentration contribution should be eliminated. To do this firstly the reduced viscosity $\eta_{red}$ and inherent viscosity $\eta_{inh}$ have to be defined (Harding, 1997).

$$\eta_{red} = (\eta_{rel} - 1/c) \tag{2.28}$$

$$\eta_{inh} = (\ln \eta_{rel}/c) \tag{2.29}$$

Due to the effects of non-ideality – derived from exclusion volume, backflow and charge effects – and associative phenomena, the reduced and inherent viscosities depend in a further way on concentration. Therefore, they are conventionally measured at a series of concentration and extrapolated back to zero concentration. In addition, the intrinsic viscosity (mL $g^{-1}$) is defined as the method of extrapolated reduced and inherent viscosities to zero concentration (van Holde, 1985; Harding, 1997). Extrapolating the reduced and inherent viscosities can be applied using two main forms namely Huggins form (Huggins, 1942) and Kraemer form (Kraemer, 1938), respectively according to the following equations:

$$((\eta_{rel} - 1)/c) = [\eta](1 + K_H[\eta]c) \tag{2.30}$$

$$(\ln \eta_{rel}/c) = [\eta](1 - K_K[\eta]c) \tag{2.31}$$

In these equations $K_H$ and $K_K$ are the coefficients of Huggins and Kraemer, respectively. Furthermore, the Solomon-Ciuta equation is another useful relation that can be used for obtaining the intrinsic viscosity at one concentration, which is a combination of the Huggins and Kraemer equations (see, e.g. Harding, 1997; Harding, 2012; Morris et al., 2014).

$$[\eta] \sim (1/c) \cdot [2(\eta_{rel} - 1) - 2\ln(\eta_{rel})]^{1/2} \quad (2.32)$$

In this study, the various procedures have been applied at different concentration then extrapolated to zero concentration to obtain the intrinsic viscosity.

## 2.4.2 Pressure Imbalance Differential Viscometry

This method measures the relative viscosity based on the difference in pressure – pressure drop instead of flow time – between solution and solvent flow through metal capillaries and can be fitted on-line to SEC-MALS. It provides an alternative to classical Ostwald viscometry and is particularly useful for the heterogeneous system since SEC can supply separation of these before entry into the viscometer. This utilises the fluid analogue of a Wheatstone bridge electrical circuit for estimation the relative viscosity of solution flowing relative to solvent flowing (Figure 2.10).

The principle of the differential pressure measurement is described as follows. Initially during the baseline conditions solvent flows in all four capillaries (R1, R2, R3 and R4) and the pressure across the bridge is zero. As the sample solution enters the delay volume from the SEC column, the configuration is such that solution flows through R1, R2 and R3 whilst solvent from a reservoir is still flowing through R4. Thus the pressure imbalance or difference measurement is dependent on the different viscosity between the solvent flow in R4 and solution flow in R3 (see, e.g. Harding, 1997).

Accordingly to a combination of pressure imbalance $\Delta P$ and the device inlet pressure $IP$, the specific viscosity $\eta_{sp}$ of the solution can be determined by the following equation:

$$\eta_{sp} = \eta/(\eta_0 - 1) = 4\Delta P/(IP - 2\Delta P) \quad (2.33)$$

where $\eta$ and $\eta_0$ are the solution and the solvent viscosities. Knowledge of determination both $\eta_{sp}$ and $c$ utilizing the differential viscometer and refractometer – coupled on-line to the SEC-MALS – respectively allows estimating the intrinsic viscosity of solution $[\eta]$ from equation (2.32). Therefore, as the pressure transducer is very sensitive, sufficiently low concentration can be applied so that $\eta_{red} \sim [\eta]$, and no extrapolation to zero concentration is required (Harding, 1997, 2012).

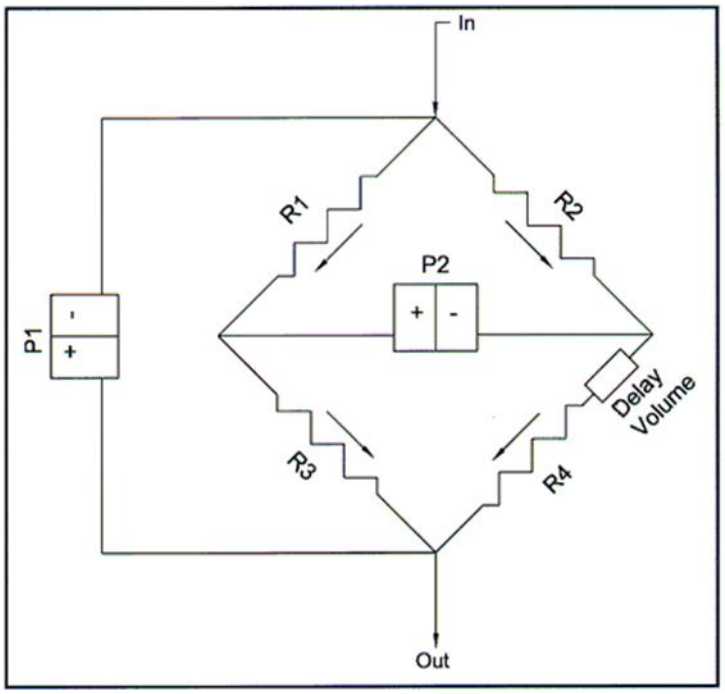


**Figure 2.10:** Schematic diagram of four capillary bridge design of pressure imbalance viscometer. Adapted from Harding (1997).

# 2.5 MICRO-DIFFERENTIAL SCANNING CALORIMETRY (micro-DSC)

Calorimetry is a method used to establish the relationship between the change of temperature and physical properties of macromolecules. One of the important advantages of calorimetry is measuring the intrinsic thermal properties without requirement for chemical modification or extrinsic probes. Therefore, the change of temperature is measured according to time, and has been frequently applied in chemistry, biology, biochemistry, biotechnology and pharmaceutical sciences (Privalov and Potekhin, 1986; Höhne et al., 2003). The measurement of "caloric" has been known since in the middle of the 18$^{th}$ century, several types of calorimeters were introduced; amongst these various types the differential scanning calorimeter (DSC) has become a popular and widely used, which is developed for more flexible application (Höhne et al., 2003).

DSC is a technique able to assess thermally induced transition, which occurs in a sample at different temperatures (increase or decrease) versus time. It is commonly carried out for biological macromolecules to observe the variation of phase transitions, and in particular conformation transitions (Gill et al., 2010).

The general principle of a DSC experiment is as follows: both solution and solvent cells are heated at constant rate along with increased temperature over time. The difference in the heat energy absorbed by the solution and solvent cells required to keep temperature equal is recorded. In regards of equal temperature, more energy is needed for the solution compared to solvent due to

the presence of the molecule of interest. That is corresponding to the different in changes of heat capacity, which provides information about the thermally induced transitions for the solution (Cooper et al., 2000; Gill et al., 2010; Bruylants et al., 2005). Therefore, the results of the position, sharpness and shape of transitions scan are affected by changes in the conformation, since the structure state of the macromolecules are sensitive to the thermal properties yielded from DSC experiments (Gill et al., 2010).

DSC can be distinguished based on the mechanism of operation into two types: heat-flux DSC and power-compensated DSC. The pans of solution and solvent materials are placed into a thermoelectric disk surrounded by a furnace in the case of heat-flux DSC. At linear heating rate the furnace is heated, and a thermoelectric disk used to transfer the heat to the solution and solvent pans. The difference of the temperature between solution and solvent is measured through area thermocouples, where the thermal equivalent of Ohm's law is applied to determine the heat flow (Danley, 2002):

$$q = \Delta T / R \tag{2.34}$$

where, $q$ is solution heat flow, $\Delta T$ difference of the temperature (solution and solvent), whereas $R$ is resistance of thermoelectric disk. However, in the second type a power – compensated DSC separate furnace were used for both solution and solvent pans. The difference in thermal power demanded to maintains the same temperature for both solution and solvent, is estimated and plotted as function of temperature or time (Zucca et al., 2004).

# 2.6 COMBINED HYDRODYNAMIC APPROACHES

The differences observed for the hydrodynamic properties of large molecular weight macromolecules (such as polysaccharides and mucin) in solution are not only due to their large size, but also their greater non-ideality (through molecular co-exclusion and charge effects), and massive variety of shapes along with flexibilities (Tombs and Harding, 1998; Harding,2005). Thus, hydrodynamic techniques have been applied to ascertain the distribution of molecular weight, overall conformation, flexibility and quaternary interaction. In the case of a more detailed picture of conformation many methods have been utilized based on the combination of two or more biophysical properties namely, sedimentation coefficient, molecular weight and intrinsic viscosity (Morris et al., 2014). Some of the most applicable procedures relevant to macromolecules will be described briefly in the following paragraphs.

## 2.6.1 Wales-van Holde Ratio (R)

One of the simplest indicators assessing the macromolecular conformation flexibility is the Wales and van Holde ratio. It is dependent on the sedimentation concentration dependence coefficient, $k_s$ and the intrinsic viscosity$[\eta]$.

$$R = k_s/[\eta] \tag{2.35}$$

The limits are ~1.6 for a compact sphere or a (non-draining) random coil (Creeth and Knight, 1965), and ~ 0.15 for the rod structure. This method can be affected by self-association and intermolecular electrostatic repulsive

faeces, but we assume these are negligible as there is little or no self-association at low concentrations and polyelectrolyte suppression using a salt solution of appropriate ionic strength (see, e.g. Tombs and Harding, 1998).

### 2.6.2 Mark-Houwink-Kuhn-Sakurada (MHKS) or Power Law Relations

The knowledge of the hydrodynamic parameters – intrinsic viscosity or sedimentation coefficient – of a macromolecule in solution is contributed by its molecular weight and conformation. Thus, the molecular conformation can be obtained through the molecular weights dependency of a number of hydrodynamic parameters such as intrinsic viscosity$[\eta]$, sedimentation coefficient$\left(s^o_{20,w}\right)$, root-mean-square radius$\left(R_g\right)$, and translational diffusion coefficient$\left(D^o_{20,w}\right)$. These relations are achieved by following equation – for those only used in this study – for example viscosity (see, e.g. Harding et al., 1991; Harding, 2005; Morris et al, 2014):

$$[\eta] = K_\eta M^a \tag{2.36}$$

and by plotting the double log of $[\eta]$ versus $M_w$, (Figure 2.11) from the intercept and the slope the $K_\eta$ and $a$ are obtained, respectively. The gross macromolecular conformation can be estimated by the exponent $a$ value, which value is related to the conformation and stiffness. Value of $a \sim 0$ is seen for macromolecule adopting the compact sphere or highly branched conformation, whereas the range of $a$ values from 0.5-0.8 correspond to a random coil molecule, and $a$ values approaching 1.8 and beyond are seen for molecule with

more chain stiffness (e.g. with rigid rod conformation) (see, e.g. Harding et al., 1991; Tombs and Harding, 1998).

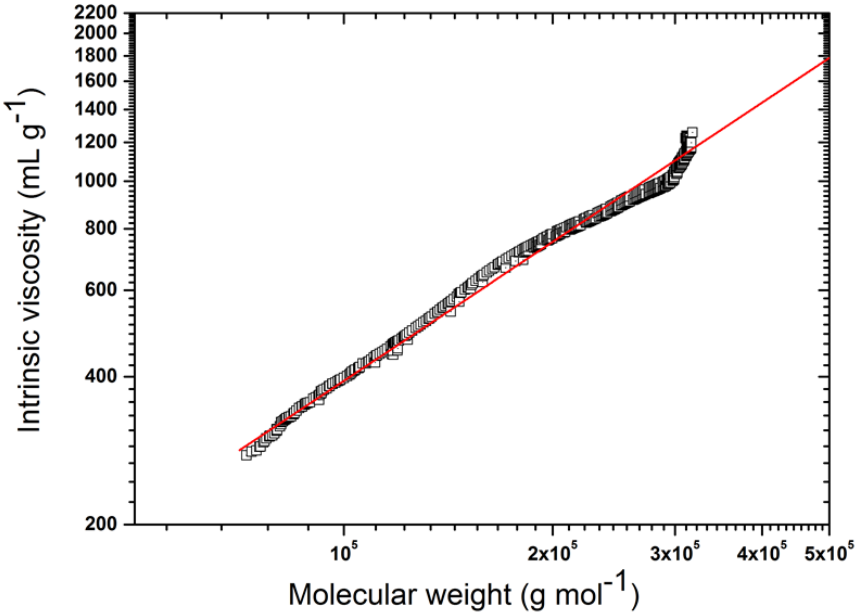


**Figure 2.11:** Example of a Mark–Houwink–Kuhn–Sakurada (MHKS) power law double logarithmic plot for chitosan CHIT1 (see *Chapter 5*) from an on-line differential pressure viscometer ViscoStar coupled to SEC-MALS. The plot is of intrinsic viscosity [η] as a function of elution volume (ordinate) versus molecular weight $M_w$ as a function of elution volume.

A second power law relation combines the sedimentation coefficient and the molecular weight as shown in equation 2.37.

$$s^o_{20,w} = K_s M^b \tag{2.37}$$

where both $K_s$ and $b$ parameters are yielded from the intercept and slope of plotting the double log of $s^o_{20,w}$ versus $M_w$ (Figure 2.12). This is analogous to the relation of intrinsic viscosity with molecular weight, but the $b$ values of ~ 0.67 has been established for compact sphere or highly branched

macromolecules, 0.4-0.5 for random coils, and ~ 0.15 for rigid rods (see, e.g. Harding et al., 1991; Tombs and Harding, 1998).

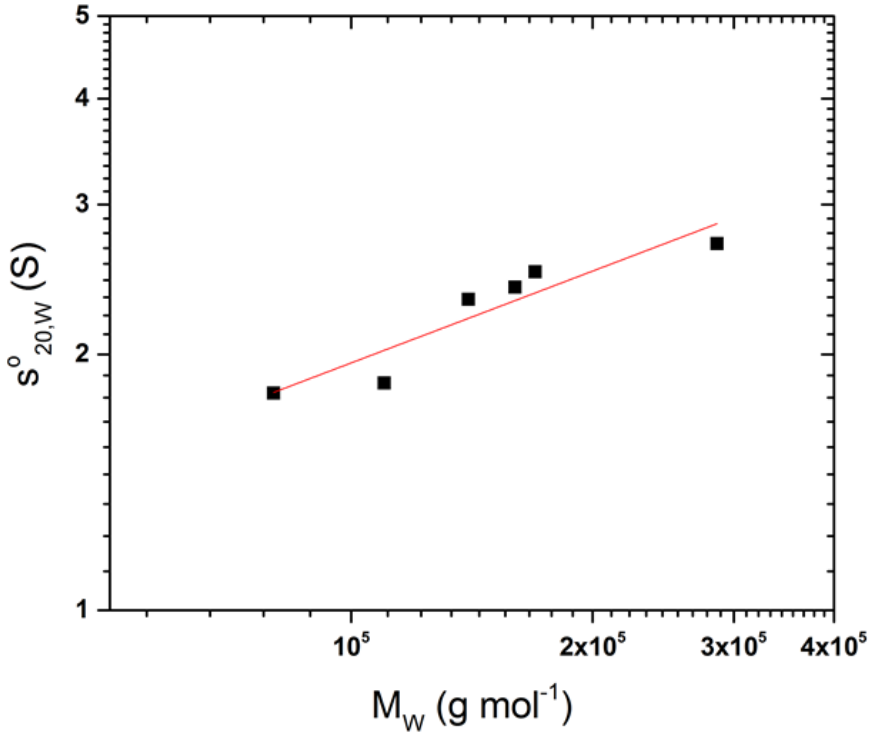


**Figure 2.12:** Example of Mark–Houwink–Kuhn–Sakurada (MHKS) power law double logarithmic plot of $s^o_{20,w}$ *vs* $M_w$ for chitosan samples (see *Chapter 5*).

## 2.6.3 Conformation Zoning

In terms of gross conformation, an extension of the Haug triangle representation of the conformation of macromolecules (in particular polysaccharides) was given by Pavlov and colleagues (1997 and 1999), suggesting the use of five conformation types or zones ranging from Zone A (extra rigid rod) to Zone E (globular or branched) (Figure 2.13). Thus, the conformation of macromoleculer can be estimated in a semi-empirically manner utilising the conformation zoning approach, in which all zones are tailored around sedimentation measurement (Harding, 2005). Based on the

knowledge of the intrinsic sedimentation coefficient, $[s]$ along with the concentration dependence of the sedimentation coefficient, $k_s$ and mass per unit length, $M_L$, a plot of $k_s M_L$ versus $[s]/M_L$ is used to estimate the overall conformation of the macromolecule. The $[s]$ parameter can be obtained through the following equation:

$$[s] = \{s^0 \eta_0 / (1 - \bar{\upsilon} p_0)\} \quad (2.38)$$

where $\eta_0$ and $\rho_0$ are the viscosity and the density of the solvent, respectively and $\bar{\upsilon}$ the partial specific volume of the macromolecular. Therefore, another relation was described for representing the conformation of macromolecular in solution utilising the information of molecular weight $M_w$, intrinsic viscosity, $[\eta]$and mas per unit length, $M_L$ (Pavlov et al., 1999).

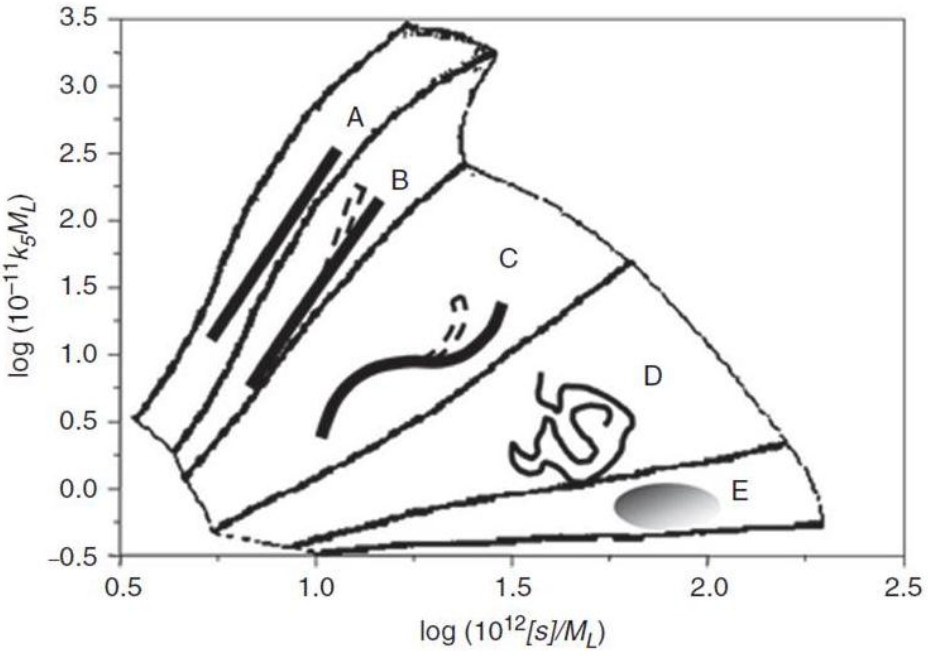


**Figure 2.13:** The sedimentation conformation zoning plot, which helps to define zones: A: extra rigid rod, B: rigid rod, C: semi-flexible coil, D: random coil, E: globular/heavily branched structure. Adapted from Pavlov *et al.*, (1997).

## 2.6.4 Estimation of the Persistence Length ($L_p$) and Mass Per Unit Length ($M_L$)

Both persistence length ($L_p$) and mass per unit length ($M_L$) are terms quantitatively used to describe the linear flexibility of polymer chains. The $L_p$ is analogous worm-like chains, and is defined as the average projection length along the initial direction of the polymer chain, whereas $M_L$ is the mass of the molecules divided by its length (see, e.g. Tombs and Harding, 1998). In theory, $L_p$ has limitation for strict random coil (where $L_p$ = 0) and for the stiff rods (where $L_p$ = ∞). However, for practical consideration the limitations often quoted is $L_p$ ~ 1-2 nm for random coils (e. g. pullulan) and $L_p$ ~ 200 nm for a stiff rod (e.g. schizophyllan) (see, e. g. Tombs and Harding, 1998; Morris et al., 2014). Nevertheless, a number of methods have been applied to estimate the linear flexibility of polymer chains. The choice of appropriate models provide an optimum measurement for the polymer flexibility, which is influenced by excluded volume effects (Kök et al., 2009).

### 2.6.4.1 Bushin-Bohdanecky Method

For a semi-flexible polymer, the Bushin-Bohdanecky method is most commonly used for estimating the persistence length of chains, and has been applied for a wide range of macromolecules (e.g. polysaccharides and glycoconjugate vaccines). Based on the knowledge of intrinsic viscosity and molecular weight values, the relationship of $(M_w^2/[\eta])^{1/3}\ vs\ M_w^{1/2}$ can be plotted, and the $L_p$ calculated from the slope, if the $M_L$ is provided, via the following equation (Bohdanecky, 1983; Bushin et al., 1981):

$$\left(\frac{{M_w}^2}{[\eta]}\right)^{1/3} = A_0\, M_L\, \phi^{-1/3} + B_o \phi^{-1/3} \left(\frac{2L_p}{M_L}\right)^{-1/2} {M_w}^{1/2} \quad (2.39)$$

where $\phi$ is the Flory-Fox constant (2.86 x $10^{23}$ $mol^{-1}$) whiles, $A_0$ and $B_o$ are tabulated coefficients (Bushin et al., 1981). Similarly, $M_L$ can be obtained from the same plot if the $L_p$ is known.

### 2.6.4.2 Yamakawa-Fujii Method

Another approach for estimating the persistence length of polymer chains is the Yamakawa-Fujii method, which utilizes the information of sedimentation coefficient and molecular weight. Plotting $s^o_{20,w}\ vs\ (M_w)^{1/2}$ led us to obtain the $L_p$ and $M_L$ from the slope, with prior knowledge of either $L_p$ or $M_L$. Although the original equation by Yamakawa and Fujii (1973) was misprinted, the corrected relation was provided by Freire and Garcia de la Torre (1992):

$$s^o = \frac{M_L\,(1-\bar{\upsilon}\rho_o)}{3\,\pi\,\eta_0\,N_A}\; x\; \left[1.843\left(\frac{M_w}{2M_L L_P}\right)^{1/2} + A_2 + A_3\left(\frac{M_w}{2M_L L_P}\right)^{-1/2} + \cdots\right] \quad (2.40)$$

where $A_2$ = -ln (d/2$L_p$) and $A_3$= 0.1382 if the $L_p$ is much higher than the chain diameter, *d* (Yamakawa and Fujii, 1973).

Although the Bushin-Bohdanecky and the Yamakawa-Fujii methods present us with a practical way of measuring these otherwise elusive parameters, nevertheless, they both have a limitation, since information about either $L_p$ or $M_L$ is required for obtaining the other parameter. As a result, both relations have been combined into a new algorithm to facilitate the calculation of both parameters through a global fitting of precisely determined experimental quantities/parameters such as sedimentation coefficient, intrinsic viscosity and

molecular weight data of the polymer (Ortega and Garcia de la Torre, 2007) – (see section 2.6.4.3).

### 2.6.4.3 Global Approach Method (HYDFIT)

Both $L_p$ and $M_L$ can be estimated using a global approach namely (Multi-HYDFIT algorithm) based on the minimisation of a target function ($\Delta$), which considers data set of sedimentation coefficient and intrinsic viscosity for different molecular weights (see, e.g. Ortega and Garcia de la Torre, 2007). In order to find the best values of $M_L$ and $L_p$ and the chain diameter $d$, the method performs a minimization procedure for a target function utilizing the equations of Bushin-Bohdanecky (2.39) and Yamakawa and Fujii (2.40). It has been confirmed by extensive simulation of the values returned for $M_L$ and $L_p$ are insensitive to $d$ value, due to that is usually fixed (Ortega and Garcia de la Torre, 2007), and also can be calculated through following equation:

$$d = (4M_L\bar{\upsilon}/\pi N_A)^{1/2} \tag{2.41}$$

where $\bar{\upsilon}$ is partial specific volume, and $N_A$ Avogadro constant.

In principal Multi-HYDFIT utilized the Monte Carlo simulation in terms of the rigid-body treatment for flexible structures to calculate the structural parameters ($L_p$, $M_L$ and $d$) of a wormlike macromolecule. In this procedure, the properties such as radius of gyration, $R_g$, sedimentation coefficient, $s$, translational diffusion, $D_t$ and intrinsic viscosity, [η] are initially evaluated for individual conformations using rigid-body hydrodynamic calculation in particular bead models of wormlike chain. The procedure repeated to estimate

different conformations, and then the average conformation obtained as rigid particles (Amoros, Ortega and Garcia de la Torre 2011). Therefore, these properties are transformed into equivalent radii, $a_Y$ $(a_G, a_T, a_I)$ which are considered function of molecular weight. The equivalent radii, $a_Y$ is defined as the radius of an equivalent sphere having the same value as the determined property (see, e.g. Ortega and Garcia de la Torre, 2007). The equivalent radii for the properties (*Rg*, *s*, *Dt* and [η] ) are calculated using following equations:

$$a_G = \sqrt{\frac{5}{3}}\, R_g \tag{2.42}$$

$$a_T = \frac{k_B\, T}{6\,\pi\,\eta_0 D_t} \tag{2.43}$$

$$a_I = \left(\frac{3M[\eta]}{10\pi N_A}\right) \tag{2.44}$$

where $\eta_0$, is the solvent viscosity, *M* is the molecular weight, *T* is the absolute temperature, and $k_B$ and $N_A$ are the Boltzmann and Avogadro constants.

However, $a_Y$ $(a_G, a_T, a_I)$ can be expressed as ($L_p$,$M_L$, and *d*) in the case of the wormlike chain. Then the minimization of the target function can be evaluated by optimizing the parameters from the following relation.

$$\Delta^2\,(L_P, M_L, d) = \frac{1}{N_s}\sum_{i=1}^{N_s}\left[(\sum_Y W_Y)^{-1}\,\sum_Y W_Y\,\left(\frac{a_{Y\,(cal)} - a_{Y\,(exp)}}{a_{Y\,(exp)}}\right)^2\right] \tag{2.45}$$

where $N_s$ is the number of samples in multi-sample analysis, $W_Y$ is the statistical weight for equivalent radii, $a_Y$ and the subscripts cal and exp represent values from calculated and experimental values respectively. In the following studies we mainly focus on the equivalent radii resulting from the sedimentation coefficient, ($a_T$ ) and from the intrinsic viscosity ($a_I$).

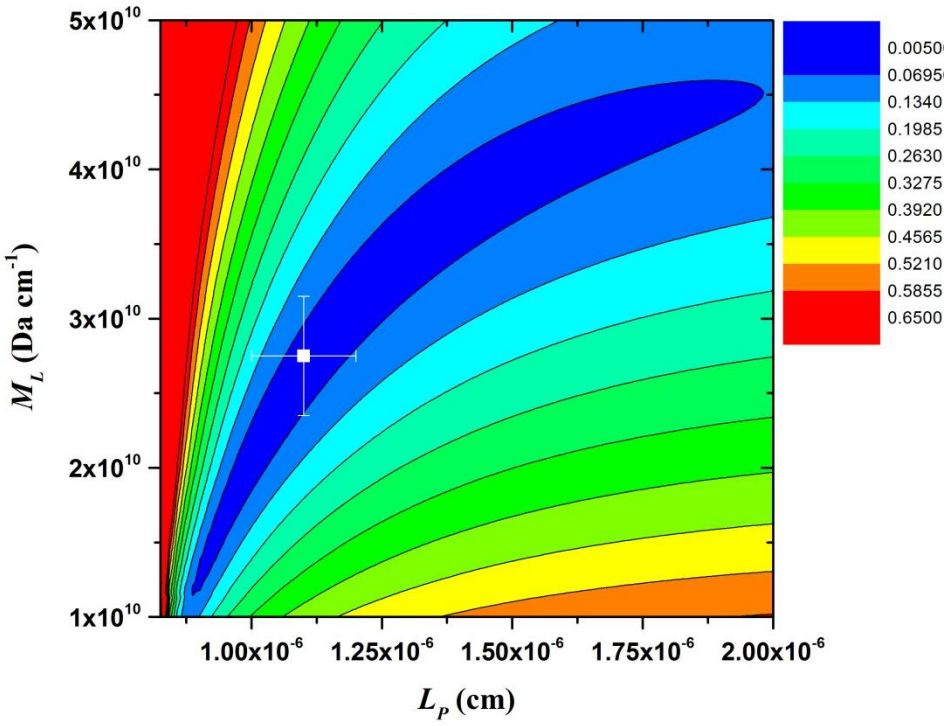


**Figure 2.14:** Contour plots of the mucin Nov13. The target function, $\Delta$ calculated based on variables values of $L_p$ and $M_L$, and are represented on the full colour spectrum from blue ($\Delta$ = 0.005) to red ($\Delta \geq 0.65$) (see *Chapter 7*).

The variable parameters floats in order to find a minimum of the multi-sample target function, $\Delta$ for $L_p$ and $M_L$. Consequently, dimensionless estimate of the target function is calculated through the agreement between the theoretical calculated values – of sedimentation coefficient and intrinsic viscosity for a particular molecular weight, persistence length and mass per unit length – and the experimentally measured parameters (see, e.g. Ortega and Garcia de la Torre, 2007; Morris et al., 2008). Over the range of values for $M_L$ and $L_p$ target function are calculated, the final data is represented as contour plots, a full colour spectrum ranging from blue to red, where $L_p$ (cm) in the x-axis and $M_L$ (Da $cm^{-1}$) in the y-axis (Figure 2.14).

# CHAPTER 3

# MOLECULAR CONFORMATION STUDY OF LAMBDA CARRAGEENAN IN AQUEOUS SOLUTION

We now consider the first of the marine polysaccharide namely lambda carrageenan. The study examined the molecular conformation of lambda carrageenan in aqueous solution. The microwave irradiation (sealed vessel microwave bomb) method was used in order to achieve the true molecular solubility and prevent formation of any aggregates or superstructure of polysaccharides. This method appears to break the main chain of the polysaccharide and increase the macromolecular solubility. Thus, this methodology was applied for two different lambda carrageenan samples, to generate more preparations for this study. Then preparations were assessed to obtain various hydrodynamic parameters by a combination of analytical ultracentrifugation, size-exclusion chromatography, light scattering and capillary viscometry, to estimate their heterogeneity and conformation in aqueous solvent.

## 3.1 INTRODUCTION

Carrageenans are a family of linear polysaccharides repeating galactose units with different sulphate groups and anhydro-bridges. These sulphated polysaccharides are combined alternately by $\alpha$-(1,3) and $\beta$-(1,4) glycosidic

bonds (Imeson, 2009). Carrageenans are found in "red" seaweeds (*Rhodophyceaea*) and the most important members of the family are kappa (κ), lambda (λ), and iota (ι). *Chondrus crispus* is the main source of kappa and lambda and iota and kappa are extracted from *Eucheuma spinosum* and *cottonii* (see, for example, Campo, Kawano, Silva and Carvalho, 2009). The diversity of the chemical structures of the carrageenan types are due to the different 3,6-anhydrogalactose and ester sulphate group content. Variation in structure gives unique characteristics for each type, including gel strength, viscosity, temperature stability, synergism and solubility. For example, the high number of sulphate groups causes the carrageenan molecule to be more water soluble, whereas anhydro-bridges produce a hydrophobic behaviour (Tombs and Harding, 1998; Hoefler, 2001).

Lambda carrageenan is the most soluble with three sulphate groups per disaccharide repeat and as it contains no 3,6 anhydrogalactose residues it cannot form gels (Figure 3.1). The high viscosities of its solutions and inability to form gels have made lambda carrageenan a popular thickening agent (Therkelsen, 1995; Bonferoni et al., 1994). The difference in rheological behaviour (in particular forming thermoreversible gels) between lambda carrageenan and both (kappa and iota) is due to the absence of an anhydro-bridge. The 3,6-anhydro is a prerequisite for ring inversion to occur with $^4C_1$ conformation forming a $^1C_4$ chair which is required to make a gel. Failure of the lambda carrageenan to invert into a $^4C_1$ chair prevents gelation. In addition, the degree of sulphation has a further inhibitory effect on gelation of lambda carrageenan (Coultae, 2009; van De Velde et al., 2002). Nevertheless, it has recently been shown that lambda carrageenan gelation is possible induced by

trivalent iron ions, which has extended its priority beyond a viscosity enhancing agent (Running et al., 2012).

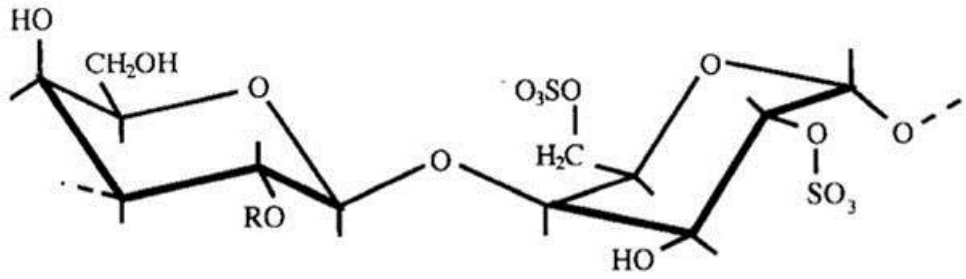


**Figure 3.1**: Lambda carrageenan repeat unit. Adapted from Perez *et al.*, (1996).

The ester sulphate groups have made carrageenans a highly negatively charged molecule, allowing it to interact with other positively charged macromolecules (proteins or polysaccharides). Earlier studies have been carried out on protein carrageenan interactions, showing that, as result of the interaction aggregation of sulphated polysaccharides with proteins are protected from losing solubility (Langendorff et al., 1999; Weinbreck et al., 2004). In particular, interaction was observed for the mixture of lambda carrageenan, rather than kappa or iota, with gluten proteins; a mixture used in dough ingredients to improve bread volume (León et al., 2000). Moreover, a study by Langendorff and his co-workers (2000) confirmed attractive interactions occurred between the most highly charged form lambda carrageenan and casein micelles under different conditions of temperature. However, interactions with other polysaccharides have been observed between lambda carrageenan and chitosan at a weight ratio of 3:1 respectively, and the complex showed interesting properties use for

drugs release (Hugerth et al., 1997; Shumilian and Shchipunov, 2002). It has also been found that the complex physicochemical properties (such as mechanical stabilities and swelling behaviours) have been affected by several factors, in particular weight ratio and salt concentrations (Tapia et al., 2004). Furthermore, enhancing the knowledge of carrageenans and their polyelectrolyte complexes properties – strong negative charge, gelling and viscosity – enables the improvement of their utilization in food, pharmaceutical and healthcare industries (see, for example, Li et al., 2014).

Lambda carrageenan has long been used as a thickening agent and for its water binding effectively in foods and biopharmaceutical products: the higher capacity of binding water make it more hydrated at room temperature and the highest sulphate content seems to reduce the tendency for self-interactions (Imeson, 2009). Mostly, lambda carrageenan has been used to stabilise food products such as milk, ice cream, coffee-whitener, milk shake, chocolate milk, and fruit drink (Therkelsen, 1995; Tombs and Harding, 1998). One of its most exciting uses in pharmaceuticals is controlled release of drugs, especially at the earlier stage of the release process (Bonferoni et al., 1994). Lambda carrageenan has also shown potent immunogenic activity against HIV and some tumours (Nakashima et al., 1987; Zhou et al., 2004). Thus, critical to understanding the functional properties of this molecule is an understanding of its fundamental properties of homogeneity, molecular weight, conformation and flexibility.

Progress has been made in earlier studies on the properties of these molecules – for example Slootmaekers et al (1991a,b) have considered the sedimentation, viscosity and light scattering behaviour of a lambda carrageenan of M~ 610000

g. $mol^{-1}$ and Berth et al (2008) have considered the use of light scattering, viscosity and multi-angle laser light scattering coupled to size exclusion chromatography of a larger lambda carrageenan (M~ 920,000 $g.mol^{-1}$). We take advantage of recent advances in analytical ultracentrifugation in particular improvements in the extraction of the sedimentation coefficient to deal with the problem of the high concentration dependence through non-ideality. Two samples of lambda carrageenan with different molecular weight were irradiated for varying times using microwave heating in a high pressure vessel to estimate their hydrodynamic parameters (e. g. molecular weight, sedimentation coefficient, and intrinsic viscosity) and conformational behaviour in aqueous solution.

## 3.2 MATERIALS

Two lambda carrageenan samples GM-λ690 and TF-λ730 were kindly provided by Glycomix Ltd (Reading, United Kingdom) and CPKelco, (Lille Skensved, Denmark), respectively. Both samples were used as supplied without any further purification and assumed to be of similar composition. A stock solution of 3.0 mg $mL^{-1}$ for both GM-λ690 and TF-λ730 were made up in deionised distilled water then dialysed into phosphate-chloride buffer solution supplemented with NaCl to an ionic strength 0.1M and pH 7.0 (Green, 1933). The concentration was measured (after dialysis) using an Atago (Fairfax, Canada) DD-5 refractometer calibrated with glucose standards. The solutions of native lambda carrageenan GM-λ690 and TF-λ730 were then exposed to microwave (see, e.g. Wood et al, 2002) heating in an 800 W

microwave oven (Panasonic UK Ltd. Bracknell, UK) using a high pressure vessel for different time periods that facilitated producing different molar masses. The temperature and pressure within the "bomb" were not measured. Heating for 15 seconds generated GM-λ850 and TF-λ870 and heating for 30 seconds produced GM-λ460 and TF-λ340. Heating for longer periods (more than 30 second) led to discoloration of the samples.

# 3.3 METHODS

## 3.3.1 Sedimentation Velocity (SV)

Sedimentation velocity in the analytical ultracentrifuge was used to probe the heterogeneity of solutions as well as to measure the sedimentation coefficient (Harding, 1992; 2005a). Polysaccharide samples (~400µl) after serial dilution by dialysate and the phosphate buffer dialysate (400µl) at pH 7.0 and ionic strength (0.1M) were injected into sample and reference channels, respectively of a double sector 12.0 mm optical path length epoxy cells with sapphire windows. The Rayleigh interference optical system was used for recording concentration profiles and the movement of the sedimentation boundary in the analytical ultracentrifuge cell (see, e.g. Harding, 2005b). An initial low rotor speed of 3000 rpm was accelerated to a rotor speed of 40,000 rpm after time was allowed for vacuum formation (≤ 50 microns) and for temperature equilibration (i.e. 20.0 $^{o}$C). Scans were taken at 2 min intervals for a run time of ~ 24 hours. The standard conditions of density and viscosity of water at 20.0 $^{o}$C were used for adjustment of the sedimentation coefficients $s$ to $s_{20,w}$ values (Schachman, 1959). The data was analysed using the SEDFIT procedure (Dam

and Schuck, 2004) which solves the Lamm equation describing the change of concentration distribution with radial position with time in terms of a distribution of sedimentation coefficients, g*(s) vs *s*, where the (*) indicates that the distribution of sedimentation coefficients has not been corrected for diffusion effects (see, e.g. Harding, 2005b). The (differential) distribution of sedimentation coefficients g*(s) can be defined as population – weight fraction – of species with a sedimentation coefficient between *s* + *ds* (Dam and Schuck, 2004; Harding, 2005a). The sedimentation coefficient expressed in terms of the standard conditions of the viscosity and density of water at 20.0 $^{o}$C, $s_{20,w}$. To eliminate the effects of non-ideality (co-exclusion and any residual polyelectrolyte effects) a plot of the reciprocal of the sedimentation coefficient ($1/s_{20,w}$) against concentration, $c$ (g mL$^{-1}$) was made and from the intercept at infinite dilution $c$=0, the value free of these effects was found: $s^{o}_{20,w}$ (units seconds, s, or Svedbergs, S, where 1S = $10^{-13}$s). The following relation (Gralén, 1944) was used for the extrapolations:

$$(1/s_{20,w}) = (1/s°_{20,w}).(1+k_s.c) \qquad (3.1)$$

where $k_s$ is the "Gralen" coefficient (unit – mL g$^{-1}$). Analysis of the change in sedimentation coefficient distributions was used to ascertain the presence of an interaction.

## 3.3.2 Sedimentation Equilibrium (SE)

Samples were prepared at concentration of 0.3 mg mL$^{-1}$, after dialysis for 24 hours at the ambient temperature in phosphate-chloride buffer solution

supplemented with NaCl (PBS) at ionic strength (0.1M). Sedimentation equilibrium experiments were performed using the Beckman (Palo Alto, California, U.S.A.) Optima XL-I analytical ultracentrifuge equipped with Rayleigh interference optics and an automatic on-line data capture system. The modified long (20.0 mm) optical path length double-sector cells with sapphire windows were loaded with (~ 80 μl) of dialysed sample and a matching amount of reference buffer (dialysate) in appropriate channels. The balanced cells were then loaded into an analytical 8-hole titanium rotor An50-Ti and placed in the analytical ultracentrifugation. After time was allowed for vacuum formation (≤ 50 microns) and for temperature equilibration (20.0 $^{o}$C), the rotor was then accelerated to 4000 rpm; rotor speeds were selected to be sufficiently apart to give a good solute distribution (Scott and Schuck, 2005). Using the Rayleigh interference optical system, scans were taken every one hour and equilibrium was reached after approximately 72 hours. A record of the relative concentration distribution of the solute at equilibrium was analysed to give the weight average apparent molecular weight $M_{w,app}$ using the SEDFIT-MSTAR algorithm implemented by Schuck and co-workers. (Schuck et al., 2014) based on the algorithm of Cölfen and Harding (Cölfen and Harding, 1997) and the $M^*$ function of Creeth and Harding (1982). Using the long path length cells (20.0 mm) allowed us to worke at low loading concentration, which is still yielded a sufficient signal. Thus, non-ideality effects will be small and hence the apparent weight average molecular weight will be approximately equal to the true weight average molecular weight $M_w$ *at* such concentration (Harding, 2005b). A partial specific volume value of 0.53 mL $g^{-1}$ was used for the analyses for all lambda carrageenan samples.

### 3.3.3 Size Exclusion Chromatography Coupled to Multi Angle Light Scattering (SEC-MALS)

The macromolecular characteristics and integrity of the lambda carrageenan samples were also determined in terms of polydispersity and molecular weight using SEC-MALS (Wyatt, 1992, 2013); a technique which has been successfully applied to polysaccharide characterisation since Horton et al., (1991). It contains an X-Act 4 channel degassing unit (Jour Research, Sweden), Jasco intelligent HPLCPump-PU-1580 (E) (Jasco, Tokyo, Japan), fitted with a Spark-Holland Marathon Basic autosampler (Spark Holland, Emmen, The Netherlands) combined with a guard column and TSK-G6000PW and G4000PW columns connected in series (Tosoh Bioscience, Tokyo, Japan), and a columns temperature regulator (Anachem, Luton, U.K.). DAWN®HELEOS-$^{TM}$II, an 18-angle light scattering detector was used (for light scattering intensity) for the measurement of absolute molecular weight, size and conformation of macromolecules in solution (Wyatt Technology Corporation, California, U.S.A.). A ViscoStar$^{TM}$ viscometer online differential viscometer was used to measure the intrinsic viscosity (Technology Corporation, California, U.S.A.). Also an Optilab® rEX refractive index detector in series is used to measure the concentration (Wyatt Technology Corporation, California, U.S.A.). Solutions of lambda carrageenan samples prepared at a concentration of 0.5 mg mL$^{-1}$ were filtered through a 0.45 μm syringe filter (Whatman, Maidstone, England) - to remove any insoluble material or dust prior to being injected into the auto-sampler. The phosphate-chloride buffer (pH=7 and I=0.1) was pumped at a flow rate 0.8 mL min$^{-1}$ through the column system. At ambient temperature each solution (100 μl) was injected into the columns.

ASTRA$^{TM}$ (Version 5.1.9.1) software (Wyatt Technology, Santa Barbara, U.S.A.) was used for collection and analysis using all 18 MALS angles along with the concentration data from the on-line differential refractometer. A linear fit to the "Debye" plot of $Kc/R_\theta$ *vs* $sin^2(\theta/2)$, where the terms have their usual meaning (see, for example Wyatt 2013) was used for calculating the absolute weight average molecular weight ($M_w$) using the following values for the refractive index increment: lambda carrageenan *dn/dc* = 0.116 mL $g^{-1}$ (Slootmaekers et al., 1991b). Because of the low concentrations after dilution on the columns no correction for non-ideality was assumed necessary.

### 3.3.4 Capillary and Differential Pressure Viscometry

The relative viscosities $\eta_{rel}$ of lambda carrageenan native and heated samples in ranging concentration ($c$) from 0.1 – 1.0 mg $mL^{-1}$ were measured from the ratio of flow times of solution to solvent using a 2 mL Ostwald viscometer. The U-tube viscometry was suspended in an accurate temperature regulated water bath. The temperature was kept constant at (20.00 ± 0.01) °C throughout by using a coolant system. Because of the low concentrations no correction for solution density was necessary (Harding, 1997). The reduced ($\eta_{red}= (\eta_{rel}-1)/c$) and inherent ($\eta_{inh} = (\ln\eta_{rel})/c$) viscosities were extrapolated to infinite dilution to eliminate non-ideality effects using both the (Huggins, 1942) and (Kraemer, 1938) approaches:

$$\eta_{red} = [\eta] (1+K_H [\eta] c) \quad (3.2)$$

$$\eta_{inh} = [\eta] (1- K_K [\eta] c) \quad (3.3)$$

where the intrinsic viscosity [η] is taken as the mean of intercepts from Eqs. (3.2) and (3.3) and $K_H$ and $K_K$ are the Huggins and Kraemer constants, respectively. To avoid possible ambiguities through transition from the dilute to the semi-dilute region [η] was also estimated from the Solomon-Ciuta relation, essentially a combination of the Huggins and Kraemer lines (see, e.g. Harding 1997):

$$[\eta] \approx (1/c)[2(\eta_{rel} - 1) - 2 \ln (\eta_{rel})]^{1/2} \quad (3.4)$$

It is normally carried out at a given concentration; but it was used at the same concentration series as Huggins and Kraemer in order to confirm the results determined from both equations. Furthermore, relative viscosities were also estimated from a Viscostar (Wyatt Technology) differential pressure viscometer linked on-line to the SEC-MALS system (Harding, 1997). Because of the higher sensitivity of the sensors and the high dilution from the column, eqn (3.4) was used to obtain [η] without a concentration extrapolation.

# 3.4 RESULTS

## 3.4.1 Sedimentation Coefficient and Sedimentation Coefficient Distribution

The results of sedimentation velocity experiments for lambda carrageenan (GM-λ690 and TF-λ730) and their preparations (heated 15s (GM-λ850 & TF-λ870) and 30s (GM-λ460 & TF-λ340)) are analysed in terms of table of data (Table 3.1). The sedimentation coefficient, *s* was obtained for all samples at

serial concentrations using the least squares ls-g*(s) method of Dam and Schuck (2004). The ls-g* (s) distribution method demonstrates the highly pureity and the good solubility of all lambda carrageenan samples, represented by unimodal distribution plots (Figure 3.2): a shoulder at the highest concentration peaks were seen for all samples, suggestive of the presence of higher molecular weight material.

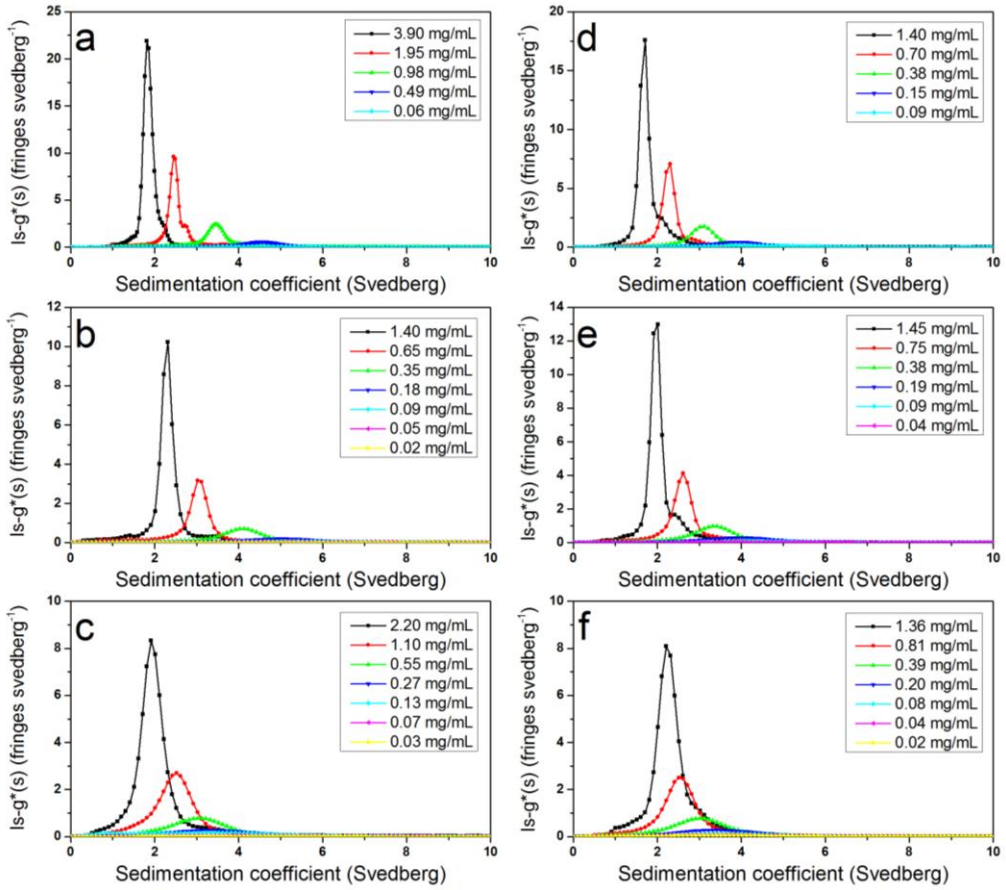


**Figure 3.2:** Sedimentation coefficient distribution profiles using least squares g*(s) method of SEDFIT obtained from sedimentation velocity experiment for lambda carrageenan samples (a) GM-λ690 (b) GM-λ850 (c) GM-λ460 (d) TF-λ730 (e) TF-λ870 (f) TF-λ340.

The values of apparent weight average $s_{20,w}$ however, all increased with decrease in concentration, showing no evidence of reversible associative behaviour. Even across the small range of concentrations used there was considerable concentration dependence of the sedimentation coefficient through the effects of non-ideality as found earlier by Slootmaekers co-workers (Slootmaekers et al., 1991a).

**Table 3.1**: Summary of $s^{\circ}_{20,w}$ and $k_s$ results for all lambda carrageenan unheated and heated samples.

| Sample | $s^{\circ}_{20,w}$ (S) | $k_s$ (mL g$^{-1}$) |
|---|---|---|
| **GM-λ690** | 5.4±0.4 | 495±55 |
| **GM-λ850** | 6.2±0.3 | 1280±105 |
| **GM-λ460** | 4.5±0.3 | 595±80 |
| **TF-λ730** | 5.0±0.3 | 925±105 |
| **TF-λ870** | 5.3±0.3 | 1130±160 |
| **TF-λ340** | 3.2±0.2 | 555±70 |

Figure 3.3 also shows the reciprocal plots of sedimentation coefficient vs concentration extrapolated to infinite dilution using Equation 3.1 for all samples. In particular the determination of the concentration dependence of sedimentation, $k_s$ is yielded information about conformation, interparticular interaction and properties of particles.

However, an increase in sedimentation coefficient value was observed for both lambda carrageenan samples heated for a short time (15 s) compared to unheated. This could reflect the final dispersity of the higher molecular weight material. Heating for a short time (15 s) exhibited good dispersibility without

degradation. The values of lambda carrageenan samples (GM-λ460 & TF-λ340) describe a decrease in sedimentation coefficient with additional 15s heating confirming depolymerisation of lambda carrageenan chains.

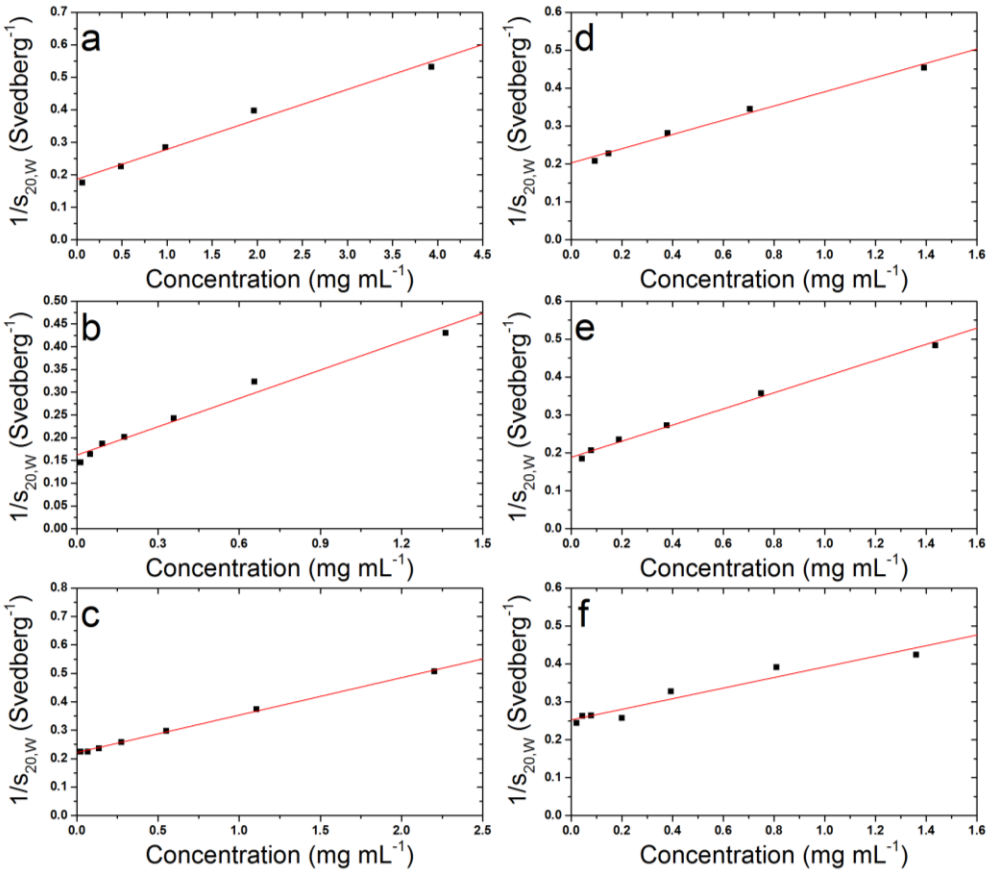


**Figure 3.3:** Concentration dependence (reciprocal) of the sedimentation coefficient plot (after correction to standard solvent conditions) for lambda carrageenan samples (a) GM-λ690 (b) GM-λ850 (c) GM-λ460 (d) TF-λ730 (e) TF-λ870 (f) TF-λ340.

## 3.4.2 Estimation of Molecular Weight

The weight average molecular weight results for lambda carrageenan samples (unheated and heated) were obtained from sedimentation equilibrium

experiment in analytical ultracentrifugation (Table 3.2). Intriguingly the value for the 15 s microwave heated samples (GM-λ850 and TF-λ870) yielded a slightly higher molecular weight than that of unheated samples (GM-λ690 and TF-λ730). This may reflect the final dispersion of higher molecular weight material. Heating for a short time (15 s) again exhibited good dispersibility without degradation consistent with sedimentation coefficient data. Heating for an additional 15 second (30 s) led to clear chain scission with a clear reduction in molecular weight (samples GM-λ460 and TF-λ340). Further application of heat led to discoloration of the sample, and such samples were not used for further characterisation. Figure 3.4 presents weight average molecular weight ($M_w$) yielded using SEDFIT-MSTAR.

**Table 3.2**: Summary of molecular weights *($M_w$)* results for lambda carrageenan unheated and heated samples from sedimentation equilibrium and SEC-MALS.

| **samples** | **$10^{-3}$ x $M_w$ (g $mol^{-1}$)[a]** | **$10^{-3}$ x $M_w$ (g $mol^{-1}$)[b]** | **Polydispersity index [b]** |
|---|---|---|---|
| **GM-λ690** | 590±90 | 690±40 | 1.10 |
| **GM-λ850** | 840±60 | 850±50 | 1.80 |
| **GM-λ460** | 460±30 | 460±30 | 1.02 |
| **TF-λ730** | 650±60 | 730±40 | 1.10 |
| **TF-λ870** | 850±50 | 870±40 | 1.85 |
| **TF-λ340** | 340±30 | 340±20 | 1.02 |

a : molecular weight obtained from sedimentation equilibrium
b : molecular weight obtained from SEC-MALS

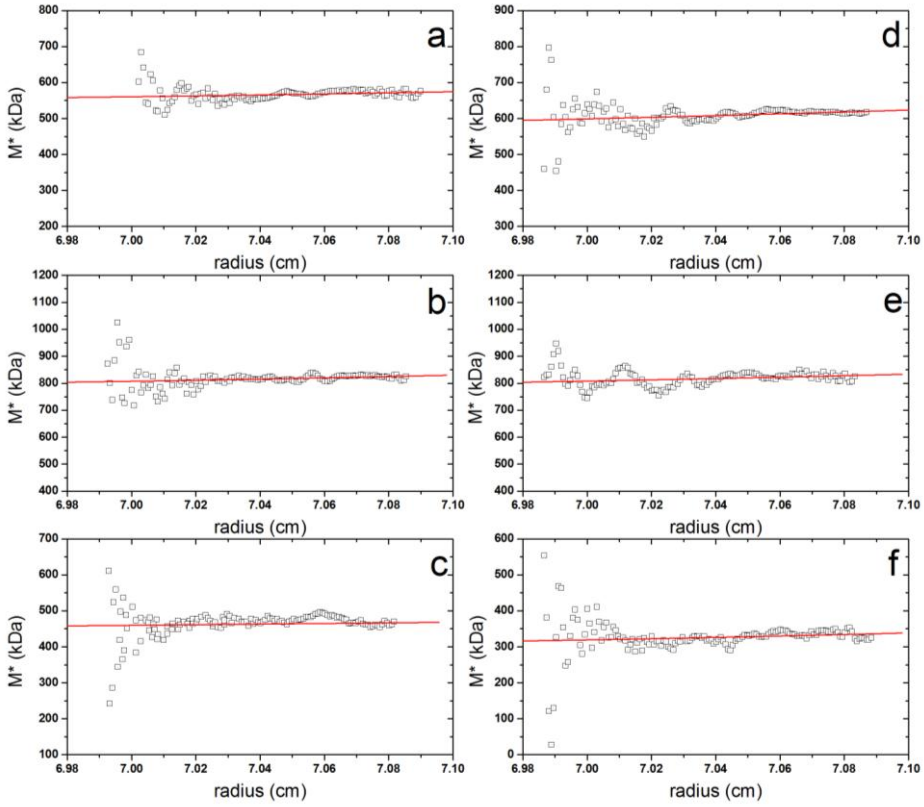


**Figure 3.4:** Molecular weight plots for lambda carrageenan samples GM-λ690, GM-λ850, GM-λ460 (a, b and c, respectively), TF-λ730, TF-λ870 and TF-λ340 (d, e and f, respectively) using SEDFIT-MSTAR: *M** versus *r* plot (open squares) and fit based on the *M** transformation of the *c(M)* fit of the raw data (red line): the value of *M** extrapolated to the cell base = $M_{w,app}$ the apparent weight average molecular weight for whole distribution.

Using long optical path length cells (20.0 mm) allowed us to work at relatively low concentration (0.3 mg $mL^{-1}$). This helped to minimize the non-ideality arising from co-exclusion and polyelectrolyte effect. Thus, at this loading concentration the apparent molecular weight $M_{w,app}$ is ~$M_w$ the true or ideal weight average molecular weight.

However, it was possible to obtain the weight average molecular weight and its distribution for each elution volume (*V*) or slice using size exclusion

chromatography coupled to multi angle light scattering (SEC-MALS). Since the concentration was also recorded as a function of elution *V* from refractive index (RI) detectors. For each lambda carrageenan sample the molecular weight results were then measured based on this method and are reported in (Table 3.2). Unimodal elution profiles were yielded for all lambda carrageenan samples showing homogeneous preparations and again consistent with sedimentation coefficient distribution data: a broader distribution was also observed for each sample indicative of the presence of higher material (Figure 3.5 a and b). Within the error estimate the weight average molecular weight results obtained for each lambda carrageenan from SEC-MALS are consistent with those found by sedimentation equilibrium.

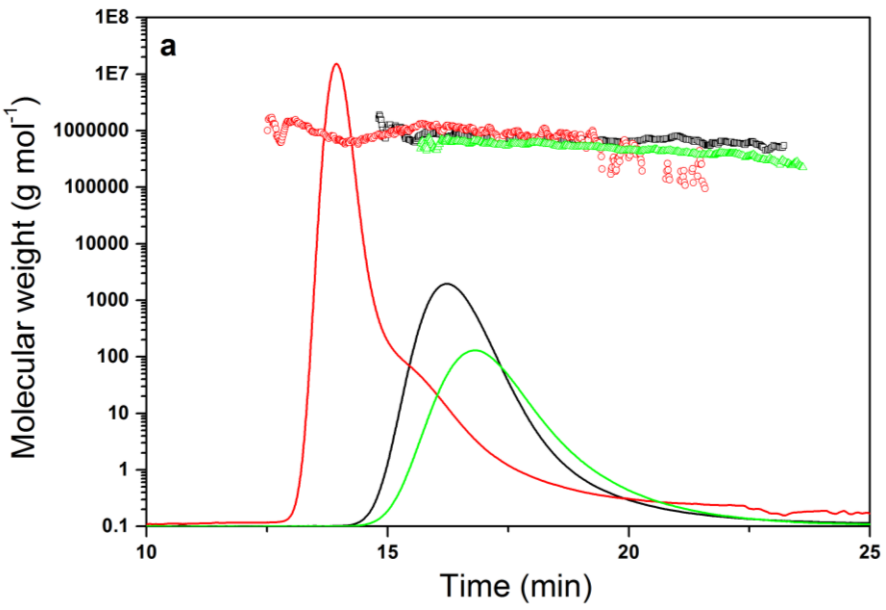


**Figure 3.5a**: Elution profiles of the lambda carrageenan samples GM-λ690 (black line), GM-λ850 (red line) and GM-λ460 (green line) examined by SEC-MALS at concentration 0.5 mg $mL^{-1}$. The horizontal black (open square), red (open circle) and green (up triangle) lines correspond to SEC-MALS calculated molecular weights for lambda carrageenan samples GM-λ690, GM-λ850 and GM-λ460, respectively.

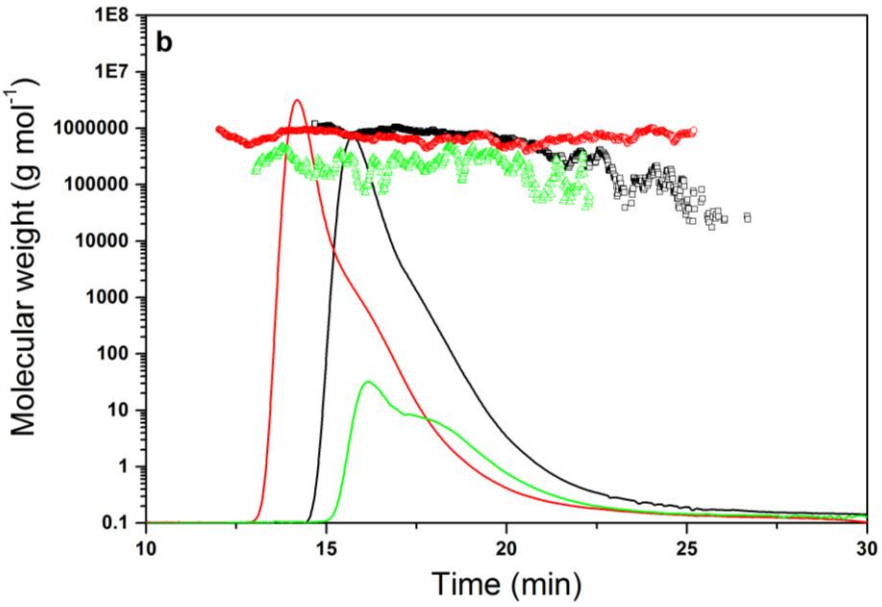


**Figure 3.5b**: As (Figure 3.5a) but the analysis of lambda carrageenan samples TF-λ730 (black), TF-λ870 (red) and TF-λ340 (green) at concentration 0.5 mg $mL^{-1}$.

### 3.4.3 Intrinsic Viscosity

The intrinsic viscosity values for lambda carrageenan samples, reported in Table 3.3, showed a good linear extrapolation in all cases for Huggins, Kraemer and Solomon-Ciuta plots (Figure 3.6). Heating both lambda carrageenan samples (GM-λ690 TF-λ730) for a short time (15 s) led to an increase in the intrinsic viscosity, which again confirms the dispersion of higher molecular weight material and is consistent with sedimentation coefficient and molecular weight results. A further 15 second heating induced the degradation of the polymer chain, and yielded a decrease in intrinsic viscosity: the results also confirm the deplymerisation of lambda carrageenan chains and correspond to sedimentation coefficient and molecular weight results.

**Table 3.3:** Intrinsic viscosity values for lambda carrageenan unheated and heated samples from capillary viscometry and differential pressure viscometry (Viscostar in SEC-MALS).

| Sample | Intrinsic viscosity [η] (mL g $^{-1}$) | | | |
|---|---|---|---|---|
| | Capillary viscometry | | | Online Viscostar ™ |
| | Huggins | Kraemer | Solomon-Ciuta | |
| **GM-λ690** | 1120±100 | 1260±60 | 1230±70 | 1300±50 |
| **GM-λ850** | 1570±20 | 1600±25 | 1600±25 | 1550±30 |
| **GM-λ460** | 1060±10 | 1070±10 | 1080±10 | 1050±20 |
| **TF-λ730** | 940±10 | 960±5 | 960±5 | 970±10 |
| **TF-λ870** | 1080±40 | 1080±35 | 1080±35 | 1050±30 |
| **TF-λ340** | 640±30 | 630±30 | 635±30 | 700±40 |

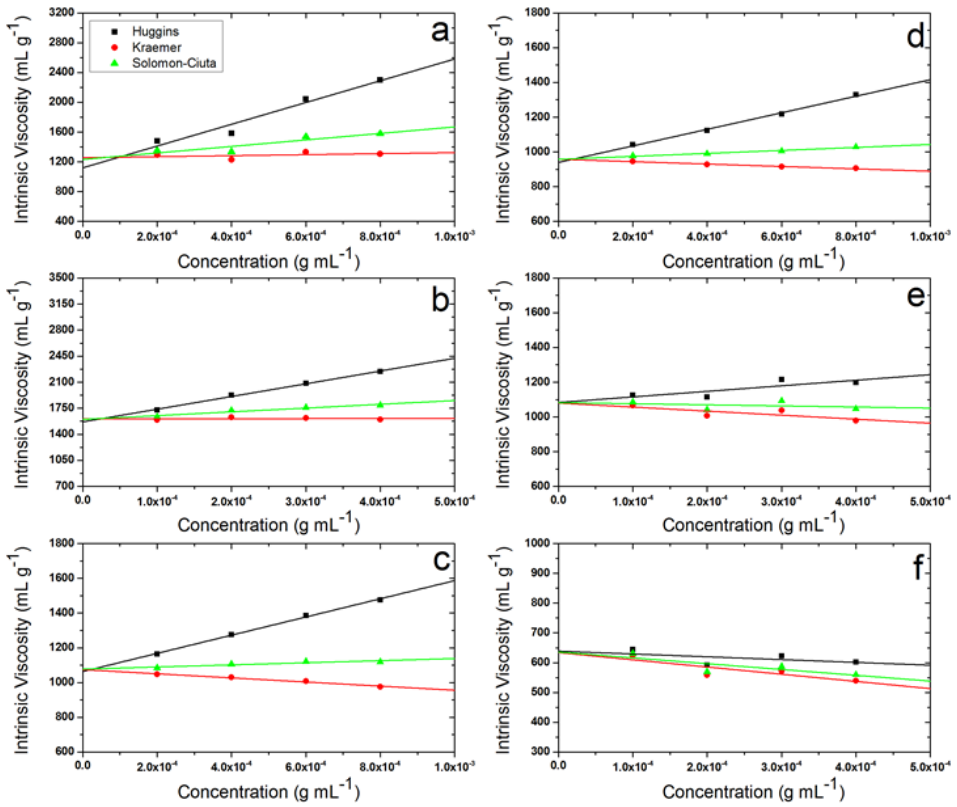


**Figure 3.6:** The intrinsic viscosity plot from capillary viscometry: Huggins, Kraemer and Solomon-Ciuta extrapolations for (a) GM-λ690, (b) GM-λ850, (c) GM-λ460, (d) TF-λ730, (e) TF-λ870 and (f) TF-λ340.

The values of the intrinsic viscosity, particularly for the GM-λ690 and TF-λ730 samples, are similar to other non-gelling viscosifying agents used in industry, such as the galactomannans and glucomannans.

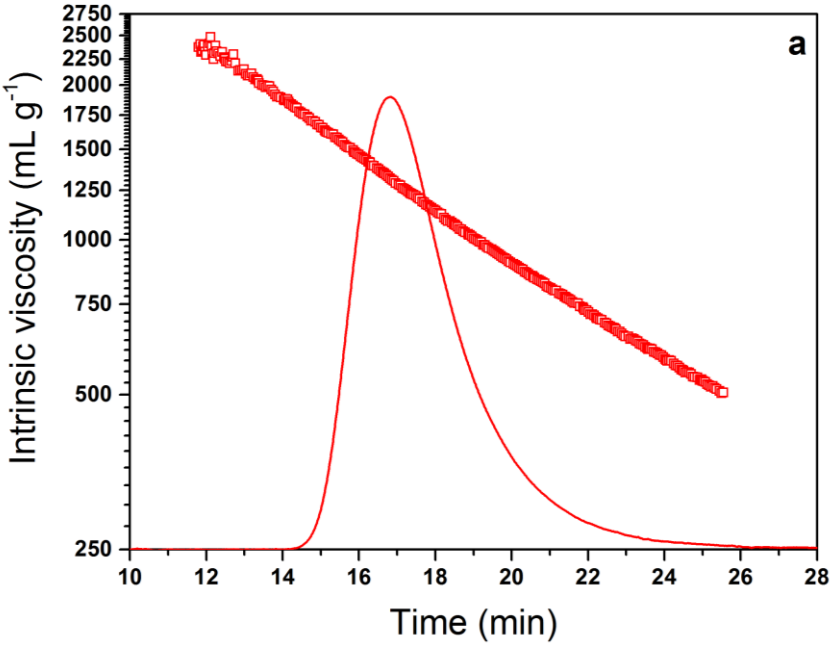


**Figure 3.7a**: Intrinsic viscosity (mL $g^{-1}$) plot (red line) versus retention time (min) for GM-λ460 from the differential pressure viscometer (Viscostar coupled to SEC-MALS). The red squares correspond to SEC-MALS calculated intrinsic viscosity.

However, Table 3.3 also reports the intrinsic viscosity for all lambda carrageenan samples obtained from the differential pressure viscometry with SEC-MALS. The average [η] for the whole undistrbuated sample can be specified as well as the intrinsic visocisty [η] ($V_e$) as function of elution volume $V_e$. The results confirmed the dispersion of higher material and deplymerisation phenomenons for samples heated for 15 s and 30 s, respectively, and are in excellent agreement with those from capillary

viscometry. Figure 3.7 (a) and (b) show examples of intrinsic viscosity profile against time for GM-λ460 and TF-λ340 respectively. Both demonstrate the decrease of intrinsic viscosity with the decrease of sample concentration.

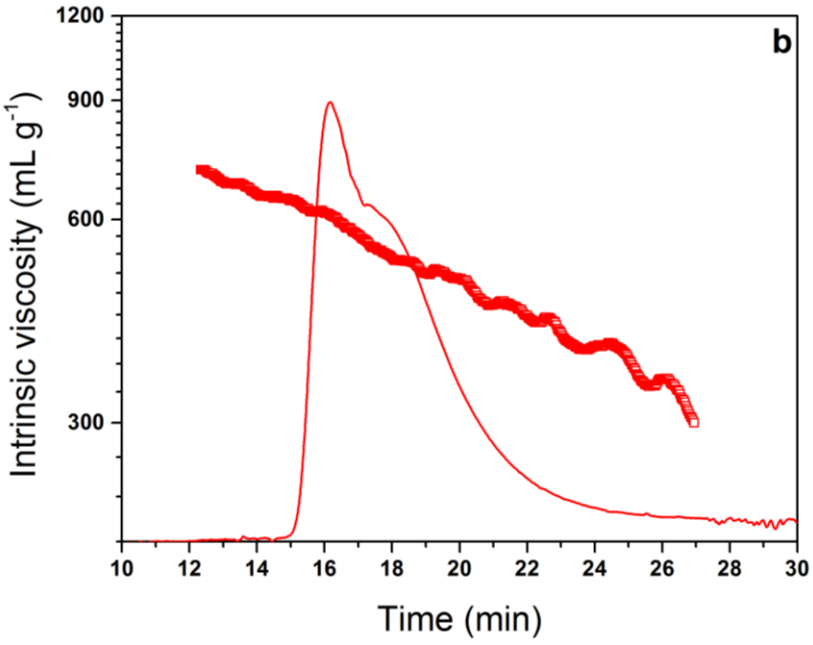


**Figure 3.7b**: Intrinsic viscosity (mL $g^{-1}$) plot (red line) versus retention time (min) for TF-λ340 from the differential pressure viscometer (Viscostar coupled to SEC-MALS). The red squares correspond to SEC-MALS calculated intrinsic viscosity

### 3.4.4 Conformational Analysis

Lambda carrageenan has a greater range of capabilities such as immunogenic activity against HIV and some tumours: thus the effectiveness of its functional properties depend on size, shape and conformation in solution. Various exciting methods designed to study the molecular conformational behaviour. Some of the most applicable methods have been applied for lambda carrageenan samples in this study.

### 3.4.4.1 Wales-van Holde Ratio (R):

The Wales-van Holde (1954) ratio $R = k_s / [\eta]$ provides a useful indicator of a molecular conformation of flexibility. The limits are ~ 1.6 for a compact sphere or a (non-draining) random coil (Creeth and Knight, 1965), and ~ 0.15 for rods (see, for example, Tombs and Harding, 1998). Values of the Wales-van Holde ratio have been yielded using the results of the concentration dependence coefficient or the Gralen parameter; $k_s$ (determined from the sedimentation coefficient), and intrinsic viscosity (from the capillary viscometry) for each lambda carrageenan sample, are reported in Table 3.4.

**Table 3.4:** Wales-van Holde ration for lambda carrageenan unheated and heated samples.

| Sample | $k_s$ / [η] |
|---|---|
| **GM-λ690** | 0.4 |
| **GM-λ850** | 0.8 |
| **GM-λ460** | 0.6 |
| **TF-λ730** | 1.0 |
| **TF-λ870** | 1.0 |
| **TF-λ340** | 0.9 |

From the results of Wales-van Holde ration it appears that the GM-λ samples (690, 850 and 460) are adopting a semi-flexible structure ($R$ = ~0.4-0.8) and is similar to those of konjac glucomannan (Kök et al., 2009) and Pectin (Morris et al., 2000). However, the TF-λ samples (730, 870 and 340) are consistent with a more flexible structure ($R$ = ~ 1), possibly extended than a random coil and consistent with a value previously estimated for kappa carrageenan (Harding et al., 1997).

### 3.4.4.2 Mark-Houwink-Kuhn-Sakurada Power Law Relationship:

Hydrodynamic parameters – molecular weight, sedimentation coefficient and intrinsic viscosity– obtained from analytical ultracentrifugation (sedimentation velocity and equilibrium), SEC-MALS and capillary viscometry experiments were further used to study the gross conformation of lambda carrageenan (GM-λ and TF-λ) (Harding et al., 1991). Taking advantage of the fact that heating for different times resulted in different weight-average molecular weights, $M_w$ this facilitated the use of the "Mark-Houwink-Kuhn-Sakurada " (MHKS) power law relation linking both sedimentation coefficient, $s^o_{20,w}$, and intrinsic viscosity, [η]with molecular weight, $M$

$$s^o_{20,w} = K_s \ M^{\,b} \tag{3.5}$$

$$[\eta]=K_\eta \ M^{\,a} \tag{3.6}$$

Values of the MHKS exponents *a* and *b* can be used as another method of assessing the conformation of polymer chain based on the knowledge of the general conformations by HAUG triangle (Tombs and Harding, 1998). Compact sphere, random coil and rigid rod are extremes of macromolecular conformation are placed at the corners of the HAUG triangle, and are the limits of exponents *a* and *b* reported in Table 3.5. Solvent draining effects – where the solvent within the domain of a coiled molecule is free to travel at its own velocity – can also affect these parameters but these are usually small compared to the strong hydrodynamic forces between the macromolecular segments and following Tanford (1961) these are assume negligible. Figure 3.8 shows the logarithmic plots of sedimentation coefficient, $s^o_{20,w}$ versus molecular weight $M_w$ and intrinsic viscosity, [η] versus molecular weight $M_w$

for lambda carrageenan samples GM-λ (a and b respectively) and TF-λ (c and d respectively).

**Table 3.5:** Mark-Houwink-Kuhn-Sakurada Power Low exponents. Adapted from Harding, (2005b).

| Shape | *a* | *b* |
|---|---|---|
| **Compact sphere** | 0 | 0.67 |
| **Random coil** | 0.5-0.8 | 0.4-0.5 |
| **Rigid rod** | 1.8 | 0.15 |

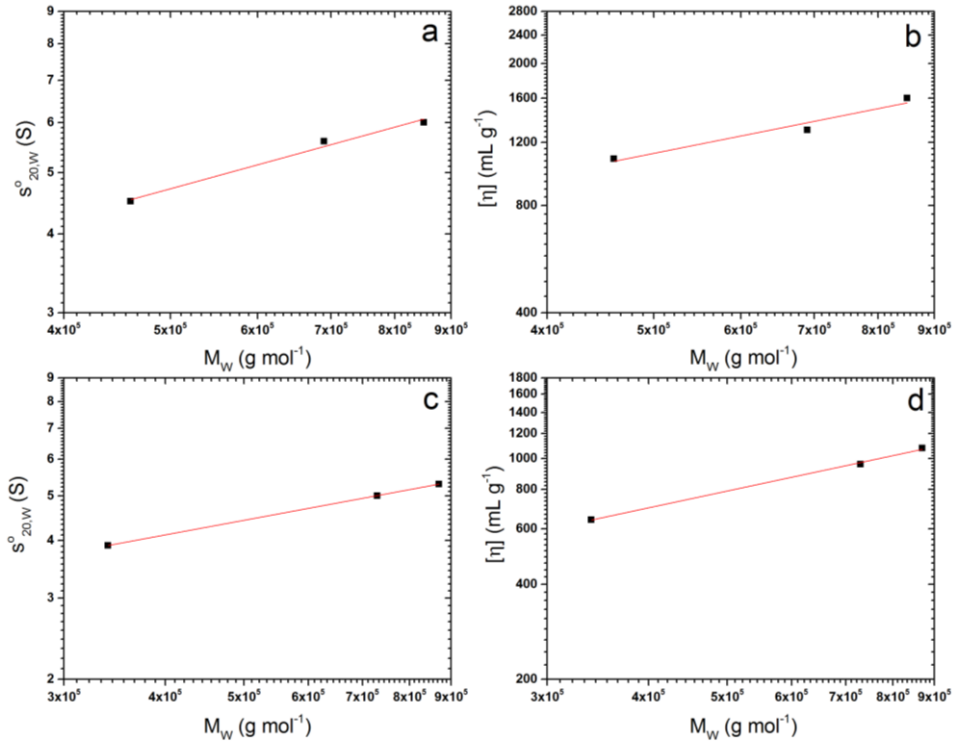


**Figure 3.8:** The Mark-Houwink-Kuhn-Sakurada (MHKS) plots for lambda carrageenan samples (GM-λ and TF-λ): (a) and (c) plots of $s^o_{20,w}$ *vs* $M_w$ for both lambda carrageenan samples GM-λ and TF-λ respectively, whereas (b) and (d) plots of [η] *vs* $M_w$ again for GM-λ and TF-λ respectively.

The values obtained of $a$ = (0.62 ± 0.1) and (0.60 ± 0.02) for both lambda carrageenan GM-λ and TF-λ respectively, are consistent with a flexible coil

conformation. The results are in an excellent agreement with that of $a$ = 0.83 (Berth et al., 2008). Whereas, the values of $b$ = (0.48 ± 0.05) and (0.32 ± 0.02) for both GM-λ and TF-λ, respectively, are again indicative of a flexible coil type molecule, which is consistent with result of $b$ = (0.32 ± 0.01) for konjac glucomannan (Kök et al., 2009).

### 3.4.4.3 Molecular Conformation Zoning

The molecular conformation type or zoning (Pavlov et al., 1999; Pavlov et al., 1997) enables an estimate of the "overall" solution conformation of a macromolecule in solution ranging from Zone A (extra-rigid rod ) to Zone E ( globular or branched ). Thus, it is represented the conformation of polymer in solution based on mass per unit length, $M_L$ and persistent length, $L_p$ parameters. Also one of the important experimental parameters is the intrinsic sedimentation coefficient, $[s]$, which can be estimated from the sedimentation coefficient, $s^o_{20,w}$ using the following relation:

$$[s] = \left[ s^o \eta_o \Big/ (1 - \bar{\upsilon}\, \rho_o) \right] \tag{3.7}$$

where $\eta_o$, is the viscosity of the solvent, $\rho_o$ is the density of the solvent and $\bar{\upsilon}$ , is the partial specific volume (0.53 mL $g^{-1}$ for lambda carrageenan). The concentration dependence of sedimentation coefficient, $k_s$ (mL $g^{-1}$) is also utilised, which is obtained from sedimentation coefficient distribution. The mass per unit length, $M_L$ (~ 610 g $mol^{-1}$ $nm^{-1}$) of lambda carrageenan is used (Berth et al., 2008).

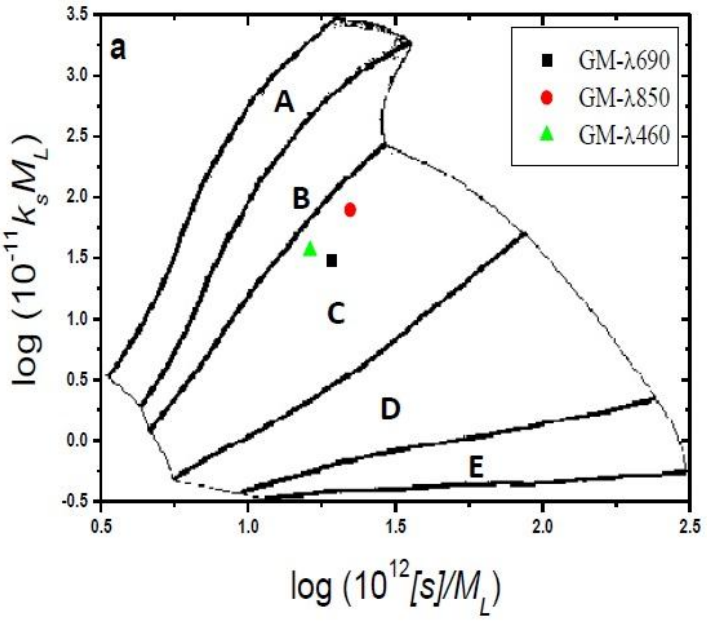


**Figure 3.9a:** The conformation zoning plot for lambda carrageenan samples GM-λ690, GM-λ850 and GM-λ460, are adopted semi-flexible coil structures (zone C), whereas zone A: Extra-rigid rod; zone B: Rigid rod; zone C: Semi-flexible coil; zone D: Random coil and zone E: Branched.

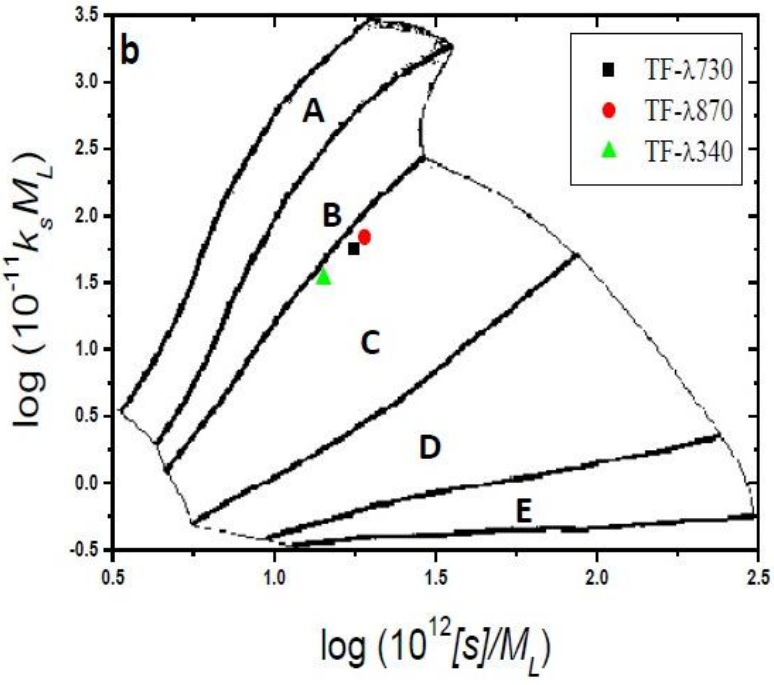


**Figure 3.9b:** The conformation zoning plot for lambda carrageenan samples TF-λ730, TF-λ870 and TF-λ340, are adopted semi-flexible coil structures (zone C).

Figure 3.9 (a) and (b) show logarithmic plots of $k_s$. $M_L$ versus $[s]/M_L$, with the five zonal types being represented for each lambda carrageenan sample (GM-λ690, GM-λ850 and GM-λ460) and (TF-λ730, TF-λ870 and TF-λ340), respectively. From the previous plots it appeared that both lambda carrageenan samples (GM-λ and TF-λ) adopted semi flexible structures at zone (C), and were more extended than a random coil consistent with those obtained from Wales-van Holde ratio and MHKS methods. Further, the results are in excellent agreement with computer modelling of lambda carrageenan conformation based on x-ray scattering data (Le Questel *et al.*, 1995).

### 3.4.4.4 Estimation of the Persistence Length $L_p$ and Mass Per Unit Length $M_L$

The flexibility of linear polymer chains can be represented by terms of the persistence length, $L_p$ and mass per unit length, $M_L$, where $L_p$ is defined as the average projection length along the initial direction of the polymer chain and $M_L$ is the mass of the molecules divided by its length (Tombs and Harding, 1998). Theoretically, persistence length has limitation for the cases of perfect random coil = 0 and for the stiff rod = ∞ , whilst the practical limitation is $L_p \sim$ 1-2 nm for random coils (e. g. pullulan) and $L_p \sim$ 200 nm for a stiff rod (e.g. schizophyllan) (see, e. g. Tombs and Harding, 1998). Thus the flexibility of lambda carrageenan conformation can be identified using the values of persistence length and mass per unit length. Several methods are applied here to estimate these two parameters ($L_p$ and $M_L$).

#### 3.4.4.4.1 Bushin-Bohdanecky method

This method is one of the most popular methods used for estimating the persistence length of polymer chains particularly for semi-flexible conformation, which has been applied for the range of polysaccharides. Both $L_p$ and $M_L$ can be estimated using this method based on the knowledge of intrinsic viscosity and molecular weight values via the following equation (Bohdanecky, 1983; Bushin *et al.*, 1981):

$$\left(\frac{{M_w}^2}{[\eta]}\right)^{1/3} = A_0\, M_L\, \phi^{-1/3} + B_o \phi^{-1/3} \left(\frac{2L_p}{M_L}\right)^{-1/2} {M_w}^{1/2} \qquad (3.8)$$

where $\phi$ is the Flory-Fox constant (2.86 x $10^{23}$ $mol^{-1}$) and $B_o$ is taken as ~ 1.10 and $A_0$ as ~ 1.32 (Bushin et al., 1981). The value of mass per unit length $M_L$ of lambda carrageenan (~ 610 g $mol^{-1}$ $nm^{-1}$) was used in this study obtained from (Berth et al., 2008). Also $M_L$ can be calculated from the mass of each monosaccharide monomer divided by length (*m/l*), where *l* is the diameter of the monosaccharide ~ 0.5 nm (Picout et al., 2002).

Figure 3.10 (a) and (b) show plots of $(M_w^2/[\eta])^{1/3}\ vs\ M_w^{1/2}$ for both lambda carrageenan GM-λ and TF-λ respectively, and $L_p$ can be estimated from the slope using the previous relation and values of $B_o$ , $A_0$ and $M_L$. Although $M_L$ might be yielded from the intercept of this method plot, it is very sensitive to estimation of $A_0$ (Bohdanecky, 1983). From the previous plots, a slope of (0.73±0.04) and (0.86±0.02) were obtained for GM-λ and TF-λ respectively, which yielded $L_p$ values of ~ (16±1) nm for GM-λ and ~ (12±1) nm for TF-λ. Subsequently, lambda carrageenan TF-λ shows more flexibility compared to

that of GM-λ and in general both agreed with previous estimates of lambda carrageenan flexibility by (Vannest, Slootmaekers and Reynaers, 1996).

### 3.4.4.4.2 Yamakawa-Fujii method

Yamakawa-Fujii is another approach used to estimate the persistence length of polymer chains based on the information of sedimentation coefficient. Plotting of sedimentation coefficient against molecular weight $s^o_{20,w}\ vs\ (M_w)^{1/2}$ led us to obtain the $L_p$ and $M_L$ from the slope and intercept, respectively, but it is required information about either $L_p$ or $M_L$. Unfortunately, the original equation relating the sedimentation coefficient with persistence length given by Yamakawa and Fujii (1973) was misprinted; thus Freire and Garcia de la Torre (1992) were provided the corrected relation:

$$s^o = \frac{M_L\,(1-\bar{\upsilon}\rho_o)}{3\,\pi\,\eta_0\,N_A}\,x\left[1.843\left(\frac{M_w}{2M_LL_P}\right)^{1/2} + A_2 + A_3\left(\frac{M_w}{2M_LL_P}\right)^{-1/2} + \cdots\right] \quad (3.9)$$

where $A_2$ = -ln (d/2$L_p$) and $A_3$= 0.1382 if the $L_p$ is much higher than the chain diameter, d (Yamakawa and Fujii, 1973). From the plots $s^o_{20,w}\ vs\ (M_w)^{1/2}$ of Yamakaw-Fujii method, a slopes of (6.87±0.76) x $10^{-16}$ for GM-λ and (6.2±0.5) x $10^{-16}$ for TF-λ were obtained Figure 3.10 (c) and (d), respectively. Utilizing equation 3.9 and fixed $M_L$ of 610 g mol$^{-1}$ nm$^{-1}$ yielded an $L_p$ of (15.2 ±0.5) for GM-λ and (18±1) for TF-λ. The $L_p$ value of lambda carrageenan GM-λ consistent with that obtained from Bushin-Bohdanecky, whereas TF-λ did not, and indicates a more extended conformation.

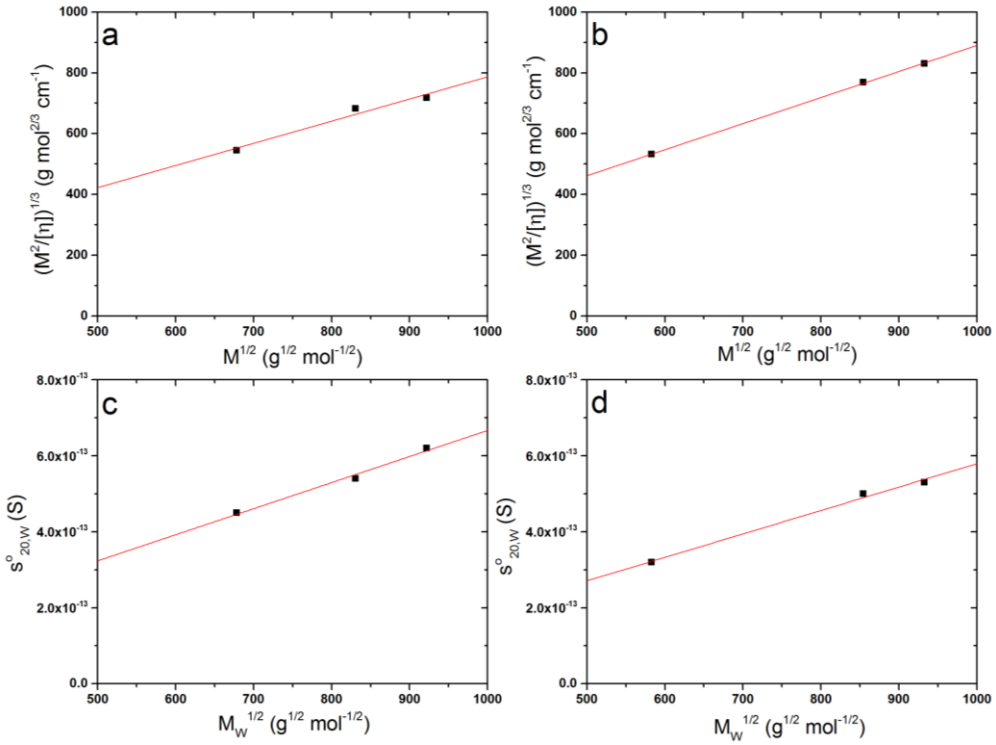


**Figure 3.10:** Show Bushin-Bohdanecky plots for lambda carrageenan (a) GM-λ and (b) TF-λ. Also the plots of Yamakawa-Fujii for lambda carrageenan (c) GM-λ and (d) TF-λ.

### 3.4.4.4.3 Global Analysis method (HYDFIT)

It can clearly be observed that using different approaches provide their own bias on results (Bohdanecky and Petrus, 1991; Patel, et al., 2008; Picout et al., 2002), hence a new software package namely "HYDFIT" has been created by Ortega and García de la Torre to resolve this problem (Ortega and García de la Torre, 2007). In the Multi-HYDFIT program, the persistent length, $L_p$, mass per unit length, $M_L$ and diameter, $d$ parameters can be estimated from data sets of sedimentation coefficient and intrinsic viscosity (also radius of gyration and translational diffusion if available) for different molecular weights. In the strategy of the program, these data sets are transformed into the equivalent

radii, to perform a minimisation procedure for obtaining the best values of those parameters ($L_p$, $M_L$ and $d$) satisfying the Bushin-Bohdanecky (Bushin et al., 1981; Bohdanecky, 1983) and Yamakawa and Fujii (1973) equations. Inclusive simulations have shown that the results returned for $L_p$ and $M_L$ is relatively insensitive to the chain diameter, $d$ consequently this is usually fixed (Ortega & García de la Torre, 2007). Then the Multi-HYDFIT optimizes the parameters in order to find the minimisation of the target function, based on the following equation:

$$\Delta^2\,(L_P, M_L, d) = \frac{1}{N_s}\sum_{i=1}^{N_s}\left[(\sum_Y W_Y)^{-1}\ \sum_Y W_Y\ \left(\frac{a_{Y\,(cal)} - a_{Y\,(exp)}}{a_{Y\,(exp)}}\right)^2\right] \qquad (3.10)$$

Thus the target function is presented as a dimensionless estimate of the convention among the theoretical calculated values (of sedimentation coefficient and intrinsic viscosity for a particular molecular weight, persistence length and mass per unit length) and the experimentally measured parameters (see, e.g. Ortega & García de la Torre, 2007; Amoros et al., 2011). In this study the sedimentation coefficient, intrinsic viscosity and molecular weight data points are used as input in Multi-HYDFIT for both lambda carrageenan samples (GM-λ and TF-λ). Consequently, minimum values of the target function ($\Delta$ = 0.04 and 0.06) correspond to the best estimate values of persistence length, $L_p$ (18±0.2) nm and (10±0.3) nm and mass per unit length, $M_L$ (650±50) Da nm$^{-1}$ and (600±20) Da nm$^{-1}$ for GM-λ and TF-λ, respectively Figures 3.11 a and b.

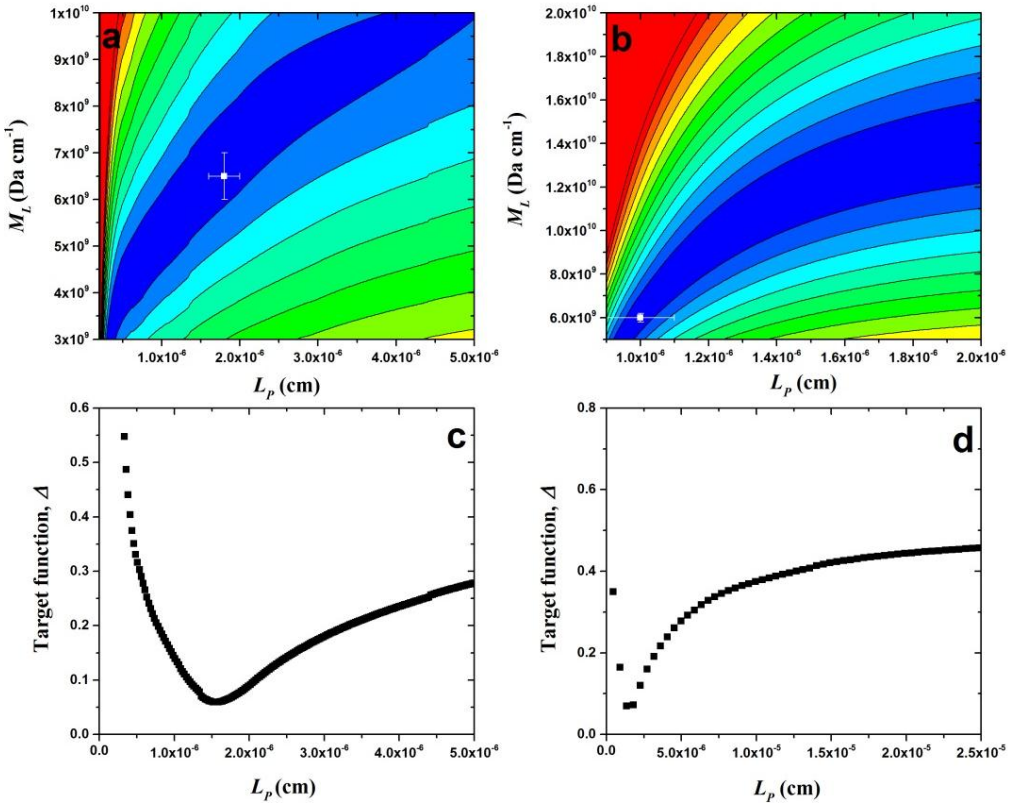


**Figure 3.11:** Global flexibility analysis (Multi-HYDFIT) for lambda carrageenan samples. (**a** & **b**) Contour plots of GM-λ and TF-λ, respectively. The target function, $\Delta$ calculated based on variables values of $L_p$ and $M_L$, and are represented on the full colour spectrum from blue to red. (**c** & **d**) Plots of target function ($\Delta$) vs. Persistence length ($L_p$) for GM-λ and TF-λ, respectively.

The second case where the diameter, *d* and also $M_L$ are fixed, $L_p$ was found to be (16±1) nm and (15±1) nm for GM-λ and TF-λ, respectively (Figures 3.11 c and d). These values are consistent with a semi-flexible structure, and are in good agreement with previous studies (Vannest, Slootmaekers and Reynaers, 1996; Berth et al., 2008).

## 3.5 DISCUSSION

The influence of the pre-treatment for the solutions of lambda carrageenan using a microwave bomb at different heating times have been shown using three different approaches based on sedimentation coefficient, $s^{o}_{20,w}$, molecular weight, $M_w$ and intrinsic viscosity, [η]: resulting in different samples of lambda carrageenan with variant molecular weights. The behaviour observed here for lambda carrageenan however, was not similar to that (depolymerisation) yielded for konjac glucomannan when treated using microwave in a high-pressure vessel, which presents good dispersability without degradation within a short time. However, degradation of the polymer was induced by longer times and higher temperatures (see, e.g. Kök et al., 2009; Wang, wood, & Cui, 2002).

The conformation of the polysaccharide in solution plays an important role in the structure- function relationship and in interaction with other biopolymer (Tombs and Harding, 1998). Evidently both lambda carrageenans (GM-λ and TF-λ) have considerable flexibility, as judged from both the viscometric and analytical ultracentrifuge behaviour. Conformation zoning therefore showed that both (GM-λ and TF-λ) most likely adopt a semi-flexible conformation (Zone C) with possibility of more extended than a random coil. Consequently, this conclusion seems to reinforce earlier observations by Slootmaekers et al. (1991b) and Berth et al. (2008). Characterisation of macromolecules using more than one hydrodynamic technique is preferred to avoid bias in the results for any methods used. In terms of the persistence length, $L_p$ and mass per unit length, $M_L$ different approaches (e. g. Bushin-Bohdanecky, Yamakawa-Fujii

and Multi-HYDFIT) have been used based on intrinsic viscosity, sedimentation coefficient and molecular weight data for estimation the flexibility of linear and flexible polysaccharides (both lambda carrageenans). Estimation again has confirmed the previous suggestion of a flexible structure, with possibility of more extended than a random coil.

The concentration dependence of the (weight average) sedimentation coefficient (with clear decrease and increase in concentration) in itself shows no clear evidence of any significant reversible association or dissociation in solution, at least under the conditions studied. The behaviour also is very different from the associative behaviour seen using analytical ultracentrifugation in for example arabinoxylans (Patel et al, 2007) – which shows a tendency for weak reversible self-association – and also more recently in amino-celluloses, the latter which exhibits step-wise, protein like association into dimers, trimers, tetramers, etc. (Heinze et al., 2011). An earlier study using analytical ultracentrifugation on kappa carrageenan also showed no evidence for reversible associative phenomena (based on both sedimentation velocity and also sedimentation equilibrium analysis). It is possible that this may have been obscured by the strong co-exclusion (molecular obstruction) non-ideality in solution, requiring more than one non-ideality virial term for the representation of solute distributions at sedimentation equilibrium (Harding et al., 1997).

In this regard it is interesting to consider what the source of the shoulder observed at the highest concentration observed in this study for lambda carrageenan might be. Multi-Gaussian analysis of the g(s) vs *s* profiles (Figure 3.12) shows for all samples the 2nd component has a sedimentation coefficient

approximately 1.1x that of the main component, and the relative proportion of the 2nd component relative to the main component is approximately 40%. This component may be an impurity although its appearance only at the highest concentration indicates it might be an association product.

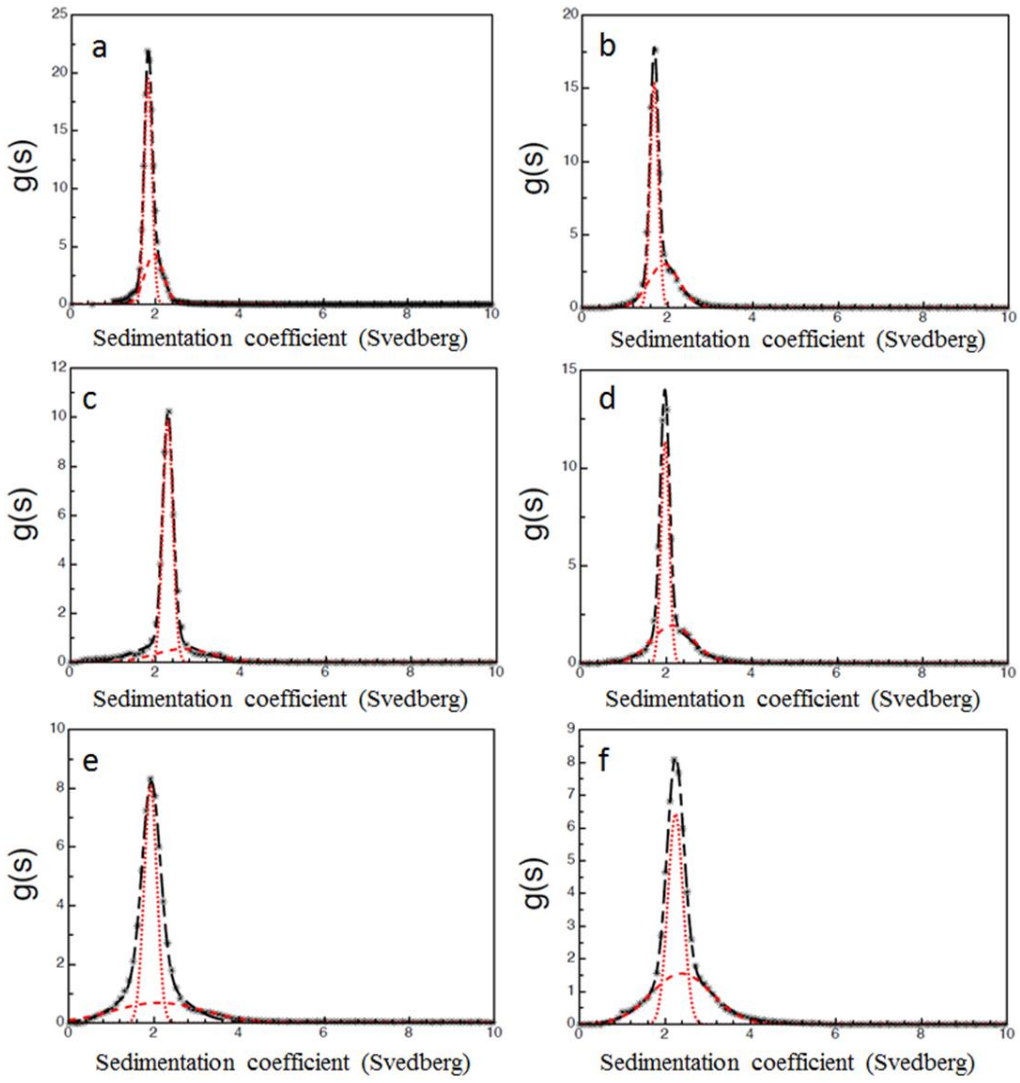


**Figure 3.12:** Multi-Gaussian fit of the highest concentration g(s) vs *s* profiles for lambda carrageenan samples GM-λ690, GM-λ850, GM-λ460 (a, c and e respectively), TF-λ730, TF-λ870 and TF-λ340 (b, d and f respectively). In each case two components are resolved, with the sedimentation coefficient of the faster component being approximately 1.1x greater than that of the slower component.

In perspective, it would be interesting to compare the properties of the different classes of carrageenans using modern analytical ultracentrifugation, with its now greater resolving power over a wide range of solvent and preparation conditions to see if this method provides any evidence of dimerization/double helix formation as originally suggested by Rees, Morris, Thom, and Madden (1992) for all three main classes (kappa, iota and lambda).

# CHAPTER 4

# HYDRODYNAMIC INVESTIGATION OF THE OLIGOMERIC STATE OF THE MAIN CLASSES OF CARRAGEENAN (KAPPA, IOTA AND LAMBDA) IN SOLUTION

In this chapter we now extend our study on lambda carrageenan in relation to the other major carrageenans, namely kappa and iota. The oligomeric and conformational states of the three main classes of carrageenan (kappa, iota and lambda) are investigated under conditions that promote either coil or helical conformations based on addition of salt (e.g. 0.1 M NaCl, NaI, and PBS) using hydrodynamic and thermodynamic methods. We take advantage of recent advances of these methods to see if new light could be thrown on the long-standing issue of whether carrageenans are a monomer (single helix) or dimer (double helix) in the so-called ordered state.

## 4.1 INTRODUCTION

Carrageenan is the generic term for a family of water-soluble linear sulphonated polysaccharides extracted from the *Rhodophyceaea* class of red seaweeds. The basic structure is a repeating unit of galactose and 3,6 anhydro-bridges, combined alternately by α-(1,3) and β-(1,4) glycosidic bonds (Imeson, 2009). The most commercially important carrageenan types are kappa (κ), iota (ι) and lambda (λ). The main source of lambda is *Chondruscrispus*, whereas

iota and kappa are isolated from *Eucheumaspinosum* and *Eucheumacottonii*, respectively (see, e. g. Campo et al., 2009). The characteristic differences among carrageenans are due to the varying proportions and linkage positions of their 3,6-anhydrogalactose and ester sulphate substituents (Figure 4.1). Variations in the chemical structure for each type of carrageenan are responsible for their unique characteristics, including gel strength, viscosity, temperature stability, synergism and solubility (see, Tombs and Harding, 1998).

Carrageenans are used extensively in food applications (Bonferoni et al., 1994; Therkelsen, 1995), oil recovery enhancement (Iglauer et al., 2011) and pharmaceutical and healthcare products (see, e.g. Zhou et al., 2004; Farias et al., 2000; Carlucci et al., 1999), as either gelling agents, natural thickeners or formulation stabilizers. The feature of gel formation for iota and kappa carrageenan has been considered to involve a conformation transition from a 'disordered' coil state at higher temperature to an 'ordered' helical state at lower temperature (Morris et al., 1980; Viebke et al., 1995). The helical form is required for gelation: lambda carrageenan cannot form a helix owing to steric hindrance; and consequently is unable to form a gel (Coultate, 2009, van de Velde et al., 2002). The ionic environment plays a significant role in the helical stability of both kappa and iota carrageenans, which follows the Hofmeister series (e.g. $Rb^+ > Cs^+ > K^+ > NH_4^+ > Na^+ > Li^+$) (Morris, 1990; Piculell, 1995; Therkelsen, 1995). The iodide ion also has an effect on helical stability of kappa carrageenan, which is reported to stabilise the helical form but represses helix aggregation and gelation ability (Ciancia et al., 1997).

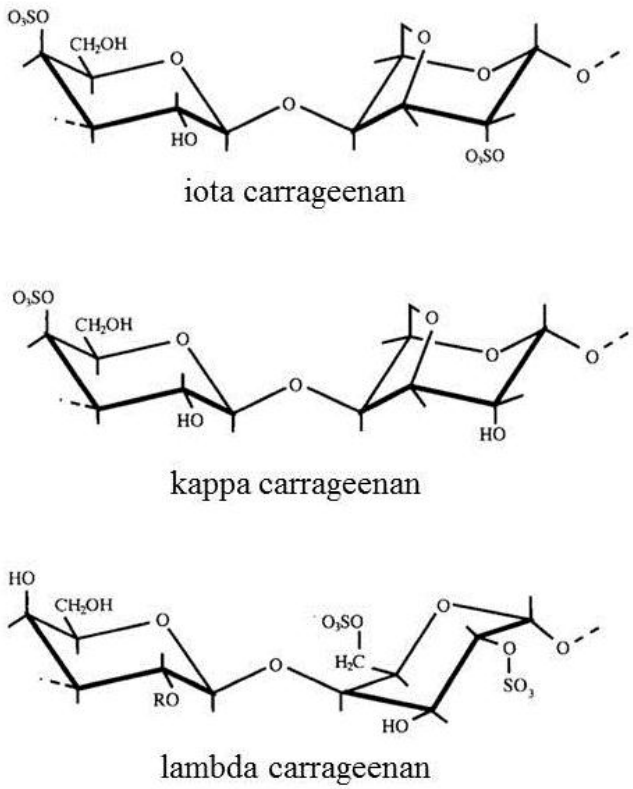


**Figure 4.1:** Chemical structure of iota (ι), kappa (κ) and lambda (λ) commercial carrageenans. Adapted from Perez et al., (1996).

Although Anderson and co-workers had proposed a double helical conformation for kappa and iota carrageenans in gels based on X-ray fibre diffraction studies (Anderson et al., 1969), the debate is still open whether the so-called ordered conformations of kappa and iota carrageenans are single or double helices. The possibility of one of these conformations has drawn the attention of many researchers and has been investigated for many years. Morris and his colleagues for example have shown a doubling of the molecular weight for iota carrageenan even in the absence of gelation (gelation phenomena promoted by different counterions), suggesting a double-helical conformation (Morris et al., 1980). Another study using multi-angle light scattering coupled with size exclusion chromatography (SEC-MALS) measured the change in

molecular weight of degraded and non-degraded kappa and iota carrageenans under defined conditions for disordered and ordered conformations by Viebke et al., (1995). The experimental results from this study showed approximately doubling in the molecular weight for the carrageenans at helix state suggesting a double helix formation. These observations have been supported by kappa carrageenan examined in 0.1 M NaCl (coil) and 0.1 M NaI (helix) at room temperature using flow field-flow fractionation (FFFF-MALS) which also seemed to point to kappa carrageenan having formed double helices (Wittgren et al., 1998; Viebke and Williams, 2000). On the other hand, Smidsrød and his group of researchers at Trondheim in Norway have reported a single helix conformation for kappa carrageenan in the ordered state (Smidsrød et al., 1980; Smidsrød and Grasdalen, 1984), showing no evidence for double chains. A further study by Vanneste and co-workers showed the existence of iota carrageenan in a single helix conformation at both NaI and NaCl solutions using static light scattering (Vanneste et al., 1994). Measurements performed by Cuppo and Reynaers using wide angle laser light scattering for kappa carrageenan in solutions of both NaI and NaCl showed no change in molecular weight which gives further support of kappa carrageenan adopting a single helix conformation (Cuppo and Reynaers, 2002).

Understanding the behaviour and function of carrageenans and how they can be used is dependent on the knowledge of their biophysical properties such as molecular weight and distribution of molecular weight (Harding, 2005a). Thus, molecular weight is considered one of the most powerful parameters to distinguish whether carrageenans exist in solution as a single helix or a double helix conformation: if doubling of the molecular weight of the carrageenans in

the ordered state can be confirmed then this would represent the dimerization of carrageenans (although not necessarily double helix). As indicated in the discussion above several studies have been performed to estimate the molecular weights or "molar masses" for carrageenans in solution using multi-angle light scattering (MALS), and light scattering coupled with size exclusion chromatography, SEC (Slootmaekers et al., 1991a, Hjerde et al., 1994, Viebke et al., 1995, Ciancia et al., 1997, Cuppo and Reynaers, 2002, Berth et al., 2008). An alternative separation medium, namely flow field-flow fractionation, has also been used rather than traditional SEC (Wittgren et al., 1998, Viebke and Williams, 2000). However, rarely have molar masses of carrageenans been measured using analytical ultracentrifugation based on sedimentation equilibrium (Harding et al., 1997). The absolute molar mass (weight, number and z-average) and molar mass distribution can be estimated, using analytical ultracentrifugation taking advantage of recent advances (Dam and Schuck, 2004; Harding et al., 2011; Harding, 2012; Schuck et al, 2014).

In this present study the properties of the different classes of carrageenans (kappa, iota and lambda) have now been investigated in different solvent conditions. Initially thermal transition has been studied in order to assess the influence of ions and solvent on carrageenan conformation using Micro-Differential Scanning Calorimetry (micro-DSC). This technique was used in conjunction with SEC-MALS, viscometry and analytical ultracentrifugation (AUC), to see if a modern and combined hydrodynamics with thermodynamic approaches can help to resolve or at least to throw new light on the long-standing issue of whether carrageenans are a single helix or double helix in the ordered state. AUC methods are particularly well suited to address this problem

as they have intrinsic separation ability without the need for separation media or immobilisation materials which might otherwise disrupt or interfere with any interaction phenomena (see, e.g. Harding, 2005b; Harding, 2012). In a recent study of lambda carrageenan using analytical ultracentrifugation based on sedimentation velocity, no clear evidence was observed for a reversible or partially reversible association or dissociation in aqueous solution (Almutairi et al., 2013) under limited solvent conditions. That study is now extended to a range of solvent conditions and to the other main carrageenan types.

## 4.2 MATERIALS

The carrageenan samples (kappa, iota and lambda) were kindly provided by CPKelco, Lille Skensved, Denmark. The samples were used as supplied without any further purification. Carrageenan (kappa, iota and lambda) powders were dissolved in 50 mL solvent solutions, either (i) sodium iodide (0.1 M NaI), (ii) phosphate chloride buffer solution containing sodium phosphate, sodium chloride, potassium phosphate and potassium chloride (PBS 0.1 M and pH 7.0), (iii) sodium chloride (0.1 M NaCl). Two more solvents were used for kappa: (iv) dimethyl sulfoxide (DMSO 100%), and (v) dimethylsulfoxide (DMSO 80%) mixed with sodium iodide (NaI 20%). The solutions were heated to approximately 80 $^{o}$C for 30 mins to obtain maximum dispersion under stirring (Viebke et al., 1995) and then cooled to room temperature prior to measurements. The concentration was measured using an

Atago (Tokyo, Japan) DD-7 Digital differential refractometer calibrated with glucose standards.

## 4.3 METHODS

### 4.3.1 Micro-Differential Scanning Calorimetry (micro-DSC)

The thermal events of carrageenan samples were characterised in a Micro-Differential Scanning Calorimeter (DSC III Setaram, Caluire, France). Approximately 0.8 g of each carrageenan solutions were sealed into the DSC cells made from Hastalloy. The reference cell was filled with the same weight of the corresponding solvent and coordinated for heat capacity with the sample. Sample and reference cells were initially cooled to a starting temperature of 0 °C to equilibrate. Cells were then run at a scanning rate of 1 °C $min^{-1}$ from 0 to 95 °C, cooled and rerun while all steps were recorded. Some experiments were run at 0.5 and 0.25 $^{o}C$ $min^{-1}$ to check the dependence on the scanning rate. Enthalpy values were calculated using Setaram software with a spline interpolated baseline, based on an extension of the trace before and after the thermal event. Enthalpy values were normalised per gram of polysaccharide in the sample.

### 4.3.2 Sedimentation Velocity (SV)

Sedimentation velocity in the analytical ultracentrifuge was used to probe the heterogeneity of solutions as well as to measure their sedimentation coefficient

(Harding, 1992, Harding, 2005b). Carrageenan samples (400µl) and reference buffer (400µl) were injected into sample and references channels, respectively, of double sector 12.0 mm optical path length cells. Aluminium expoxy or, when DMSO was the solvent, Kel-F centerpieces were used. The Rayleigh interference optical system was used for recording concentration profiles and the movement of the sedimentation boundary in the analytical ultracentrifuge cell (Harding, 2005b). An initial low rotor speed of 3000 rpm was adjusted to a rotor speed of 40,000 rpm. The standard conditions of density and viscosity of water at 20.0℃ were used for adjustment of the sedimentation coefficients *s* to $s_{20,w}$ values (Schachman, 1959). Scans were taken at 2 min intervals for a run time of ~ 24 hours. The data was analysed using the SEDFIT procedure (Dam and Schuck, 2004) which solves the Lamm equation describing the change of concentration distribution with radial position with time in terms of a distribution of sedimentation coefficients, g(s) vs *s*, where *s* is the sedimentation coefficient. The (differential) distribution of sedimentation coefficients g(s) can be defined as population – weight fraction – of species with a sedimentation coefficient between $s + ds$ (Dam and Schuck, 2004, Harding, 2005a). The sedimentation coefficient is expressed in terms of the standard conditions of the viscosity and density of water at 20.0°-°C, $s_{20,w}$. To eliminate the effects of non-ideality (co-exclusion and any residual polyelectrolyte effects) a plot of the reciprocal of the sedimentation coefficient ($1/s_{20,w}$) against concentration, *c* (g $mL^{-1}$) was made. From the intercept at infinite dilution c=0, the value free of these effects was found: $s^o_{20,w}$ (units seconds, s, or Svedbergs, S, where $1S = 10^{-13}s$). The following relation was used for the extrapolations (Gralén, 1944):

$$(1/s_{20,w}) = (1/s°_{20,w}).(1+k_s.c) \quad (4.1)$$

where $k_s$ is the "Gralen" coefficient (mL $g^{-1}$). Analysis of the change in sedimentation coefficient distributions was used to ascertain the presence of an interaction.

### 4.3.3 Sedimentation Equilibrium (SE)

Samples were prepared at a concentration of 0.3 mg $mL^{-1}$, after dialysis for 24 hours at the ambient temperature in the appropriate solvent. Sedimentation equilibrium experiments were performed using the Beckman (Palo Alto, California, U.S.A.) Optima XL-I analytical ultracentrifuge equipped with Rayleigh interference optics and an automatic on-line data capture system. The modified long (20.0 mm) optical path length double-sector cells with sapphire windows were loaded with ~80 μl of dialysed sample and a matching amount of reference buffer dialysate in appropriate channels. The balanced cells were then loaded into an analytical 8-hole titanium rotor An50-Ti and placed in the AUC. After time was allowed for vacuum formation (≤ 50 microns) and for temperature equilibration (20.0°C), the rotor was then accelerated to 4000 rpm; rotor speeds were selected to be sufficiently apart to give a good solute distribution (Scott and Schuck, 2005). Using the Rayleigh interference optical system, scans were taken every one hour and equilibrium was reached after approximately 72 hours. A record of the relative concentration distribution of the solute at equilibrium was analysed to give the weight average apparent molecular weight $M_{w,app}$ using the SEDFIT-MSTAR algorithm implemented by

Schuck and co-workers (Schuck et al., 2014) based on the algorithm of Cölfen and Harding (Cölfen and Harding, 1997) and the *M** function of Creeth and Harding (1982).

### 4.3.4 Size Exclusion Chromatography Coupled to Multi Angle Light Scattering (SEC-MALS)

Molecular weight (weight averages) of the carrageenan samples were also estimated by using the independent technique of SEC-MALS (Wyatt, 1992, 2013), a technique which has been successfully applied to polysaccharide characterisation since Horton et al., (1991). The present set-up comprised a series of size-exclusion chromatography (SEC) columns, namely TSK G6000PW and TSK G4000PW, protected by a similarly packed guard column (Tosoh Bioscience, Tokyo, Japan) coupled on-line to a "Helios" multi-angle light scattering (MALS) and refractive index (OptilabrEX) detectors (Wyatt Technology, Santa Barbara, USA). Solutions prepared at concentrations of 0.8 mg $mL^{-1}$ were filtered through a 0.45 μm syringe filter (Whatman, Maidstone, England) - to remove any insoluble material or dust prior to being injected into the columns. The buffer was pumped at a steady, pulse-free flow rate of 0.8 mL $min^{-1}$ through the column system. ASTRA (Version 5.1.9.1) software (Wyatt Technology, Santa Barbara, U.S.A.) was used to analyse the data. A linear fit to the "Debye" plot of $Kc/R_\theta$ *vs* $sin^2(\theta/2)$, where the terms have their usual meaning (see, e. g. Wyatt 2013) was used for calculating the absolute weight average molecular weight ($M_w$) using the following values for the refractive index increment: kappa *dn/dc* = 0.111 mL $g^{-1}$, iota *dn/dc* = 0.127 mL

$g^{-1}$ (Theisen et al., 2000) and lambda *dn/dc* = 0.116 mL $g^{-1}$ (Slootmaekers et al., 1991b). Because of the low concentrations after dilution on the columns no correction for non-ideality was assumed necessary.

### 4.3.5 Capillary and Differential Pressure Viscometry

The relative viscosities $\eta_{rel}$ of carrageenans (kappa, iota and lambda) samples in ranging concentrations ($c$) ranging from 0.1 – 1.0 mg $mL^{-1}$ were measured from the ratio of flow times of solution to solvent using a 2.0 mL Ostwald viscometer. The U-tube viscometry was suspended in an accurate temperature regulated water bath. The temperature was kept constant at (20.0 ± 0.01) °C throughout by using a coolant system. Because of the low concentrations no correction for solution density was necessary (Harding, 1997). The reduced ($\eta_{red}= (\eta_{rel}-1)/c$) and inherent ($\eta_{inh} = (\ln\eta_{rel})/c$) viscosities were extrapolated to infinite dilution to eliminate non-ideality effects using both the (Huggins, 1942) and (Kraemer, 1938) approaches:

$$\eta_{red} = [\eta] (1+K_H [\eta] c) \quad (4.2)$$

$$\eta_{inh} = [\eta] (1- K_K [\eta] c) \quad (4.3)$$

where the intrinsic viscosity $[\eta]$ is taken as the mean of intercepts from equations (4.2) and (4.3) and $K_H$ and $K_K$ are the Huggins and Kraemer constants, respectively. To avoid possible ambiguities through transition from the dilute to the semi-dilute region $[\eta]$ was also estimated from the Solomon-

Ciuta relation, essentially a combination of the Huggins and Kraemer lines (see, e.g. Harding 1997):

$$[\eta] \approx (1/c)\,[2(\eta_{rel}-1) - 2\ln(\eta_{rel})]^{1/2} \qquad (4.4)$$

Relative viscosities were also estimated from a Viscostar (Wyatt Technology) differential pressure viscometer linked on-line to the SEC-MALS system (Harding, 1997). Because of the higher sensitivity of the sensors and the high dilution from the column, equation (4.4) was used to obtain [η] without a concentration extrapolation.

# 4.4 RESULTS

## 4.4.1 Thermal Behavior of Carrageenans

Carrageenans samples were studied using differential scanning calorimetry. The micro-DSC thermograms of the kappa, iota and lambda carrageenans in three different aqueous solutions (namely 0.1 M PBS, NaI and NaCl) are shown in Figure 4.2a-c. First, the effect of ions on conformational transition was evaluated for kappa carrageenan, where one peak was generally observed in both cooling and heating curves at these different solvents. These exothermic and endothermic peaks are referred to helix formation (in some cases also helix aggregation), the melting of the cross-linked helices if any, and of the helical segments, respectively (Figure 4.2a). In the presence of the NaI the thermal transition is shifted to higher temperatures as compared to both NaCl and PBS. Also, the thermal hysteresis on cooling decreases in the cases

of NaI and NaCl compared to that of PBS. The thermal hysteresis is related with inter-helical aggregation (Viebke et al., 1998; Takemasa and Nishinari, 2004; Burova et al., 2006). These results suggest that kappa carrageenan is disordered/ordered from helix to random coil state and vice versa upon heating/cooling in all salt solutions, indicated by the presence of endothermic/exothermic peaks. However, NaI increases the stability of helices, indicated by the location of the transition peaks at higher temperatures (Viebke et al., 1998; Takemasa and Nishinari, 2004). Nevertheless, the slight thermal hysteresis observed for kappa carrageenan in NaI and NaCl suggests reduced the helix aggregation and hence no gel formation. The thermal hysteresis may depend on the scan rate. Moritaka and co-workers showed that the gelation temperature of kappa carrageenan in NaCl was elevated by slowing the cooling rate (Moritaka et al., 2007).

In the current study, some experiments were performed at lower scanning rate (0.5 and 0.25 °C $min^{-1}$) to check this dependency. Indeed, in the case of kappa carrageenan in NaI, the slight thermal hysteresis was reduced at lower scanning rate and was negligible when extrapolating to zero. The same could be applied for kappa carrageenan in NaCl, meaning no helix aggregation. In the case of kappa carrageenan in PBS, the large thermal hysteresis cannot be neglected even when extrapolating to zero the scan rate, evidencing helix aggregation and gel formation.

Sodium is present as the major percentage of cations in all salt solutions; therefore the different behaviour observed in NaI might come from iodide anion. It has been previously reported that NaI promotes the formation of isolated helices because the electrostatic repulsion among helices with bound

iodide should be higher than that of the other conditions due to the high charge density, and prevents from effect of aggregation of helices (Viebke et al., 1998; Takemasa and Nishinari, 2004). Additionally, the small percentage of potassium cations in PBS may contribute to the thermal hysteresis observed for kappa carrageenan and hence in the gel formation, since it is well known that kappa carrageenan is sensitive to potassium cations.

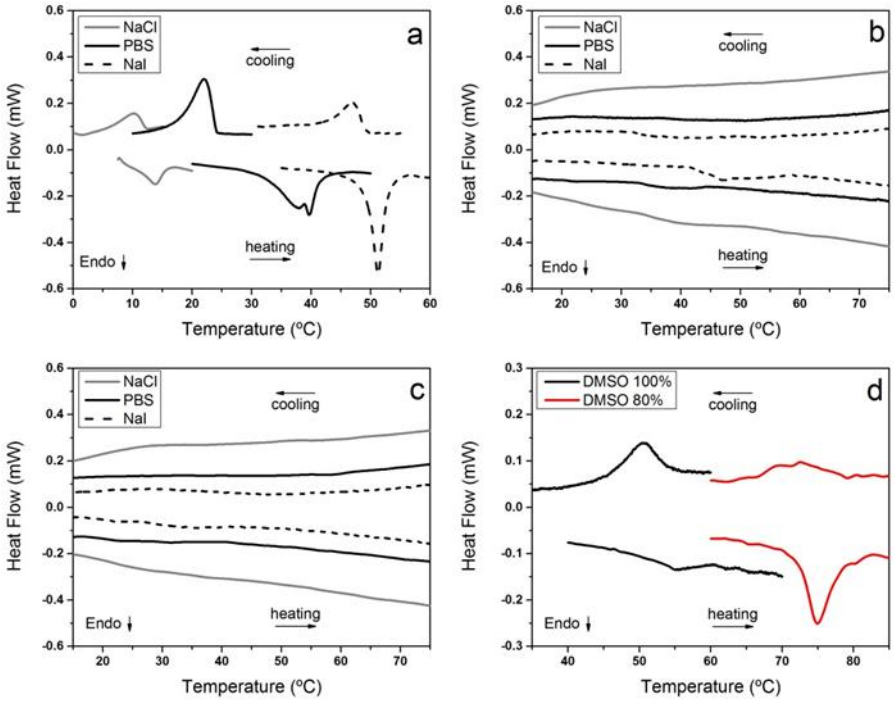


**Figure 4.2:** Micro-DSC trace of carrageenans (0.15%) in aqueous solution (0.1M NaCl, PBS and NaI); (a) kappa, (b) iota and (c) lambda, whereas (d) gives a comparison of micro-DSC traces of kappa in DMSO (100% and 80%).

In the case of iota carrageenan (Figure 4.2b), a small endothermic peak is detected in NaI on heating, within the same range of temperature as for kappa carrageenan, which seems to be very broad on cooling (exothermic). This suggests at least melting and formation of some helical segments, respectively (Grinberg et al., 2001). On the other hand, it has been reported that lambda

carrageenan is not able to go through the coil-to-helix transition and remains as a random coil in aqueous solution without forming gels (De Ruiter and Rudolph, 1997). In this regard Figure 4.2c shows no evident transition peaks for lambda carrageenan in either salt solution.

Figure 4.2d shows the thermal behaviour of kappa carrageenan in DMSO solvent (100%) or diluted DMSO (80% DMSO and 20% NaI). As a general trend, the effect of this solvent is to shift the transition peaks of kappa carrageenan to higher temperature values as compared to aqueous solutions in the presence of NaI, NaCl and PBS, likewise keeping low thermal hysteresis. These results suggest helix-coil/coil-helix conformational transitions, although little or no inter-helical aggregation, hence, no gel formation as reported previously (Rochas and Rinaudo, 1982).

### 4.4.2 Sedimentation Coefficient and Sedimentation Coefficient Distribution

The sedimentation coefficient, *s* values were measured for kappa, iota and lambda carrageenans in the different solvents at various concentrations using the ls-g*(s) method of SEDFIT (Dam and Schuck, 2004) (Table 4.1). Analysis of the g*(s) distributions profiles displayed the classical linear increase in sedimentation coefficient value with the decrease in concentration for each carrageenan. Figure 4.3a-f shows the sedimentation coefficient distributions or g*(s) vs *s* profiles for kappa carrageenan at different solvents (0.1 M NaCl, 0.1 M NaI, 0.1 M PBS and DMSO). Unimodal distributions were generally seen for kappa carrageenan in all solvents, except 0.1 M PBS. The (apparent)

sedimentation coefficient distributions of kappa in PBS at (20 $^{o}$C) shows broad distributed peaks that reflects the gelation behaviour in agreement with micro-DSC results, which reduced at 30 $^{o}$C (Figure 4.3c and d).

**Table 4.1:** Summary of $s^{\circ}_{20,w}$ and $k_s$ results for kappa, iota and lambda carrageenans in different solvents.

| Sample | Solvent | $s^{\circ}_{20,w}$ (S) | $k_s$ (mL g$^{-1}$) |
|---|---|---|---|
| **kappa** | 0.1M NaCl | 4.2±0.1 | 790±30 |
| | 0.1M NaI | 4.6±0.2 | 720±100 |
| | 0.1M PBS | 7.0±0.3 | 510±90 |
| | 0.1M PBS[a] | 5.2±0.2 | 890±150 |
| | DMSO 100% | 3.0±0.1 | 170±20 |
| | DMSO 80% | 3.0±0.2 | 400±80 |
| **iota** | 0.1M NaCl | 6.8±0.4 | 400±50 |
| | 0.1M NaI | 7.0±0.2 | 440±30 |
| | 0.1M PBS | 7.3±0.3 | 770±70 |
| | 0.1M PBS[a] | 7.1±0.5 | 850±100 |
| **lambda** | 0.1M NaCl | 5.6±0.2 | 720±50 |
| | 0.1M NaI | 5.7±0.2 | 330±50 |
| | 0.1M PBS | 5.5±0.1 | 520±20 |
| | 0.1M PBS[a] | 5.8±0.2 | 840±40 |

a: sedimentation velocity experiment performed at temperature of 30 $^{o}$C

The ls-g*(s) profile of iota (in 0.1 M NaI, NaCl and PBS) however, displayed bimodal distribution at the highest concentration peak, but not lower concentrations which represents either minor contamination of kappa or existence of high molecular weight material (Figure 4.4a-c). The distribution profile of iota in PBS at (30 $^{o}$C) shows unimodal distribution, except the shoulder present at the highest concentration (Figure 4.4d).

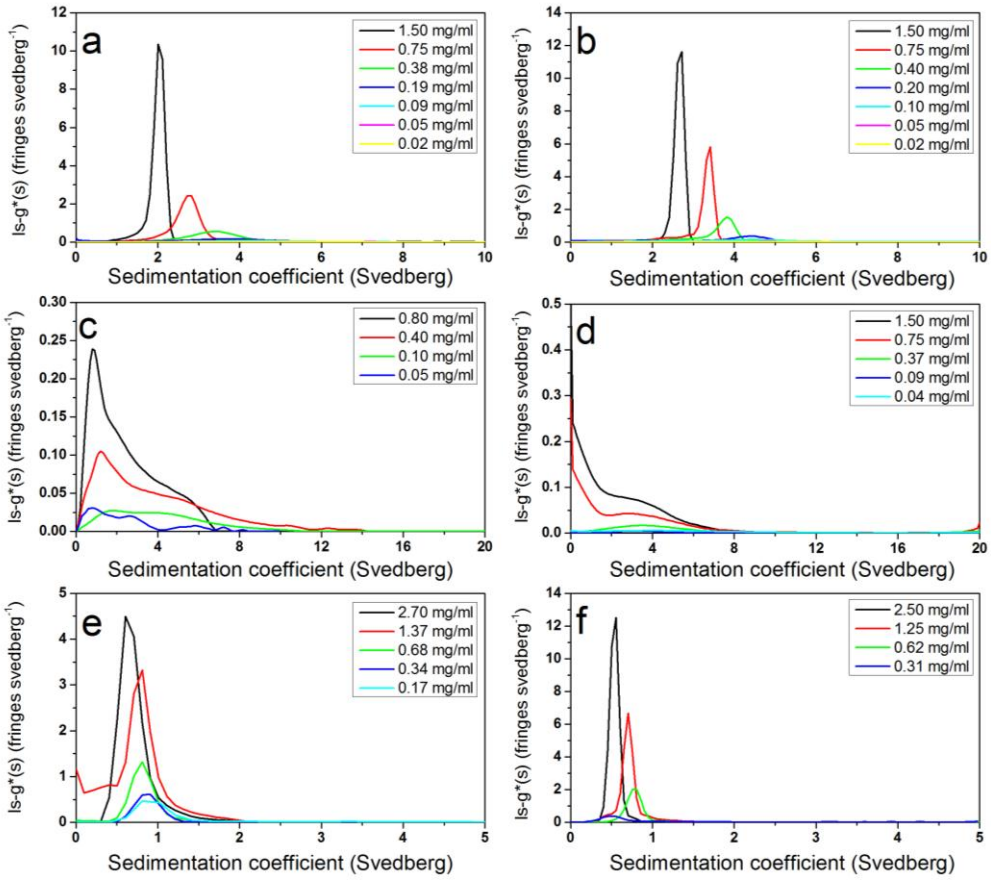


**Figure 4.3:** Sedimentation coefficient distribution profiles using least squares g*(s) method of SEDFIT obtained from sedimentation velocity experiment for **kappa carrageenan** samples at different conditions (a) NaCl (b) NaI (c) PBS 20.0$^{o}$C (d) PBS 30.0$^{o}$C (e) DMSO 100% (f) DMSO 80%.

Finally, plots of g*(s) vs *s* for lambda carrageenan in all cases (0.1 M NaI, NaCl and PBS (20 and 30 $^{o}$C)) show homogenous distribution with unimodal system, likewise a shoulder at highest concentration peaks were yielded for all cases which propose high molecular weight lambda (Figure 4.5a-d). The behaviour seen here agreed with that observed in the recent study for lambda carragenana using analytical ultracentrifugation (Almutairi et al., 2013).

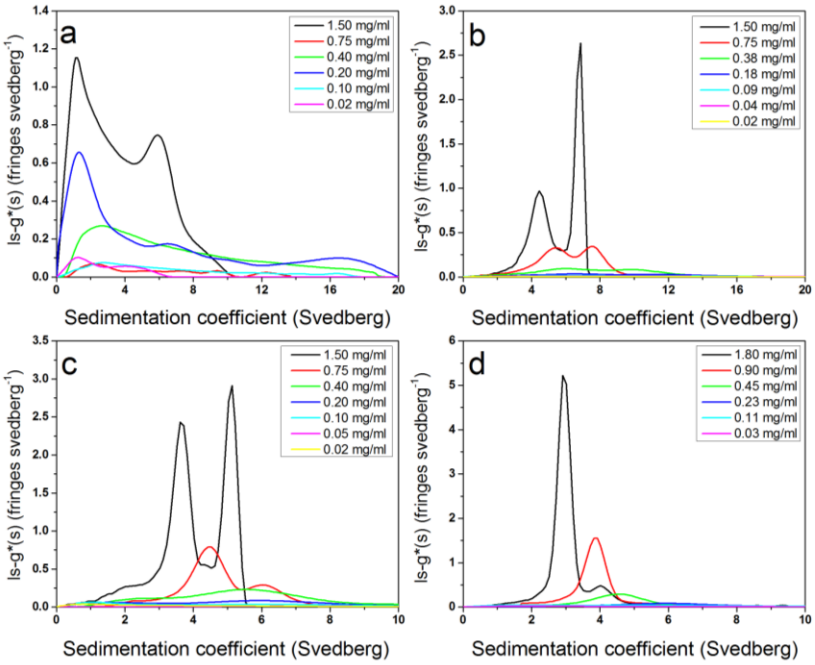


**Figure 4.4:** Sedimentation coefficient distribution profiles using least squares g*(s) method of SEDFIT obtained from sedimentation velocity experiment for **iota carrageenan** samples at different conditions (a) NaI (b) NaCl (c) PBS 20.0$^{o}$C (d) PBS 30.0$^{o}$C.

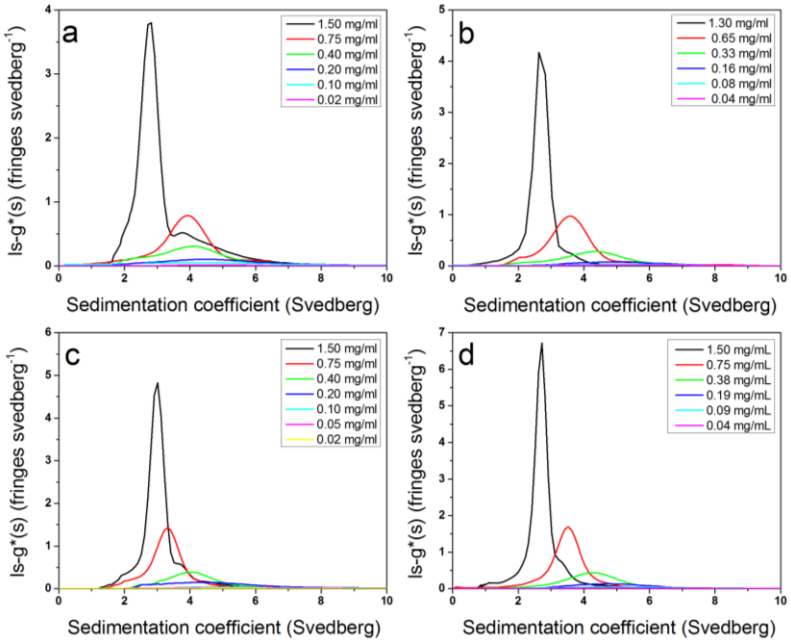


**Figure 4.5:** Sedimentation coefficient distribution profiles using least squares g*(s) method of SEDFIT obtained from sedimentation velocity experiment for **lambda carrageen** samples at different conditions (a) NaI (b) NaCl (c) PBS 20.0 $^{o}$C (d) PBS 30.0$^{o}$C.

Furthermore, to eliminate the non-ideality effects, $s_{20,w}$ values (or the reciprocals thereof) were extrapolated to zero concentration to obtain $s^{\circ}_{20,w}$ using the reciprocal plots ($1/s_{20,w}$) vs. concentration for all three carrageenans (kappa, iota and lambda) as shown in (Figure 4.6, 4.7 and 4.8). Generally this gives more reliable estimates for $s^{\circ}_{20,w}$ and the concentration dependence of sedimentation, $k_s$ which are reported in (Table 4.1).

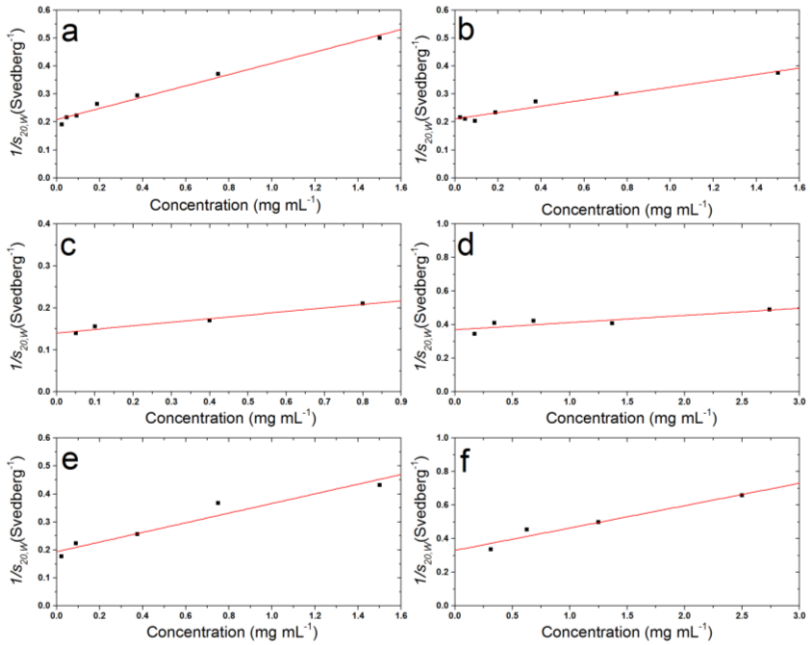


**Figure 4.6:** Concentration dependence (reciprocal) of the sedimentation coefficient plot (after correction to standard solvent conditions) for **kappa carrageenan** samples at different conditions (a) NaCl (b) NaI (c) PBS 20.0$^{o}$C (d) PBS 30.0$^{o}$C (e) DMSO 100% (f) DMSO 80%.

Under similar conditions (temperature and rotor speed) carrageenans (kappa, iota and lambda) have different weight average sedimentation coefficient in different solvents. This might reflect the different behaviour of carrageenans in different salt types (Ciancia et al., 1997). The reciprocal plots of sedimentation coefficient vs concentration confirmed the linear trend on sedimentation

coefficient value which increases with decreasing concentration indicative of classical non-ideal behaviour.

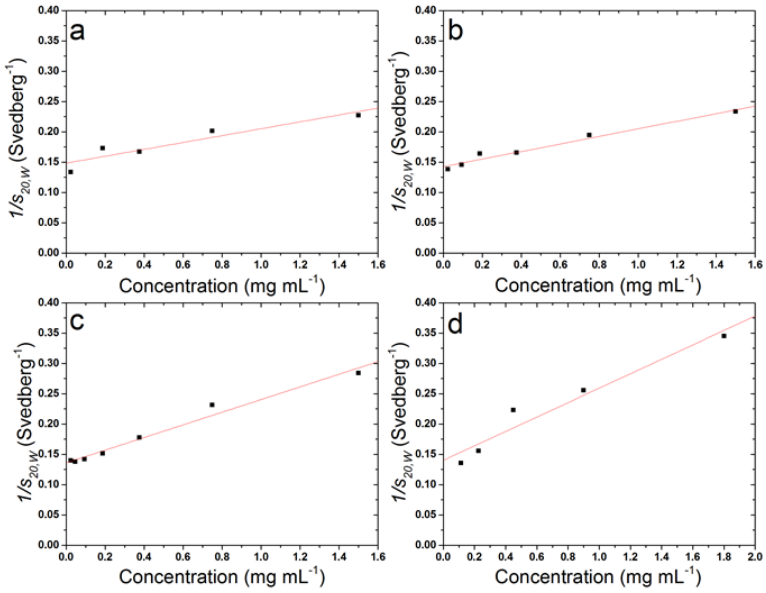


**Figure 4.7:** Concentration dependence (reciprocal) of the sedimentation coefficient plot (after correction to standard solvent conditions) for **iota carrageenan** samples at different conditions (a) NaCl (b) NaI (c) PBS 20.0$^{o}$C (d) PBS 30.0$^{o}$C.

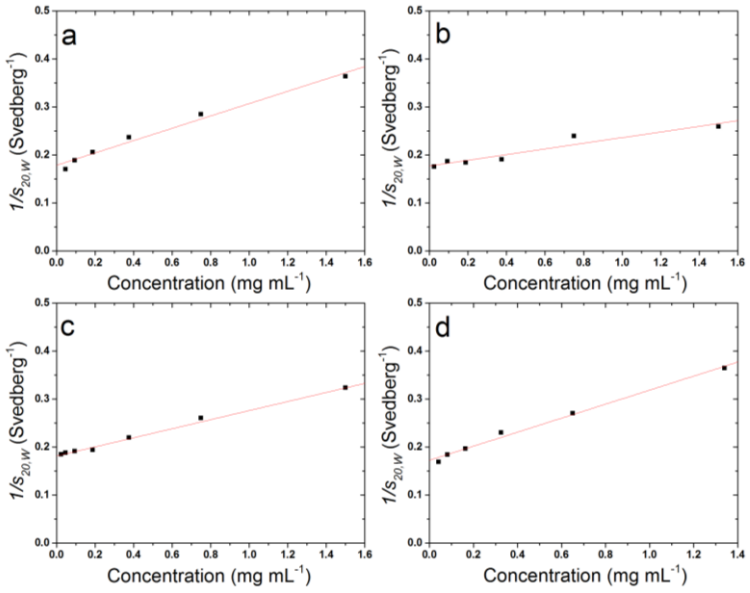


**Figure 4.8:** Concentration dependence (reciprocal) of the sedimentation coefficient plot (after correction to standard solvent conditions) for **lambda carrageenan** samples at different conditions (a) NaCl (b) NaI (c) PBS 20.0$^{o}$C (d) PBS 30.0 $^{o}$C.

### 4.4.3 Estimation of Molecular Weight

Weight average molecular weight values for carrageenans (kappa, iota and lambda) at different solvents (0.1 M NaCl, 0.1 M NaI, 0.1 M PBS and DMSO) were estimated from sedimentation equilibrium using SEDFIT-MSTAR (Figures 4.9, 4.10 and 4.11) and are reported in Table 4.2. For polydisperse system in particular carrageenan it is well established that non-ideality increases with increasing the loading concentration (Harding et al., 1997).

**Table 4.2:** Summary of weight average molecular weight *($M_w$)* results for kappa, iota and lambda carrageenans in different solvents.

| Sample | Solvent | $10^{-3}$ x $M_w$ (g mol$^{-1}$)[b] | $10^{-3}$ x $M_w$ (g mol$^{-1}$)[c] | $10^{-3}$ x $M_w$ (g mol$^{-1}$)[d] |
|---|---|---|---|---|
| **kappa** | 0.1M NaCl | 180±5 | 220±20 | nd |
| | 0.1M NaI | 375±15 | 360±10 | 420±70 |
| | 0.1M PBS | nd | 610±30 | 580±100 |
| | 0.1M PBS[a] | nd | 600±20 | nd |
| | DMSO 100% | 260±20 | nd | nd |
| | DMSO 80% | 300±20 | nd | nd |
| **iota** | 0.1M NaCl | 720±20 | 690±30 | nd |
| | 0.1M NaI | 680±50 | 600±50 | 685±75 |
| | 0.1M PBS | 550±20 | 650±40 | 590±60 |
| | 0.1M PBS[a] | 630±10 | 620±20 | nd |
| **lambda** | 0.1M NaCl | 520±10 | 500±20 | nd |
| | 0.1M NaI | 530±15 | 470±40 | 602±40 |
| | 0.1M PBS | 540±15 | 580±40 | 630±70 |
| | 0.1M PBS[a] | 550±10 | 530±10 | nd |

nd : not determined
a : experiment performed at temperature of 30.0 $^{o}$C
b : molecular weight obtained from sedimentation equilibrium
c : molecular weight obtained from extended Fujita methods
d : molecular weight obtained from SEC-MALS

Thus, working at low concentration (0.3 mg $mL^{-1}$) and a reasonable ionic strength (0.1 M) helped to minimize the non-ideality arising from co-exclusion and the polyelectrolyte effect. The assumption is made that the apparent molecular weight at this loading concentration $M_{w,app}$ is the true or ideal weight average molecular weight, $\sim M_w$ (Harding, 2005b; Schuck, etal., 2014). Within the range of solvents used, iota has the highest weight average molecular weight followed by lambda then kappa which are consistent with sedimentation coefficient results. Values are in excellent agreement with those obtained previously (Slootmaekers et al., 1991a; Viebke et al., 1995; Ciancia et al., 1997).

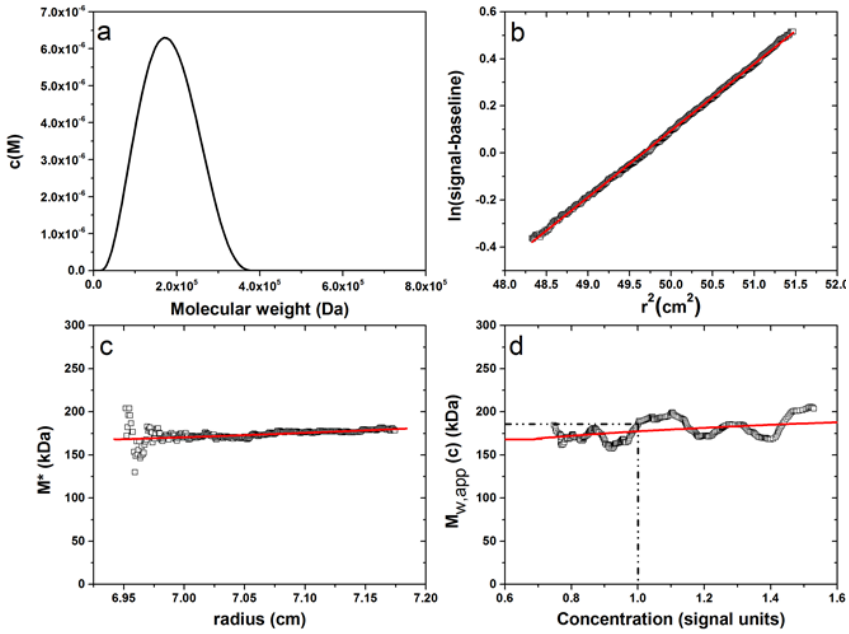


**Figure 4.9:** The analysis of **kappa carrageenan** in 0.1 M NaCl at a loading concentration of 0.3 mg $mL^{-1}$ (a) molecular weight distribution, *c(M) vs. M* plot; (b) log concentration ln *c(r) vs.* $r^2$ plot, where *r* is the radial distance from the centre of rotation; (c) *M* vs. r* plot: the value of *M** extrapolated to the cell base = $M_{w,app}$ the apparent weight average molecular weight for the whole distribution. (d) Point or local apparent weight average molecular weight at radial position r (open circle) plotted against the local concentration c(r). Dotted line gives the estimate for $M_{w,app}$ at **the hinge point**.

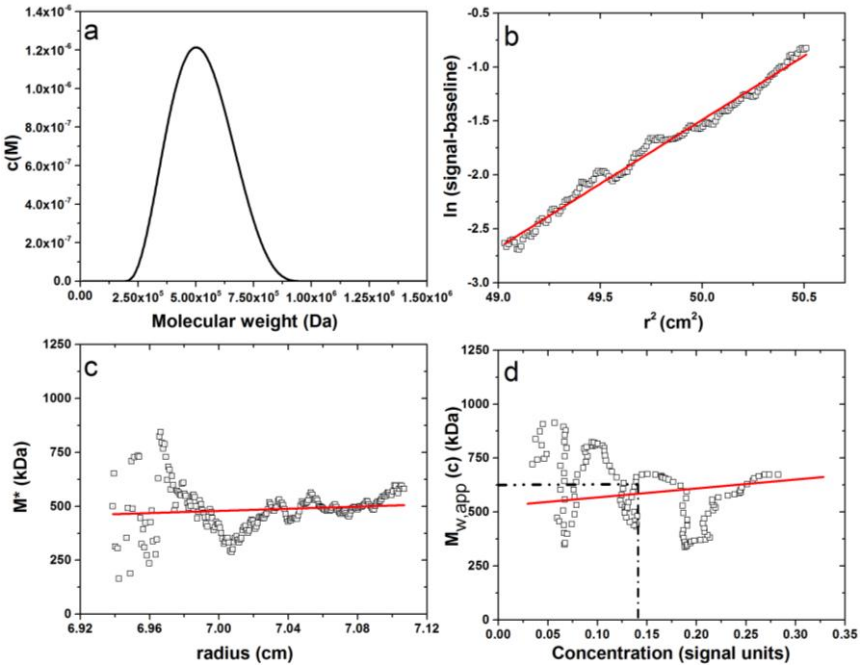


**Figure 4.10:** As (Figure 4.9) but the analysis of **iota carrageenan** in PBS 0.1M at a loading concentration (0.3 mg $mL^{-1}$). $M_{w,\,app}$ from extrapolation of $M^*$ to cell base = 550 kDa, and the fitted lines are defined in the legend Figure 4.9.

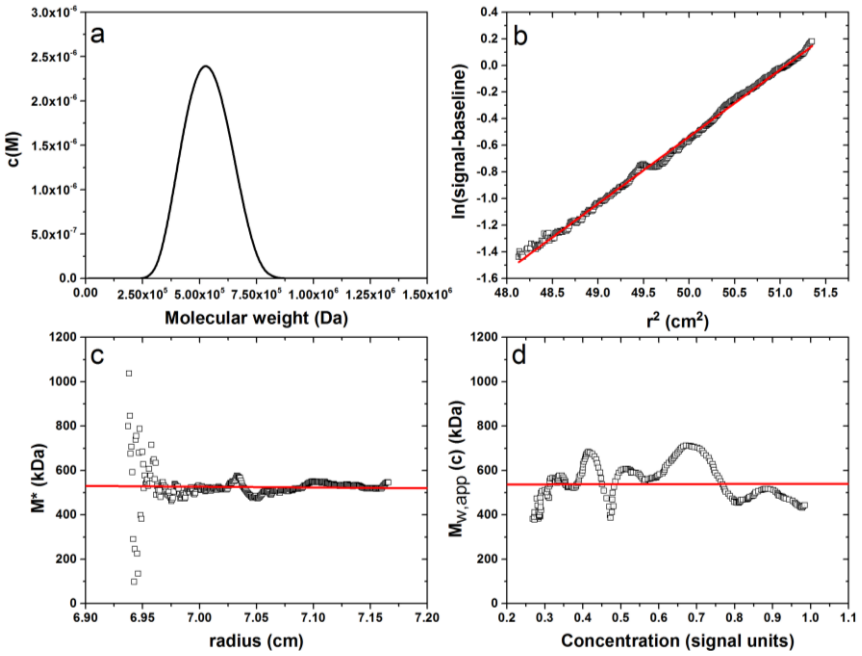


**Figure 4.11:** As (Figure 4.9) but for the analysis of **lambda carrageenan** in PBS 0.1M at a loading concentration (0.3 mg $mL^{-1}$). $M_{w,\,app}$ from extrapolation of $M^*$ to cell base = 540 kDa, and the fitted lines are defined in the legend Figure 4.9.

Furthermore, within the error estimate both iota and lambda show similar weight average molecular weights for all solvents used. In contrast, it can be clearly seen that weight average molecular weight of kappa approximately double in NaI solution than that yielded in both solvents NaCl and DMSO. The doubling of the molecular weight should be taken as indicator for a double helix conformation.

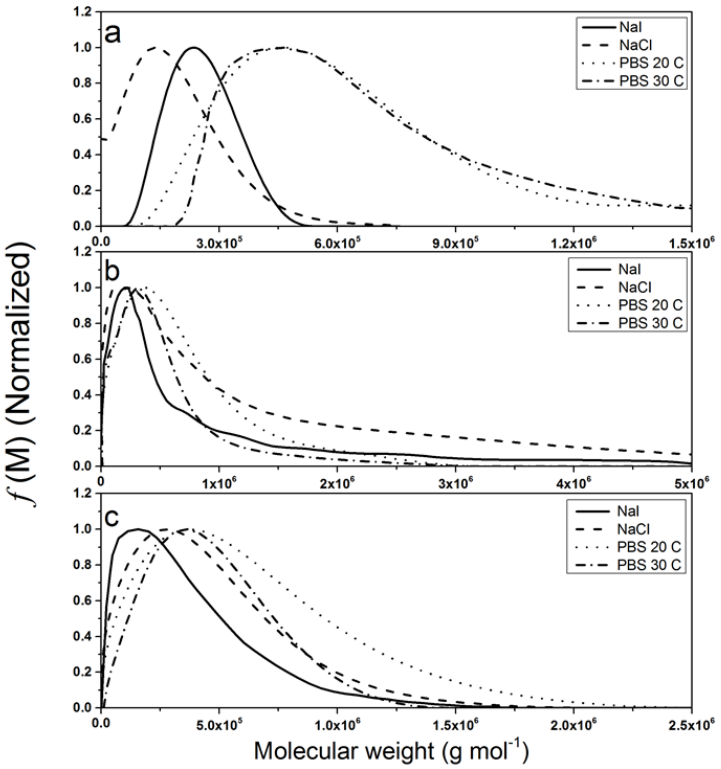


**Figure 4.12:** Molecular weight distribution for carrageenan samples at different solvents obtained from transformation of the g(s) versus *s* distribution at concentration (0.2 mg $mL^{-1}$), using the Extended Fujita method of Harding et al., (2011) (a) kappa (b) iota (c) lambda.

However, the molecular weight of kappa in PBS could not be measured using sedimentation equilibrium, due to the presence of gel at the cell base which made analysis of the radial distribution data difficult. Consequently, the molecular weight of kappa as well iota and lambda carrageenans (in PBS, NaI

and NaCl) were estimated by transforming a distribution of sedimentation coefficient (*s*) into a distribution of weight average molecular weight utilising the combination of Fujita (1962) equation $f(M) = g(s) \cdot (ds/dM)$ with $s = K_s M^b$ (Harding et al., 2011). Figure 4.12 shows the distributions of molecular weight obtained for carrageenan samples at different solvents. The influence of non-ideality arising from both co-exclusion and polyelectrolyte effects is again minimized by working at low concentration (0.2 mg $mL^{-1}$) and ionic strength (0.1 M). Values are in reasonably good agreement with those found using sedimentation equilibrium (Table 4.2). In the case of kappa in PBS solvent at both temperatures the weight average molecular weights obtained, indicating that kappa is forming double helices and then aggregating which coincides with the onset of the ordered-disordered transition seen by micro-DSC.

SEC coupled to MALS was also performed for carrageenan samples to estimate the molecular weight. The order-disorder transition was not induced by changing temperature as previously (Viebke et al., 1995; Viebke and Williams, 2000), the addition of salt only was used and the measurement was carried out at room temperature. As we were unable to calculate molecular weight for carrageenan in 0.1 M NaCl using SEC-MALS due to the technical issue with instrumentation (SEC-MALS) in our laboratory. The carrageenan only examined at 0.1 M NaCl and PBS. Values of weight average molecular weight for carrageenans (kappa, iota and lambda) in different solvents (0.1 M NaI and PBS) obtained using SEC-MALS are reported in Table 4.2. With the SEC-MALS system low concentration can be injected, taking advantage of the high sensitivity of the light scattering detector, and influence of non-ideality is

neglected in the measurement. The concentration is diluted in columns and become much lower than the initial loading concentration to be about 0.1 mg $mL^{-1}$ or less (Wyatt, 2013).

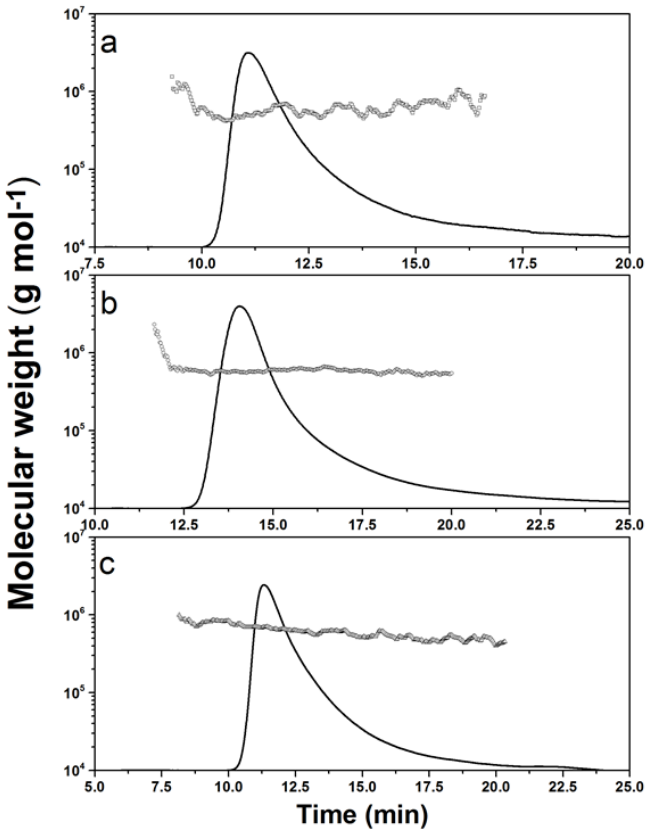


**Figure 4.13**: Example of elution profile of carrageenan samples and PBS 0.1M buffer (a) kappa, (b) iota and (c) lambda (black line) examined by SEC-MALS at concentration 0.8 mg $mL^{-1}$. The horizontal black lines (open square) correspond to SEC-MALS calculated molecular weights.

The elution profiles of molecular weight vs retention time estimated for kappa, iota and lambda carrageenans in both PBS (Figure 4.13) and NaI (not shown) demonstrated unimodal peaks, showing homogeneous preparations and again consistent with sedimentation coefficient distribution data at low concentrations. Difference in molecular weights and polydispersities reflect corresponding difference in molecular distribution and elution time for

carrageenans. Within experimental error estimate values of molecular weight from SEC-MALS are consistent with those obtained previous from sedimentation equilibrium and velocity of the systems studied.

### 4.4.4 Intrinsic Viscosity

The intrinsic viscosity values of kappa, iota and lambda carrageenans obtained using standard Ostwald capillary viscometry are reported in Table 4.3 and showed in all cases a good linear extrapolation from the Huggins, Kraemer and Solomon – Ciuta plots.

**Table 4.3:** Summary of intrinsic viscosity [η] results for kappa, iota and lambda carrageenans in different solvents obtained from capillary viscometry and on line ViscoStar.

| **Sample** | **Solvent** | **intrinsic viscosity [η] (mL $g^{-1}$)** | | | |
|---|---|---|---|---|---|
| | | **capillary viscometry** | | | **On line ViscoStar** |
| | | Huggins | Kraemer | Solomon-Ciuta | |
| **kappa** | 0.1M NaCl | 900±40 | 900±20 | 910±30 | nd |
| | 0.1M NaI | 2240±100 | 2450±60 | 2430±70 | 2600±160 |
| | 0.1M PBS | 970±70 | 1060±70 | 1030±70 | 1220±60 |
| | DMSO 100% | 1740±40 | 1620±40 | 1670±40 | nd |
| | DMSO 80% | 1080±20 | 1090±20 | 1090±20 | nd |
| **iota** | 0.1M NaCl | 1260±15 | 1250±10 | 1250±15 | nd |
| | 0.1M NaI | 1130±150 | 1260±120 | 1230±70 | 1020±50 |
| | 0.1M PBS | 1520±150 | 1550±90 | 1550±100 | 1200±70 |
| **lambda** | 0.1M NaCl | 1040±180 | 1040±90 | 1050±100 | nd |
| | 0.1M NaI | 990±70 | 980±50 | 980±60 | 1100±60 |
| | 0.1M PBS | 1320±110 | 1270±90 | 1290±90 | 1200±70 |

nd : not determined

Figures 4.14 and 4.15 show the corresponding plots of intrinsic viscosity versus concentration (g $mL^{-1}$) for carrageenans at different solvents (0.1 M NaCl, NaI, PBS and DMSO (100 and 80%)). Kappa in NaI presented the highest intrinsic viscosity value compared to that in NaCl, PBS and DMSO. The differences were clearly seen among kappa at all solvents, resulting from different conformations (ordered and disordered) adapted in each solutions at room temperature (Figure 4.14).

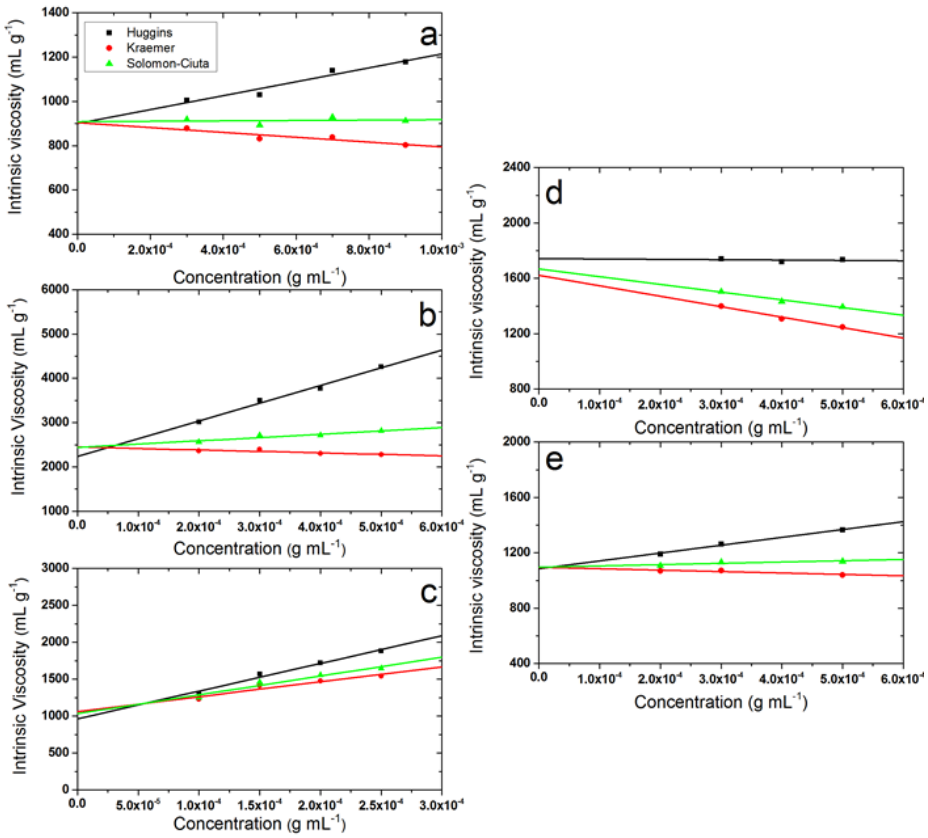


**Figure 4.14:** Intrinsic viscosity plots from capillary viscometry: Huggins, Kraemer and Solomon-Ciuta extrapolations for **kappa carrageenan** (a) NaCl (b) NaI (c) PBS 20.0$^{o}$C (d) DMSO 100% and (e) DMSO 80%.

Furthermore, working at low concentrations, (1.0 – 2.5 x $10^{-4}$) g $mL^{-1}$, showed a decrease in the intrinsic viscosity results for the kappa in PBS upon structure

aggregation formation, and consistent with that found previously (Richardson and Goycoolea, 1994). Within the error estimate iota and lambda showed similar intrinsic viscosity results for all solvents, namely 0.1 M NaCl, NaI and PBS (Figure 4.15). However, Table 4.3 also reports the intrinsic viscosity for all carrageenans at only two solvents (0.1 M NaI and PBS) from ViscoStar on line with SEC-MALS, and in excellent agreement with those from capillary viscometry.

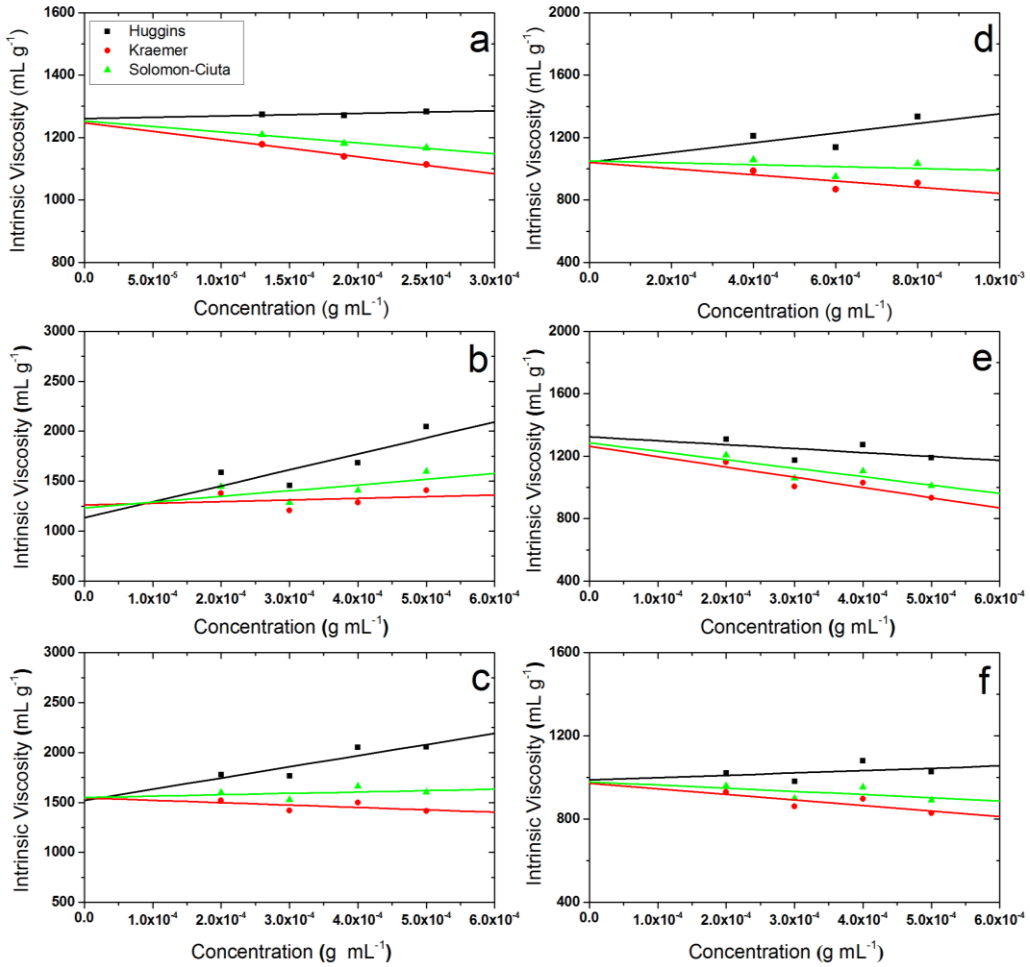


**Figure 4.15:** The intrinsic viscosity plot from capillary viscometry: Huggins, Kraemer and Solomon-Ciuta extrapolations for **iota carrageenan** (a, b and c) and **lambda carrageenan** (d, e and f) at different solvents NaCl, NaI and PBS 20.0$^{o}$C, respectively.

## 4.5 DISCUSSION

The influences of salt type and concentration on carrageenans have been explored and different behaviour has been seen. For instance sodium iodide (NaI 0.1M) has been claimed previously to enhance the formation of the ordered helical conformation at room temperature whilst sodium chloride (NaCl 0.1M) has been shown to favour the disordered conformation (Grasdalen and Smidsrod, 1981; Viebke et al., 1995; Ciancia et al., 1997; Cuppo and Reynaers, 2002). In the present study, thermal transition has been studied in order to assess the influence of different solvents (0.1 M NaCl, NaI, PBS and DMSO (100 and 80%)) on carrageenan conformation using micro-DSC. Clearly carrageenan is thermo-reversible, hence a coil-to-helix transition followed in some cases by aggregation among helices forming a three dimensional structure gel network takes place upon cooling (Takemasa and Nishinari, 2004). As shown in Figure 4.2 (a) for kappa, the presence of NaI shifts the thermal transition to higher temperatures compared to NaCl and PBS solutions. This can be explained by the increasing the stability of the helix. Moreover, it decreases the thermal hysteresis on cooling as compared to PBS, suggesting helical formation but not gel formation. A similar behaviour was observed in the presence of DMSO (100% and 80%), which confirmed the helix ordered conformation and no gel formation (Figure 4.2d). According to Rochas and co-workers, kappa carrageenan arranges in water as a double helix ordered conformation, unlike the mono-helix ordered conformation displayed in DMSO. This single helix conformation is characterised by a broadening of the transition and a symmetrical melting-curve (Rochas and Rinaudo, 1982). These behaviours observed for carrageenan in different solvents however, have

inspired us to try and address the question as to whether either single or double helices are present or responsible for the so-called ordered conformation.

Analytical ultracentrifugation, and in particular sedimentation velocity, offers the possibility to estimate the conformation and flexibility of polysaccharides in terms of their weight average sedimentation coefficient – a measure of the size and shape of the macromolecules – and sedimentation coefficient distribution (Harding, 2005b). Iota has the highest weight average sedimentation coefficient $s^{\circ}_{20,w}$ followed by lambda and then kappa. It may have been expected that different $s^{\circ}_{20,w}$ values of the carrageenans is ascribed to the different size (molecular weight) and conformation of these macromolecules: suggests that iota has either a more compact structure or the largest molecular weight (or both); while lambda has extended flexible coil and kappa the most rigid structure, as was previously observed (Morris, 2001; Almutairi et al., 2013; Harding et al., 1997, respectively). However, the broadness of the sedimentation coefficient distribution and the large sedimentation coefficient value for kappa in PBS (0.1 M) represents the gelation behaviour, which might be induced by the small percentage of potassium cations in PBS. The behaviour seen here is different from what was observed for kappa in PBS (Potassium $K^+$ free) using analytical ultracentrifugation, which did not form gelation (Harding et al., 1997). Moreover, the helix - coil transition was induced by increasing the temperature of the measurement to be (30.0 $^{o}$C) for carrageenans in PBS solution. A decrease in sedimentation coefficient was observed for kappa, whereas iota and lambda did not; this suggests that a slight change might have occurred in the conformational state of kappa carrageenan (Table 4.1).

Thus, it is interesting to analyses kappa carrageenan in NaCl – a favorable solvent of the disordered conformation – a decrease on the sedimentation coefficient was yielded, which might be interpreted in a double helix formation. Furthermore, in the presence of the DMSO solvents (at both 100% and 80%) sedimentation coefficient values of kappa reduced to be (approximately 3.1±0.1 S), and might be attributed to the ability of DMSO to disrupt the ordered conformation of polysaccharides at higher concentration ~91 % (Member and Morris, 1995). The discrepancy of the results obtained for kappa carrageenan in DMSO solvent from micro-DSC and AUC based on sedimentation velocity and equilibrium can be attributed to efficiency of the solvent to disrupt the ordered conformation. That can clearly been seen, DMSO was not completely disrupt the ordered conformation of kappa carrageenan. However, earlier studies using sedimentation velocity for kappa showed a similarity in sedimentation coefficient results at both 0.1 M NaCl and NaI (Slootmaekers et al., 1991b). It is possible that this might be due to the different procedures used for preparation of the kappa carrageenan solutions. In this study carrageenan solutions were prepared by heating at approximately 80.0 $^{o}$C for 30 min.

In this regard we can now compare the sedimentation coefficient values estimated for carrageenans (in this study) with what might be expected or predicted for helix and coil conformations utilizing the Mark-Houwink-Kuhn-Sakurada (MHKS) relation. Following Studier (1965) this method has been based on the assumption that the molecular weight of a dimer is twice that of monomer; thus sedimentation coefficient results for a helical conformation can be predicted theoretically through the following equation:

$$s^{o}_{20,w\,(dimer)} = 2^{b} \,.\, s^{o}_{20,w\,(monomer)} \qquad (4.5)$$

derived from MHKS relation ($s^{o}_{20,w} = K_s\, M^{b}$), where the exponent (b) in the case of a theoretically perfect rod = 0.15, and for a coil = 0.4-0.5 (see, e.g. Tombs and Harding 1998). The predicted sedimentation coefficient values in dimer state for both iota and lambda carrageenans appear to be higher compared with experimentally determined in dimer (helix) ordered, while kappa remain similar (Table 4.4). The excellent agreement between the predicted and experimental sedimentation coefficient values for kappa carrageenan again indicates a double helix conformation.

**Table 4.4**: Predicted sedimentation coefficient values based on experimental data for carrageenans.

| Sample | $s^{o}_{20,w}$ Experiment [a] | | $s^{o}_{20,w}$ Predicted (Dimer) [b] |
|---|---|---|---|
| | Coil (monomer) NaCl | Helix (Dimer) NaI | |
| **kappa** | 4.2±0.1 | 4.6±0.2 | 4.6 |
| **iota** | 6.8±0.4 | 7.0±0.2 | 7.5 |
| **lambda** | 5.6±0.2 | 5.7±0.2 | 6.2 |

a : sedimentation coefficient values obtained experimentally, in sodium chloride solution (NaCl) – according to the claims of other studies – adopts a coil conformation, while in sodium iodide solution (NaI) adopts a helix conformation.
b : predicted sedimentation coefficient obtained in dimers form using $s^{o}_{20,w\,(\mathrm{dimer})} = 2^{b}\, s^{o}_{20,w(\mathrm{monomer})}$ ,where the molecular weight in dimer is double of monomer.

Although the sedimentation coefficient is a representativel measure of the size (e. g. the seed globulins and ribosomes), it also depends on conformation. Therefore absolute molecular weight can be estimated using sedimentation equilibrium in the analytical ultracentrifugation as well as SEC-MALS. Over the range of solvents (e.g. PBS 20.0, 30.0$^{o}$C, NaCl and NaI) the weight average

molecular weights for iota and lambda carrageenan remain relatively constant, with no sign of reversible associative as studied by the sedimentation equilibrium experiment. These results are consistent with sedimentation coefficient results, whilst there is no clear evidence of double helix conformation for both iota and lambda as previously supported (Vannest et al., 1994; Bongaerts et al., 2000). On the other hand, the higher weight average molecular weight obtained for kappa in NaI compared to those in NaCl and DMSO suggest a double helix formation, which is in good agreement with previous studies (Morris et al., 1980; Viebke et al., 1995; Wittgren et al., 1998). This finding is likewise consistent with sedimentation coefficient results obtained using sedimentation velocity experiment. the molecular weight provided by SEC-MALS for kappa in PBS was higher and also eluted earlier compared to other solvent (0.1 M NaI). This may reflect a sort of high level of aggregation due to the presence of potassium as seen in the micro-DSC and sedimentation velocity data (Ciancia et al., 1997). Another approach of estimating molecular weight for kappa in PBS is using the Extended Fujita method based on sedimentation velocity (Harding et al. 2011), showed higher molecular weight in a good agreement with SEC-MALS results, which might be affected again by gelation behaviour (Figure 4.12).

One of the simplest parameters providing information about conformation and conformational change is the intrinsic viscosity. In the case of iota and lambda carrageenan in 0.1 M NaI this not associated with any increase of intrinsic viscosity compared to these substances in both 0.1 M NaCl and PBS. This is in excellent agreement with sedimentation coefficient and molecular weight resultspreviously reported by Ciancia and co-worker (Ciancia et al., 1997).

Under similar conditions, kappa carrageenan showed approximately a doubling in intrinsic viscosity (Figure 4.13). This would indicate the high rigidity of kappa molecules in the ordered conformation and be consistent with a double helix conformation consistent with an earlier found for kappa and xanthan (Chronakis et al., 2000).

# CHAPTER 5

# HYDRODYNAMIC CHARACTERISATION OF CHITOSAN AND ITS INTERACTION WITH TWO POLYANIONS: DNA AND XANTHAN

In this chapter another group or family of marine polysaccharides is considered: chitosan a soluble polycationic derivative of insoluble chitin. Commercial ("C") and in-house laboratory ("L") prepared chitosan samples extracted from crustaceous shells with different molecular weights and degrees of acetylation (25% and 15%) were characterised with regards to (i) weight-average molecular weight ($M_w$); (ii) sedimentation coefficient ($s^o_{20,w}$) distribution, and (iii) intrinsic viscosity ([η]). Therefore, the physical properties estimated for chitosan provided us the basis for investigating the interaction with two polyanions DNA and xanthan (another double helical high molecular weight molecule) using the principle of co-sedimentation.

## 5.1 INTRODUCTION

Chitosan is the generic term for a family of linear, copolymeric polysaccharide derivatives of chitin extracted from the exoskeletons of crustaceans or the cell walls of *Basidomycete* fungi. The basic structure of chitosan consists of 2-amino-2-deoxy-$\beta$-D-glucopyranose units linked through a $\beta$-(1,4) linkage, with a high degree of *N*-acetylation (Figure 5.1). It is very similar to cellulose, except that at the C-2 position, the acetylamino group is replaced by the hydroxyl group (Tombs and Harding, 1998). The amine groups of chitosan are

much easier to protonate in an acidic medium, resulting in a positively charged polysaccharide with a high charge density. This characteristic is important, as it makes chitosan water soluble and a potential bioadhesive, facilitating the binding of negatively charge macromolecules (Hejazi and Amiji, 2003). The diversity of chitosans in solution depends on 3 degrees of freedom, namely their molecular weight, degree of acetylation (DA) and also the distribution of acetyl group along the main chain (Venugopal, 2011).

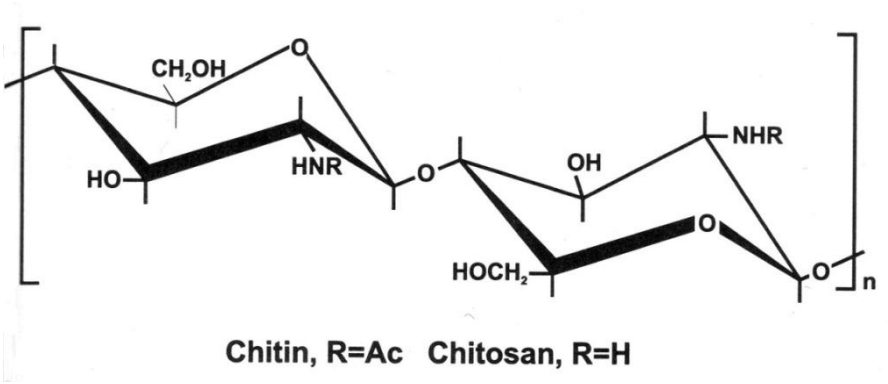


**Figure 5.1:** Chemical structure of chitosan. Adapted from Tombs and Harding, (1998). Ac=acetyl.

Chitosan has many distinctive properties including biocompatibility, biodegradability, hemocompatiblity, antibacterial activity, nontoxic, antitumor, fungistatic and anticholesteremic (Rinaudo, 2006). As a result of these properties, chitosan has received a great deal of interest for use in the food (No et al., 2007), cosmetic (Ravi Kumar, 2000), and pharmaceutical industries (Morris et al., 2010). Additionally, specific complexes of chitosan with oppositely charged polyelectrolytes have yielded three-dimensional networks or "hydrogels" and these have potential for controlled drug release from drug delivery systems as well as protecting the drug from degradation in the

gastrointestinal tract. The efficacy and efficiency of chitosan can be altered by changing the chemical structure (e.g. molecular weight) and reaction conditions (e.g. ionic strength), which involves electrostatic interaction and hydrogen and hydrophobic bonds. Such interactions are attracting attention in biomedical research areas, in particular, drug delivery (e.g. chitosan-carrageenan) and gene delivery (e.g. chitosan-DNA) (Il'ina and Varlamov, 2005; Jayakumar et al., 2010). However, understanding the behaviour of chitosans in the presence of other macromolecules is dependent on knowledge of its own molecular properties in solution, particularly how molecular weight and conformation impact on the behaviour of chitosans.

The study of molecular properties such as conformation and molecular weight for chitosan in solution is important to comprehend its properties and functions. Thus, molecular weight (primarily the weight average $M_w$) or "molar mass" estimations for various chitosan preparations in solution have in the past been investigated using either multi-angle light scattering (MALS), or light scattering coupled with size exclusion chromatography, or SEC alone (Rinaudo et al., 1993; Berth et al., 1998; Cölfen et al., 2001). Due to the possibility of adverse polycationic interactions with column materials, use of a second independent method for molecular weight determination is nonetheless useful and analytical ultracentrifugation (AUC) – which has an inherent fractionation property without the need for columns or membranes – is useful in this regard (Fee et al., 2003), using the complementary tools of sedimentation velocity or sedimentation equilibrium.

In their interactions with macromolecules and other ligands, the conformation of chitosans can also play an important role, and, depending on the source,

molecular size range, and degree of acetylation DA (or degree of de-acetylation) conformations can range from semi-flexible to stiffer conformations (Cölfen et al., 2001; Fee et al., 2003; Morris et al., 2009), with sedimentation and viscometry also playing a key role in these evaluations.

There is increasing interest in chitosan interactions with polyelectrolytes of opposite charge, for example, chitosan-mucin glycoprotein mucoadhesive interactions used for nasal and oral drug delivery (see, Harding, 2003; Harding, 2006). Sedimentation velocity has been used previously to assay the efficacy of these interactions where results are reflected in a change in the sedimentation coefficient of the complex with respect to that of pure component. The different optical properties of the interacting components have also been assessed. Chitosans have also been considered along with other polycationic molecules for use as histone analogues for condensing DNA.

In this study, the properties of different samples of chitosan were investigated in solution to assess structural integrity in terms of sedimentation coefficient, molecular weight, distribution of molecular weight, intrinsic viscosity and overall conformational flexibility. Sedimentation velocity along with sedimentation equilibrium in the AUC were used with SEC-MALS and viscometry in order to provide important information, which will support any strategy planned to investigate whether the interaction occurred between chitosan and other polyelectrolytes of opposite charge in particular DNA and for comparison another polyanions claimed to have a double helical conformation, namely xanthan. However, the degree of interaction has been measured by comparing the distribution/weight average of sedimentation coefficient for the complex to those of individual.

# 5.2 MATERIALS

Commercially available chitosans (CHIT1, CHIT2, CHIT3 and CHIT4) were obtained from Sigma Aldrich (USA). A further two chitosans (CHIT5 and CHIT6) hitherto referred to as "laboratory chitosans" were prepared at the Teagasc Food Research Centre, Ashtown, Dublin 15, Ireland. Degrees of acetylation (DA) were found to be approximately 25% for CHIT1 to CHIT5 and 15% for CHIT6, as assayed using NMR (Almutairi et al., 2015). Samples were used as supplied without any further purification. The chitosan samples were dissolved in I= 0.2 M acetate buffer (pH 4.3) with stirring for 24 h and used directly for all experiments. For sedimentation equilibrium experiments the samples were dialysed against the buffer solution overnight. DNA samples were kindly provided by Dr. Alan Mackie, Institute of Food Research (Norwich, UK) in stock solution (5.0 mg $mL^{-1}$) and were diluted in phosphate buffered saline (PBS) at an ionic strength of 0.1 M and pH 7.4.

A stock solution of xanthan (supplied by Dupont, Paris), referred to as "xanthan – STD" (Erten et al., 2014) was prepared by dissolving a known amount in distilled deionised water, with gentle stirring for 3 hours followed by overnight dialysis against phosphate-chloride buffer supplemented with NaCl at pH 7.0 and an ionic strength of 0.1M. The concentrations, $c$ (g $mL^{-1}$) of the stock of chitosans and xanthan solutions were measured using an Atago (Japan) DD-7 refractometer calibrated with glucose standards. The mixtures of DNA-chitosan and xanthan-chitosan were prepared by adding equal volumes and concentration.

# 5.3 METHODS

## 5.3.1 Sedimentation Velocity (SV)

As before (Chapters 3 and 4) an Optima XL-I (Beckman Instruments, Palo Alto, USA) equipped with Rayleigh interference optics was used. Sample (400µl) and reference buffer (400µl) were injected into sample and reference channels, respectively, of double sector 12.0 mm optical path length cells. The Rayleigh interference optical system was used to record changes in the concentration versus radial displacement profiles with time. An initial low rotor speed of 3000 rpm was used to check for the presence of any large sedimenting species and then adjusted to a rotor speed of 40,000 rpm. The standard conditions of density and viscosity of water at 20.0℃ were used for adjustment of the sedimentation coefficients *s* to $s_{20,w}$ values (Schachman, 1959). The data was analysed using the SEDFIT procedure (Dam and Schuck, 2004), which solves the Lamm equation describing the change of concentration distribution with radial position with time in terms of a distribution of sedimentation coefficients, g(s) vs *s*, where *s* is the sedimentation coefficient. To eliminate the effects of non-ideality (co-exclusion and any residual polyelectrolyte effects) a plot of the reciprocal of the sedimentation coefficient ($1/s_{20,w}$) against concentration, *c* (g $mL^{-1}$) was made and from the intercept at infinite dilution *c*=0, the value free of these effects was found: $s^{o}_{20,w}$ (units seconds, s, or Svedbergs, S, where $1S = 10^{-13}s$). However, the curve fitting module MULTIG (A. J. Rowe, NCMH) in pro FIT™ (QuantumSoft, Switzerland) was used to yield the percentage of unreacted DNA material in the complexes of chitosan and DNA.

### 5.3.2 Sedimentation Equilibrium (SE)

Sedimentation equilibrium experiments were performed also using the Optima XL-I analytical ultracentrifuge. The optical path length (12.0 mm) double-sector cells with sapphire windows were loaded with (~80 μl) of dialysed sample and a matching amount of reference buffer dialysate in appropriate channels. The balanced cells were then loaded into an analytical 8-hole titanium rotor An50-Ti and placed in the AUC. After time was allowed for vacuum formation (≤ 50 microns) and for temperature equilibration (20.0°C), the rotor was then accelerated to 10,000 rpm. Using the Rayleigh interference optical system, scans were taken every one hour and equilibrium was reached after approximately 72 hours. Records of the relative concentration distribution of the solute at equilibrium was analysed to give the apparent weight average molecular weight $M_{w,app}$ using the SEDFIT-MSTAR algorithm (Schuck et al., 2014). To account for non-ideality, the conventional/reciprocal of the apparent weight average molecular weight $1/M_{w,app}$ determined over a range of concentrations, $c$, were extrapolated to zero concentration (Harding, 2005a).

### 5.3.3 Size Exclusion Chromatography Coupled to Multi Angle Light Scattering (SEC-MALS)

Molecular weight (weight averages) of all chitosan samples were also estimated by using the independent technique of SEC-MALS (Wyatt, 1992, 2013), and considered in detail in *Chapter 2*. As before the size-exclusion chromatography (SEC) system used comprised a series of columns, namely TSK G6000PW and TSK G4000PW, protected by a similarly packed guard

column (Tosoh Bioscience, Tokyo, Japan) coupled on-line to a "Helios" multi-angle light scattering (MALS) and refractive index (OptilabrEX) detectors (Wyatt Technology, Santa Barbara, USA). Solutions prepared at injected concentrations of 0.5 mg $mL^{-1}$ were filtered through a 0.45 μm syringe filter (Whatman, Maidstone, England) - to remove any insoluble material or dust prior to being injected into the columns. The buffer was pumped at a steady, pulse-free flow rate of 0.8 mL $min^{-1}$ through the column system. ASTRA (Version 5.1.9.1) software (Wyatt Technology, Santa Barbara, U.S.A.) was used to analyse the data. The absolute weight average molecular weight ($M_w$) was obtained based on information of the refractive index increment value: chitosan $dn/dc$ = 0.163 mL $g^{-1}$ (Rinaudo et al., 1993). Because of the low concentrations after dilution on the columns no correction for non-ideality was assumed necessary, and $M_{w,app} = M_w$, the ideal weight average molecular weight.

## 5.3.4 Capillary and Differential Pressure Viscometry

As before (chapter 3 and 4) the relative viscosities $\eta_{rel}$ of chitosan samples in concentration ($c$) ranging from 0.1 – 1.0 mg $mL^{-1}$ were measured using a 2mL Ostwald viscometer at temperature of (20.00 ± 0.01) °C. The reduced ($\eta_{red} = (\eta_{rel}-1)/c$) and inherent ($\eta_{inh} = (\ln\eta_{rel})/c$) viscosities were extrapolated to infinite dilution to eliminate non-ideality effects using both the Huggins and Kraemer approaches. As an additional check, a combined relation due to Solomon and Ciuta was also used (see, e.g. Harding, 1997).

$$[\eta]\sim(1/c).\left[2\left(\eta_{sp}-ln(\eta_{rel})\right)\right]^{1/2} \quad (5.1)$$

Relative viscosities were also estimated from a Viscostar (Wyatt Technology) differential pressure viscometer linked on-line to the SEC-MALS system (Harding, 1997). The differential pressure drop from solution flow versus solvent flow yielded $\eta_{rel}$ and then the reduced viscosity $\eta_{red}$. Then because of the high dilutions from the column, the assumption that the intrinsic viscosity ~ reduced viscosity can be reasonably made.

$$[\eta]\sim \eta_{red} \quad (5.2)$$

The average [η] for the whole undistributed sample can be specified as well as the intrinsic viscosity [η]($V_e$) as a function of elution volume $V_e$. Because of the higher sensitivity of the sensors and the high dilution from the column, eqn 5.1 was used to obtain [η] without a concentration extrapolation.

# 5.4 RESULTS

## 5.4.1 Sedimentation Coefficient and Sedimentation Coefficient Distribution

Chitosan samples were first of all characterised by sedimentation velocity in the analytical ultracentrifuge to establish their molecular integrity using the least squares ls-g*(s) method of Dam & Schuck (2004). The sedimentation coefficient, $s^o_{20,w,}$ yielded for all samples ranging from 1.8 S to 2.7 S as reported in (Table 5.1) presented different molecular weights (size). As has been known sedimentation coefficient principally depends on the size (as well

the conformation); the low molecular weight chitosan being the lowest (1.8 ± 0.1) S and the high molecular weight chitosan being the highest (2.7 ± 0.1) S. These results are also within the expected range for chitosans (Cölfen et al., 2001; Fee et al., 2003; Morris et al., 2009). Unimodal distributions were seen in all cases for the apparent sedimentation coefficient distributions; showing that the samples are homogeneous (Figure 5.2).

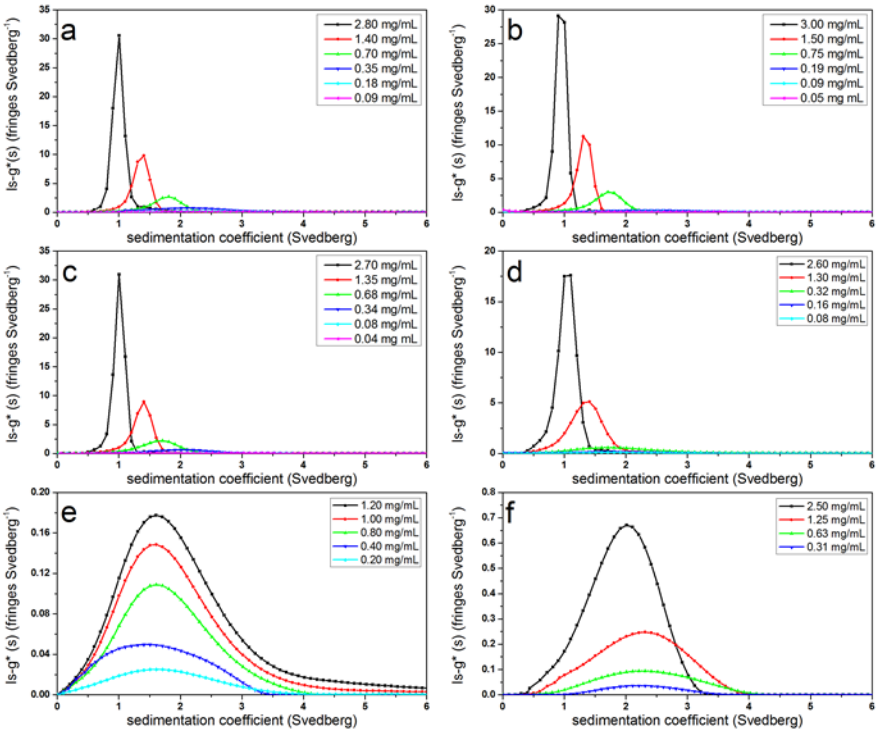


**Figure 5.2:** Sedimentation coefficient distribution profiles using least squares g*(s) method of SEDFIT obtained from sedimentation velocity experiment for chitosan samples (a) CHIT1 (b) CHIT2 (c) CHIT3 (d) CHIT4 (e) CHIT5 (f) CHIT6.

However, values of the weighted average $s_{20,w}$ increased with decrease in concentration, showing no evidence of associative effects. In addition the concentration dependence was considered even at the small range of concentration used, was indicative of non-ideality (Figure 3). The higher values of concentration dependence observed for commercial samples (CHIT1 to

CHIT4) but not for the laboratory-prepared samples (CHIT5 and CHIT6), which is reflected by very high non-ideal behaviour (Table 5.1).

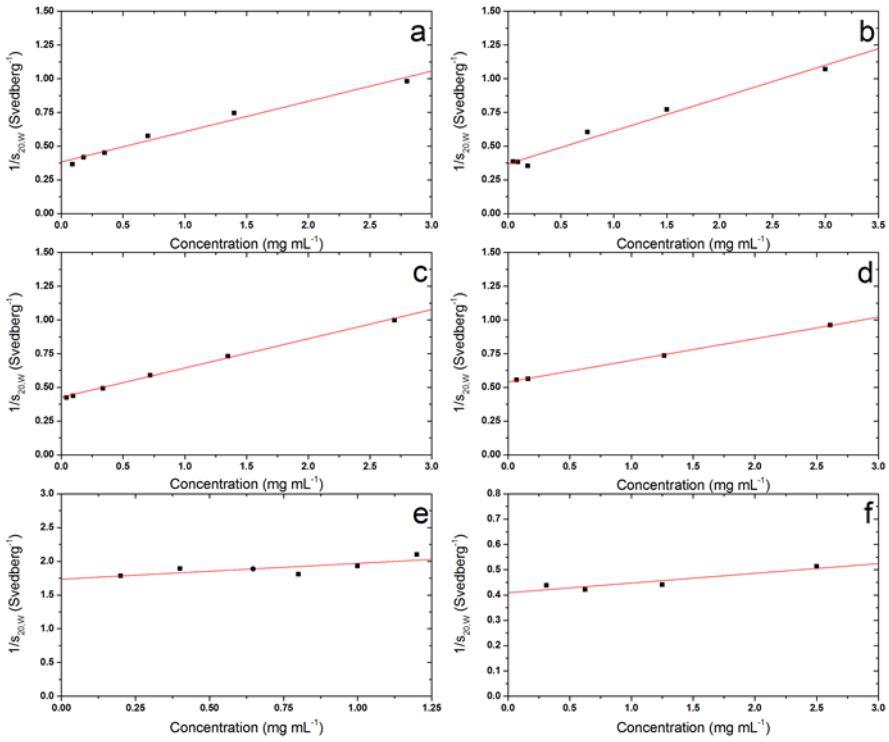


**Figure 5.3:** Concentration dependence (reciprocal) of the sedimentation coefficient plot (after correction to standard solvent conditions) for chitosan samples (a) CHIT1 (b) CHIT2 (c) CHIT3 (d) CHIT4 (e) CHIT5 (f) CHIT6.

**Table 5.1**: Summary of $s^{\circ}_{20,w}$ and $k_s$ results for all chitosan Commercial ("C") and in-house laboratory ("L") prepared samples.

| Sample | $s^{\circ}_{20,w}$ (S) | $k_s$ (mL g$^{-1}$) |
|---|---|---|
| **CHIT1** | 2.5±0.2 | 650±50 |
| **CHIT2** | 2.7±0.2 | 750±70 |
| **CHIT3** | 2.3±0.1 | 600±30 |
| **CHIT4** | 1.85±0.1 | 300±10 |
| **CHIT5** | 1.8±0.1 | 100±30 |
| **CHIT6** | 2.4±0.1 | 120±30 |

## 5.4.2 Estimation of Molecular Weight

Absolute molecular weight can be estimated using SEC-MALS as well as sedimentation equilibrium in the analytical ultracentrifugation. The weight average molecular weight of all chitosan samples initially was estimated from sedimentation equilibrium. Although working at low concentration (0.3 mg $mL^{-1}$) and a reasonable ionic strength (0.2 M) helped to minimize the non-ideality arising from co-exclusion and polyelectrolyte effect, for some polysaccharides (including chitosan) these effects can still be significant. The assumption is made that the apparent molecular weight at this loading concentration $M_{w,app} \sim M_w$ the true or ideal weight average molecular weight is not valid (Harding, 2005a; Schuck et al., 2014). Consequently, such effects can normally be vanished by performing a series of measurements at different loading concentration and extrapolate back to zero concentration.

Each chitosan sample was run at different concentration ranges from (0.5 -2.0 mg $mL^{-1}$), and weight average molecular weights were obtained using SEDFIT-MSTAR (see, for example Figure 5.4). The plot of $M_{w,app}$ versus concentration for commercial samples (CHIT1 to CHIT4) gave a non-linear extrapolation, showed a significant concentration dependence consistent with non-ideal behaviour and is in agreement with sedimentation velocity results (Figure 5.5 a). At the same time a simple second order polynomial fit was used to yield the molecular weight values and are reported in (Table 5.2). Similar behaviour has been observed for other polysaccharides such as alginate (Horton et al., 1991b) and hyaluronic acid at high molecular weight (Hokputsa et al., 1993).

**Table 5.2**: Summary of weight average molecular weights *($M_w$)* results for chitosan samples from sedimentation velocity, equilibrium and SEC-MALS.

| samples | $10^{-3}$ x $M_w$ (g mol$^{-1}$)[a] | $10^{-3}$ x $M_w$ (g mol$^{-1}$)[b] | $10^{-3}$ x $M_w$ (g mol$^{-1}$)[c] |
|---|---|---|---|
| **CHIT1** | 170±10 | 170±5 | 160±10 |
| **CHIT2** | 230±10 | 260±10 | 220±20 |
| **CHIT3** | 130±10 | 140±5 | 120±20 |
| **CHIT4** | 85±5 | 110±20 | 90±10 |
| **CHIT5** | 95±10 | 85±5 | 95±10 |
| **CHIT6** | 170±30 | 170±10 | 140±30 |

a : molecular weight obtained from sedimentation equilibrium
b : molecular weight obtained from SEC-MALS
c : molecular weight obtained from sedimentation velocity and the Extended Fujita method

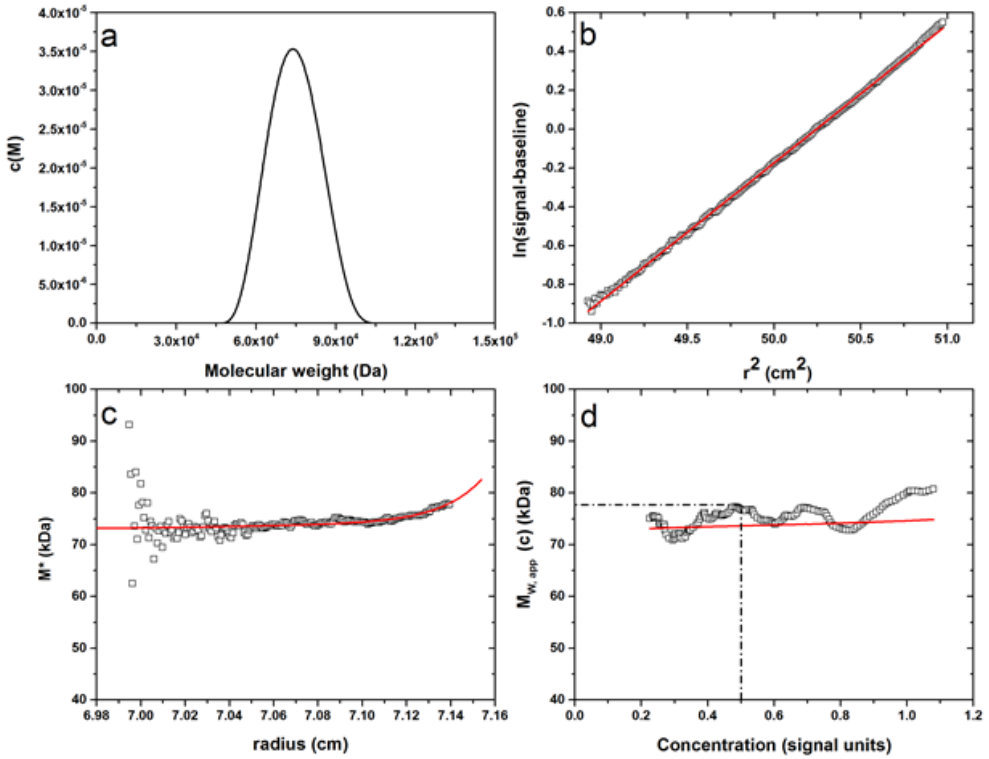


**Figure 5.4:** As (Figure 4.9) but the analysis of **CHIT4** at a loading concentration of (0.5 mg mL$^{-1}$). $M_{w,\,app}$ from extrapolation of $M^*$ to cell base = 80 kDa, and the meaning of the fitted lines in "c" and "d" are explained in the legend Figure 4.9.

Although the conventional plot of $M_{w,\ app}$ versus concentration gave a linear extrapolation for the laboratory-prepared samples (CHIT5 and CHIT6), the results obtained were insufficient. Thus, the reciprocal plot of $1/M_{w,\ app}$ versus concentration was applied (Figure 5.5 b), and again gave a linear extrapolation, whilst molecular weight values are presented in (Table 5.2).

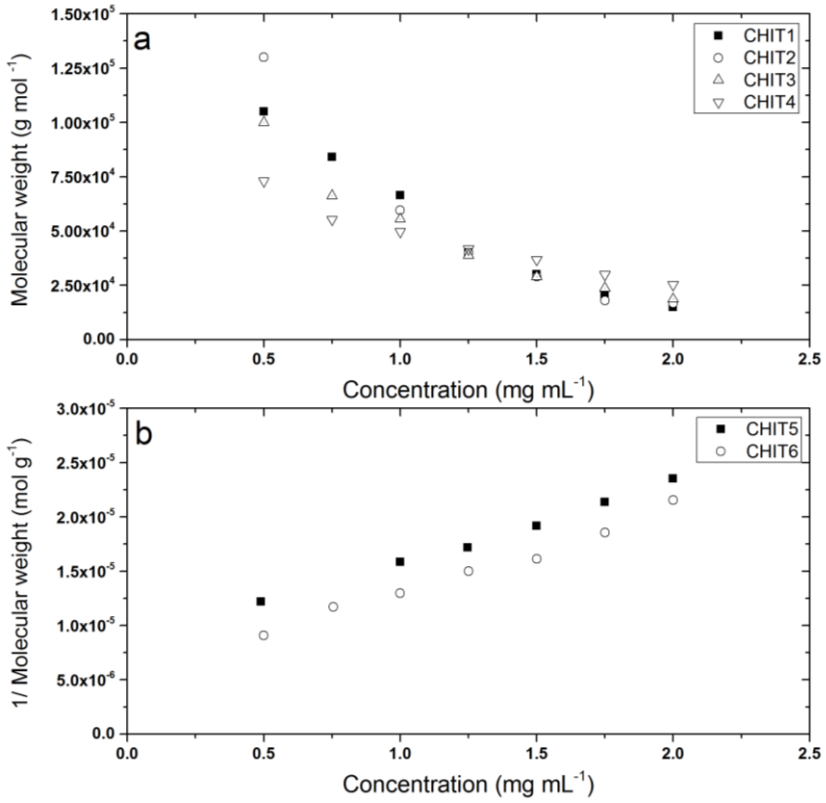


**Figure 5.5:** Plots of the apparent weight average molecular weight ($M_{w,app}$) against concentration c (g mL$^{-1}$): (a) the conventional plot ($M_{w,\ app}$ *vs c*), the molecular weight ($M_w$) value obtained is to $M_{w,\ app} = M_w + a_1c + a_2c^2$; (b) the reciprocal plot ($1/M_{w,\ app}$ *vs c*), the $M_w$ value obtained is to $1/M_{w,\ app} = 1/M_w\ (1+2BM_w\ c)$, where *B* is the second thermodynamic virial coefficient (mL mol g$^2$).

However, with the SEC-MALS system the non-ideality effects are usually small in the experiment, due to the ability of the light scattering detector (high

sensitivity) for working at the low concentrations that can be injected. The sample concentration is diluted by the columns and becomes much lower than the initial loading concentration usually 0.1 mg $mL^{-1}$ or less (Wyatt, 2013). Molecular weight versus retention time for chitosan samples obtained from SEC-MALS showed earlier elution times for commercial samples (CHIT1 to CHIT4), in contrast to that of laboratory prepared samples (CHIT5 and CHIT6) despite similar molecular weights were observed (Figure 5.6).

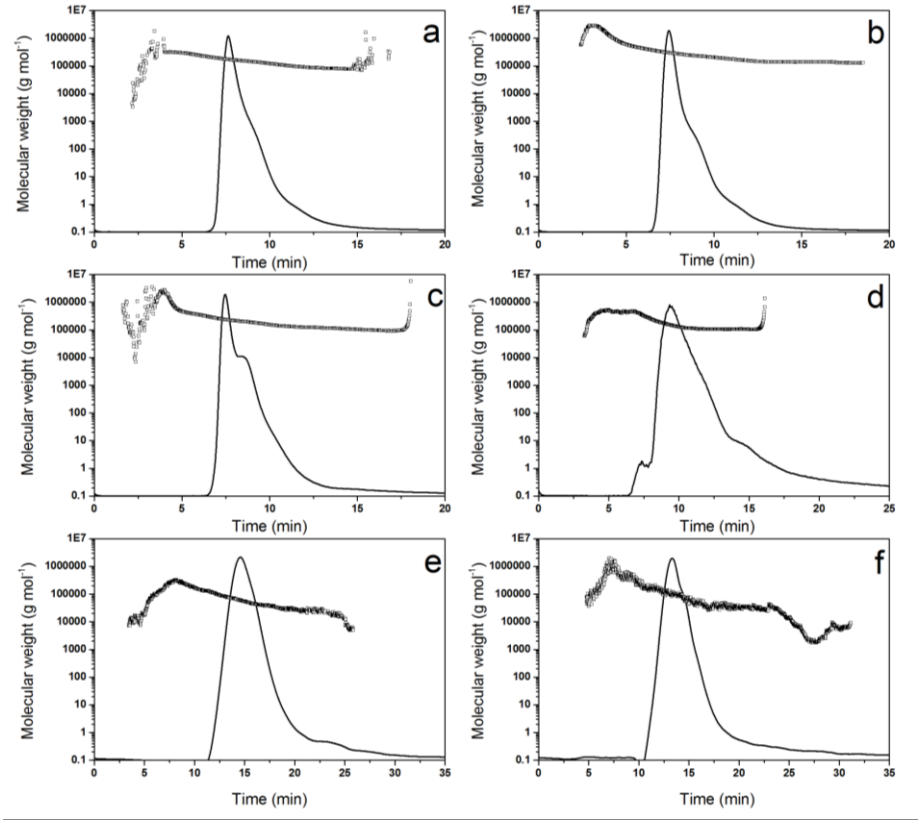


**Figure 5.6:** Elution profile of commercial and laboratory prepared chitosan samples in 0.2 M, pH 4.3, acetate buffer, (a) CHIT1 (b) CHIT2 (c) CHIT3 (d) CHIT4 (e) CHIT5 (f) CHIT6 (black line) examined by SEC-MALS at concentration 0.5 mg $mL^{-1}$. The open squares correspond to SEC-MALS calculated molecular weights.

This may represent the different conformation adapted in solution for the commercial and laboratory prepared chitosan samples. Within experimental error a better agreement was observed between the two independent methods of sedimentation equilibrium and SEC-MALS for the weight average molecular weights of all chitosan samples (Table 5.2); and values are similar to those found previously (Errington et al., 1993; Fee et al., 2003).

A third approach of estimating molecular weight was applied to the chitosan samples by transforming a distribution of sedimentation coefficient g(*s*) vs *s* into a distribution of molecular weight, *f*(*M*) vs *M* using the Extended Fujita method of *Harding et al.* (Harding et al., 2011).

The transformation is as follows:

$$f(M) = (\mathrm{d}s/\mathrm{d}M).\ g(s) \tag{5.3}$$

with

$$M = (s/\kappa_s)^{1/b} \tag{5.4}$$

and

$$\mathrm{d}s/\mathrm{d}M = b.\kappa_s^{\ 1/b}.s^{(b-1)/b} \tag{5.5}$$

*b* is a conformation parameter that has already been estimated for chitosan (Fee et al., 2003) and $\kappa_s$ can be found from equation (5.4) provided that at least one value of *M* (e.g. $M_w$ from sedimentation equilibrium) is known for one value of *s* (e.g. the weight average *s* value). The distributions so obtained (Figure 5.7) were again consistent with those obtained from sedimentation equilibrium and SEC-MALS.

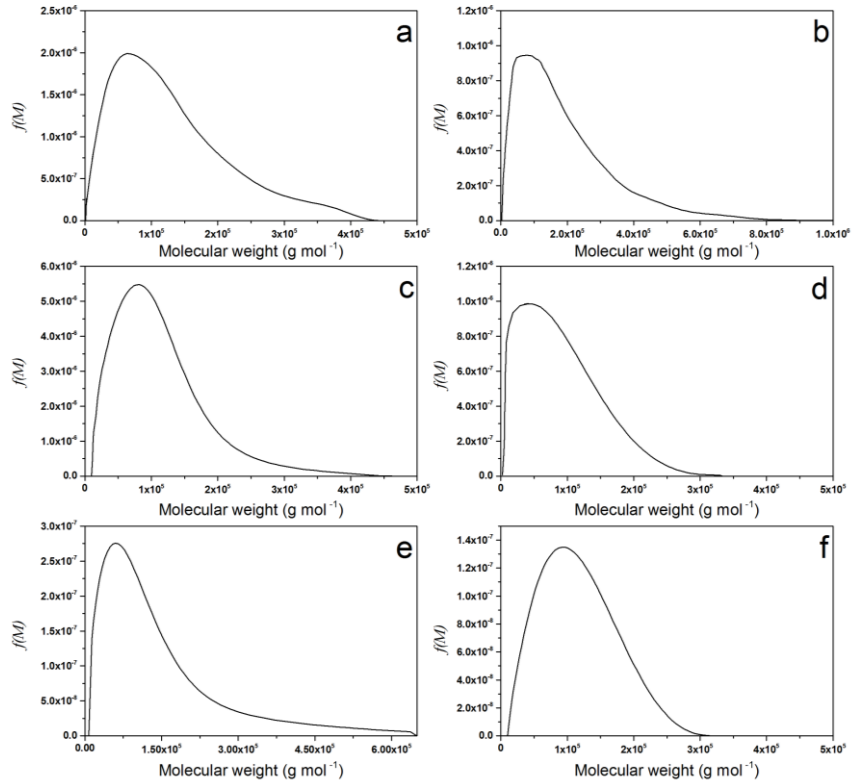


**Figure 5.7:** Molecular weight distribution for all chitosan samples in 0.2 M, pH 4.3, acetate buffer obtained from transformation of the g(s) versus *s* distribution at concentration (0.2 mg $mL^{-1}$), using the Extended Fujita method of Harding et al., (2011) (a) CHIT1 (b) CHIT2 (c) CHIT3 (d) CHIT4 (e) CHIT5 (f) CHIT6.

## 5.4.3 Intrinsic Viscosity

Intrinsic viscosity values of chitosan samples obtained using standard Ostwald capillary viscometry are reported in Table 5.3, and showed in all cases a good linear extrapolation from the Huggins, Kraemer and Solomon – Ciuta plots (Figure 5.8). Clearly the differences were seen among chitosan samples, resulting from different sources and preparation of these samples. The viscosity of the chitosan samples is also influenced by heterogeneity in molecular weight and degree of acetylation (Muzzarelli and Muzzarelli, 2009). The intrinsic

viscosity result of CHIT1 is higher than that of the CHIT2 although the molecular weight is less. This could be indicative of a much stiffer chain for the CHIT1. However, laboratory-prepared samples (CHIT5 and CHIT6) showed less intrinsic viscosity values compare to those of commercial samples in a similar range of molecular weights. This might be due to the different conformations of chitosan samples appearing in solution, which are influenced by degree of acetylation (Terbojevich et al., 1991; Wang et al., 1991).

**Table 5.3:** Intrinsic viscosity values of ("C") and ("L") chitosan samples obtained from capillary viscometry and differential pressure viscometry (Viscostar in SEC-MALS).

| **Sample** | **Intrinsic viscosity [η] mL $g^{-1}$** | | | |
|---|---|---|---|---|
| | **Capillary viscometry** | | | **Online Viscostar™** |
| | **Huggins** | **Kraemer** | **Solomon-Ciuta** | |
| **CHIT1** | 830±20 | 815±15 | 825±15 | 885±20 |
| **CHIT2** | 775±50 | 805±20 | 810±25 | 820±5 |
| **CHIT3** | 730±10 | 740±5 | 740±5 | 730±5 |
| **CHIT4** | 440v5 | 430±5 | 435±5 | 500±10 |
| **CHIT5** | 132±10 | 132±5 | 132±5 | 230±20 |
| **CHIT6** | 295±10 | 295±5 | 295±5 | 300±20 |

Table 5.3 also shows the intrinsic viscosity for chitosan samples from ViscoStar on-line with SEC-MALS, and is in excellent agreement with those yielded from capillary viscometry except for those of CHIT5 and CHIT6. The results of intrinsic viscosity are also within the range previously determined (Morris et al., 2009).

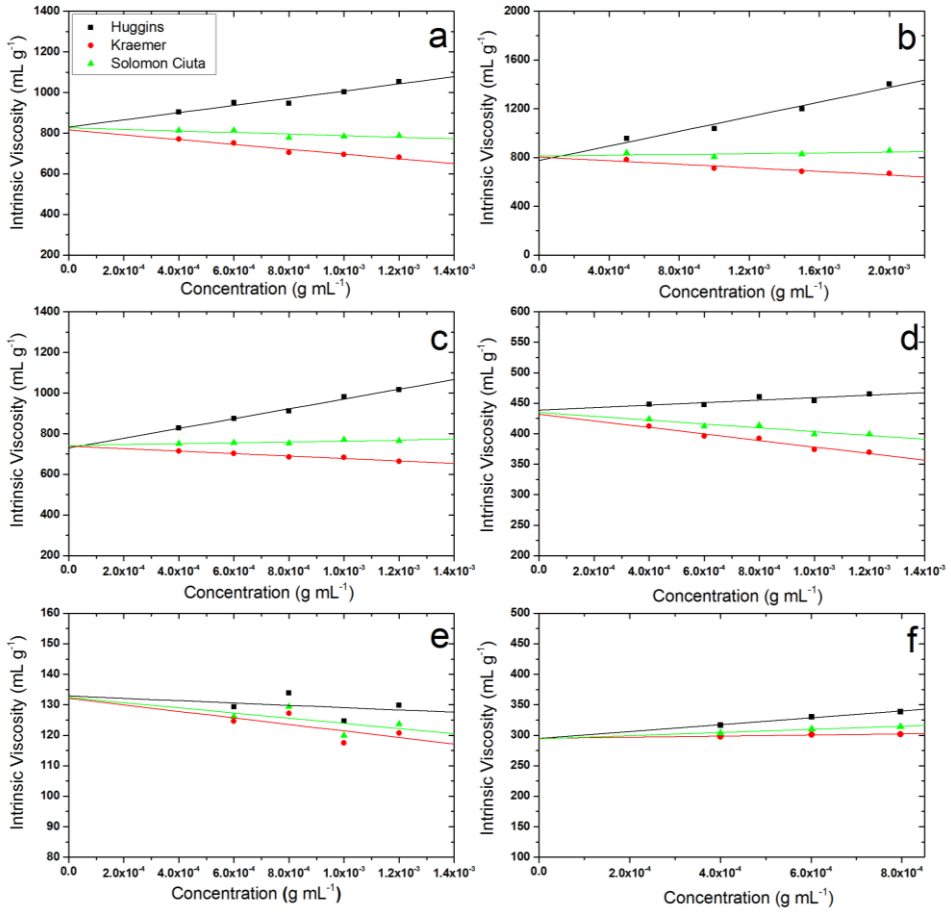


**Figure 5.8:** The intrinsic viscosity plots from capillary viscometry: Huggins, Kraemer and Solomon-Ciuta extrapolations for chitosan samples (a) CHIT1 (b) CHIT2 (c) CHIT3 (d) CHIT4 (e) CHIT5 (f) CHIT6.

## 5.4.4 Conformational Analysis

Biophysical properties such as sedimentation coefficient, intrinsic viscosity and molecular weight are all linked to yield a useful indicator for conformation and flexibility of chitosan in solution using two levels of approach: (i) general overall conformation types (coil, rod, and sphere) and (ii) in terms of persistence lengths ($L_p$) use for estimation of the flexibility of linear and flexible structures.

### 5.4.4.1 Mark-Houwink-Kuhn-Sakurada Power Law Relationship

The Mark-Houwink-Kuhn-Sakurada (MHKS) relation is one of the simplest methods used to provide useful information of polysaccharides conformation and flexibility (see, Harding et al., 1991). According to the equation molecular weight is related to sedimentation coefficient:

$$s^{o}_{20,w} = K_s M^b \qquad (5.6)$$

we found an exponent $b$ = (0.35 ± 0.06) (Figure 5.9), i.e. between the limits of rod (0.15) and coil (0.4-0.5). Within the error estimate the value is similar to those obtained previously by Cölfen *et al.*, and Fee *et al.*, (Cölfen et al., 2001; Fee et al., 2003).

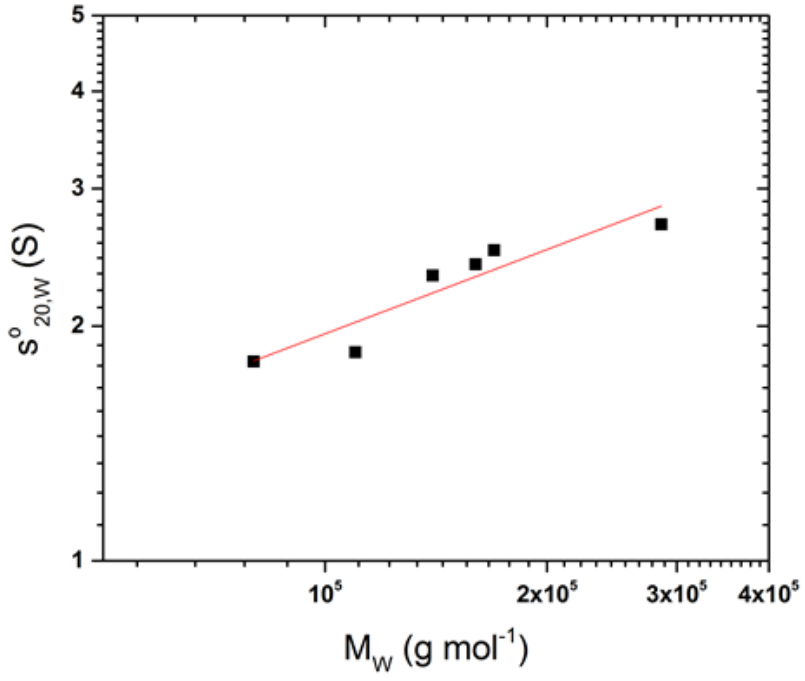


**Figure 5.9:** Mark–Houwink–Kuhn–Sakurada (MHKS) power law double logarithmic plot of $s^{o}_{20,w}$ *vs* $M_w$ for all chitosan samples.

Although the sedimentation coefficient is the absolute marker for conformation and flexibility in solution, it is still less sensitive to indicate change in molecular weight compared to intrinsic viscosity (Harding, 2012). However, taking advantage of the feature of viscostar coupled on-line to SEC–MALS system allowed using (MHKS) power law relation linking [η] (from the Viscostar™) with $M_w$ (from SEC–MALS):

$$[\eta] = K_\eta M^a \tag{5.7}$$

for each elution volume of the chitosan distribution. Figure 5.10 shows a plot in terms of double logarithmic of intrinsic viscosity $[\eta](V_e)$ as function of elution volume $V_e$ versus molecular weight, $M_w(V_e)$ also as a function of elution volume $V_e$. The MHKS exponents ($a$) obtained for each chitosan are reported in Table 5.4. The values of $a$ for the chitosans are all consistent with semi-flexible type of molecules (the limits are 0.5-0.8 for a flexible coil, 0 for a compact sphere and 1.8 for a rigid rod), and again in good agreement with previous studies (Errington et al., 1993; Cölfen et al., 2001; Fee et al., 2003; Morris et al., 2009). It was previously reported that increasing the degree of acetylation leads to hydrogen bridges occurring between chitosan acetylated units, producing a more extended conformation or stiffer chain (Draget, 1996; Hu et al., 2007). Consequently, a lower degree of acetylation leads to a more flexible structure (see, also Brugnerotto, Desbrières, Roberts, and Rinaudo, 2001). Although no clear difference was seen in the present study between the chitosan with the lowest DA (CHIT6) compared with the others, this may be because the differences in DA are relatively modest.

**Table 5.4:** Mark-Houwink-Kuhn-Sakurada (MHKS) power law exponent *a*, from SEC-MALS and Wales-van Holde ration, *R* for chitosan samples.

| Sample | MHKS *a* | $R = k_s/[\eta]$ |
|---|---|---|
| **CHIT1** | 0.98±0.01 | 0.75 |
| **CHIT2** | 0.92±0.01 | 0.90 |
| **CHIT3** | 0.98±0.01 | 0.83 |
| **CHIT4** | 0.90±0.01 | 0.60 |
| **CHIT5** | 0.70±0.01 | 0.45 |
| **CHIT6** | 0.85±0.01 | 0.40 |

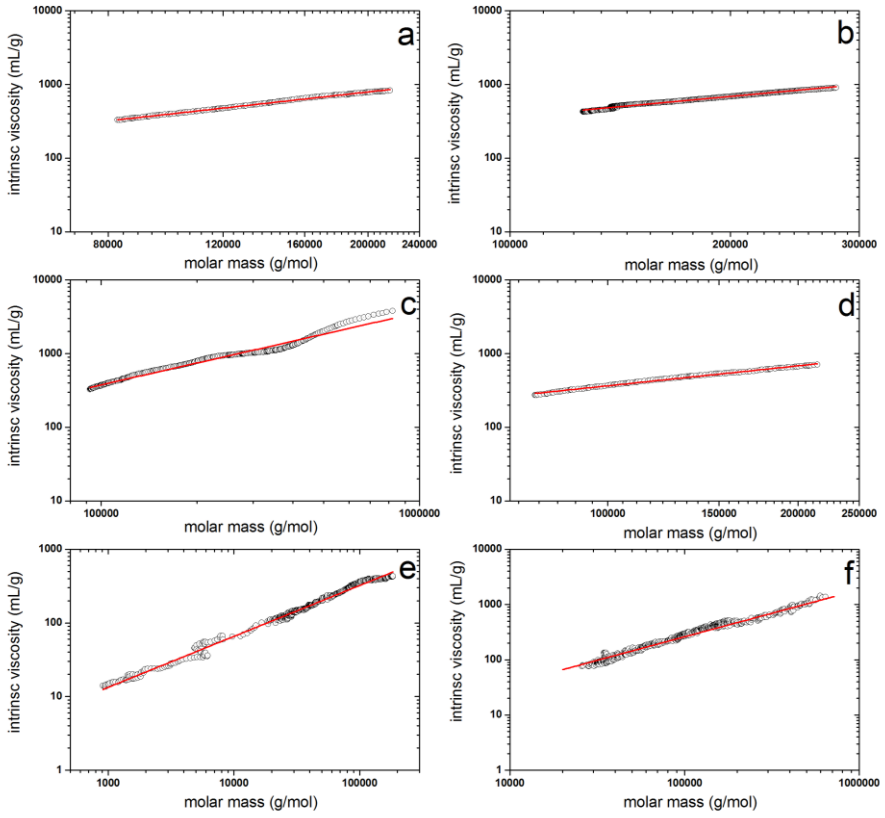


**Figure 5.10:** Mark–Houwink–Kuhn–Sakurada (MHKS) power law double logarithmic plot from on-line differential pressure viscometery coupled to SEC-MALS. The plot is of intrinsic viscosity [η] as a function of elution volume (ordinate) versus molecular weight $M_w$ as a function of elution volume. For chitosan samples (a) CHIT1 (b) CHIT2 (c) CHIT3 (d) CHIT4 (e) CHIT5 (f) CHIT6.

### 5.4.4.2 Wales-van Holde Ratio (R)

Please refer to section 3.4.4.1. As a further check for conformation, the Wales–van Holde (1954) ratio, $R = k_s/[\eta]$ was used, based on knowledge of the concentration-dependence coefficient, $k_s$ from sedimentation velocity experiment and intrinsic viscosity [η] from on-line differential pressure viscometery coupled to SEC-MALS. The values are reported in Table 5.4, and it appears that all chitosan samples are again consistent with semi-flexible structures ($R \sim 0.4–0.9$). Also the results appear similar to those found previously by Cölfen *et al.,* and Morris *et al.* (Cölfen et al., 2001; Morris et al., 2009).

### 5.4.4.3 Molecular Conformation Zoning

Please refer to section 3.4.4.3. Figure 5.11 shows a molecular conformation zone plot of $k_s\ M_L$ vs $[s]/M_L$ for chitosan commercial samples (CHIT1 to CHIT4) and in-house laboratory-prepared (CHIT5 and CHIT6). It appears that commercial chitosan samples adapted a rigid rod structure at zone (B), whilst in house laboratory-prepared at zone (C) within the range of semi-flexible structure. Thus, the results obtained seem to be consistent with those yielded from the MHKS approach, and reinforce those previously found by Morris *et al.* (Morris et al., 2009).

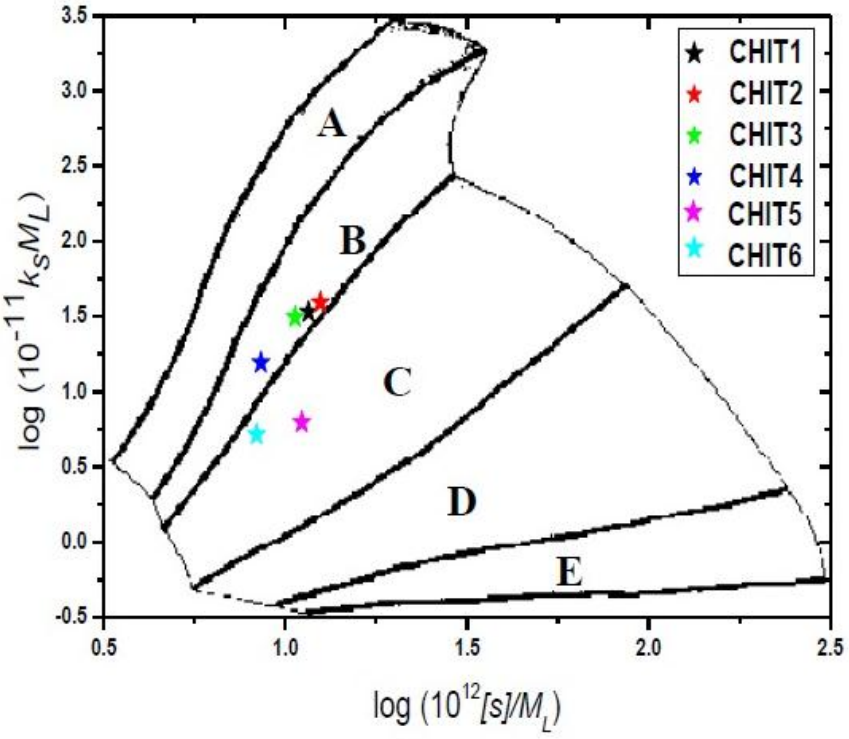


**Figure 5.11:** The conformation zoning plot for chitosan samples, commercial (CHIT1 to CHIT4) and in house laboratory-prepared (CHIT5 and CHIT6) adopted rigid rod structures at (zone B) and semi-flexible coil structures (zone C), respectively.

### 5.4.4.4 Estimation of the Persistence Length $L_p$ and Mass Per Unit Length $M_L$:

In terms of studying flexibility of chitosan samples, as determined in the range of rigid rod and semi-flexible coil structures by general conformation methods, more advanced analyses can now be applied. Several approaches are applied here to measure the chain flexibility in terms of persistence length $L_p$ and mass per unit length $M_L$ (refer to section 3.4.4.4).

#### 5.4.4.4.1 Bushin-Bohdanecky method

In this study the Bushin-Bohdanecky method was used (refer to section 3.4.4.4.1) to estimate both $L_p$ and $M_L$ based on information of molecular weight values (from sedimentation equilibrium) and intrinsic viscosity (from on-line differential pressure viscometery in SEC-MALS) by appling the following equation (Bohdanecky, 1983; Bushin et al., 1981):

$$\left(\frac{{M_w}^2}{[\eta]}\right)^{1/3} = A_0\, M_L\, \phi^{-1/3} + B_o \phi^{-1/3} \left(\frac{2L_p}{M_L}\right)^{-1/2} {M_w}^{1/2} \qquad (5.8)$$

From the slope $L_p$ can be calculated using the above equation, where, $\phi$ is the Flory-Fox constant (2.86 x $10^{23}$ mol$^{-1}$), $B_o$ taken as $\sim 1.10$ (Bohdanecky, 1983) and $M_L \sim 450$ g mol$^{-1}$ nm$^{-1}$ obtained from Morris *et al.,* (2009). Figure 5.12 shows a plot of $(M_w^2/[\eta])^{1/3}\ vs\ M_w^{1/2}$ for commercial chitosan and in-house laboratory-prepared samples in general satisfactory fits were obtained. Thus, from the previous plot a slope of (0.82±0.11) was obtained, and yielded an $L_p$ value of (10±1) nm, which is in excellent agreement with that obtained by (Vold, 2004).

#### 5.4.4.4.2 Yamakawa-Fujii method

Another method used for calculating the $L_p$ is that of Yamakawa-Fujii (refer to section 3.4.4.4.2), which utilises information of sedimentation coefficient and molecular weight. Again from the slope of the plot $s^o_{20,w}\ vs\ (M_w)^{1/2}$, the $L_p$ and $M_L$ can be obtained but information is required about either $L_p$ or $M_L$ using following equation:

$$s^o = \frac{M_L\,(1-\bar{\upsilon}\rho_o)}{3\,\pi\,\eta_0\,N_A}\,x\left[1.843\left(\frac{M_w}{2M_LL_P}\right)^{1/2} + A_2 + A_3\left(\frac{M_w}{2M_LL_P}\right)^{-1/2} + \cdots\right] \quad (5.9)$$

Figure 5.13 shows the slope of 4.9 E-13± 6.2 E-14was obtained for chitosan commercial and in - house laboratory-prepared samples. Consequently, equation 5.9 was applied with a fixed $M_L$ of ~ 450 g mol$^{-1}$ nm$^{-1}$ and yielded $L_p$ of (18±1), which is indicative of a rigid rod type conformation and consistent with that previously found by Morris et al., (2009). Therefore, the result is considerably higher than that obtained from the Bushin-Bohdanecky method, but still well within the flexible rod type conformation.

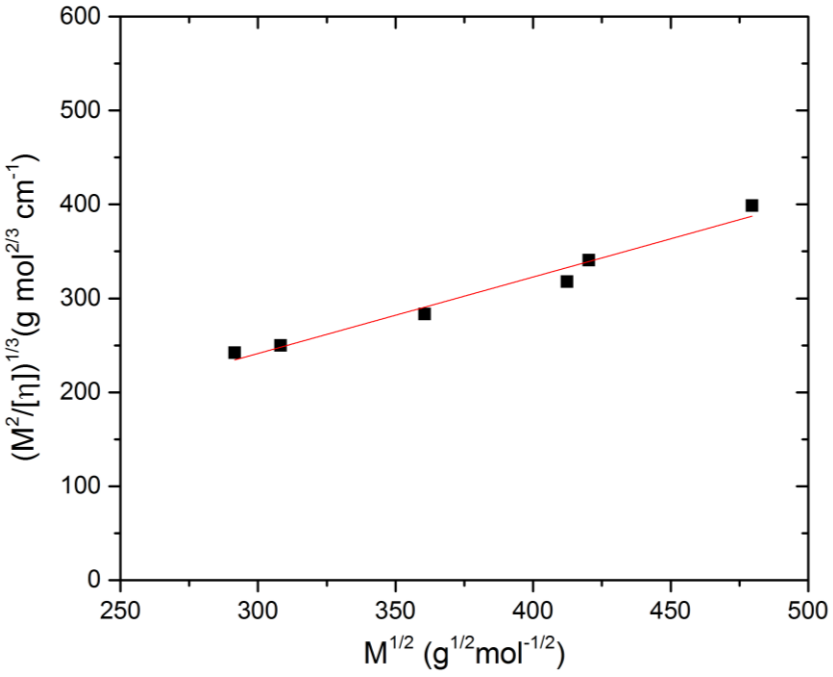


**Figure 5.12:** Bushin-Bohdanecky plot for commercial (CHIT1 to CHIT4) and in-house laboratory-prepared (CHIT5 and CHIT6) chitosan samples, where $L_p$ = (10 ± 1) nm from the slope.

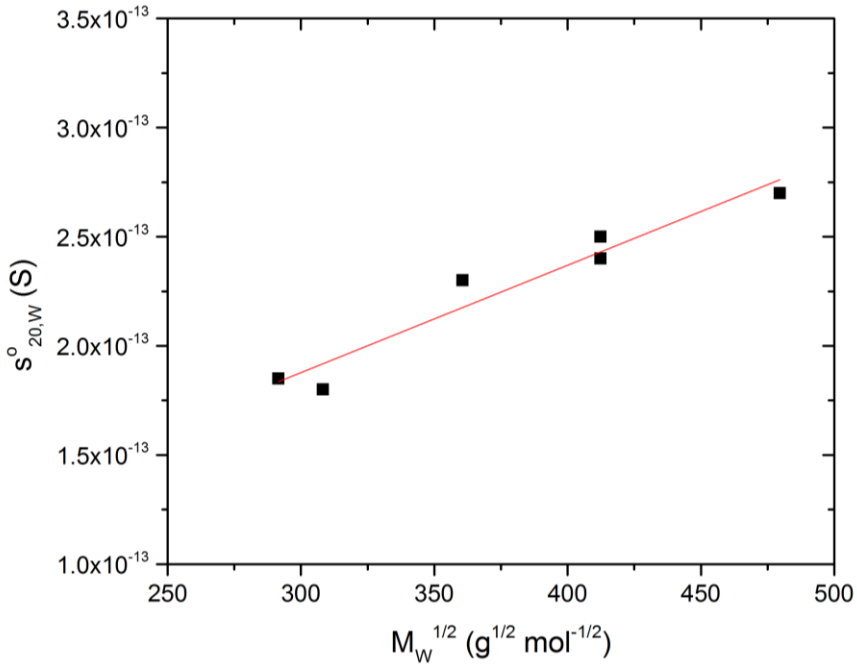


**Figure 5.13:** Yamakawa-Fujii plot for commercial (CHIT1 to CHIT4) and in-house laboratory-prepared (CHIT5 and CHIT6) chitosan samples, where $L_p$ = (18 ± 1) nm from the slope.

#### 5.4.4.4.3 Global analysis method (HYDFIT)

It can clearly be seen that different methods can bias the results (Bohdanecky and Petrus, 1991; Patel, et al., 2008; Picout et al., 2002), thus a new software package namely "HYDFIT" has created by Ortega and García de la Torre to resolve this problem (Ortega and García de la Torre, 2007). This algorithm takes into consideration data sets of both intrinsic viscosities and sedimentation coefficients for different molecular weights, which is used to estimate the best values of persistence lengths $L_p$ and mass per unit length $M_L$ based on minimisation of a target function $\Delta$. Although estimation of the chain diameter $d$ provided by the Multi-HYDFIT, it is usually fixed in the case of finding $L_p$

and $M_L$ results, because they are insensitive to $d$ values (Ortega and García de la Torre, 2007; Amoros et al., 2011).

In this study two cases have been considered to estimate both $L_p$ and $M_L$. Firstly we fixed $d$ and treated $L_p$ and $M_L$ as variables, thus the minimum value of the target function $\Delta$ was yielded on the contour plot for each chitosan sample (Figure 5.14.).

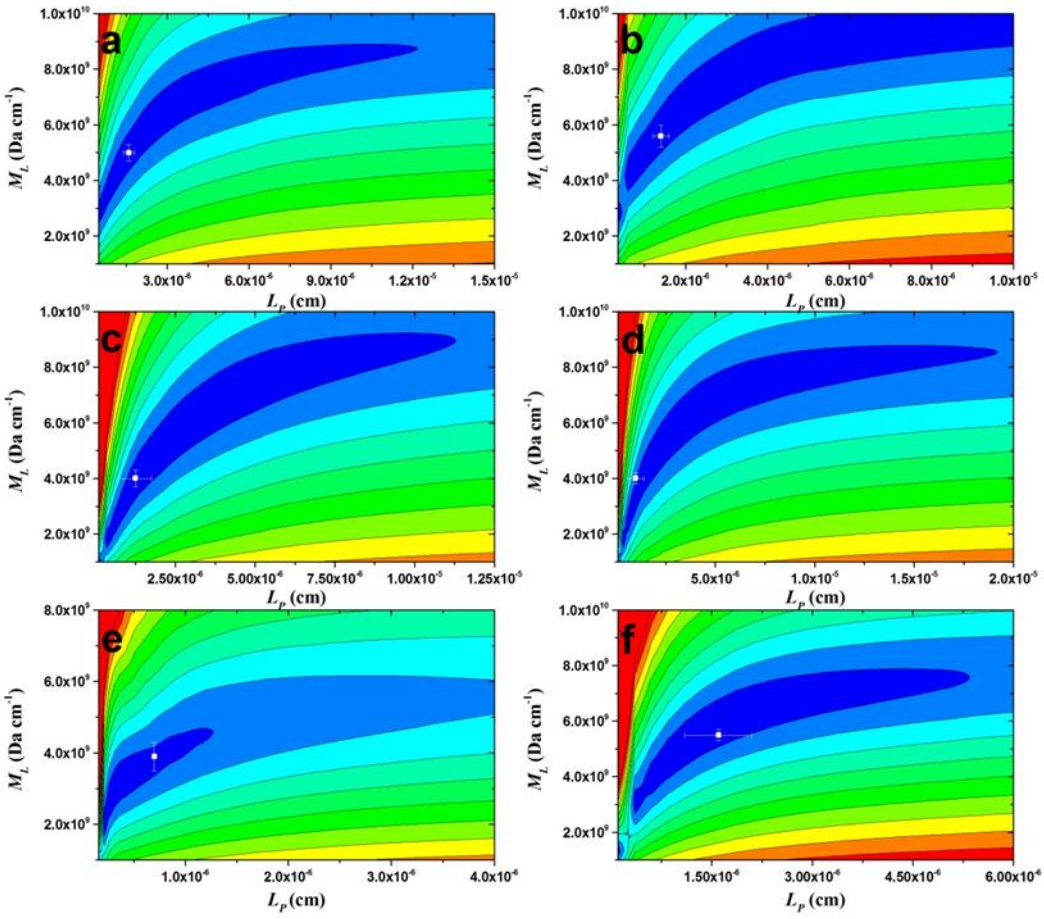


**Figure 5.14:** Contour plots of chitosan samples (a) CHIT1 (b) CHIT2 (c) CHIT3 (d) CHIT4 (e) CHIT5 and (f) CHIT6. The target function, $\Delta$ calculated based on variables values of $L_p$ and $M_L$, and are represented on the full colour spectrum from blue ($\Delta$ = 0) to red ($\Delta \geq 0.95$).

The values estimated are in the range 7-16 nm for $L_p$, whereas 390-560 Da nm$^{-1}$ for $M_L$, and given in Table 5.5. The small differences between chitosan samples in persistence length and mass per unit length are reflected in the intrinsic viscosity and the sedimentation coefficient. In the second case where both the diameter and the mass per unit length are fixed hence the persistence length and the minimization plots for chitosan samples are shown in (Figure 5.15). All the values are in good agreement with those calculated when both $L_p$ and $M_L$ were treated as variables (Table 5.5), and are consistent with semi-flexible rod structure and previous studies (Berth et al., 1998; Cölfen et al., 2001; Vold, 2004; Morris et al., 2009).

**Table 5.5:** Summary of the persistence length $L_p$ and the mass per unit length $M_L$ values for chitosan samples.

| **Sample** | **$L_p$ (nm)** | | **$M_L$ (Da nm$^{-1}$)** |
|---|---|---|---|
| | ***a*** | ***b*** | |
| **CHIT1** | 16±0.2 | 16±1.0 | 500±30 |
| **CHIT2** | 14±0.2 | 15±0.2 | 560±40 |
| **CHIT3** | 10±1.0 | 9±1.0 | 400±30 |
| **CHIT4** | 7.0±0.4 | 6.0±0.5 | 400±20 |
| **CHIT5** | 7.0±0.1 | 6.5±0.1 | 390±40 |
| **CHIT6** | 16±1.0 | 16±1.0 | 550±20 |

*a* : calculated when both $L_p$ and $M_L$ were treated as variables
*b*: calculated when both *d* and $M_L$ were fixed

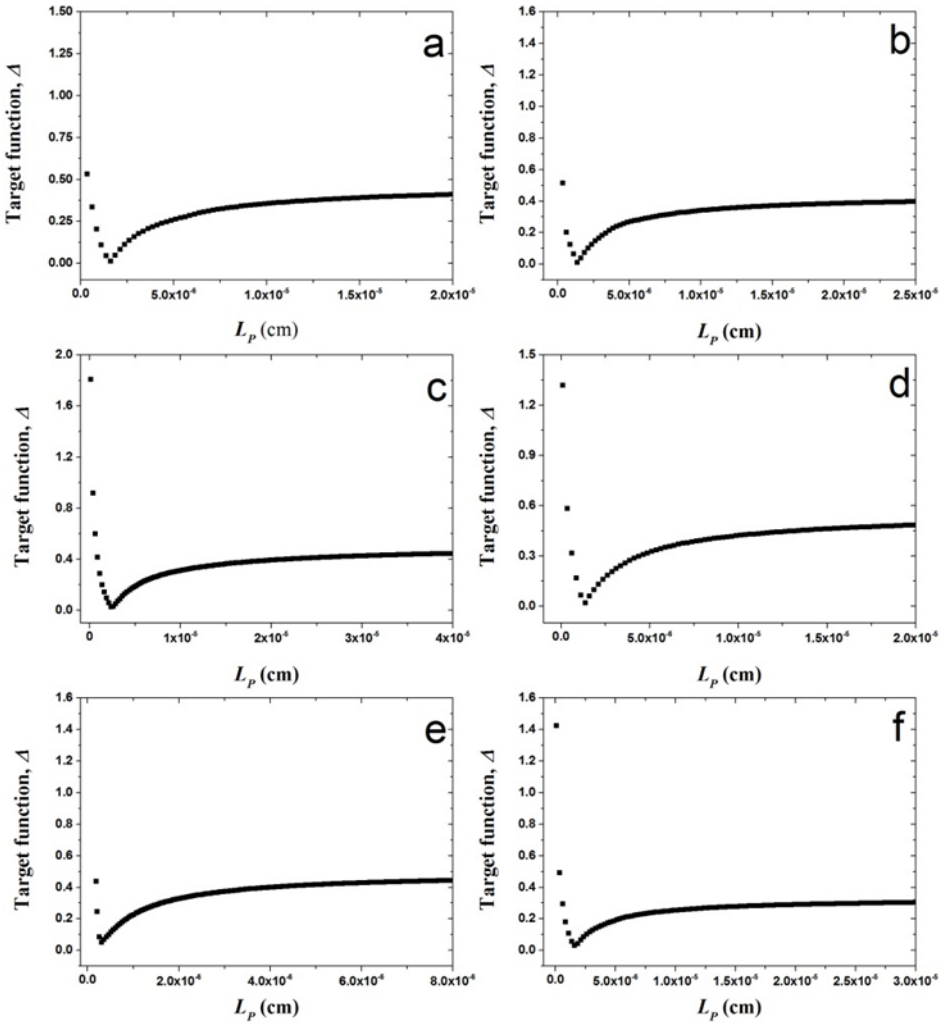


**Figure 5.15:** Plots of target function ($\Delta$) vs. persistence length ($L_p$) for chitosan samples (a) CHIT1 (b) CHIT2 (c) CHIT3 (d) CHIT4 (e) CHIT5 and (f) CHIT6.

## 5.4.5 Interaction with Two Polyanions: DNA and Xanthan

Chitosans have received considerable interest for the development of therapeutic drug delivery systems, due to their polycationic properties, biocompatibility, biodegradability and antibacterial activity. Progress has been made in this study on the characterisation of the hydrodynamic parameters for chitosan - for examples molecular weight and conformation- allowed us to

investigate the interaction of this substance with other polyanions macromolecules in particular DNA and xanthan.

### 5.4.5.1 Chitosan-DNA Interaction

We use the principle of co-sedimentation in the analytical ultracentrifuge – previously successfully employed to study chitosan-mucin interactions (Harding 2003, 2006) – to explore this situation further. Previously, it was shown that the efficacy of chitosan binding with DNA is reduced as the molecular weight decreased and the degree of acetylation increased (Kiang et al., 2004). Solutions of the two chitosan samples CHIT5 and CHIT6 with different molecular weights and also degrees of acetylation were studied in mixtures with the DNA of $M_w$, estimated from the Extended Fujita method of Harding et al (2011) to be approximately 300 kDa.

Firstly, CHIT5, CHIT6 and DNA were characterised separately at a concentration of 1.0 mg $mL^{-1}$ and a temperature of 20.0 $^0$C, using analytical ultracentrifugation based on sedimentation velocity. Unimodal distributions were seen in all cases, and the apparent weight average sedimentation coefficient $s_{20,w}$ obtained for CHIT5, CHIT6 were 1.9S and 2.3S, respectively and 6.8S for DNA as reported in (Table 5.6). Each chitosan preparation was then mixed in a 1:1 w/w ratio with the DNA to a total concentration of 1.0 mg $mL^{-1}$. A clear shift to a high *s* value is observed in both cases, with nothing sedimenting at the rate of uncomplexed chitosan suggesting that the interaction had gone to completion (Figure 5.16): a shoulder of the complexes observed, suggestive that some unreacted DNA appears remaining. Furthermore, the

effect of the molecular weight has appeared clearly on the interaction; showing a greater distribution /apparent weight average sedimentation coefficient $s_{20,w}$ for the CHIT6 (higher molecular weight) compared to that of the CHIT5 (lower molecular weight). The degree of acetylation effect also observed, providing a greater $s_{20,w}$ distribution at low acetylation ratio (CHIT6) compared to that of a higher acetylation ratio (CHIT5). Therefore, this result is in excellent agreement with a more recent study in which interaction of chitosan with oligodeoxynucleotide yielded changes in the sedimentation velocity behaviour of the mixture compared to controls in the analytical ultracentrifugation (Niebel et al., 2014).

**Table 5.6:** Sedimentation coefficients at $s_{20,w}$ at a total concentration of 1.0 mg $mL^{-1}$, for chitosan, DNA, xanthan and chitosan-DNA and chitosan-xanthan complexes.

| sample | $s_{20,w}$ (S) | %unreacted chitosan | %unreacted DNA | %unreacted xanthan |
|---|---|---|---|---|
| **CHIT5** | 1.9 | | | |
| **CHIT6** | 2.3 | | | |
| **DNA** | 6.8 | | | |
| **Xanthan** | 4.8 | | | |
| **CHIT5-DNA** | 17 | 0 | 28 | |
| **CHIT6-DNA** | 20 | 0 | 17 | |
| **CHIT5-xanthan** | 10 | 0 | | 0 |
| **CHIT6-xanthan** | 10 | 0 | | 0 |

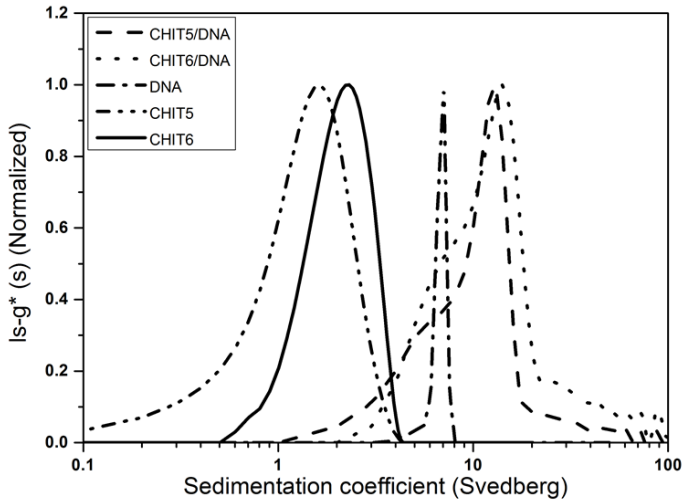


**Figure 5.16:** Normalized sedimentation coefficient distribution profiles obtained from sedimentation velocity experiment for unmixed controls and mixture for chitosan samples (CHIT5 and CHIT6) with DNA.

### 5.4.5.2 Xanthan-chitosan Interaction

Xanthan is another negatively charged polymer that can generate the strong and weak hydrogel form in the solution. Therefore, the characteristics of xanthan-chitosan hydrogels have been extensively studied for over two decades (Dumitriu et al., 1994; Martínez-Ruvalcaba, 2007; Shchipunov et al., 2010). We now reinforce this with a co-sedimentation study. The molecular weight of the xanthan (xanthan-STD) was found previously to be ~3.2 x $10^3$ kDa using sedimentation equilibrium in the analytical ultracentrifuge (Erten et al., 2014).

The sedimentation velocity profile of xanthan was first characterised at 1.0 mg $mL^{-1}$ yielding a unimodal g(s) vs *s* plot with weighted-average $s_{20,w}$ of 4.8S. Then the 1:1 by weight mixtures with CHIT5 and CHIT6 at a total concentration of 1.0 mg $mL^{-1}$, were studied and the results were shown in Figure 5.17 and Table 5.6. As with chitosan-DNA, all the chitosan was

complexed, and no residual chitosan or xanthan were left behind for both CHIT5 and CHIT6 complexes. Weighted average $s_{20,w}$ for the complexes of 10.3S and 10.1S for CHIT5-xanthan and CHIT6-xanthan, respectively were obtained.

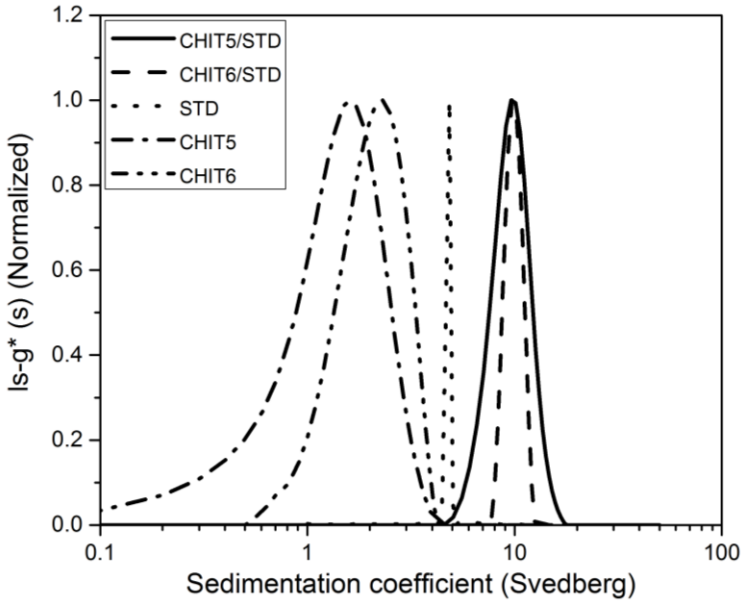


**Figure 5.17:** Normalized sedimentation coefficient distribution profiles obtained from sedimentation velocity experiment for unmixed controls and mixture for chitosan samples (CHIT5 and CHIT6) with xanthan-STD.

## 5.5 DISCUSSION

Conformation in addition to molecular weight plays an important role in the ability to use chitosan for drug delivery and its interaction with polyanionic polymers (Tombs and Harding, 1998). Therefore, commercial (C) and in-house laboratory (L) prepared chitosan samples with different molecular weights and degrees of acetylation (25% and 15%) have been characterised with regard to their weight-average molecular weight ($M_w$), sedimentation coefficient ($s^o_{20,w}$)

distribution, and intrinsic viscosities ([η]). Unimodal distributions were seen from sedimentation coefficient distributions and elution profiles from SEC-MALS. $M_w$ values obtained for each sample by sedimentation equilibrium measurements, and these were in excellent agreement with those obtained from SEC-MALS.

Knowledge of the dependence of [η] with $M_w$ now permits us to investigate the conformation of our chitosans. Following Tanford (1961) we make the reasonable assumption that complications through molecular draining effects and other non-conformational effects are small. Evidently, chitosan samples are all a consistent semi-flexible rod type conformation of molecules, with greater flexibility observed for CHIT5 sample. Results have been confirmed by the Wales-van Holde ratio and molecular conformation zoning methods. The discrepancy observed in the conformational flexibility of chitosan samples may refer to very different chemical composition, molecular weight and ionic strength (Varum and Smidsrød, 2004). Therefore, it is appropriate to characterize macromolecules using more than one hydrodynamic method. In terms of the persistence length different approaches (e. g. Bushin-Bohdanecky and Yamakawa-Fujii) have been used to estimate the flexibility of linear and flexible structures. Thus, results most likely adopt a semi-flexible rod type conformation in good agreement with those calculated from MHKS and Wales-van Holde ratio and appear to reinforce earlier estimations by Cölfen et al., (2001) and Morris et al., (2009). Charactisating the physical properties of chitosans in solution provided important biophysical information and having understood their nature we can now with some confidence approach their behaviour in mixture with the DNA and xanthan.

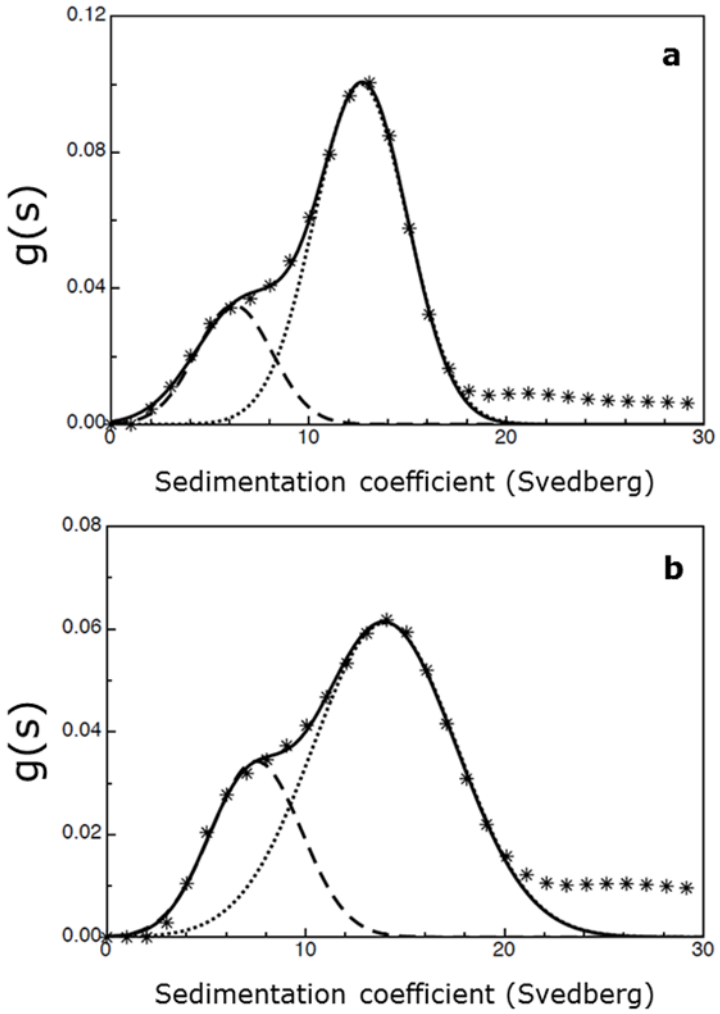


**Figure 5.18:** Multi-Gaussian fit using MULTIG (locally written software, run under pro Fit™, Quansoft, Zurich) (a) Multi-Gaussian fit to the CHIT5-DNA mixture and (b) Multi-Gaussian fit to the CHIT6-DNA mixture. With the routine MULTIG fitting was initially performed manually via the interactive *Preview Window*, floating the position (*s* value), area and standard deviation of each peak.

The principle of co-sedimentation was then used to monitor the interactions of the two different molecular weights of L chitosans with two polyanions, DNA and xanthan (another double helical high molecular weight molecule). Interactions were clearly observed and quantified from the changes in the

sedimentation coefficient distribution of the mixture compared to unmixed controls using sedimentation velocity. The interactions appeared to show a strong dependence on molecular weight. The relevance of this for DNA condensation applications is indicated.

In this regard from the shoulder of the complex, some unreacted DNA appears to be remaining (Figure 5.16 and 5.17). Multi-Gaussian analysis of the g(s) vs *s* distribution for the complex using the routine MULTIG suggests ~ 28% DNA had not interacted for CHIT5 (Figure 5.18 a) and ~17% for CHIT6 (Figure 5.18 b). The *s*-distribution of the complex is very broad, even on a logarithmic scale, with material in excess of 100S, with the larger molecular weight chitosan CHIT6 showing the highest degree of complexation. With the latter this may prove useful for the assay of potential chitosan based materials for the condensation of DNA in gene therapies, particularly if used in conjunction with imaging probes as successfully combined in the analysis of chitosan mucoadhesive phenomena (Deacon et al, 2000).

# CHAPTER 6

# HYDRODYNAMIC STUDIES ON A MIXTURE OF NON-DIGESTIBLE CARBOHYDRATES

Recent work has shown that the combination (proprietary mixture) of three non-digestible carbohydrates namely konjac glucomannan, xanthan and sodium alginate involved synergistic non-covalent interactions (Abdelhameed et al., 2010; Harding et al., 2011a; Harding et al., 2012), offering beneficial properties for therapeutic purposes. In this part of the study, the possibility of replacing the polyanionic seaweed sodium alginate with different polyanionic seaweed namely lambda carrageenan was investigated. Looking for a favourable mixture can possibly help to improve satiety and the obesity problem from food.

## 6.1 INTRODUCTION

Non-digestible carbohydrate – also referred to as dietary fibre – has always formed a substantial part of the human diet, however changes in diet in the last two hundred years has lead to a reduction in the overall intake by the consumer. A lack of dietary fibre intake is associated significantly with being overweight or obese, dyslipidemia, type two diabetes, heart disease, and gastrointestinal disorders (Smith et al., 2014). The constituents of dietary fibre are non-digestible carbohydrate and lignin, which are considered as having beneficial physiological effects for human health. These effects are related to

physical properties such as viscosity, volume and water-holding capacity. In particular viscous fibre reduces the incidence of coronary heart disease by interaction or absorption of dietary fat and cholesterol (Jenkins et al., 2000).

A significant number of dietary fibres are obtained from seaweed (mainly agar, carrageenan, alginate etc.), and have been used in the human diet for at least three thousand years (Lahaye, 1991; Tombs and Harding, 1998). To illustrate this point, the market for seaweeds – an important source of dietary fibre – has been growing continuously 1-3 % per year due to their high consumption in the food and pharmaceutical industries (Bixler and Porse, 2011). The impact of seaweed on human health (e.g. obesity and diabetes) is as results of its behaviour in the alimentary tract such as dispersibility in water, viscosity, binding ability, absorptive capacity and fermentability (Kendall et al., 2010).

Seaweed polysaccharides are just one group of dietary fibre polysaccharides: nowadays, interest is growing in the use of combinations of dietary fibres, which have a greater effect than a single fibre component. Especially for consumers who have an insufficient fibre intake. One particular proprietary product in this category, which is used as a food supplement, is PolyGlycopleX®, (α-D-glucurono-α-D-manno-β-D-manno-β-D-gluco), (α-L-gulurono-β-D-mannurono), β-D-gluco-β-D-mannan (PGX®). PGX® and PolyGlycopleX® are both trade names belonging to InovoBiolgic Inc., Calgary, Alberta, Canada. PGX® is produced from a mixture of proprietary proportions of powders of konjac glucomannan, xanthan and alginate that has been subjected to a proprietary process (EnviroSimplex®) including heat input after mixing the solid components. The combination appears to give high viscosities and offers beneficial properties for therapeutic purposes (Vuksan et

al., 2000). The high viscosity obtained from this combination was somewhat unexpected, which led to the recent investigation to examine whether interactions were occurring between the three components considered to be accounting for this unexpected behaviour.

The synergistic interaction of polysaccharide mixtures in concentrated solution has been well proven in rheological studies. The interaction of binary mixtures, for instance konjac glucomannan and xanthan has been shown that and a strong thermoreversible gel network is formed (Shatwell, Sutherland, Ross-Murphy, and Dea, 1991). A study in dilute solution using analytical ultracentrifugation (AUC) has supported these observations, which identified a significant interaction between xanthan – as the dominant component – and konjac glucomannan, but this interaction was very sensitive to the ionic strength of the aqueous medium (Dhami, 1996). In a recent study, changes in the sedimentation velocity behaviour observed for PGX® compared to unmixed controls of each individual component polysaccharide in AUC; showing alginate clearly interacts with a mixture of konjac glucomannan and xanthan (Abdelhameed et al., 2010). Further, combination of AUC with nuclear magnetic resonance (NMR) and rheological measurements indicated that the interactions within PGX® were clearly non-covalent, and found to be sensitive to the ionic environment: interactions occurred at low ionic strength (Harding et al., 2011a). In fundamental dilute solution viscosity studies these observations have been supported and the presence of the alginate appeared to increase the viscosity beyond what was expected for a non-interacting mixture (Harding et al., 2012).

This study was undertaken to investigate the possibility of replacing the polyanionic seaweed alginate with another polyanionic seaweed polysaccharide, namely lambda carrageenan. Whereas alginate can show variability in terms of their repeat structure (poly M "mannuronate", poly G "guluronate" and poly MG), lambda carrageenan offer the possibility of a more consistent raw material. Previous studies by the National Centre for Macromolecular Hydrodynamics (NCMH) laboratory have shown that some carrageenans engage in weak interactions with protein (see, e.g. Morris, 2001) and it would be important to discover whether this also applies to konjac glucomannan in the presence of xanthan. Taking advantage of recent advances in AUC (Dam & Schuck, 2004; Harding et al, 2011b; Schuck et al, 2014), sedimentation velocity and equilibrium were used in conjunction with SEC-MALS and viscometry to check the molecular integrity (sedimentation coefficient, molecular weight and intrinsic viscosity) of individual preparations of lambda carrageenan, konjac glucomannan and xanthan at low ionic strength I ($10^{-3}$M) and higher I ($10^{-1}$M). The sedimentation coefficient and intrinsic viscosity were then determined for the mixture components at both ionic strengths and compared to values of a non-interacting mixture. Before we describe the materials and methods we firstly indicate the favourable properties of fibre polysaccharide konjac glucomannan, xanthan and sodium alginate, whereas lambda carrageenan has previously been well described in *Chapter 3*.

### 6.1.1 Konjac Glucomannan

Konjac glucomannan is a type of neutral glucomannan heteropolysaccharide extracted from the tubers of *Amorphophallus Konjac* C. Koch (Figure 6.1). konjac glucomannan is a β-(1,4) linked polysaccharide composed of a D-glucosyl "G" and D-mannosyl "M" with a low degree of acetyl groups that relate to its gel formation properties (see, for example Kök et al., 2009). The M:G ratio is reported as 1.6:1 and occasional branches or side chains (not shown in Figure 6.1) join through the C-3 carbons of the main-chain D-glucosyl and D-mannosyl residues (Maeda et al., 1980; Katsuraya et al., 2003). Some researchers have reported a random distribution of these residues, whereas other prefers a complex non-random distribution as the basic polymeric repeating unit has the pattern: -G-G-M-M-M-M-G-M- or –G-G-M-G-M-M-M-M- (Williams et al., 2000; Cescutti et al., 2002).

The main chain of konjac glucomannan includes acetyl groups, while deacetylation occurs and a thermally stable gel is formed with application of an alkali. The side chains occur at intervals of (50 – 60) units of the main chain attached by β- (1,3) linkage. Likewise, acetate groups on carbon 6 occur at every 9 – 19 units of the main chain (Maeda et al., 1980). Unaltered linear β-(1,4) mannans and glucans (cellulose) are both insoluble in water because of inter-chain association through hydrogen bonding, whereas konjac glucomannan by contrast is water soluble. The long side chains of the glucomannan seem to play an important role in this solubility, which inhibits intermolecular association, inter-chain H-bonding and enhanced solvation (Dea et al., 1977; Hwang and Kokini, 1991). Otherwise, the solubility is believed

predominantly to be connected with the presence of the replaceable acetyl. The precise role of the acetyl groups in promoting solubility is still an issue of argument, although the elimination of these groups makes the gelation behaviour much easier (Maeda et al., 1980).

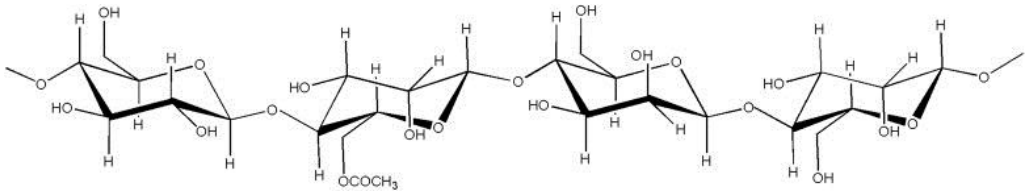


**Figure 6.1:** Chemical structure of konjac glucomannan. Adapted from Kök *et al.*, (2009).

Konjac glucomannan is widely known as a food storage polysaccharide in plants, and has been cultivated for centuries in Japan (Kök et al., 2009). The production of Japanese shirataki noodles uses konjac glucomannan flour, which is very low in calories. The feeling of fullness it gives is related to the high viscosity of konjac glucomannan solutions that delays absorption of some of the nutrients in food. The high viscosity depends on an extremely high capacity for holding water. One gram of this soluble polysaccharide can absorb up to 200 mL of water (Maeda et al., 1980; Wen et al., 2008). So commonly it is used in absorbent material such as disposable diapers and sanitary towels. Many scientists have suggested that, at low concentration konjac glucomannan has the highest viscosity of any known dietary fibre (see, e.g. Kök et al., 2009).

Konjac glucomannan has also been widely used in both food and pharmaceutical productions as a texture modifier and thickener (Kök et al., 2009). One of its most exciting uses is in the production of DNA-advanced

controlled release hydrogels as an adjunctive therapeutic agent in the treatment of thyrotoxicosis (Azezli et al., 2007; Wen et al., 2008). It has been reported to give inhibition of postprandial hypoglycaemia without any drawbacks of unpalatability and carbohydrate malabsorption (Hopman et al., 1988). In addition, it has been used in dealing with glycaemia and other related risk factors for coronary heart disease in type II diabetes (Vuksan et al., 1999).

### 6.1.2 Xanthan

Xanthan gum, was discovered at the Northern Regional Research Laboratories (USA) in the 1950s, is a polysaccharides produced by the bacterium *Xanthomonas campestris* which has subsequently become a significant industrial biopolymer (see, e.g. Margaritis and Zajic, 1978; Dhami et al., 1995; Tombs and Harding, 1998; Morris and Harding, 2009). It is an extracellular heteropolysaccharide produced by a process involving fermentation of carbohydrate by the bacterium (Davidson, 1980). The primary structure of xanthan consists of repeating pentasaccharide units formed by two glucose, two mannose and one glucuronic acid unit (Figure 6.2).

The main chain of xanthan is composed of two β-D-glucose units linked at the 1 and 4 positions. There is great similarity between the main chain of xanthan and cellulose with regards to the chemical structure (Sandford and Barid, 1983). The side chain contains two D-mannose units and a D-glucuronic acid unit, linked to every other glucose of the backbone at the 3 position. About one-half of the terminal D-mannose units have a pyruvic acid group connected by keto group to 4 and 6 positions. In addition, another mannose unit is linked

to an acetyl group at the 6 position. The consensus opinion seems to be that molecular xanthan has two conformations, namely a double helix and a random coil (Chaplin, 2009). Double stranded helical conformation could form an inflexible rod-like macromolecule, and this situation can occur when elongated single stranded chains are heated (Garcia-Ochoa et al., 2000). The ordered double helical conformation converts to the single more-flexible extended chain after treatment for some hours at 40 – 80$^{o}$C (Symes, 1980). Variable strains or fermentation conditions used may give variable degrees of acetylation and pyruvylation and this can affect the functionality.

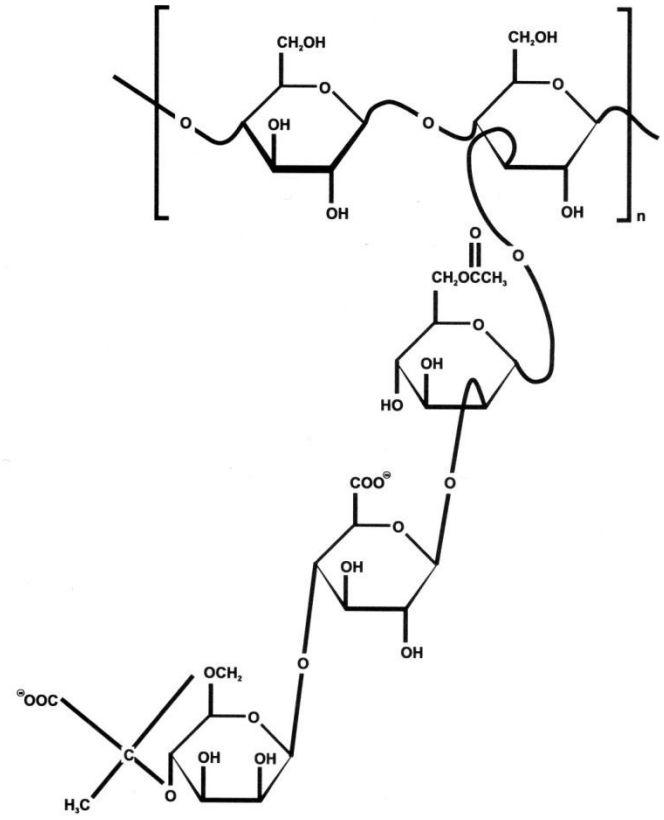


**Figure 6.2**: Chemical structure of xanthan repeat unit indicating a trisaccharide side chain with pyruvalated end mannose unit. Adapted from Tombs and Harding (1998).

Solutions of xanthan can also be highly viscous and exhibit what is known as pseudoplastic behavior: this is behavior where the viscosity decreases with increasing rate of shear stress (shear thinning effect). Xanthan became a very useful tool for many applications (food, cosmetics, oil recovery and pharmaceuticals) because of its suspending, stabilizing, thickening, emulsifying and its pseudoplasic rheological properties (Sutherland, 1996). It is also known to interact synergistically with other polysaccharides, notably galactomannans and this leads to an increase in viscosity (Foster and Morris, 1994; Dhami, 1996).

### 6.1.3 Sodium Alginate

Alginate is a hydrophilic colloidal carbohydrate located in the cell wall in the matrix of brown seaweed, which is extracted by the use of dilute alkali (Tombs and Harding, 1998; Rinaudo, 2008). In terms of molecular properties, alginate is a linear anionic polysaccharide (Figure 6.3). It is composed of (1,4) linked β-D-mannuronic (M) and α-L-gluronic acids (G), which are arranged in homopolymeric sequences of (MM and GG blocks) and heteropolymeric sequences of (MG blocks). Additionally, the M and G residues depend on the biological source and state of plant maturation (Haug et al., 1967; King, 1983).

Alginate has been widely used within food and pharmaceutical industries, because of its useful properties such as forming gels with calcium ions and retaining a significant amount of water (Pongjanyakul and Puttipipatkhachorn, 2007). The zone rich in a GG block plays an important role in the formation of these gels (Tønnesen and Karlsen, 2002). The arrangement of blocks along the

chain and also the total uronic acid composition (M and G residues ratio) have strong effect on the physiological and rheological properties of alginates and therefore on their application for example stabilizing, thickening and gelling. Alginate has the ability to form complexes with cationic and anionic polymers such as chitosan (Lee et al., 1997; Sæther et al., 2008) and sodium starch glycolate (Puttipipatkhachoron et al., 2005), as well as the non-ionic polymer konjac glucomannan (Wang and He, 2002).

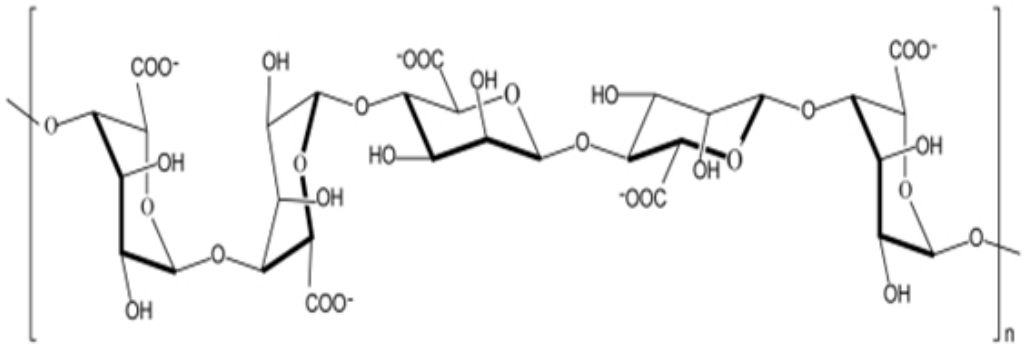


**Figure 6.3:** Chemical structure of alginate. Adapted from Tombs and Harding (1998).

## 6.2 MATERIALS

All the polysaccharides lambda carrageenan, konjac glucomannan, xanthan and their ternary mixtures were kindly provided by Glycomix (Reading, United Kingdom). The lambda carragennan, lot No. 27867; konjac glucomannan, lot No. 4229 and xanthan gum, lot No. 2761 were studied individually. Ternary mixtures were mixed together in a range of compositions as received varying

the lambda carragennan content in a range from 0% to 30% weights whilst maintaining - in the remainder of the mixture - the same constant high konjac glucomannan to xanthan gum weight ratio as in PGX®. Samples were used as supplied without any further purification. All samples were dissolved in deionised distilled water then dialysed into phosphate-chloride buffer solution (PBS) at pH=7.0 and ionic strength 0.1 M and 0.001 M. The concentrations, *c* (g $mL^{-1}$) of the stock solutions of all samples were measured using an Atago (Tokyo, Japan) DD-7 refractometer calibrated with glucose standards.

# 6.3 METHODS

## 6.3.1 Sedimentation Velocity (SV)

Please refer to (Chapter 3 section 3.3.1). An initial low rotor speed of 3000 rpm was used to check for the presence of any large sedimenting species and then adjusted to a rotor speed of 40,000 rpm. Scans were taken at 2 minutes intervals for a run time of ~16 hours.

## 6.3.2 Sedimentation Equilibrium (SE)

Please refer to (Chapter 3 section 3.3.2). Only individual polysaccharides were examined. They were prepared at a concentration of 0.3 mg $mL^{-1}$, after dialysis for 24 hours at the ambient temperature in phosphate-chloride buffer solution (PBS) at pH=7.0 and ionic strength 0.1M. The modified long (20.0 mm) optical path length double-sector cells with sapphire windows were loaded with

(~ 80 μl) of dialysed sample and a matching amount of reference buffer dialysate in appropriate channels. The rotor was then accelerated to 4000 rpm for lambda carrageenan and konjac glucomannan. However, in the case of xanthan the rotor was then accelerated to 2000 rpm.

### 6.3.3 Size Exclusion Chromatography Coupled to Multi Angle Light Scattering (SEC-MALS)

Please refer to (Chapter 3 section 3.3.3). Solutions prepared at injected concentrations of 0.5 mg $mL^{-1}$ were filtered through a 0.45 μm syringe filter (Whatman, Maidstone, England) - to remove any insoluble material or dust prior to being injected into the columns. The buffer was pumped at a steady, pulse-free flow rate of 0.8 mL $min^{-1}$ through the column system. The refractive index increment value was used for data analysis; lambda carrageenan *dn/dc* = 0.116 mL $g^{-1}$ (Slootmaekers et al., 1991b), whereas *dn/dc* = 0.15 mL $g^{-1}$ for KGM and 0.155 mL $g^{-1}$ for xanthan (Theisen et al., 2000). Because of the low concentrations after dilution on the columns no correction for non-ideality was assumed necessary, and $M_{w,app} = M_w$, the ideal weight average molecular weight.

### 6.3.4 Capillary Viscometry

As before (Chapter 3 section 3.3.4) the relative viscosities $\eta_{rel}$ of individual polysaccharides and mixtures of samples in concentration ($c$) ranging from 0.1 – 1.0 mg $mL^{-1}$ were measured using a 2 mL Ostwald viscometer at temperature of (20.00 ± 0.01) °C. The reduced ($\eta_{red} = (\eta_{rel}-1)/c$) and inherent ($\eta_{inh}$ =

($\ln\eta_{rel}$)/$c$) viscosities were extrapolated to infinite dilution to eliminate non-ideality effects using both the Huggins and Kraemer approaches. As an additional check, a combined relation due to Solomon and Ciuta was also used (see, e.g. Harding, 1997).

$$[\eta]\sim(1/c).\left[2\left(\eta_{sp}-ln(\eta_{rel})\right)\right]^{1/2} \quad (6.1)$$

# 6.4 RESULTS

## 6.4.1 Individual Polysaccharides

Characterization of the physical properties of the individual polysaccharides (namely lambda carrageenan, konjac glucomannan and xanthan) in solution is provided important biophysical information, which will supported a strategy planned to investigate whether any interaction occurred between these substances or not. Thus, sedimentation coefficient, intrinsic viscosity and molecular weight were estimated to establish molecular integrity of these individual polysaccharides using analytical ultracentrifuge (AUC), size exclusion chromatography coupled to multi-angle laser light scattering (SEC-MALS), and capillary viscometry.

### 6.4.1.1 Sedimentation Coefficient and Sedimentation Coefficient Distribution

We consider the sedimentation coefficient, *s* values for the individual polysaccharides (lambda carrageenan, konjac glucomannan and xanthan) using

sedimentation velocity (SV) (Table 6.1). The sedimentation coefficients, *s* were obtained for all individual polysaccharides at a series of concentrations and two ionic strengths (0.1M and 0.001M) using the ls-g* (s) distribution method.

**Table 6.1**: Summary of $s^{\circ}_{20,w}$ and $k_s$ results for all individual polysaccharides samples.

| Sample | | $s^{\circ}_{20,w}$ (S) | $k_s$ (mL g$^{-1}$) |
|---|---|---|---|
| **konjac glucomannan** | **0.1M** | 4.4±0.3 | 2000±150 |
| | **0.001M** | 4.4±0.4 | 1600±200 |
| **lambda carrageenan** | **0.1M** | 5.4±0.4 | 495±60 |
| | **0.001M** | 2.6±0.1 | 710±20 |
| **xanthan** | **0.1M** | 12.0±0.5 | 1510±95 |
| | **0.001M** | 11.0±0.8 | 3100±500 |

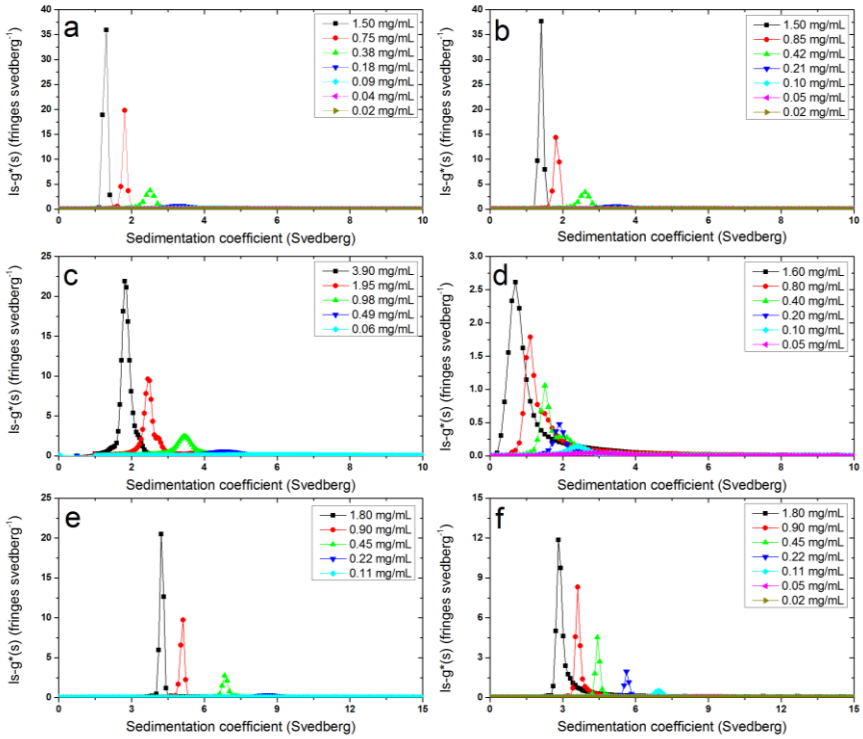


**Figure 6.4:** Sedimentation coefficient distribution profiles using least squares g*(s) method of SEDFIT obtained from sedimentation velocity experiment for all individual polysaccharides at different ionic strengths (0.1M and 0.001M) konjac glucomannan (a and b), lambda carrageenan (c and d) and xanthan (e and f) respectively.

Unimodal distributions were seen in all cases for the apparent sedimentation coefficient distributions; show that the samples are homogeneous (Figure 6.4). Note that as the ionic strength is increased non-ideality effects are suppressed through charge shielding for lambda carrageenan and xanthan, but not konjac glucomannan which is uncharged. To eliminate the non-ideality effects, $s_{20,w}$ was further extrapolated to zero concentration to obtain $s^{\circ}_{20,w}$ using the reciprocal plots ($1/s_{20,w}$) *vs.* concentration as shown in Figures 6.5. Generally, this provides more reliable estimates for $s^{\circ}_{20,w}$ and the concentration dependence of sedimentation, $k_s$ both are reported in (Tables 6.1).

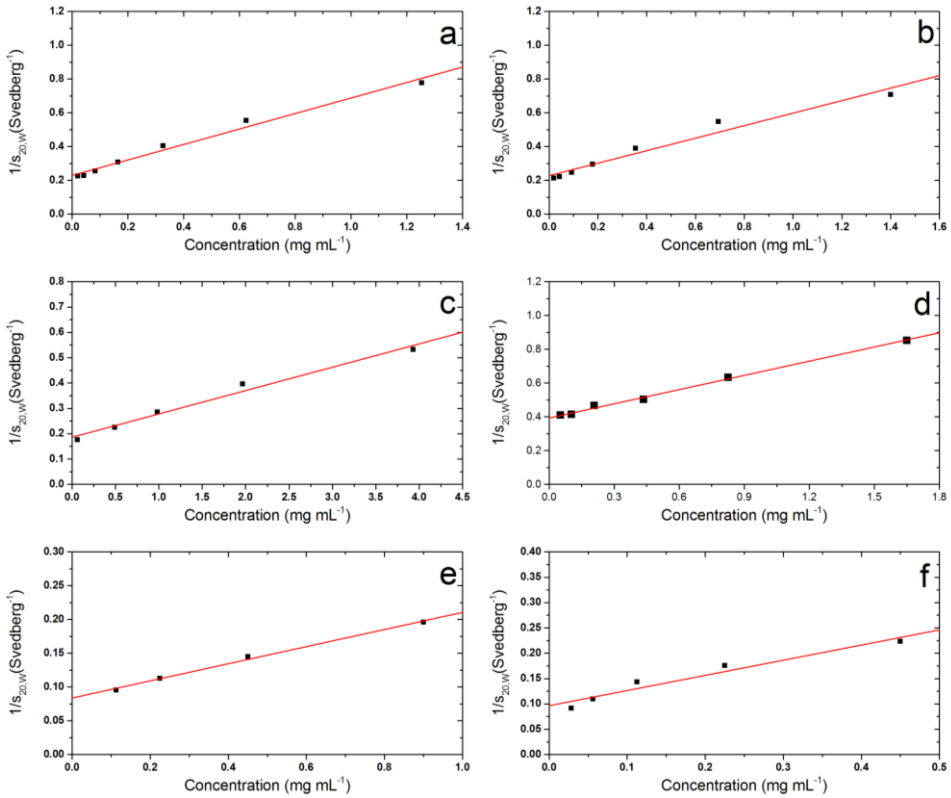


**Figure 6.5:** Concentration dependence (reciprocal) of the sedimentation coefficient plot (after correction to standard solvent conditions) for all individual polysaccharides at different ionic strengths (0.1M and 0.001M) konjac glucomannan (a and b), lambda carrageenan (c and d) and xanthan (e and f), respectively.

The results show that xanthan has the highest weight average sedimentation coefficient $s^{\circ}_{20,w}$ followed by lambda carrageenan and konjac glucomannan.

This is a consequence of the sedimentation coefficient depending principally on the molecular weight (the larger the molecule is the larger the *s*) and then the conformation (the more extended the molecule is the lower the *s*). For example, konjac glucomannan has high solubility attributing to its long side chains that have intermolecular association, which contributes to its low sedimentation (Kök et al., 2009). In accordance to Tombs and Harding (1998), xanthan is a double-stranded polysaccharide with worm-like chain which behaves like a flexible rod and a stiff coil. Furthermore, the results of lambda carrageenan and xanthan describe a decrease in weight-average sedimentation coefficient with decreased ionic strengths, whereas konjac glucomannan was not affected. This behaviour is due to very little charge shielding at very low ionic strengths (higher non-ideality), since both lambda carrageenan and xanthan are strongly polyannionic and konjac is a neutral polysaccharide with little or no charge (Ratcliff et al., 2005).

#### 6.4.1.2 Estimation of Molecular Weight

The absolute weight average molecular weight of the reaction was checked for each individual polysaccharide prior to them being mixed together, using SEC-MALS as well as sedimentation equilibrium in the analytical ultracentrifugation. The weight average molecular weights of all individual polysaccharides (lambda carrageenan, konjac glucomannan and xanthan) initially were estimated from sedimentation equilibrium and are reported in (Table 6.2). Figure 6.6 presents the weight average molecular weight $M_w$

results analysed using the SEDFIT-MSTAR procedure for all individual samples (Schuck et al., 2014). Working at relatively low concentration (0.3 mg $mL^{-1}$) helps to minimize the non-ideality arising from co-exclusion and polyelectrolyte effects. Such a low concentration is rendered possible by using the modified long (20.0 mm) optical path length cells; the apparent molecular weight at this loading concentration $M_{w,app}$ is ~$M_w$ the true or ideal weight average molecular weight (Harding, 2005a; Schuck et al., 2014).

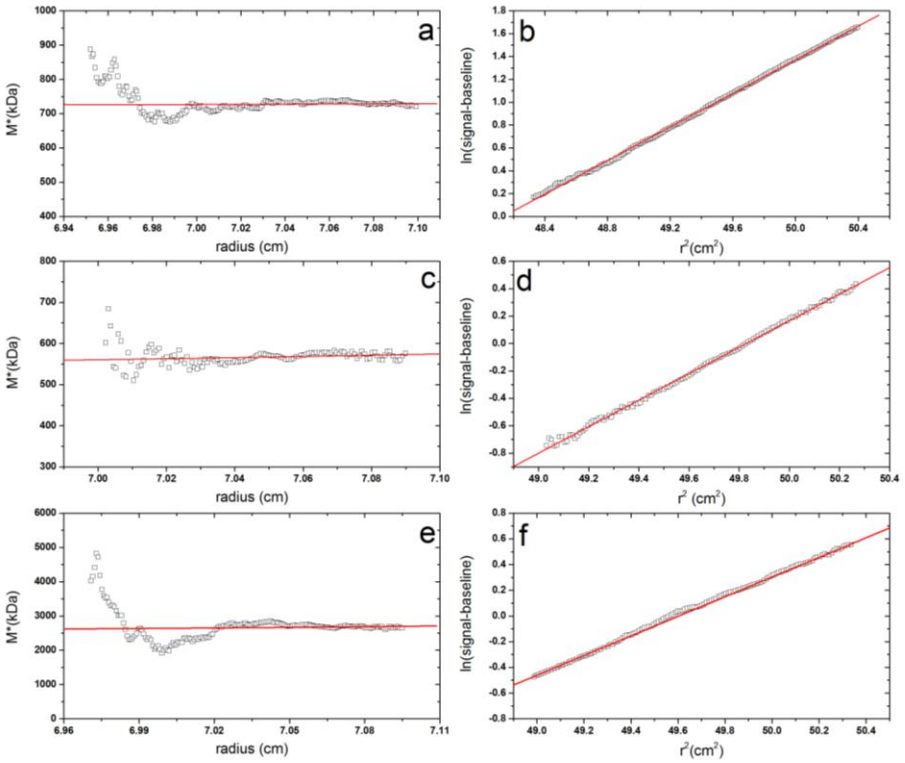


**Figure 6.6:** Molecular weight plots for konjac glucomnannan (a and b), lambda carrageenan (c and d) and xanthan (e and f) using SEDFIT-MSTAR: log concentration ln*c(r) vs.* $r^2$plot, where *r* is the radial distance from the centre of rotation; *M** versus *r* plot the value of *M** extrapolated to the cell base = $M_{w,app}$ the apparent weight average molecular weight for whole distribution.

However, values of the weight average molecular weight ($M_w$) for individual polysaccharides lambda carrageenan and xanthan obtained using SEC-MALS

are reported in Table 6.2. Within the error estimate the molecular weight results of lambda carrageenan and xanthan obtained from SEC-MALS show a good agreement, with those yielded from sedimentation equilibrium in analytical ultracentrifugation. Figure 6.7 shows plot molecular weight vs retention time for lambda carrageenan and xanthan which is demonstrated to be unimodal. Konjac glucomannan was not measured by SEC-MALS, because of an apparent anomalous reaction with the column material (Kök et al., 2009).

**Table 6.2**: Summary of molecular weights *($M_w$)* results for individual polysaccharides from sedimentation velocity, equilibrium and SEC-MALS.

| **Samples** | **$10^{-3}$ x $M_w$ (g $mol^{-1}$)[a]** | **$10^{-3}$ x $M_w$ (g $mol^{-1}$)[b]** | **$10^{-3}$ x $M_w$ (g $mol^{-1}$)[c]** |
|---|---|---|---|
| **konjac glucomannan** | 730±10 | not determined* | 800±60 |
| **lambda carrageenan** | 680±10 | 690±10 | 630±7 |
| **xanthan** | 2700±300 | 2200±200 | 2100±150 |

* : not determined due to interaction with the column
a : molecular weight obtained from sedimentation equilibrium
b : molecular weight obtained from SEC-MALS
c : molecular weight obtained from sedimentation velocity and the Extended Fujita method

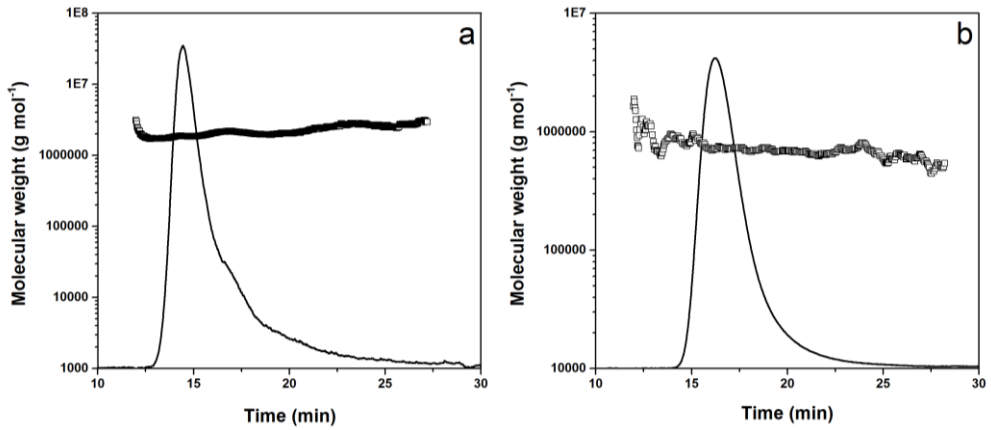


**Figure 6.7:** Elution profile (black line) for (a) xanthan and (b) lambda carrageenan in 0.1M PBS examined by SEC-MALS at concentration of 0.5 mg $mL^{-1}$. The open squares correspond to SEC-MALS calculated molecular weights.

The molecular weights for the individual polysaccharides were also estimated from sedimentation velocity and the Extended Fujita method and are presented in Table (6.2). Transforming a distribution of sedimentation coefficient (*s*) into a distribution of molecular weight was used to estimate the molecular weight by combining the Fujita (1961) equation $f(M) = g(s).(ds/dM)$ with $s^{o}_{20,w} = K_s M^b$ equation in the Extended Fujita approach of Harding et al. (2011b).

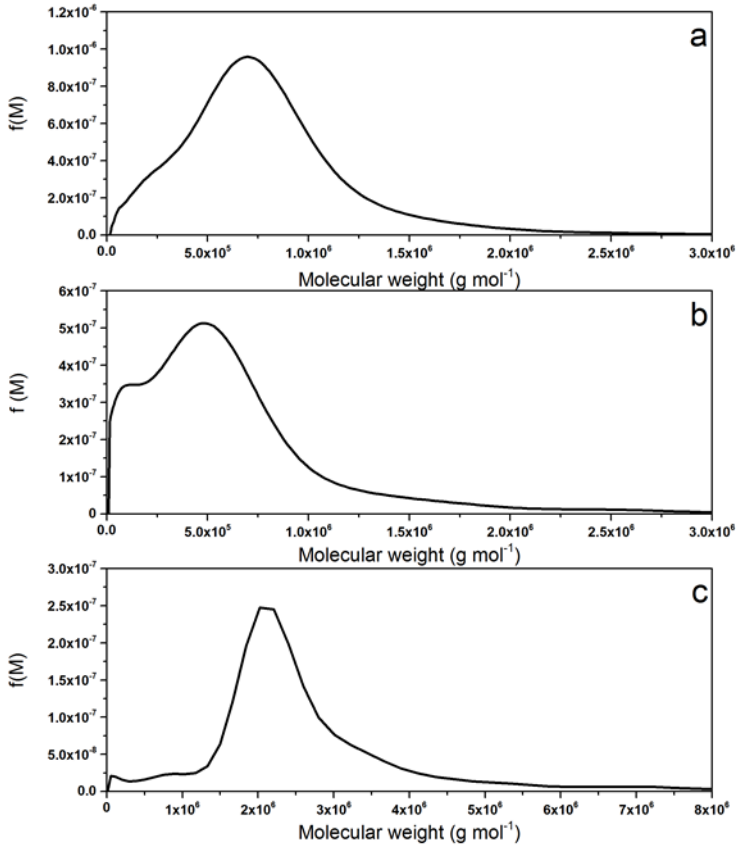


**Figure 6.8:** Molecular weight distribution for individual polysaccharides (a) konjac glucomannan, (b) lambda carrageenan and (c) xanthan in 0.1M PBS buffer obtained from transformation of the g(s) versus *s* distribution at concentration (0.2 mg $mL^{-1}$), using the *Extended Fujita* method of Harding et al., (2011b).

Figures 6.8 show *f(M)* versus molecular weight for all polysaccharides. Clearly, xanthan has the highest molecular weight followed by konjac

glucomannan and finally lambda carrageenan. The results from sedimentation velocity are in perfect agreement with those obtained from both sedimentation equilibrium and SEC-MALS in this study, as well with previous study (Harding et al., 2012).

### 6.4.1.3 Intrinsic Viscosity

The values of intrinsic viscosity obtained from the Huggins, Kraemer and Solomon-Ciuta extrapolation methods (using capillary viscometry) for individual polysaccharides are reported in Table 6.3. Figures 6.8 show the corresponding plots of intrinsic viscosity versus concentration (g $mL^{-1}$) for konjac glucomannan, lambda carrageenan and xanthan, respectively.

**Table 6.3:** Intrinsic viscosity values for individual polysaccharides konjac glucomannan, lambda carrageenan and xanthan yielded from capillary viscometry.

| **Samples** | | **Intrinsic viscosity [η] (mL $g^{-1}$)** | | |
|---|---|---|---|---|
| | | **Huggins** | **Kraemer** | **Solomon-Ciuta** |
| **konjac glucomannan** | **0.1M** | 2045±35 | 2820±160 | 2730±210 |
| | **0.001M** | 2420±380 | 2930±80 | 2730±190 |
| **lambda carrageenan** | **0.1M** | 1415±140 | 1540±70 | 1530±80 |
| | **0.001M** | 2760±190 | 2960±210 | 2940±220 |
| **xanthan** | **0.1M** | 3080±180 | 3560±90 | 3480±60 |
| | **0.001M** | 5790±670 | 6185±230 | 6240±260 |

The results clearly show the influence of ionic strength on xanthan and lambda carrageenan: when it decreases the intrinsic viscosity increases. Thus, these

results are consistent with sedimentation coefficient; corroborating that konjac glucomannan was not significantly affected by changing ionic strength (Table 6.3).

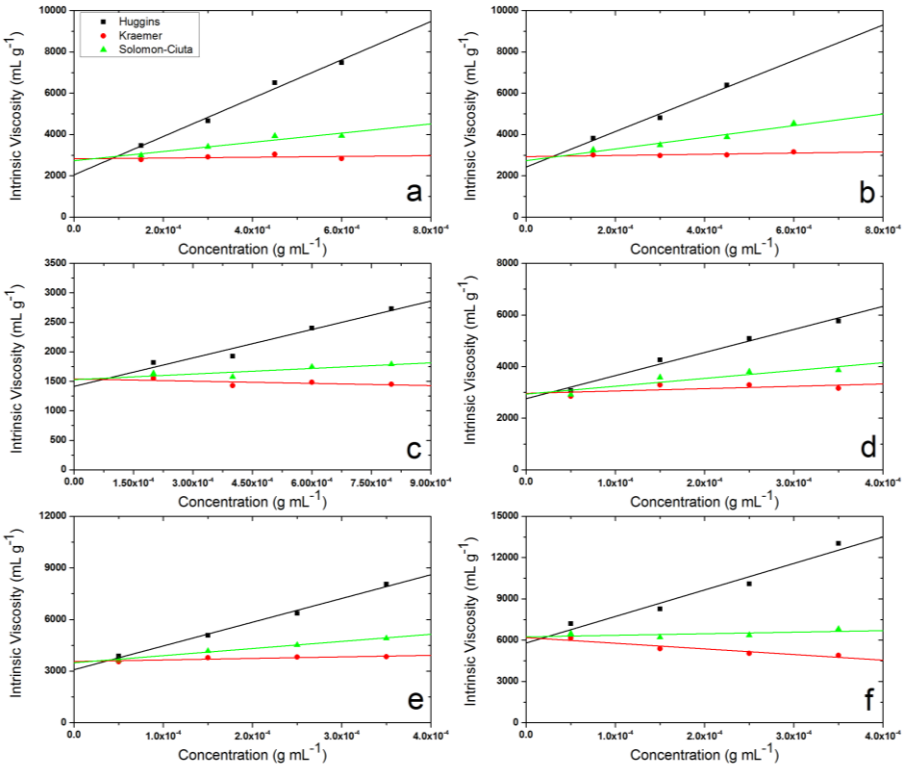


**Figure 6.9:** The intrinsic viscosity plot from capillary viscometry: Huggins, Kraemer and Solomon-Ciuta extrapolations for konjac glucomannan (a and b) lambda carrageenan (c and d) xanthan (e and f).

For both ionic strengths (0.1M and 0.001M) there is a good agreement between the results of intrinsic viscosity obtained from Huggins, Kraemer and Solomon-Ciuta extrapolations using capillary viscometry. Therefore, xanthan was the most viscous, followed by konjac glucomannan and then lambda carrageenan (at ionic strength of 0.1M), which is consistent with sedimentation coefficient and molecular weight results. A study by Harding and co-workers (2011a) showed that xanthan has a higher viscosity compared to konjac

glucomannan in rheological measurements. Furthermore, the viscosity of all individual polysaccharides gives good linear extrapolations from different extrapolation methods (Figure 6.9).

## 6.4.2 Binary Mixture of Polysaccharides

We now consider the interaction of konjac glucomannan and xanthan mixture without lambda carrageenan (C0) – where konjac glucomannan is the major species – at two different ionic strengths (0.1M and 0.001M) using analytical ultracentrifugation and capillary viscometry. This will provide a strong platform for the following experiments to examine whether there is an interaction between binary mixture polysaccharides and lambda carrageenan. The recent advances in sedimentation velocity (Dam & Schuck, 2004; Harding et al, 2011b) can also be utilised to reinforce the interaction observed previously by Dhami (1996).

### 6.4.2.1 Sedimentation Coefficient and Sedimentation Coefficient Distribution

The results of sedimentation velocity for the binary mixture konjac glucomannan and xanthan at 0.1M ionic strength are summarised in Table 6.4. The sedimentation coefficient, *s* obtained using the least squares ls-g*(s) method. Plot of reciprocal sedimentation coefficient, $s_{20,w}$ vs. concentration yielded a similar sedimentation coefficient, $s^{o}_{20,w}$ value for the konjac glucomannan control (Figure 6.10a). Figure 6.11 also showed that the

distribution profiles of binary mixture combined with individual component controls at several concentrations (2.0, 1.0, 0.5 and 0.25 mg $mL^{-1}$).

**Table 6.4:** Summary of sedimentation velocity and capillary viscometry results for the binary mixture of konjac glucomannan and xanthan samples at 0.1M and 0.001M.

| **Property** | | **Binary mixture (C0)** | |
|---|---|---|---|
| | | **0.1M** | **0.001M** |
| $s^o_{20,w}$ **(S)** | | 4.8±0.2 | 4.8±0.1* |
| $k_s$ **(mL $g^{-1}$)** | | 970±60 | 720±50 |
| **[η](mL $g^{-1}$)** | **Huggins** | 1905±25 | 3600±35 |
| | **Kraemer** | 2715±50 | 3670±65 |
| | **Solomon-Ciuta** | 2720±90 | 3790±30 |
| | **Predicted**[a] | 2880 | 3430 |

* : sedimentation coefficient of the main free peak
a : predicted intrinsic viscosity if there was no interaction

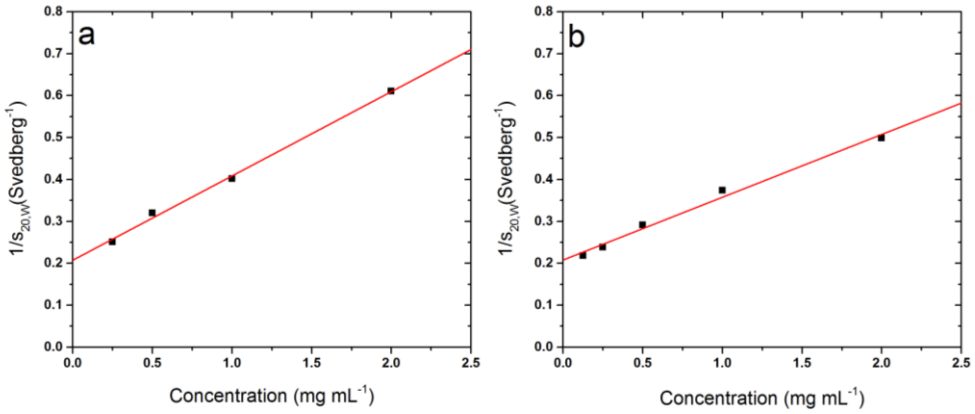


**Figure 6.10:** Concentration dependence (reciprocal) of the sedimentation coefficient plot – main free peak (after correction to standard solvent conditions) for the binary mixture of konjac glucomannan and xanthan: (a) 0.1M ionic strength and (b) 0.001M ionic strength

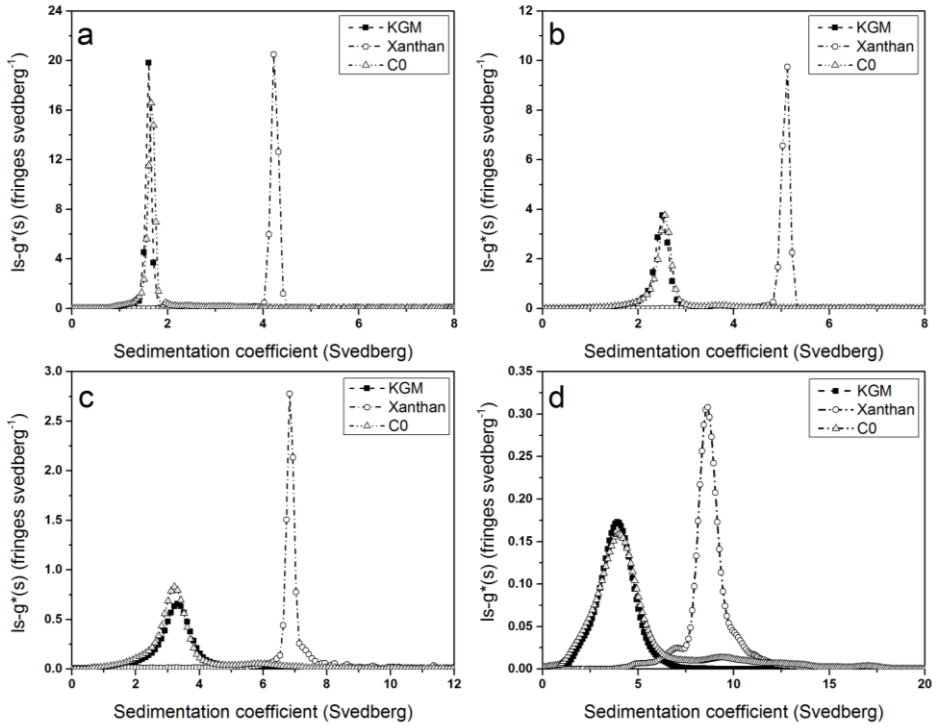


**Figure 6.11:** Sedimentation coefficient distribution profiles using least squares g*(s) method of SEDFIT obtained from sedimentation velocity experiment for the binary mixture of konjac glucomannan and xanthan with individual component controls at 0.1M ionic strength: (a) 2.00 mg mL$^{-1}$, (b) 1.00 mg mL$^{-1}$, (c) 0.50 mg mL$^{-1}$ and (d) 0.25 mg mL$^{-1}$.

The values of the weight average $s_{20,w}$ of the binary mixture increased with decrease in concentration, and seems to be in the same order as for the konjac glucomannan control, showing no evidence of interaction at higher ionic strength 0.1M. However, a significant interaction product was observed with apparent sedimentation coefficients (3.6 S) greater than that of the highest sedimenting component in the controls (Figure 6.12), for the binary mixture of konjac glucomannan and xanthan in the absence of lambda carrageenan at low ionic strength. Since synergistic polysaccharide-polysaccharide interactions are already known from rheological studies in concentrated solution (Shatwell,

Sutherland, Ross-Murphy, and Dea, 1991). Therefore, the observation of binary mixture interaction (konjac glucomannan and xanthan) was in a perfect agreement with previous studies (Foster and Morris, 1994; Dhami, 1996; Harding et al., 2011a). In addition, increase in the sedimentation coefficient of free konjac glucomannan in the mixture as compared to the individual control is consistent with reduction in a total concentration of component (Schachman, 1959).

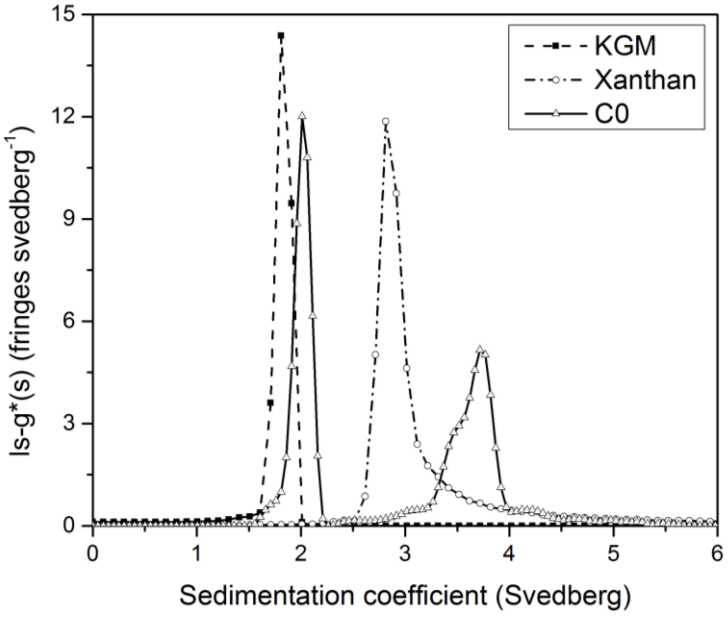


**Figure 6.12:** Sedimentation coefficient distribution profiles using least squares g*(s) method of SEDFIT obtained from sedimentation velocity experiment for the binary mixture of konjac glucomannan and xanthan with individual component controls at 0.001M ionic strength and concentration (2.0 mg $mL^{-1}$).

The apparent sedimentation coefficient values of the new product - in binary mixture - increased (14, 22 and 30 S) with decrease in the concentration (1.0, 0.5 and 0.25 mg $mL^{-1}$ respectively) (Figure 6.13). Further, the sedimentation coefficient value obtained from the reciprocal plot of the main free peak in the

binary mixture within the error estimate seems be similar to that found for the individual konjac glucomannan (Table 6.4). This finding can be explained by the fact that konjac glucomannan is the dominant component in the binary mixture.

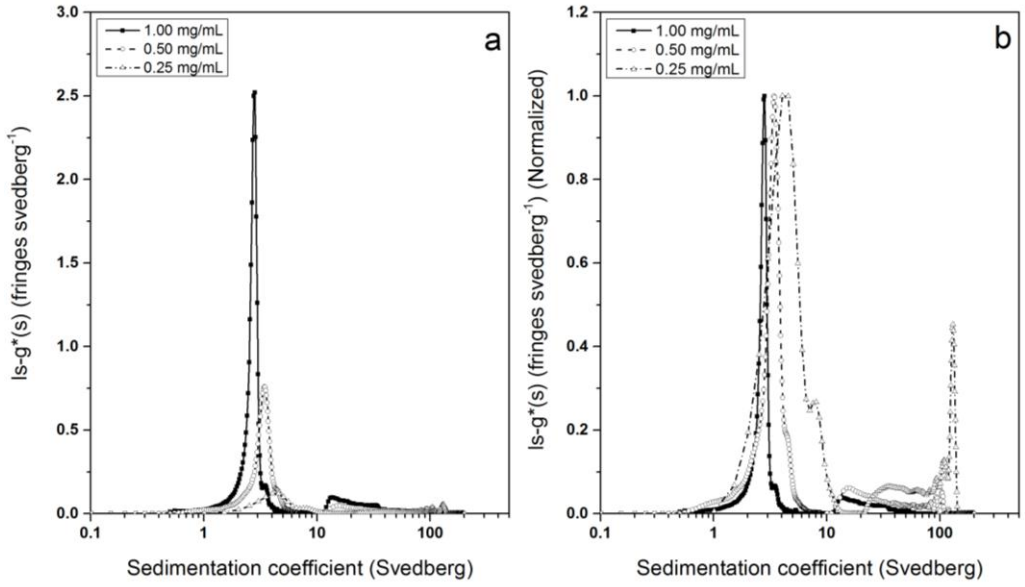


**Figure 6.13:** Sedimentation coefficient distribution profiles using least squares g*(s) method of SEDFIT obtained from sedimentation velocity experiment for (a) the binary mixture of konjac glucomannan and xanthan at 0.001M ionic strength, (b) the normalized data.

### 6.4.2.2 Intrinsic Viscosity

The intrinsic viscosity values resulting from the Huggins, Kraemer and Solomon-Ciuta extrapolation methods for the binary mixture of konjac glucomannan and xanthan (C0) investigated at both ionic strength 0.1M and 0.001M (Figure 6.14), are also reported in Table 6.4. A clear difference was observed for the binary mixture (3790 mL $g^{-1}$) compared to the predicted value for a non-interacting mixture (3430 mL $g^{-1}$) at low ionic strength 0.001M, but

not at 0.1M ionic strength; showing that the interaction occurred at 0.001M. This result is in agreement with those yielded by sedimentation velocity in analytical ultracentrifugation. Also it appears to reinforce the earlier observations obtained by (Shatwell et al., 1991; Foster and Morris, 1994; Dhami, 1996). Having understood the behaviour of the binary mixture of konjac glucomannan and xanthan we can now consider the ternary mixture with lambda carrageenan also present.

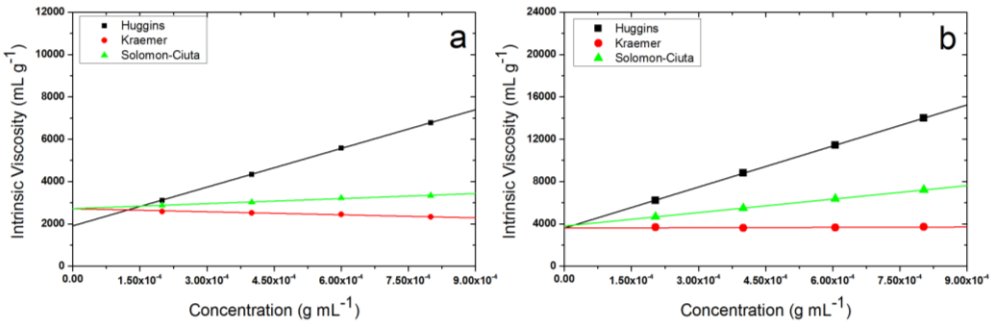


**Figure 6.14:** The intrinsic viscosity plot from capillary viscometry: Huggins, Kraemer and Solomon-Ciuta extrapolations for the binary mixture of konjac glucomannan and xanthan at tow ionic strengths (a) 0.1M and (b) 0.001M.

## 6.4.3 Ternary Mixture of Polysaccharides

In order to observe the possibility of whether or not the interaction between the components of the ternary mixture (lambda carrageenan, konjac glucomannan and xanthan) occurred at two different ionic strengths (0.1M and 0.001M); sedimentation velocity experiment in analytical ultracentrifugation and capillary viscometry were used. Changes in hydrodynamic volume of the mixtures compared to that of individual polysaccharides were measured in terms of sedimentation coefficient and intrinsic viscosity.

### 6.4.3.1 Sedimentation Coefficient and Sedimentation Coefficient Distribution

Sedimentation coefficient distributions were studied for ternary mixture solutions of lambda carrageenan - mixing ratio C30 to C0 - with konjac glucomannan and xanthan at a series concentrations and two ionic strengths (0.1M and 0.001M) (Figures 6.15 and 6.16, respectively). In solvent of ionic strength 0.1M, no clear interaction was observed for the ternary mixture at all mixing ratios, showing a sedimentation coefficient distribution corresponded to that of the lambda carrageenan control (at a ratio of C30 to C15), whereas for the konjac glucomannan control (C10 to C05) and reported in Table 6.5. This result is confirmed by the plot of the reciprocal sedimentation coefficient, $1/s_{20,w}$ vs. the concentration $c$; showing that values obtained for these solutions of mixing ratio C30 to C15 within the error estimate are similar to that of lambda carrageenan control, whereas konjac glucomannan at C10 to C05 (Figure 6.17).

**Table 6.5:** Summary of $s^{\circ}_{20,w}$ results for ternary mixture samples at different ionic strengths.

| Samples | $s^{o}_{20,w}$ (S) | | |
|---|---|---|---|
| | 0.1M | 0.001M | |
| | | Peak 1 | Peak 2 |
| **C30** | 5.4±0.2 | 2.4±0.2 | 4.3±0.5 |
| **C25** | 5.4±0.3 | 2.7±0.3 | 4.9±0.3 |
| **C20** | 5.6±0.4 | 2.6±0.2 | 4.8±0.2 |
| **C15** | 5.4±0.1 | 2.6±0.3 | 4.9±0.2 |
| **C10** | 4.6±0.5 | 3.2±0.1 | 4.4±0.2 |
| **C05** | 4.4±0.5 | 4.6±0.5 | 12.2±0.2 |

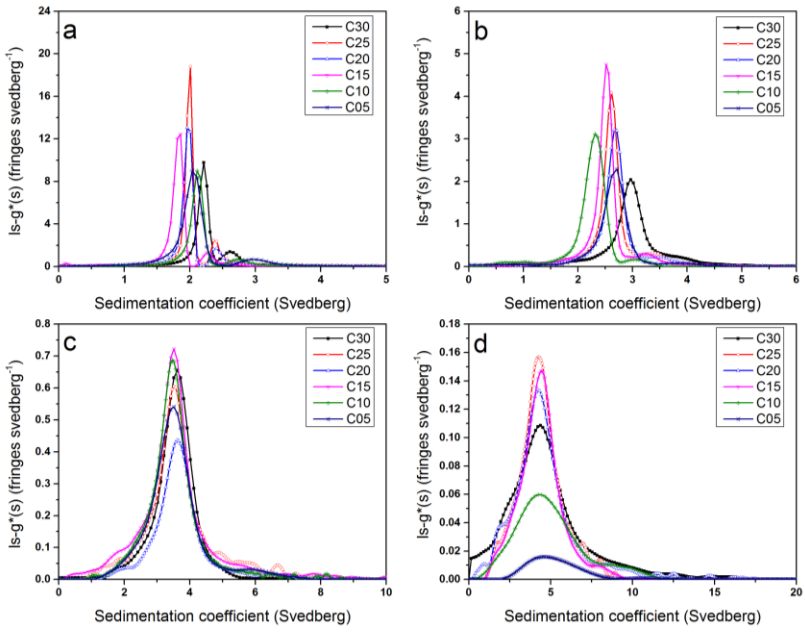


**Figure 6.15:** Sedimentation coefficient distribution profiles using least squares g*(s) method of SEDFIT for the ternary mixture of lambda carrageenan, konjac glucomannan and xanthan at 0.1M ionic strength: (a) 2.00 mg $mL^{-1}$, (b) 1.00 mg $mL^{-1}$, (c) 0.50 mg $mL^{-1}$ and (d) 0.25 mg $mL^{-1}$.

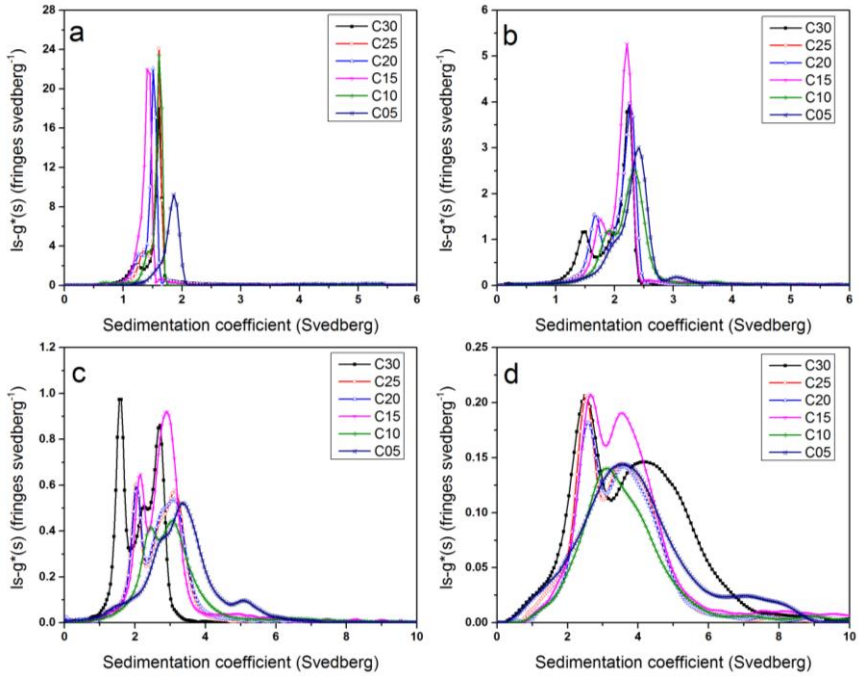


**Figure 6.16:** Sedimentation coefficient distribution profiles using least squares g*(s) method of SEDFIT for the ternary mixture of lambda carrageenan, konjac glucomannan and xanthan at 0.001M ionic strength: (a) 2.00 mg $mL^{-1}$, (b) 1.00 mg $mL^{-1}$, (c) 0.50 mg $mL^{-1}$ and (d) 0.25 mg $mL^{-1}$.

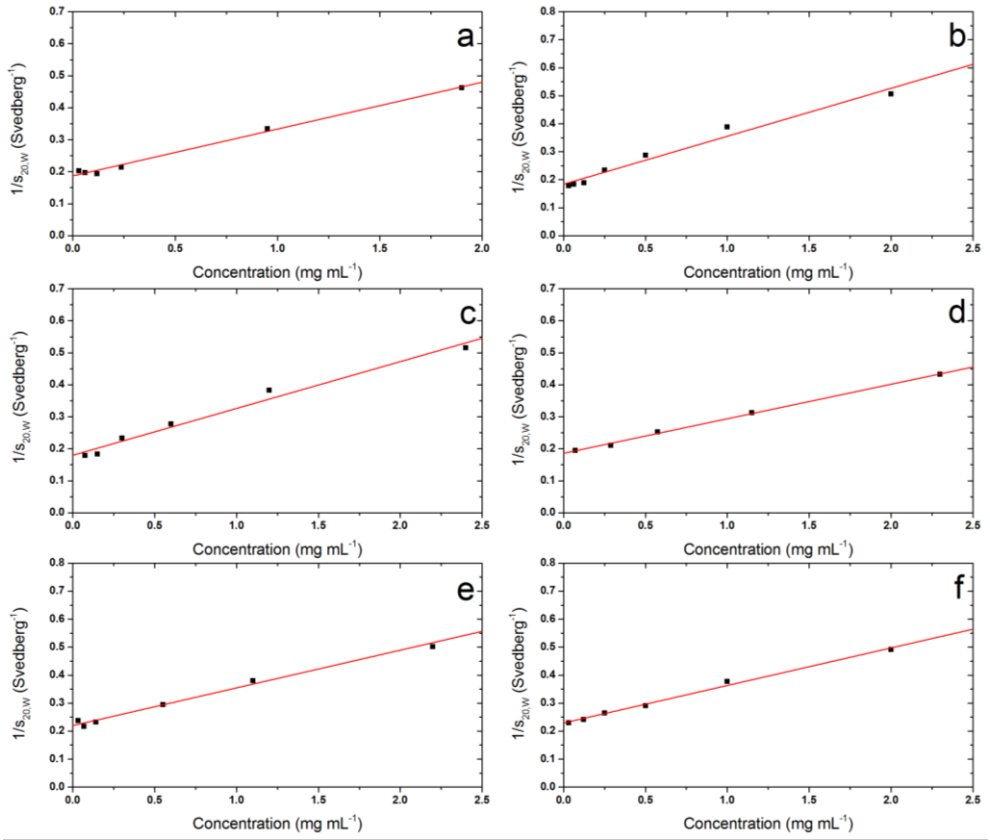


**Figure 6.17:** Concentration dependence (reciprocal) of the sedimentation coefficient plot for the ternary mixture of lambda carrageenan, konjac glucomannan and xanthan at ionic strength 0.1M: (a) C30, (b) C25, (c) C20, (d) C15, (e) C10 and (f) C05.

However, two peaks presented in the sedimentation coefficient distribution plot for the ternary mixture in the solution of low ionic strength 0.001M, which are referred to that of lambda carrageenan (mixing ratio C30 to C10) and konjac glucomannan (at C05) controls. Consequently, the results showed no evidence of an interaction occurred in the presences of lambda carrageenan at all mixing ratios. Figure 6.18 showed a good example for this behaviour of the ternary mixture for all mixing ratios (C30 to C05) combined with individual component controls at one concentration (0.25 mg $mL^{-1}$); providing no significant interaction observed at this environment (I= 0.001M). Furthermore,

the plots of $s_{20,w}$ versus concentration (Figure 6.19) also showed that the values for the first and second peaks are similar to that for the individual component lambda carrageenan and konjac glucomannan, respectively at mixing ratios (C30 to C10), whereas similar to konjac glucomanan and xanthan at (C05). These are reported in Table 6.5.

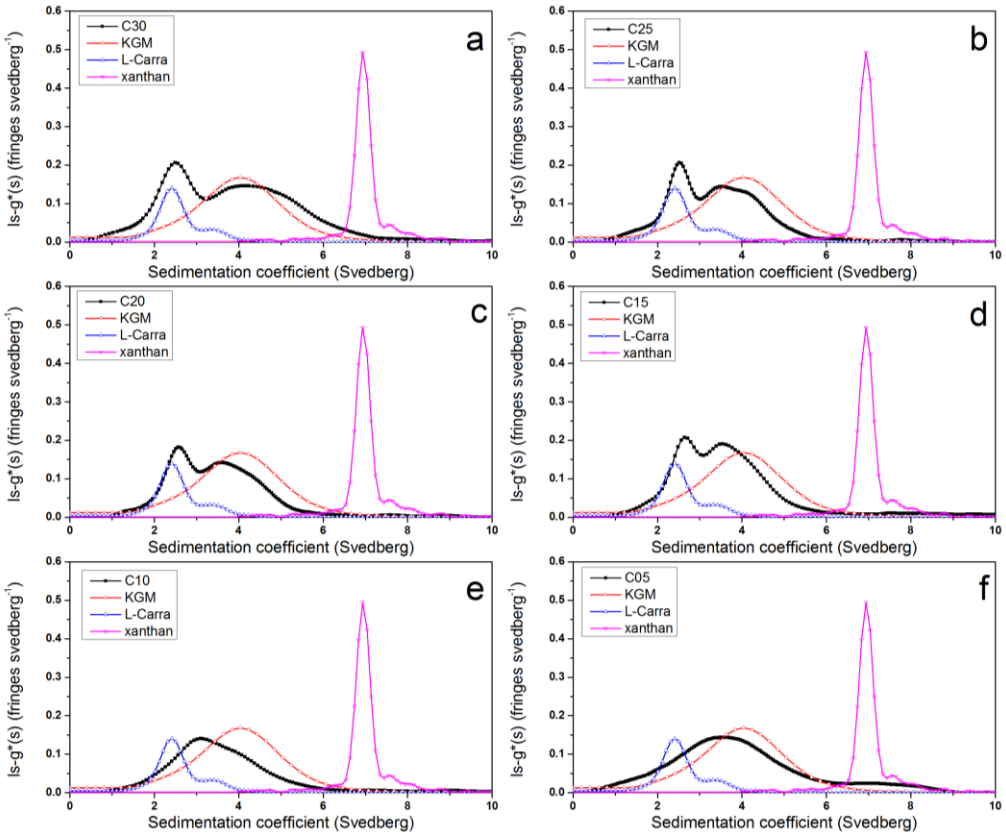


**Figure 6.18:** Sedimentation coefficient distribution profiles using the least squares g*(s) method of SEDFIT for the ternary mixture of lambda carrageenan, konjac glucomannan and xanthan at all mixing ratio (C30 – C05) companied with non-interacting species at 0.001M ionic strength and 0.25 mg $mL^{-1}$.

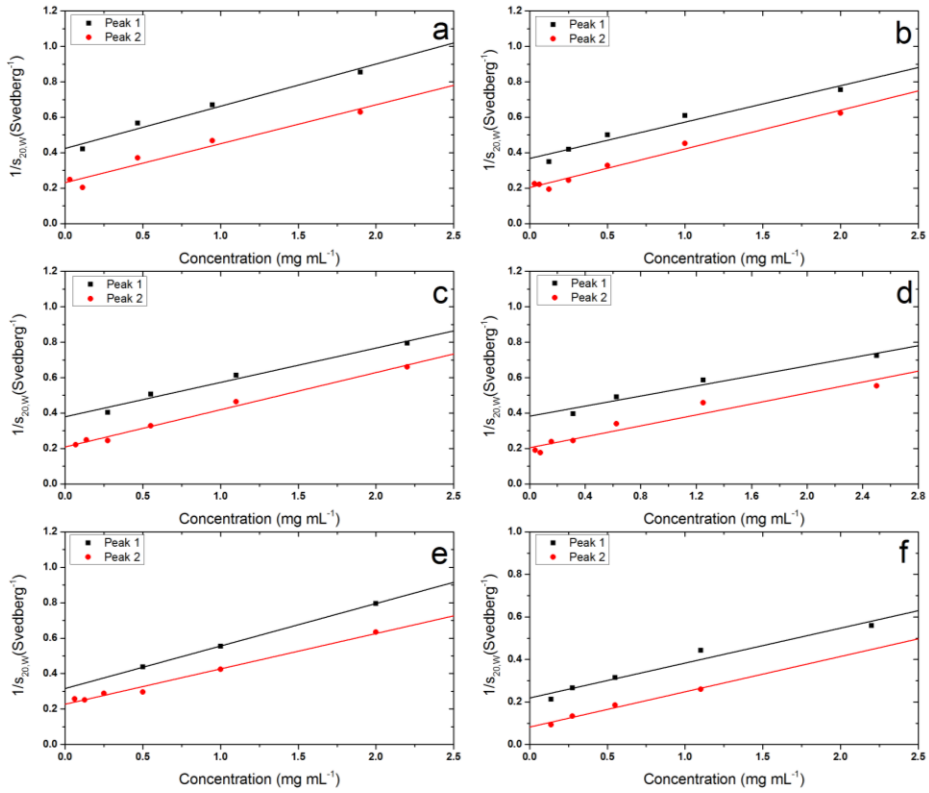


**Figure 6.19:** Concentration dependence (reciprocal) of the sedimentation coefficient plots for the ternary mixture of lambda carrageenan, konjac glucomannan and xanthan at ionic strength 0.1M: (a) C30, (b) C25, (c) C20, (d) C15, (e) C10 and (f) C05.

### 6.4.3.2 Intrinsic Viscosity

Intrinsic viscosity values resulted from Huggins, Kraemer and Solomon-Ciuta extrapolation methods for ternary mixture solutions of lambda carrageenan (maxing ratio C30 to C05) with konjac glucomannan and xanthan at ionic strength (0.1M and 0.001M) are given in (Table 6.6). The corresponding plots of intrinsic viscosity [η] (mL $g^{-1}$) versus concentration (g $mL^{-1}$) for ternary mixture solutions of lambda carrageenan with konjac glucomannan and xanthan at ionic strength (0.1M and 0.001M) are presented in Figures 6.20 and 6.21.

**Table 6.6:** Intrinsic viscosity values (mL $g^{-1}$) for ternary mixtures of lambda carrageenan, konjac glucomannan and xanthan (mixing ratios C30 to C05) at 0.1M and 0.001M ionic strengths yielded from capillary viscometry.

| Sample | | 0.1M | Predicted | 0.001M | Predicted |
|---|---|---|---|---|---|
| **C30** | **Huggins** | 1310±20 | 2170±265 | 2270±350 | 2980±360 |
| | **Kraemer** | 1360±20 | 2670±130 | 2580±120 | 3400±140 |
| | **Solomon-Ciuta** | 1350±30 | 2620±170 | 2500±180 | 3290±210 |
| **C25** | **Huggins** | 1770±120 | 2228±274 | 3100±190 | 3000±375 |
| | **Kraemer** | 1780±100 | 2760±130 | 3100±100 | 3430±130 |
| | **Solomon-Ciuta** | 1760±110 | 2670±170 | 3120±130 | 3310±210 |
| **C20** | **Huggins** | 1420±150 | 2280±280 | 1490±300 | 3020±390 |
| | **Kraemer** | 1460±115 | 2840±140 | 1990±150 | 3460±130 |
| | **Solomon-Ciuta** | 1455±130 | 2770±170 | 1875±135 | 3335±210 |
| **C15** | **Huggins** | 1820±70 | 2340±290 | 1810±60 | 3040±120 |
| | **Kraemer** | 1815±60 | 2920±140 | 1820±60 | 3490±120 |
| | **Solomon-Ciuta** | 1810±60 | 2850±180 | 1780±80 | 3360±200 |
| **C10** | **Huggins** | 1640±65 | 2390±300 | 1990±180 | 3060±410 |
| | **Kraemer** | 1740±40 | 3000±140 | 2220±75 | 3520±120 |
| | **Solomon-Ciuta** | 1720±40 | 2930±190 | 2175±85 | 3385±200 |
| **C05** | **Huggins** | 1692±96 | 2444±309 | 1910±280 | 3080±420 |
| | **Kraemer** | 1820±25 | 3080±150 | 2490±60 | 3550±110 |
| | **Solomon-Ciuta** | 1790±40 | 3010±195 | 2360±15 | 3410±210 |

However, predicted intrinsic viscosity values for the non-interacting components were calculated from the total percentage for each component in the mixture multiplied by its intrinsic viscosity, and then divided by 100. At both ionic strengths (0.1M and 0.001M) the intrinsic viscosity values for ternary mixture solution C30, C25 and C20 seem to be close to that of the individual lambda carrageenan species, whereas C15, C10 and C05 are close to

konjac glucomannan (Table 4.3). These results can be explained in terms of the dominant component in the ternary mixture, where lambda carrageenan has higher amount in C30, C25 and C20. Furthermore, the results of intrinsic viscosity values for mixture solutions from C30 to C05 within the error estimate seem be similar or lower to the predicted values for a non-interacting mixture at both ionic strengths. Thus, these observations show clearly no interaction observed within mixtures of konjac glucomannan and xanthan in the presence of lambda carrageenan, a finding supported by the results obtained from analytical ultracentrifugation based on sedimentation velocity.

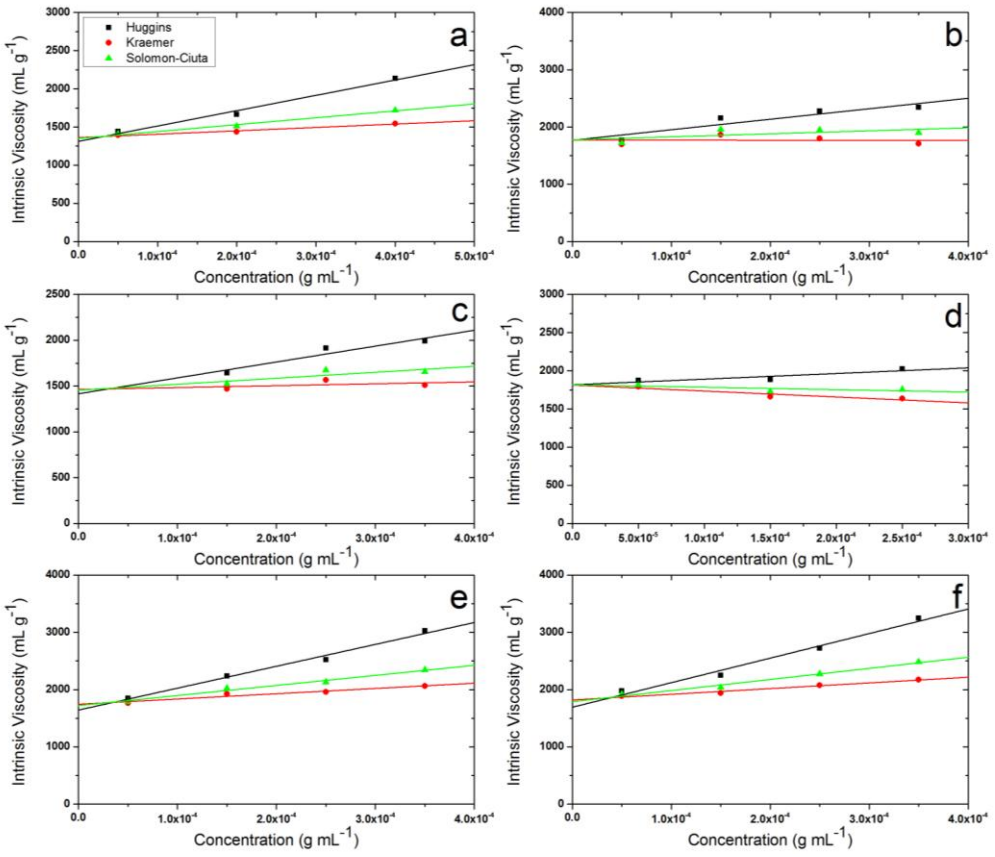


**Figure 6.20:** Intrinsic viscosity plots from capillary viscometry: Huggins, Kraemer and Solomon-Ciuta extrapolations for the ternary mixtures of lambda carrageenan, konjac glucomannan and xanthan at 0.1M ionic strength: (a) C30, (b) C25, (c) C20, (d) C15, (e) C10, and (f) C05.

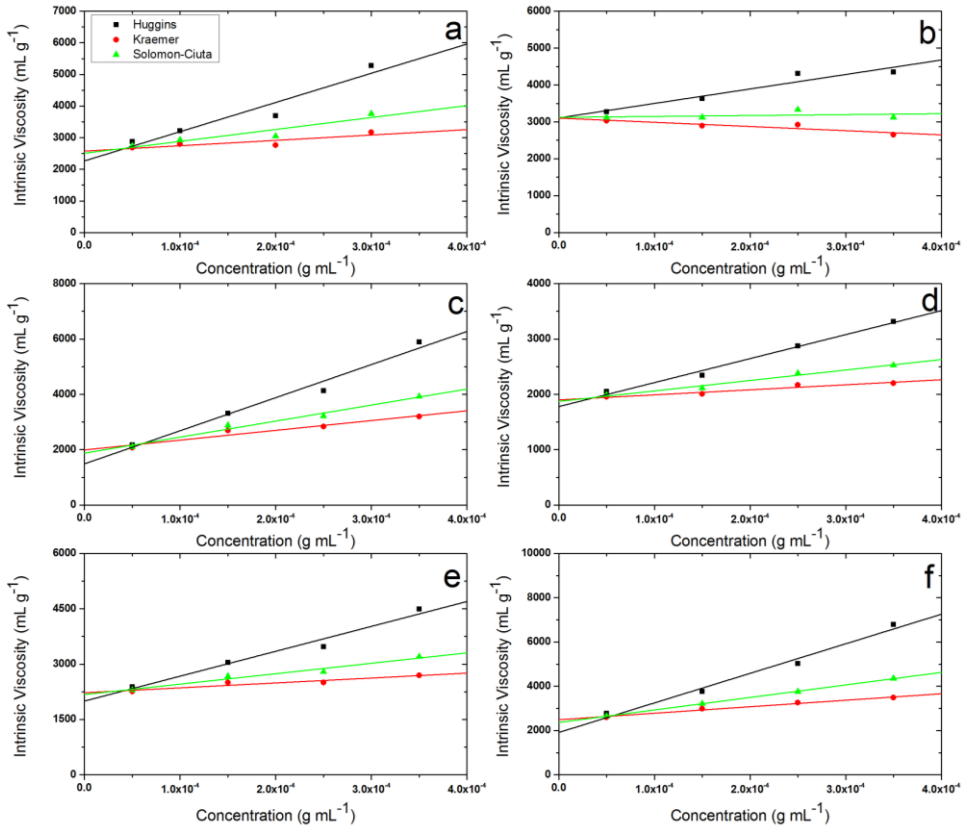


**Figure 6.21:** Intrinsic viscosity plots from capillary viscometry: Huggins, Kraemer and Solomon-Ciuta extrapolations for the ternary mixture of lambda carrageenan, konjac glucomannan and xanthan at 0.001M ionic strength: (a) C30, (b) C25, (c) C20, (d) C15, (e) C10, and (f) C05.

## 6.5 DISCUSSION

The results obtained from both sedimentation velocity in analytical ultracentrifuge and capillary viscometry, show a significant interaction between binary mixture of konjac glucmannan - as dominant component - and xanthan, which reinforces the previous results found by (Foster and Morris; Dhami, 1996; Harding et al., 2011a). The interaction appears to be ionic strength sensitive, indicating that it is electrostatic in nature. These results

allowed us to determine whether the third polysaccharide – lambda carrageenan – adds a further contribution to this interaction.

Solutions of ternary mixtures of lambda carrageenan at all mixing ratios (C30 to C05) with konjac glucomannan and xanthan were studied using the same methods. The sedimentation velocity results provided no clear evidence of an interaction between the ternary mixtures in the presence of lambda carrageenan at any of the mixing ratios. In addition, the viscosity studies showed no enhancement in the intrinsic viscosity values for ternary mixtures compared with predicted values for non-interacting mixtures. Thus, results have shown conclusively that lambda carrageenan has not interacted in ternary mixtures with konjac glucomannan and xanthan at the two ionic strengths examined (0.1M and 0.001M). This observation was in a good agreement with the Shelso study (1990), as he reported no interaction occurred between konjac glucomannan and lambda carrageenan. These findings can be interpreted in terms of the structural properties of lambda carrageenan which is unable to form an ordered structure due to the absence of an anhydro-bridge and higher charge content. As previously reported that by Goycoolea and co-workers (1995) polysaccharides forming synergistic interactions with konjac glucomannan are required to have an ordered structure; this appears not the case for lambda carrageenan. By contrast, another carrageenan type, namely kappa carrageenan has the ability to form an ordered structure, hence allowing an interaction with konjac glucomannan and formation of synergistic gels (Williams et al., 1993; Pinheiro et al., 2011).

Furthermore, alginate seaweed polysaccharides are fundamentally different from lambda carrageenan (Tombs and Harding, 1998). This is why, in contrast

to lambda carrageenen, interaction of alginate in a ternary mixture with konjac glucomannan and xanthan was observed using analytical ultracentrifugation (Abdelhameed et al., 2010) reinforced by nuclear magnetic resonance and rheological methods (Harding et al., 2011a): observations were supported by fundamental dilute solution viscosity studies, showing presence of the alginate appeared to increase the viscosity further (Harding et al., 2012). Other considerations such as the presence of mucus and mucins need also to be considered.

# CHAPTER 7

# APPLICATION OF NEW HYDRODYNAMIC METHODOLOGY TO THE STUDY OF MUCIN AND ITS INTERACTION WITH BIOPOLYMERS IN SOLUTION

Mucus is a complex mixture of space-filling glycoproteins covering for example, the alimentary and respiratory tracts and providing a protective/ defensive barrier. The most important component of mucus is mucin glycoprotein that gives mucus its high viscosity and elastic gel-like properties. The protective role of 'mucins' in gastric physiology has attracted pharmaceutical and food scientists to investigate its basic structure, viscoelastic properties and interactions. This part of the study initially focuses on the characterisation of the biophysical properties of mucin using recent advances in hydrodynamic analysis. Then, the possibility of interaction of mucin with PGX as a way of representing the mucosal environment in the alimentary tract was investigated.

## 7.1 INTRODUCTION

There has been growing interest in the use of biopolymers – in particular non-digestible carbohydrates referred to as dietary fibre – in the pharmaceutical industry for therapeutic purposes such as the treatment or control of obesity, cardiovascular disease and type 2 diabetes (Brownlee, 2011). The

physiological effect of fibre is related to the high viscosity, which is associated with reduced rates of nutrient absorption in the lumen of the intestine. It is known from analytical ultracentrifugation, rheological and NMR studies that mixtures of non-digestible fibre carbohydrates namely PolyGlycopleX (PGX) interact at low ionic strength solutions (Abdelhameed et al., 2010; Harding et al, 2011a; Harding et al., 2012a). Consequently, there has been a suggestion that this sensitive interaction might be protected by mucin glycoprotein from the disruptive effects of higher ionic strengths and exposure to bile salts in the alimentary tract by the mucus. Recent advances in biophysical methodology – especially involving analytical ultracentrifugation (AUC) – could help provide a better understanding of the mucosal environment in the gastrointestinal tract in which PGX will be in when they exert their effects.

The adherent mucus gel layer covers the alimentary tract – its thickness is generally between 150 and 700 μm – and is synthesized by specialized epithelial cells called goblet cells. It has several important functions as a barrier against pathogens and noxious substances, provides a layer permeable to exchange gases and nutrients for the underlying epithelium, and acts as a lubricant for the passage of objects (McGuckin et al., 2011). The mucus is composed primarily of water (95% – 99% by weight) together with other components such as salt, lipids (e.g. fatty acids, phospholipids and cholesterol), proteins and unconjugated carbohydrates. However, glycoprotein "mucin" is the main component which gives the mucus its high viscosity and elastic gel-like properties (see, for example, Bansil and Turner, 2006). Mucin molecules typically have a large molecular weight ranging from 0.5 to 20 MDa. These glycoproteins are composed of a polypeptide backbone containing large

amount of carbohydrate (70 - 80%), whereas protein (15 - 25%) and ester sulphate (up to 5%).

Different sources of native mucins consist of several basic unit linked together into linear arrays. The high and low glycosylated regions companied together to form a basic unit, with its low glycosylated region sensitive to proteolysis degradation. Thus, T-domains are a result of digestion other basic unit (of molecular weight approximately 400 kDa) (see, Sheehan and Carlsted, 1989). The disulphide bridge is used to link every third or fourth T-domain. These can be susceptible to the thiol reduction producing subunits of molecular weight of approximately 2 MDa (Harding, 2006).

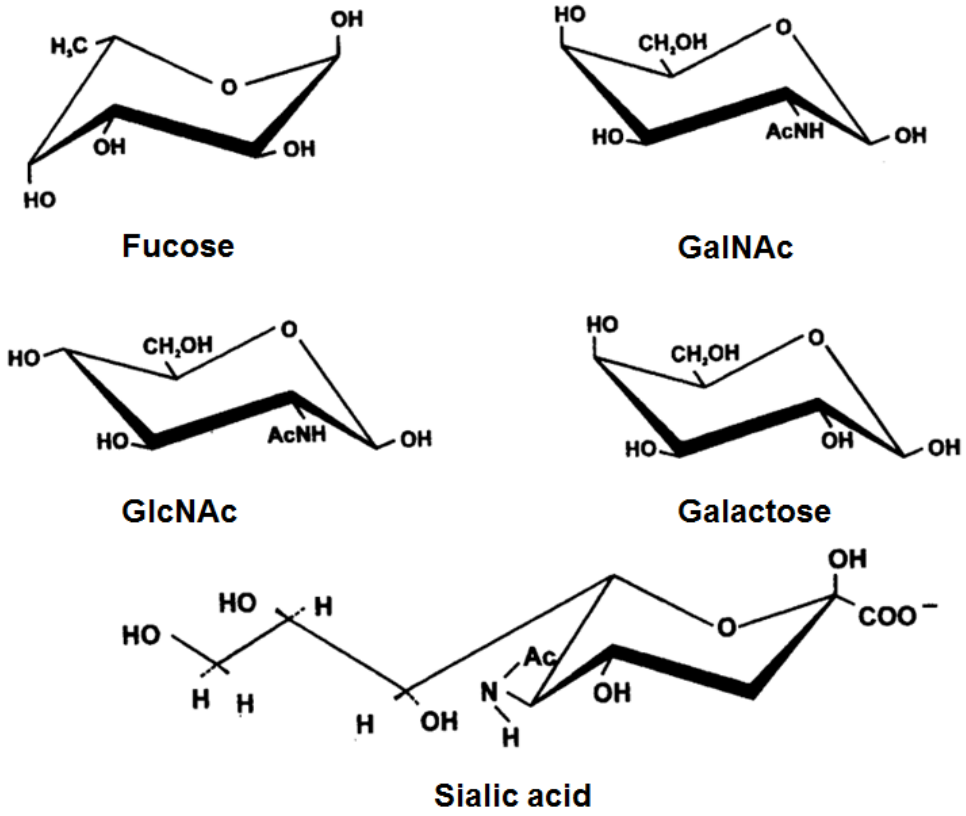


**Figure 7.1:** The principle sugars of gastrointcstinal mucins. Adapted from Harding (1989).

However, the knowledge of the primary structure of mucins is increasing and at present approximately 20 mucin genes - called MUC - have been sequenced (see, McGuckin et al., 2011). Characterisation of these genes confirmed the presence of large amount of serine, threonine and proline (amino acids that build up linear polypeptide backbone). Also sites of the O-glycosylation linked carbohydrate or glycan component to the hydroxyl side chains of serine and threonine. The carbohydrate residues are mainly galactose, fucose, N-acetylglucosamine, N-acetylgalactosamine and sialic acid (Figure 7.1). Earlier biophysical studies carried out for mucin glycoproteins provided a platform of understanding how this polymer determine and regulate the properties of mucus (Bansil and Turner, 2006; Harding, 2006).

Although analysis of mucin behaviour is critical for the understanding of its performance in health and disease as a physical and chemical barrier: determination of its hydrodynamic properties is not easy, due to its large molecular weight, polydispersity and high degree of glycosylation. The advantage of the online fractionation and analysis ability of size exclusion chromatography coupled to multi angle light scattering (SEC-MALS) has allowed us to determine the molecular weight and molecular weight distribution for macromolecules (Wyatt, 1992, 2013). The technique was applied primarily for non-ideal macromolecules such as polysaccharides in 1991 (Harding et al., 1991; Horton et al., 1991) and the first determination on mucin glycoproteins was in 1996 by Jumel and co-workers (see, Jumel et al., 1996; Jumel et al., 1997). An alternative powerful technique used to estimate absolute molecular weight is sedimentation equilibrium in the analytical ultracentrifugation (AUC) (Harding, 1989; Sheehan and Carlstedt 1989). AUC

has the advantage of not requiring any separation columns or membranes and provides a precious independent check for the results obtained from SEC-MALS with regards molecular weight; agreement between these methods gives a researcher more confidence for some of the other information from SEC-MALS (Harding, 2005). Additionally, new methodologies for analysis and representing the data (for example the "Extended Fujita method") has been proven invaluable to determine the molecular weight distributions for all classes of macromolecules (Harding et al., 2011b), extending an earlier treatment of Fujita was specifically for polymers with a random coil conformation. This method has been successfully applied to mucins (Gillis et al., 2013).

Significant progress has been made in earlier studies on the hydrodynamic proprieties of mucin (e.g. molecular weights and conformation), showing that it adopts a random-coil like conformation in solution, which in turn occupied a spheroidal domain (Harding, 1989; Sheehan and Carlstedt, 1989; Jumel et al., 1997; Deacon et al., 2000). We take advantage of the recent advances in hydrodynamic analysis to investigate three different preparations of mucin samples (isolated from pig gastric mucus) in aqueous solution. Using new approaches in sedimentation velocity analytical ultracentrifugation (AUC) (the Extended Fujita approach) and sedimentation equilibrium ("SEDFIT-MSTAR") together with size exclusion chromatography coupled to multi angle light scattering (SEC-MALS) to characterise heterogeneity and molecular weight distributions. The flexibility of a mucin in terms of persistence length ($L_p$) and mass per unit length ($M_L$), can also be estimated using further methodological advances, namely the global conformational analysis method

"Multi-HYDFIT" (Ortega and Garcia de la Torre, 2007) utilizing a combination of intrinsic viscosity and sedimentation coefficient data. The biophysical properties that obtained utilizing the new approaches of hydrodynamic analysis for mucin provides a strong platform for the following experiments carried out to examine whether there is an interaction between mucin and PolyGlycopleX (PGX) or any of its individual components.

## 7.2 MATERIALS

Three different preparations of mucin samples (Sep 13, Oct 13 and Nov 13) isolated from pig gastric were kindly provided in stock solutions (2.0 mg $mL^{-1}$) by Dr Alan Mackie, Institute of Food Research, Norwich Research Park, Colney Lane, UK. All solutions were diluted in phosphate-buffer saline (PBS) at an ionic strength of 0.1M and pH ~ 7.0 to the appropriate concentrations required for hydrodynamic characterisations.

PGX (lot No. 902310) and its individual components (namely konjac glucomannan lot No. 5217, xanthan gum lot No. 5014 and sodium alginate lot No. 5001) were supplied by Glycomix Ltd. (Reading, United Kingdom). Samples were dissolved in deionised distilled water followed by overnight dialysis against phosphate-chloride buffer at pH ~ 7.0 and ionic strength of 0.1M. The mixture of mucin (Nov 13) and PGX were prepared at different ratio 1:1 to 5:1.

# 7.3 METHODS

## 7.3.1 Sedimentation Velocity (SV)

Please refer to (Chapter 3 section 3.3.1). An Optima XL-I (Beckman Instruments, Palo Alto, USA) equipped with Rayleigh interference and absorbance optical systems, was used. An initial low rotor speed of 3000 rpm was used to check for the presence of any large sedimenting species and then adjusted to a rotor speed of 30,000 rpm for all individual mucin samples and the mixture of mucin (Nov 13) with PGX. Scans were taken at 2 minutes intervals for a run time of ~16 hours.

## 7.3.2 Sedimentation Equilibrium (SE)

Please refer to Chapter 3 section 3.3.2. The individual mucin (Sep 13, Oct 13 and Nov 13) only were examined, and were prepared at different concentrations, after dialysis for 24 hours at the ambient temperature in phosphate-chloride buffer solution (PBS) at pH=7.0 and ionic strength 0.1 M. The modified long (20.0 mm) optical path length double-sector cells with sapphire windows were loaded with (~ 80 μl) of dialysed sample and a matching amount of reference buffer dialysate in appropriate channels. The rotor was then accelerated to 4000 rpm. Equilibrium data was analysed using SEDFIT-MSTAR (Schuck et al., 2014). To account for non-ideality, the conventional/reciprocal of the apparent weight average molecular weight $1/M_{w,app}$ determined over a range of concentrations, $c$, were extrapolated to zero concentration (Harding, 1992).

### 7.3.3 Size Exclusion Chromatography Coupled to Multi Angle Light Scattering (SEC-MALS)

Please refer to Chapter 3 section 3.3.3. Mucin samples (Sep 13, Oct 13 and Nov 13) injected at concentrations of 2.0 and 1.0 mg $mL^{-1}$ were filtered through a 0.45 μm syringe filter (Whatman, Maidstone, England) - to remove any insoluble material or dust prior to being injected into the columns. The buffer was pumped at a steady, pulse-free flow rate of 0.8 mL $min^{-1}$ through the column system. The refractive index increment value used for data analysis for the mucin $dn/dc$ = 0.165 mL $g^{-1}$ (Jumel et al., 1997). Because of the low concentrations after dilution on the columns no correction for non-ideality was assumed necessary, and $M_{w,app} = M_w$, the ideal weight average molecular weight.

### 7.3.4 Differential Pressure Viscometry

A Viscostar (Wyatt Technology) differential pressure viscometer linked on-line to the SEC-MALS system was used to estimate the relative viscosities $\eta_{rel}$ for mucin samples (see, Harding, 1997). Information about the relative and reduced viscosities is obtained based on the differential pressure drop from solution flow versus solvent flow. The assumption of the intrinsic viscosity ~ reduced viscosity can be made, due to the high dilutions from the column. The average [η] for the whole undistributed sample can be specified as well as the intrinsic viscosity [η] ($V_e$) as a function of elution volume $V_e$.

$$[\eta] \sim (1/c).\left[2\left(\eta_{sp} - ln(\eta_{rel})\right)\right]^{1/2} \quad (7.1)$$

Because of the high sensitivity of the sensors and the high dilution from the column, eqn 7.1 was used to obtain [η] without a concentration extrapolation.

# 7.4 RESULTS

## 7.4.1 Sedimentation Coefficient and Sedimentation Coefficient Distribution

The sedimentation coefficient, $s_{20,w}$ results for mucin samples (Sep 13, Oct 13 and Nov 13) were obtained by sedimentation velocity in the analytical ultracentrifugation using the least squares ls-g*(s) distribution method and are reported in Table 7.1. The apparent sedimentation coefficient distributions in all cases appear to be bimodal – particularly the Oct 13 sample – and showed that the samples are heterogeneous (Figure 7.2). In addition, the ls-g*(s) distribution also displayed for all samples a classical linear increase in the values of weighted average $s_{20,w}$ with decrease in concentration.

**Table 7.1:** Summary of $s^{o}_{20,w}$ and $k_s$ results for all mucin samples.

| **Sample** | | $s^{\circ}_{20,w}$ **(S)** | $k_s$ **(mL g$^{-1}$)** |
|---|---|---|---|
| **Sep 13** | | 18±1 | 190±25 |
| **Oct 13** | **Peak 1** | 8.0±0.4 | 275±45 |
| | **Peak 2** | 13±1 | 150±20 |
| **Nov 13** | | 21.0±0.6 | 960±70 |

Values of $s^{o}_{20,w}$ provided information about the size (molecular weight) of mucin samples; showing that the mucin of Oct 13 had the lowest sedimentation

coefficient $s^{o}_{20,w}$ of 8.0±0.4S and the mucin of Nov 13 had the highest at 21.0±0.6S. These results are also within the sedimentation coefficient range of mucins obtained previously (Sheehan and Carlstedt, 1989; Dodd et al., 1998; Gillis et al., 2013).

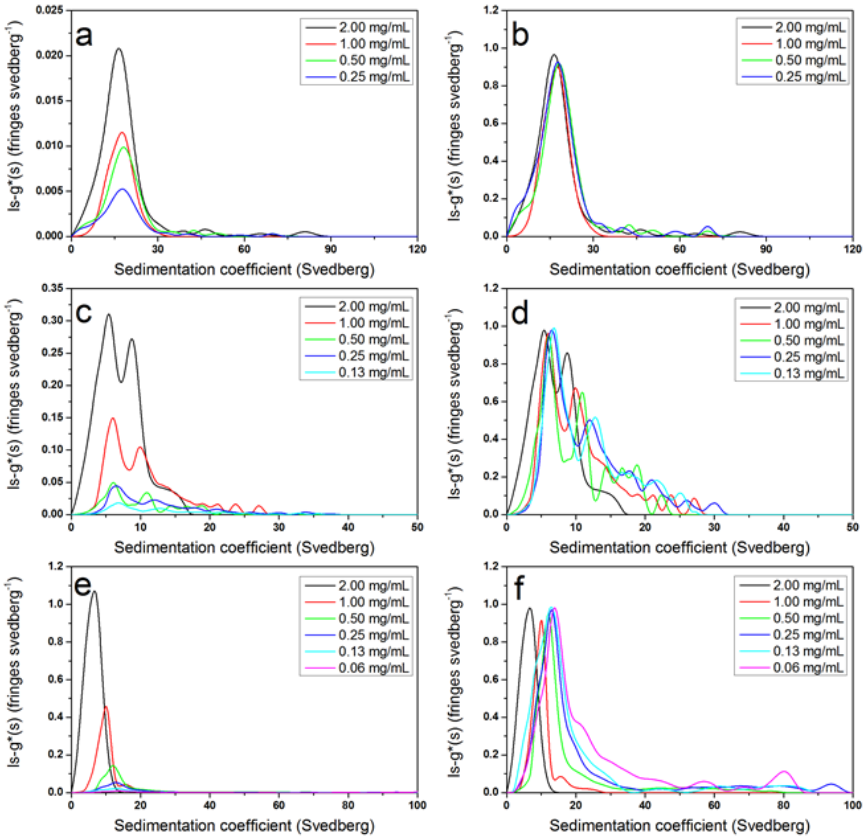


**Figure 7.2:** Sedimentation coefficient distribution profiles using least squares g*(s) method of SEDFIT obtained from sedimentation velocity experiment for all mucin Sep 13, Oct 13 and Nov 13 (a, c and e), and normalised plots (b, d and f) respectively.

The mucin samples exhibited considerable non-ideality effects due to their large volumes. To correct for that $s_{20,w}$ was further extrapolated to zero concentration to obtain $s^{o}_{20,w}$ using the reciprocal plots ($1/ s_{20,w}$) *vs.* concentration as shown in Figure 7.3. These plots are used to gives more

reliable estimates for $s^{o}_{20,w}$ , and to also help determine the concentration dependence of sedimentation, $k_s$ .

These values are reported in Table 7.1. The plots confirmed the linear increase in the value of sedimentation coefficient with decrease in concentration. The concentration dependence, $k_s$ values obtained for Nov 13 and the main peak of Oct 13 samples are in broad agreement with those yielded by Sheehan and Carlstedt (1989) for the samples have similar $s^{o}_{20,w}$. On the other hand the Sep 13 sample showed a lower $k_s$ value. This may reflect a difference on the conformation of mucin sample, since $k_s$ depends on the shape of sedimenting species the less spherical the shape of solute the higher the value of $k_s$ (Harding, 2005b).

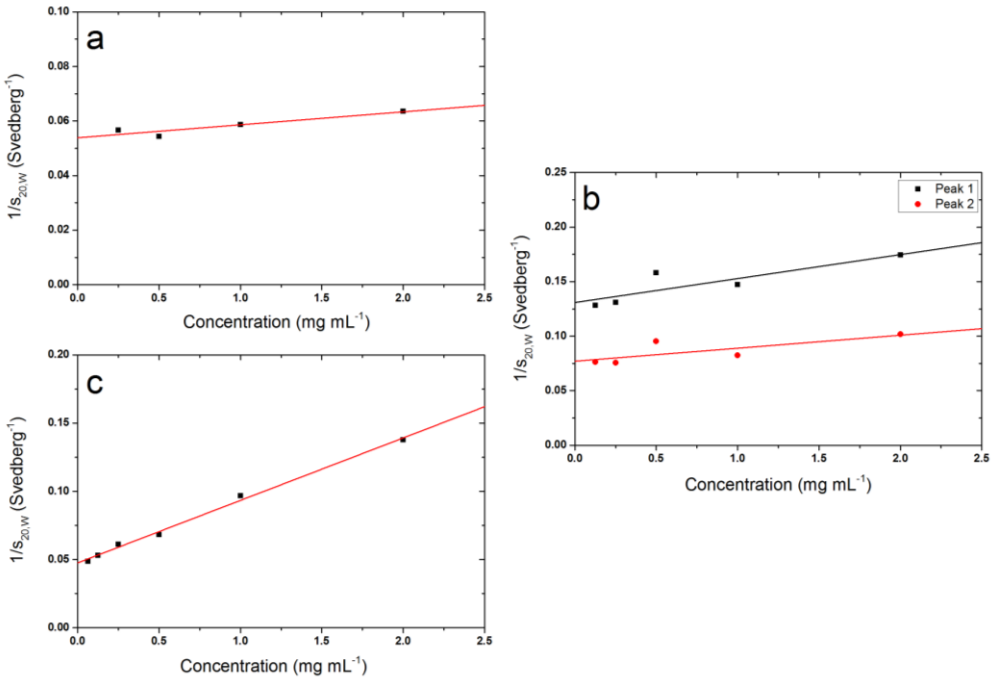


**Figure 7.3:** Concentration dependence (reciprocal) of the sedimentation coefficient plot (after correction to standard solvent conditions) for all mucin samples (a) Sep 13, (b) Oct 13 and (c) Nov 13.

## 7.4.2 Estimation of Molecular Weight

Weight average molecular weights for all mucin samples (Sep 13, Oct 13 and Nov 13) were initially obtained using SEC-MALS, and are reported in Table 7.2. The chromatogram shows two traces, first from the light scattering detector at $90^0$, and second from the viscostar detector (Figure 7.4). Both chromatograms present clearly two peaks for the Sep 13 and Oct 13 mucin samples, whereas the second peak of Nov 13 is sufficiently pronounced to be observed by the (high sensitive) viscostar detector.

**Table 7.2:** Summary of weight average molecular weight *($M_w$)* results for mucin samples from sedimentation velocity, equilibrium and SEC-MALS.

| **Samples** | **$10^{-4}$ x $M_w$ (g mol$^{-1}$)$^a$** | **$10^{-4}$ x $M_w$ (g mol$^{-1}$)$^b$** | **$10^{-4}$ x $M_w$ (g mol$^{-1}$)$^c$** | |
|---|---|---|---|---|
| | | | **Peak 1** | **Peak 2** |
| **Sep 13** | 360±10 | 380±25 | 370±30 | 49±5 |
| **Oct 13** | 110±5 | 130±6 | 200±10 | 66±2 |
| **Nov 13** | 510±30 | 710±90 | 720±50 | 27±4 |

a : molecular weight obtained from sedimentation velocity and the Extended Fujita method
b : molecular weight obtained from sedimentation equilibrium
c : molecular weight obtained from SEC-MALS

Results indicating that the samples are heterogeneous are in excellent agreement with the sedimentation coefficient distribution data. The second peak yielded for mucin samples – especially Sep 13 and Oct 13 – might be a manifestation of lower molecular weight breakdown products. The broader distribution observed for the Nov 13 mucin however, is indicative of a presence of higher molecular weight materials.

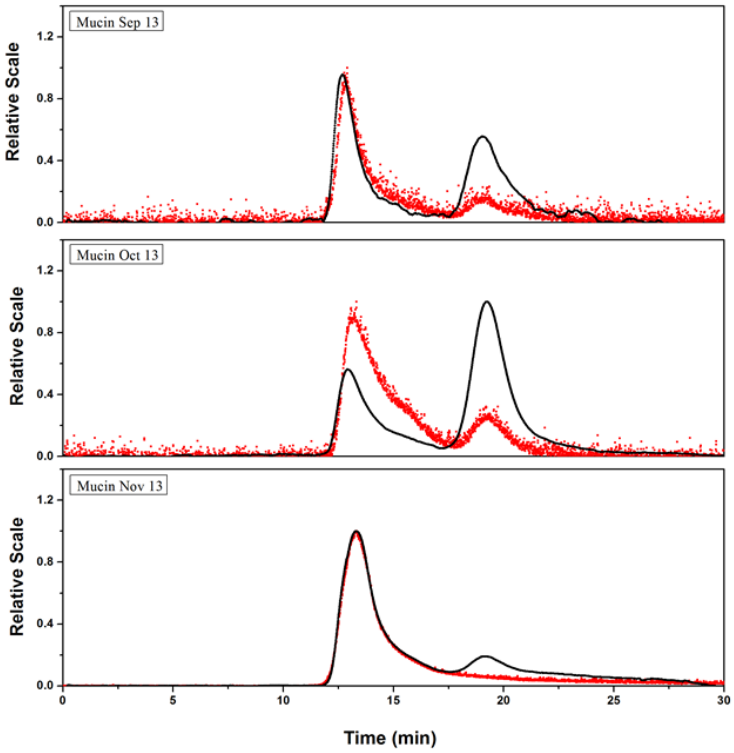


**Figure 7.4:** Elution profile for the three mucin samples at a loading concentration of 1.0 mg $mL^{-1}$. The red dot indicates light scattering at a scattering angle of $90^0$ (nb the full scattering envelope was used) and the black indicates specific viscosity.

Although all the mucin samples had been isolated from the porcine small intestine and purified using the same technique, different weight average molecular weights were obtained (see Table 7.2). The difference has also been observed based on the trace of voltage signal. Nov 13 mucin has the highest signal of the three at a similar concentration 1.0 mg $mL^{-1}$ (Figure 7.5)However, molecular weights versus retention times for mucin samples shows that a similar elution time exists for the two peaks observed (Figure 7.6). Generally, molecular weight, $M_w$ values of the main and additional peaks showed that Nov 13 has the highest $M_w$, followed by Sep 13 and then Oct 13 (Table 7.2), and consistent with results obtained previously (Sheehan and Carlstedt, 1989; Jumel et al., 1996; Fogg et al., 1996). The additional peak could indicate again

low molecular weight components, and possible resulted from the present of any protease activity in the preparation (Jumel et al., 1996).

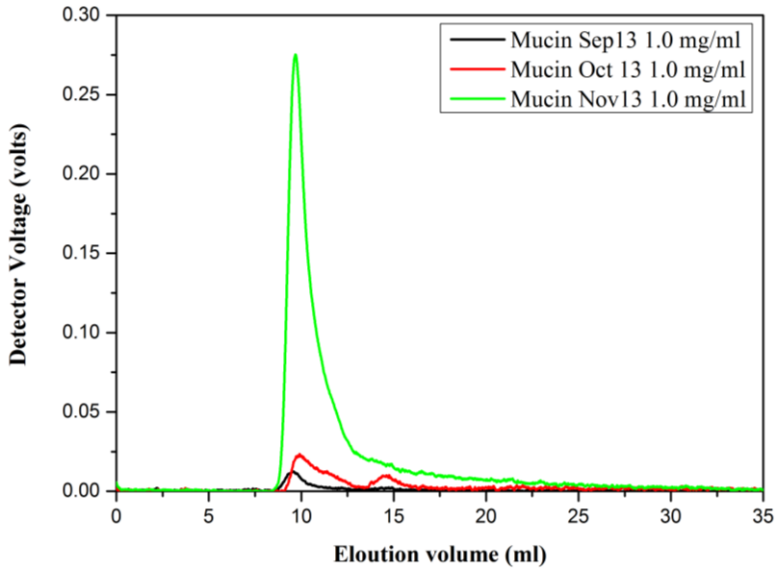


**Figure 7.5:** Elution profiles for the three mucin samples (Sep 13, Oct 13 and Nov 13) at concentration 1.0 mg $mL^{-1}$.

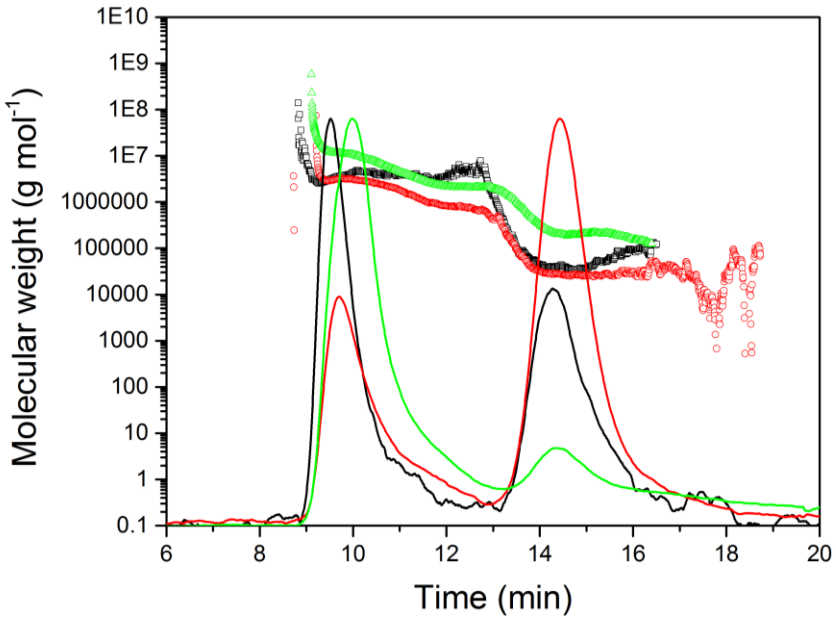


**Figure 7.6:** Elution profiles for the three mucin samples Sep 13 (black line), Oct 13 (red line) and Nov 13 (green line) examined by SEC-MALS at concentration 1.0 mg $mL^{-1}$. The horizontal black (open square), red (open circle) and green (up triangle) lines correspond to SEC-MALS calculated molecular weights for mucin samples Sep 13, Oct 13 and Nov 13, respectively.

Absolute weight average molecular weight can be estimated also using sedimentation equilibrium in the analytical ultracentrifuge. The effect of non-ideality arising from co-exclusion and polyelectrolyte behaviour is still significant, even though the measurement carried at low concentration (0.3 mg $mL^{-1}$) and a reasonable ionic strength (0.1M). Working at a series of measurements at different loading concentrations and extrapolating back to zero concentration was therefore performed to range of concentrations from (0.25 - 2.0 mg $mL^{-1}$), and weight average molecular weights were obtained using SEDFIT-MSTAR (see, for example Figure 7.7).

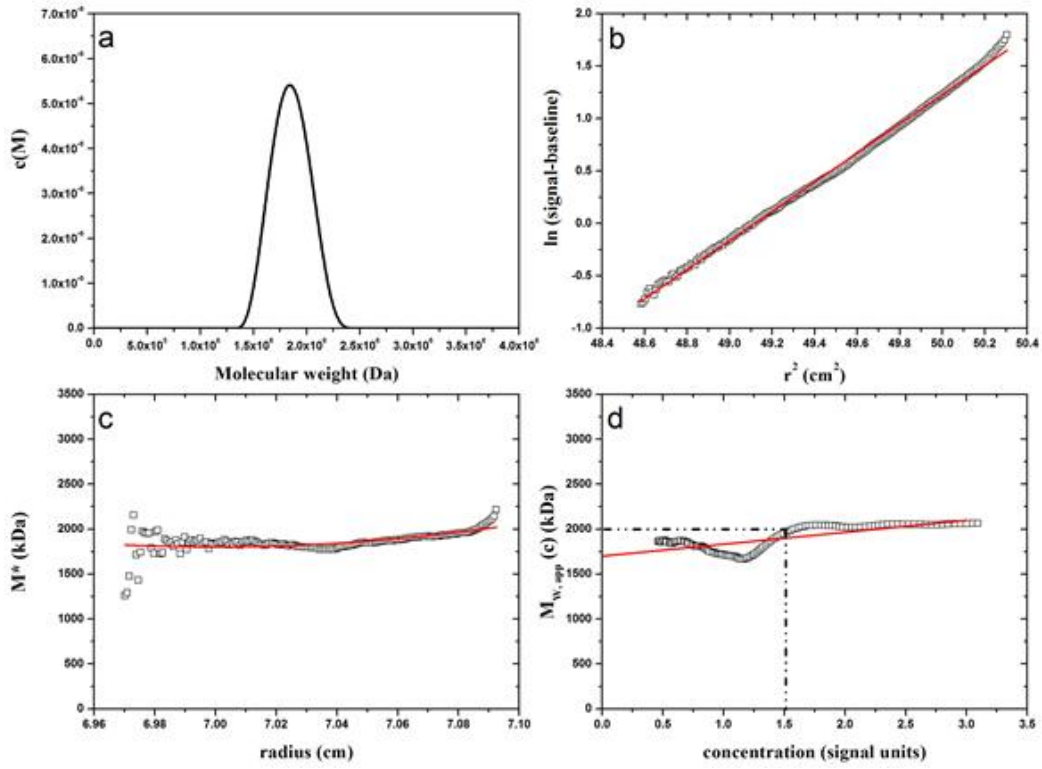


**Figure 7.7:** As (Figure 4.9) but the analysis of **Sep 13 mucin** at a loading concentration of (0.5 mg $mL^{-1}$). $M_{w,\,app}$ from extrapolation of $M^*$ to cell base = 2000 kDa, and the meaning of the fitted lines in "c" and "d" are explained in the legend Figure 4.9.

The reciprocal plot of $M_{w,app}$ versus concentration for all mucin samples (Sep 13, Oct 13 and Nov 13) gave a linear extrapolation and the values yielded are presented in Table 7.2, showed significant concentration dependence consistent with non-ideal behaviour and is agreement with sedimentation velocity results (Figure 7.8). Results were consistent with those from SEC-MALS, and values are similar to previous studies (Sheehan and Carlstedt, 1989; Jumel et al., 1996; Fogg et al., 1996).

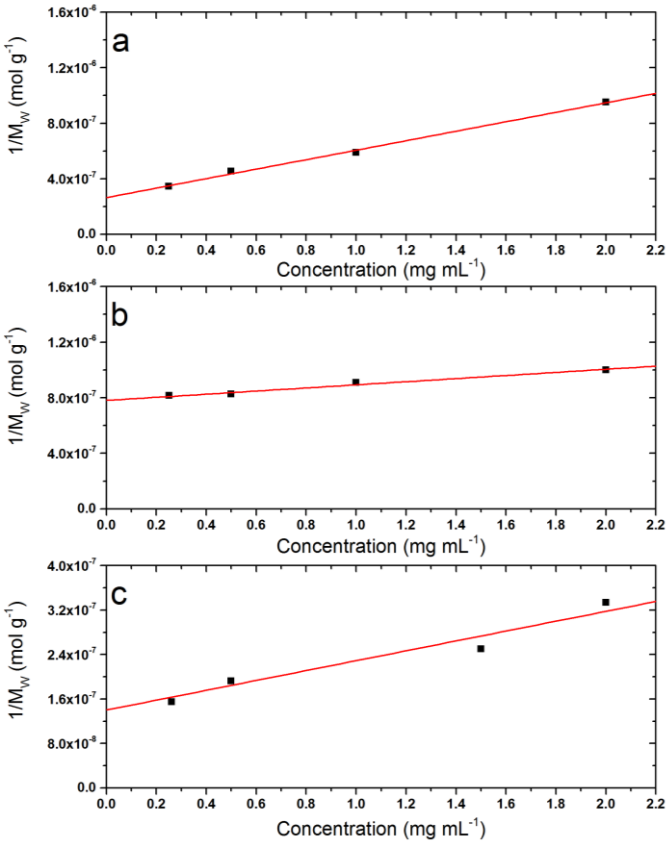


**Figure 7.8:** The reciprocal plots of the apparent weight average molecular weight ($M_{w,app}$) against concentration $c$ (g mL$^{-1}$) for mucin samples (a) Sep 13, (b) Oct 13 and (c) Nov 13.

Transforming a distribution of sedimentation coefficient g($s$) vs $s$ into a distribution of molecular weight, $f(M)$ vs $M$ was used as further methods for

estimating the molecular weight distribution of the mucin samples using the Extended Fujita method (Harding et al., 2011b). The distributions so obtained (Figure 7.9) were again consistent with those obtained from sedimentation equilibrium and SEC-MALS (Table 7.2).

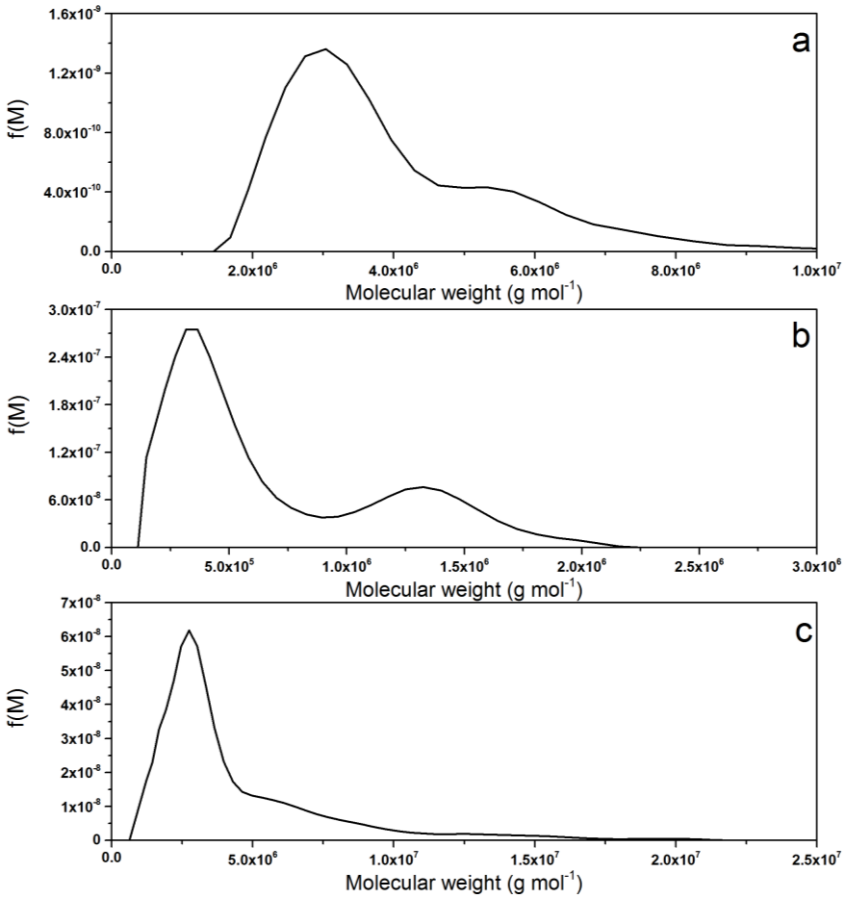


**Figure 7.9:** Molecular weight distribution for all mucin samples obtained from transformation of the g(s) versus *s* distribution at concentration (0.25 mg $mL^{-1}$), using the Extended Fujita method of Harding et al., (2011) (a) Sep 13 (b) Oct 13 and (c) Nov 13.

## 7.4.3 Intrinsic Viscosity

Intrinsic viscosity values for the mucin samples (Sep 13, Oct 13 and Nov 13) were obtained using the on-line differential pressure viscometry measurements

with SEC-MALS. The profile of intrinsic viscosity vs elution time for all mucin samples again confirmed the bimodal behaviour (Figure 7.10), and the results for both peaks are reported in Table 7.3.

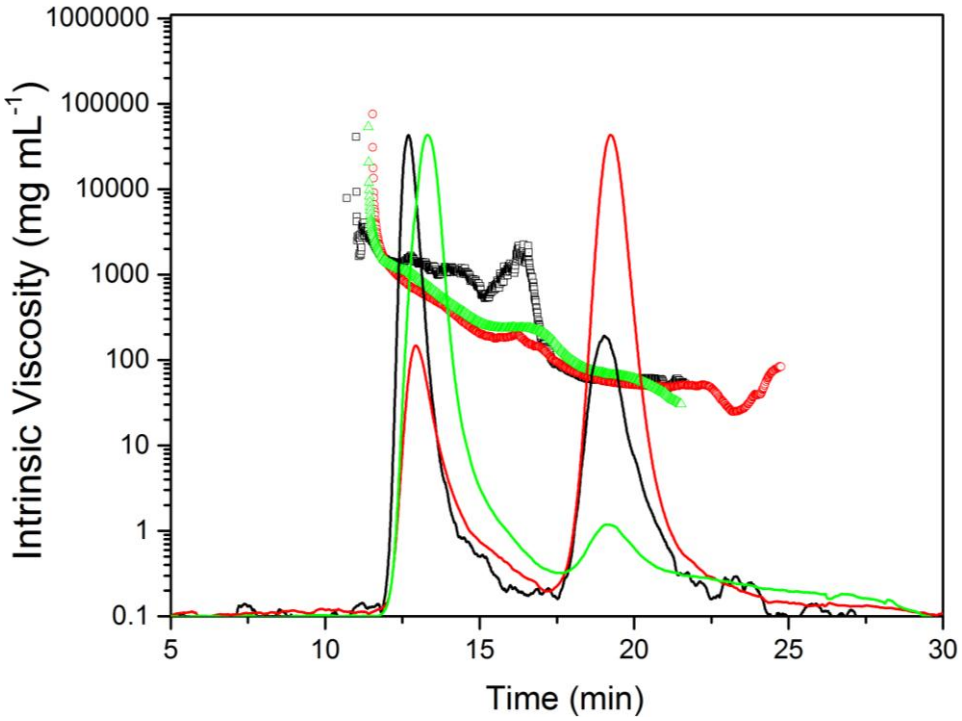


**Figure 7.10:** Elution profiles for the three mucin samples: Sep 13 (black line), Oct 13 (red line) and Nov 13 (green line) examined by SEC-MALS at concentration 1.0 mg $mL^{-1}$. The horizontal black (open square), red (open circle) and green (up triangle) lines correspond to SEC-MALS calculated intrinsic viscosity for mucin samples Sep 13, Oct 13 and Nov 13, respectively.

The results mostly showed that the Nov 13 mucin has the highest intrinsic viscosity followed by Sep 13 and then Oct 13. The results were also in excellent agreement with molecular weight and sedimentation coefficient data, as well as with a previous study by (Sheehan and Carlstedt, 1989).

**Table 7.3:** Intrinsic viscosity and MHKS power law exponent *a*, values for mucin samples yielded using the Viscostar in SEC-MALS.

| **Sample** | **Intrinsic viscosity [η] (mL g$^{-1}$)** | | **MHKS (*a*)** | |
|---|---|---|---|---|
| | Peak 1 | Peak 1 | > ~1.0 x 10$^6$ $M_w$ | < ~1.0 x 10$^6$ $M_w$ |
| **Sep 13** | 760±8 | 110±2 | 1.0±0.02 | 0.4±0.01 |
| **Oct 13** | 550±4 | 60±1 | 1.0±0.01 | 0.3±0.002 |
| **Nov 13** | 800±2 | 230±0.5 | 0.9±0.002 | 0.4±0.002 |

## 7.4.4 Conformational Analysis

Characterisation of the mucin conformation in dilute solution also provided important underpinning information before studying its molecular interactions and how it can be involved in the viscous and gelling properties, which are responsible for its protective and lubricating functions. Hydrodynamic properties – sedimentation coefficient, molecular weight and intrinsic viscosity – however, helped us to estimate the conformation and flexibility of macromolecules in solution using two levels of approach: (i) general overall conformation types (coil, rod, and sphere) and (ii) in terms of persistence lengths use for estimation flexibility of linear and flexible structures.

### 7.4.4.1 Mark-Houwink-Kuhn-Sakurada Power Law Relationship:

The conformation of mucin samples were investigated based on knowledge of the dependence of [η] with $M_w$. Following Tanford (1961) we make the

reasonable assumption that complication through molecular draining effects and other non-conformation effects are small. The feature of viscostar coupled to on-line fractionation SEC-MALS system allowed us to characterise the conformation using (MHKS) power law relation linking [η] (Viscostar™) and Mw (from SEC–MALS) as following:

$$[\eta] = K_\eta M^{a} \tag{7.2}$$

Double logarithmic plots of intrinsic viscosity [η] ($V_e$) versus molecular weight $M_w$ ($V_e$) both as function of elution volume $V_e$ for all mucin samples (Sep 13, Oct 13 and Nov 13) shown in (Figure 7.11).

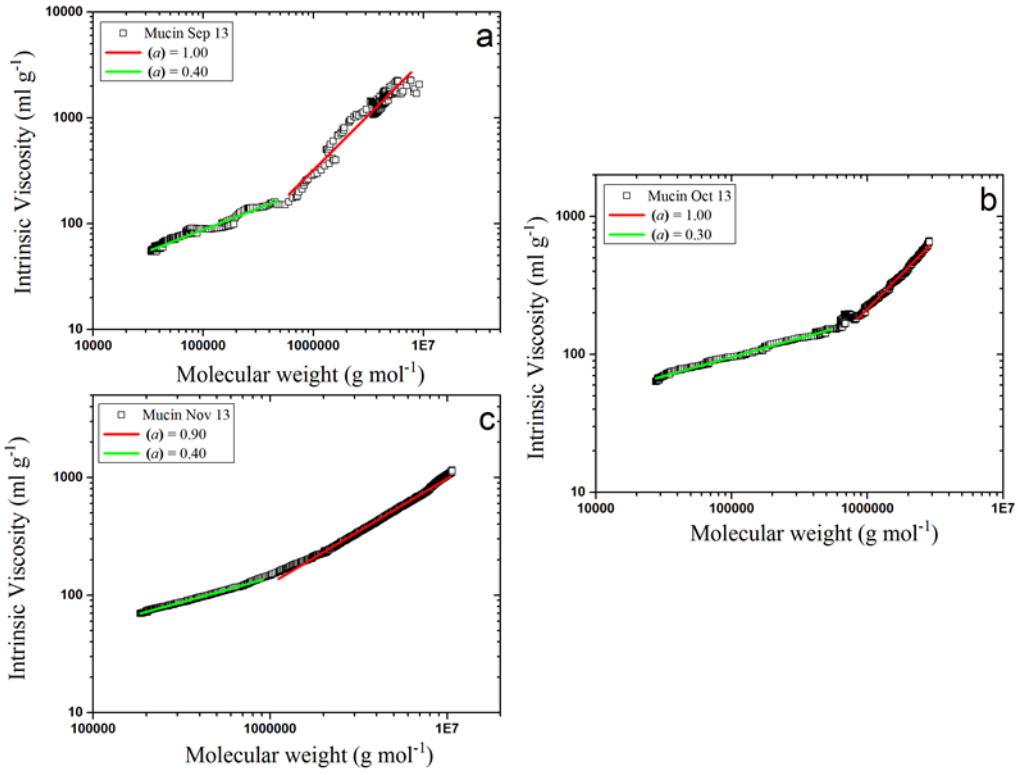


**Figure 7.11:** Mark–Houwink–Kuhn–Sakurada (MHKS) power law double logarithmic plot for mucin samples (a) Sep 13, (b) Oct 13 and (c) Nov 13 from on-line differential pressure viscometery coupled to SEC-MALS. The plot is of intrinsic viscosity [η] as a function of elution volume (ordinate) versus molecular weight $M_w$ as a function of elution volume.

Non-linear plots observed for all mucin samples indicating that, they adapted more than one conformation (Tombs and Harding, 1998). The polymer chains of these samples appear to show a change in conformation with molecular weight: those < ~1.0 x $10^6$ $M_w$ appear to be a more coiled form, and with those > ~1.0 x $10^6$ $M_w$ in a more linear semi-flexible type conformation. The behaviour seen here for mucin samples is similar to that observed for polysaccharides amylose (Rollings, 1992) and pectin (Fishman et al., 2001). The exponents (*a*) yielded for all mucin samples are reported in (Table 7.3) and in general suggested a linear macromolecule in overall of a random coil conformation and in good agreement with previous studies (Harding et al., 1983; Sheehan and Carlstedt, 1984; Jumel et al., 1997).

#### 7.4.4.2 Estimation of the Persistence Length $L_p$ and Mass Per Unit Length $M_L$:

The assessment of the conformational flexibility of a polydisperse system - using mucin glycoproteins as an example - is crucial for a proper understanding of its behaviour *in situ*, which is commanded the physical properties (e. g. viscoelastic) in such system. Several approaches are applied here to measure the chain flexibility in terms of persistence length $L_p$ and mass per unit length $M_L$ (refer to section 3.4.4.4).

#### 7.4.4.2.1 Bushin-Bohdanecky method

The estimation of $L_p$ and $M_L$ using the Bushin-Bohdanecky method (refer to section 3.4.4.4.1) requires the molecular weight and intrinsic viscosity data – in this study the data obtained from on-line differential pressure viscometery coupled to SEC-MALS. The following equation was applied (Bohdanecky, 1983; Bushin et al., 1981):

$$\left(\frac{{M_w}^2}{[\eta]}\right)^{1/3} = A_0\, M_L\, \phi^{-1/3} + B_o \phi^{-1/3} \left(\frac{2L_p}{M_L}\right)^{-1/2} {M_w}^{1/2} \qquad (7.3)$$

Using a plot of $(M_W^2/[\eta])^{1/3}\ vs\ M_W^{1/2}$ yielded slopes of (1.56±0.01) for Sep 13, (1.68±0.01) for Oct 13 and (1.76±0.01) for Nov 13 for each mucin samples (Figure 7.12). From the slope $L_p$ can be calculated using the above equation, where, $\phi$ is the Flory-Fox constant (2.86 x $10^{23}$ $mol^{-1}$), $B_o$ taking as $\sim 1.10$ (Bohdanecky, 1983) and $M_L \sim$ 3000 g $mol^{-1}$ $nm^{-1}$ obtained from (Carlstedt et al., 1993). In this way, $L_p$ has been estimated as (17±1), (15±1) and (14±1) for the mucins Sep 13, Oct 13 and Nov 13, respectively; showing that Nov 13 more flexible whereas Sep 13 exhibits less flexibility. Results in general are consistent with that obtained previously using electron microscopy (Stokke et al., 1987). However, utilizing the more traditional Bushin–Bohdanecky analysis alone is not sufficient which may lead obtain incorrect results, since it depend on the knowledge of the mass per unit length, $M_L$. Therefore, it is more appropriate to determine the conformation flexibility of macromolecules using different approaches.

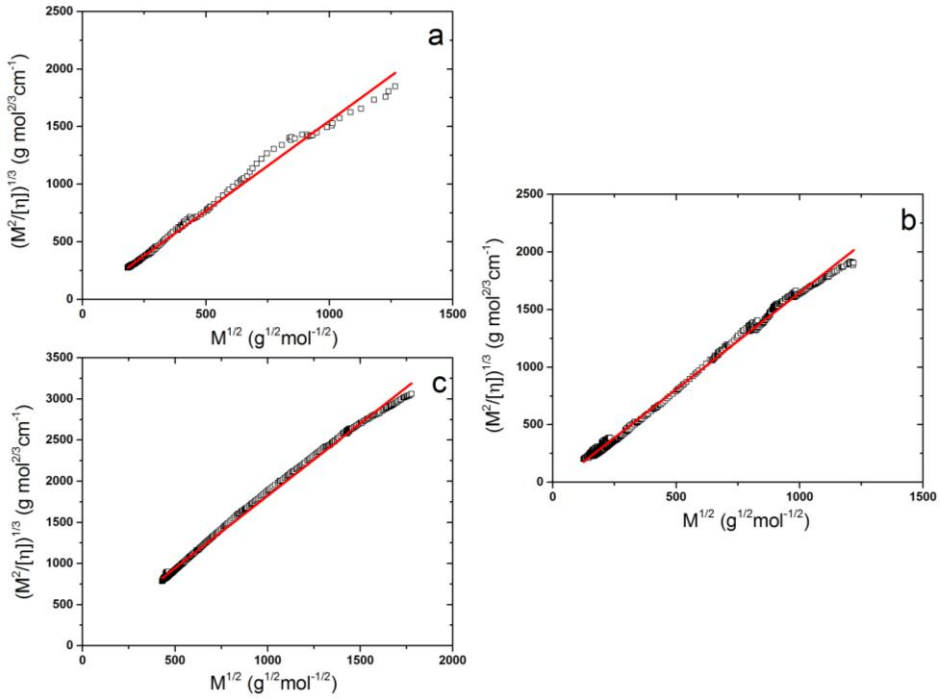


**Figure 7.12:** Bushin-Bohdanecky plots for mucin samples (a) Sep 13, (b) Oct 13 and (c) Nov 13, where $L_p$ (17±1) nm, (15±1) nm and (14±1) nm, respectively.

#### 7.4.4.2.1 Global analysis method (HYDFIT)

In study of the mucin samples (Sep 13, Oct 13 and Nov 13) we used the sedimentation coefficient, intrinsic viscosity and molecular weight data points as input in Multi-HYDFIT (refer to section 3.4.4.4.3), and then optimizes the parameters in order to find the minimisation of the target function, based on the following equation:

$$\Delta^2\,(L_P, M_L, d) = \frac{1}{N_s}\sum_{i=1}^{N_s}\left[(\sum_Y W_Y)^{-1}\ \sum_Y W_Y\ \left(\frac{a_{Y\,(cal)} - a_{Y\,(exp)}}{a_{Y\,(exp)}}\right)^2\right] \qquad (7.4)$$

The results of $L_p$, $M_L$ and $d$ parameters obtained for the mucin samples are reported in (Table 7.4). Although it has been theoretically known the

equivalent random coil $L_p = 0$, and the extra-rigid $L_p = \infty$ , the more appropriate values in practice are limits of ~ 1 nm for the random coils (e.g. pullulan) and ~ 200 nm for an extra-rigid rod (e.g. DNA) (Tombs and Harding, 1998). Consequently, the $L_p$ values estimated are ~ 2.4, 7.6 and 11 for Sep 13, Oct 13 and Nov 13, respectively suggestion that all samples are presented in the region of flexible (linear random coil). The differences can be observed among the mucin samples; Sep13 mucin has shown the more flexible chain followed by Oct13 then Nov13 the less flexible chain. An excellent agreement furthermore was obtained between the values of the $M_L$ with those found of the $L_p$ in regard the flexibility.

**Table 7.4:** Summary of the results obtained from Multi-HYDFIT for mucin samples.

| **Sample** | | $L_p$ **(nm)** | $M_L$ **(Da nm$^{-1}$)** | $d$ **(nm)** | **100xΔ** | $L/L_{;p}$ |
|---|---|---|---|---|---|---|
| **Mucin** | **Sep 13** | 2.4±0.1 | 310±70 | 1.4±0.1 | 7.0% | 40 |
| | **Oct 13** | 7.6±0.5 | 1000±40 | 6.0±0.8 | 4.3% | 4 |
| | **Nov 13** | 11±1 | 2750±400 | 10±0.5 | 3.5% | 6 |

It can clearly be seen that the stiffness of the worm-like Nov13 and Oct 13 mucin chains increase with increasing the values of $M_L$ and $d$. This is most likely because of the distribution reported for the block-wise (e.g. hairy and smooth regions) of oligosaccharide residues along the glycosylated and non-glycosylated regions of mucin structure. Note that the highest values of $M_L$ reflect the great amount of oligosaccharide, whilst highest values of $d$ indicate an extended oligosaccharide side chain. The results, listed in Table 7.4, mention that these mucin (Nov 13 and Oct 13) are consistent with a slightly

stiff linear random coil due to the amount and extended of oligosaccharide side chain. Consequently a model propose based on the original scheme given by *Jumel et al.* (1997), showing the effect of the oligosaccharides on the mucin flexibility (Figure 7.13).

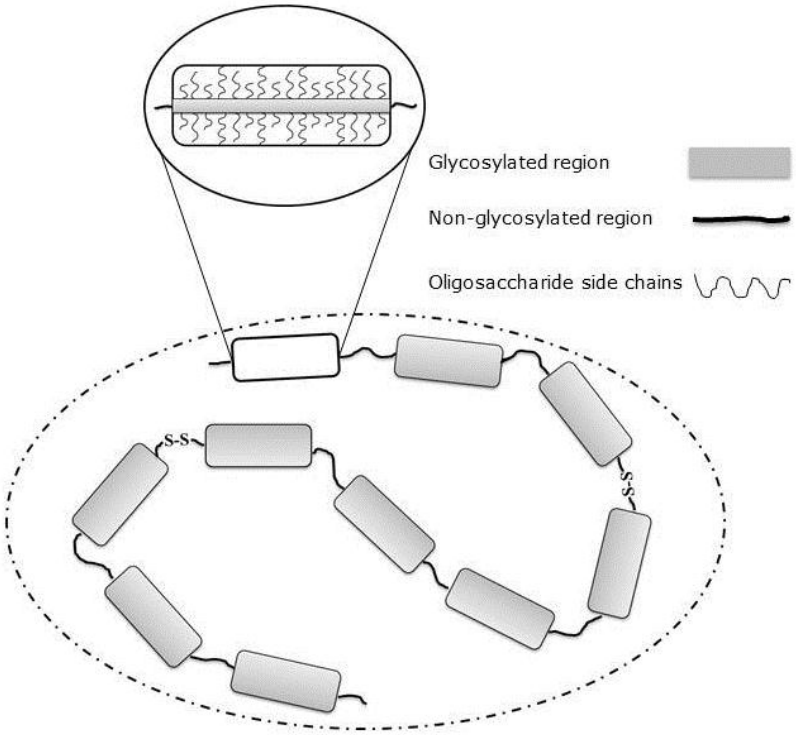


**Figure 7.13**: Schematic view for a linear random coil model of mucin, showing the influence of the oligosaccharide on the macromolecule flexibility.

The results for the mucin samples are presented in (Table 7.4), which indicated that Sep 13 exhibits high flexibility chain, while Nov 13 and Oct 13 chains look like a bending rod with less flexibility consistent with $L_p$ results. The persistence lengths, $L_p$ and mass per unit lengths, $M_L$ of mucin samples (Sep 13, Oct 13 and Nov 13) are represented as contour plot, where the full colour spectrum ranging from blue to red indicted for the values of target function, $\Delta$.

The dependence of $\Delta$ on the $L_p$, $M_L$ and $d$ were used to understand the sensitivity of the fit to each parameter, which is clarified by means of the contour plots as shown in Figure 7.14. In this plot the target function is calculated over the range of values for $L_p$ (x-axis) and $M_L$ (y-axis). Therefore, with regard fixing chain diameter, $d$ and $M_L$ the best estimates for the $L_p$ of mucin Sep 13, Oct 13 and Nov 13 are the minimum values of the target function, and found in the range of (2.0, 7.5 and 11, respectively) in excellent agreement with those calculated when $L_p$ and $M_L$ treated variable (Figure 7.15). Further, an excellent overall achieved for the typical percent deviation 100Δ, calculated based on the typical difference between the calculated and experimental values of the whole data point sets, as it shown in (Figure 7.16).

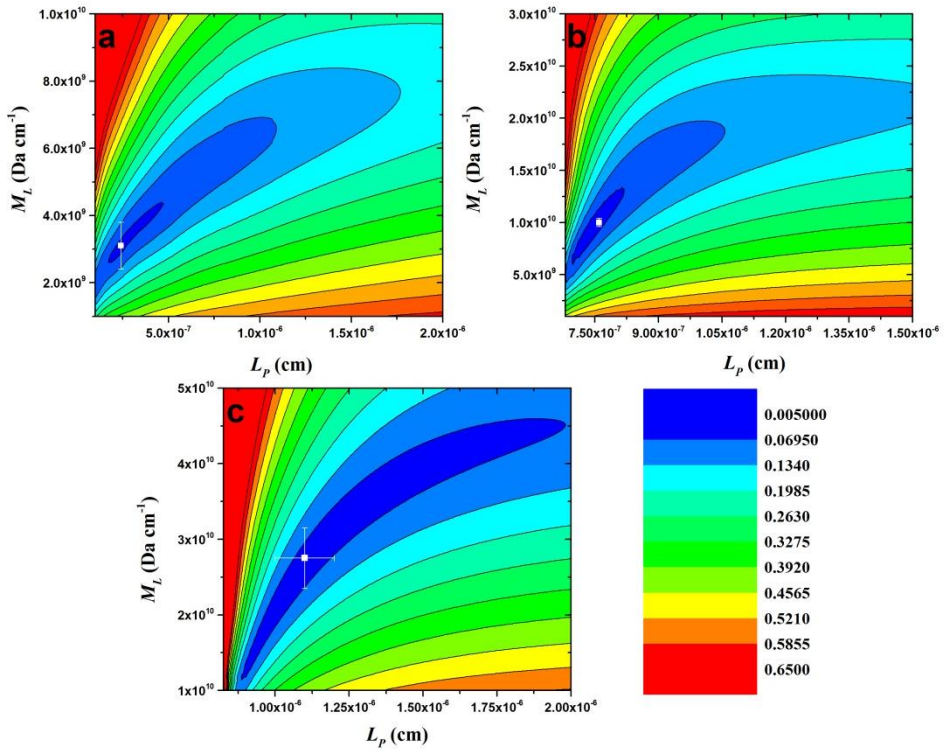


**Figure 7.14**: Contour plots of the mucin samples (a) Sep 13, (b) Oct 13 and (c) Nov 13. The target function, $\Delta$ calculated based on variables values of $L_p$ and $M_L$, and are represented on the full colour spectrum from blue ($\Delta$ = 0.005) to red ($\Delta \geq 0.65$).

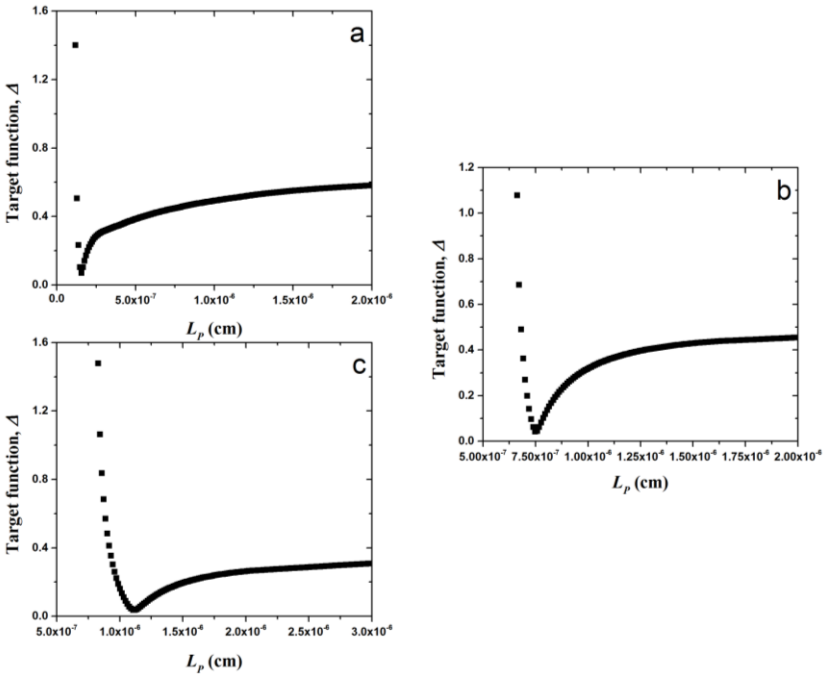


**Figure 7.15:** Plots of target function ($\Delta$) vs. Persistence length ($L_p$) for the mucin samples (a, b and c) Sep 13 (2.0±0.1), Oct 13 (7.5±0.5) and Nov 13 (11±1), respectively.

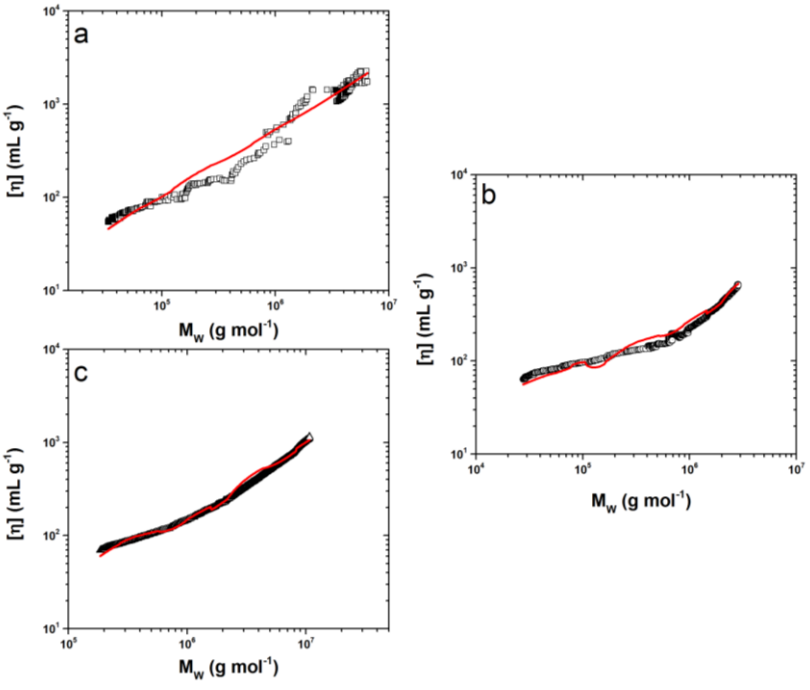


**Figure 7.16**: Plots of the experimental and calculated values for the intrinsic viscosity of the mucin samples (a, b and c) Sep 13, Oct 13 and Nov 13, respectively.

### 7.4.5 Interaction with Biopolymer Mixtures: PolyGlycopleX (PGX)

First of all PolyGlycopleX (PGX) and its individual components – konjac glucomannan (KGM), xanthan and alginate – were characterised separately to establish their molecular integrity using sedimentation velocity in the analytical ultracentrifuge. The apparent weight average sedimentation coefficient, $s_{20,w}$ for all samples were obtained at concentration of (0.5 mg $mL^{-1}$) and ionic strength of (0.1 M), presenting a unimodal distribution at all cases (Figure 7.17). Under these conditions PGX has $s_{20,w}$ of ~2.6S, KGM, ~2.4S, xanthan, ~6.4S and alginate ~2.1S.

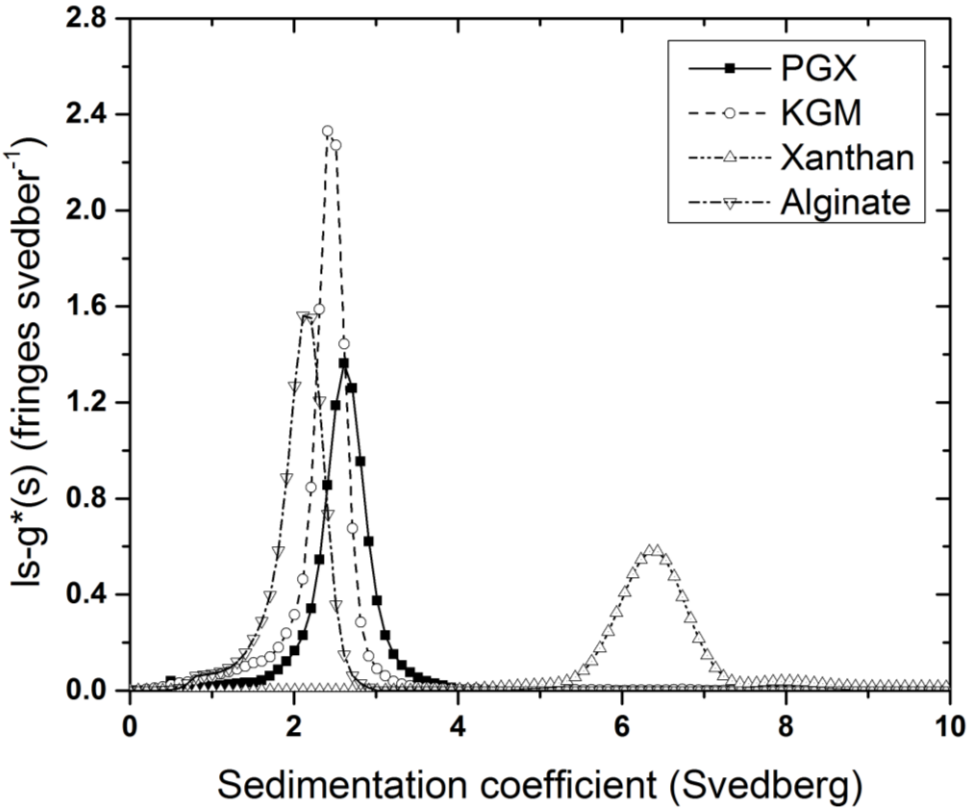


**Figure 7.17:** Apparent sedimentation coefficient distribution profile using least squares g*(s) methods for PGX and its individual components at loading concentration 0.5 mg $mL^{-1}$ and high ionic strength 0.1M.

In this study a solution of mucin sample particularly Nov 13 was mixed with PGX and its individual components solutions in 1:1 V/V ratio to a total concentration 0.5 mg $mL^{-1}$ and I= 0.1 M; then the sedimentation coefficient distributions were obtained for the mixtures (Figure 7.18).

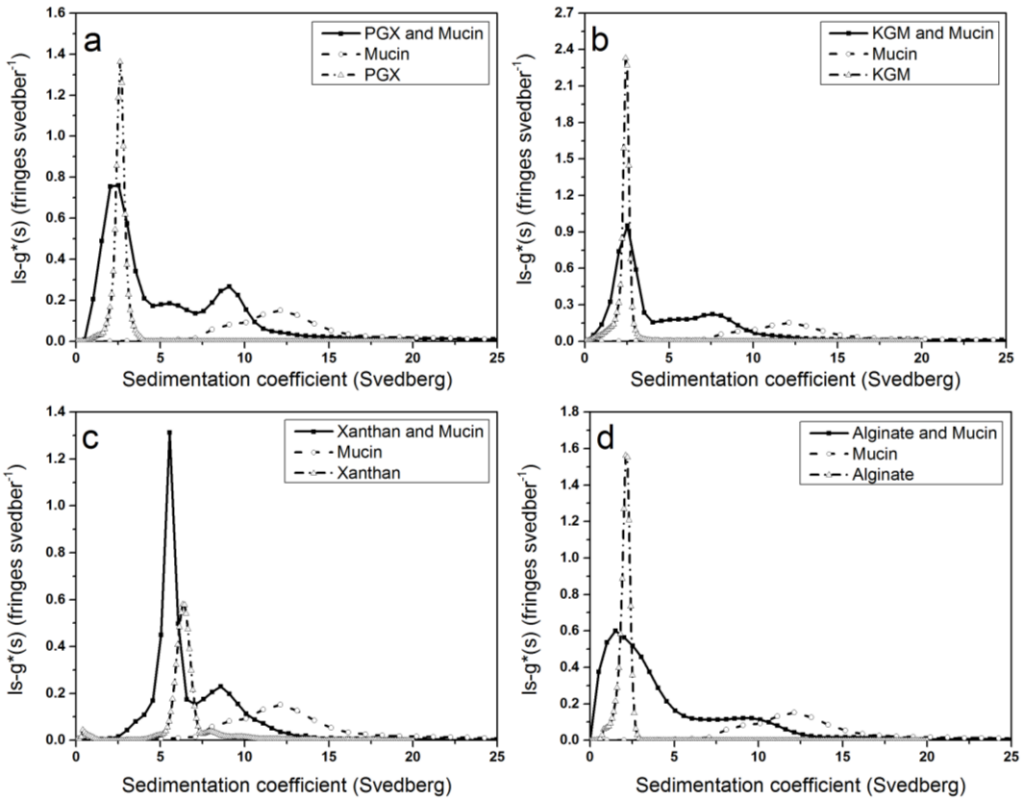


**Figure 7.18:** Apparent sedimentation coefficient distribution profile using the least squares g*(s) methods for the mixture of mucin with (a) PGX, (b) KGM, (c) xanthan and (d) alginate at a loading concentration 0.5 mg $mL^{-1}$ and high ionic strength 0.1 M.

From the plots of ls-g*(s) vs *s*, two peaks were observed for the mixture of mucin with KGM, xanthan and alginate separately, which corresponded to individual component controls; these showed no evidence of interaction here.

Therefore, the free mucin in all cases of the mixture showed a reduction in the sedimentation coefficient compared to the individual control, which may represent a high concentration of the mixture (Schachman, 1959). However, profile of sedimentation coefficient distribution for the mixture of mucin with PGX yielded a second peak, which is disappeared in the case of PGX alone at the same ionic strength (0.1M). The peak observed here is similar to that obtained for PGX at low ionic strengths by *Abdelhameed et al., and Harding et al.,* (Abdelhameed et al., 2010; Harding et al., 2011a). This behaviour seen here might be suggested that; mucin has protected the interaction observed previously for PGX at low ionic strength.

In a further investigation, the presence of the second peak was examined at the same mixing ratio (1:1) but different concentrations; scans were taken using both interference and absorbance optical systems in the analytical ultracentrifuge (Figure 7.19). The interference data showed a linear increase in sedimentation coefficient distribution with decrease concentration for the mixture exhibited concentration dependence, and also the second peak observed in all concentrations. However, the absorbance data presented only the mucin sample which has the apparent sedimentation coefficient similar to that in the interference data; confirming the second peak is related to the PGX. Furthermore, the mixture of mucin with PGX was investigated at different ratio at total concentration of 0.5 mg $mL^{-1}$ (Figure 7.20). Again the results supported that the second peak was existed at all mixing ratios.

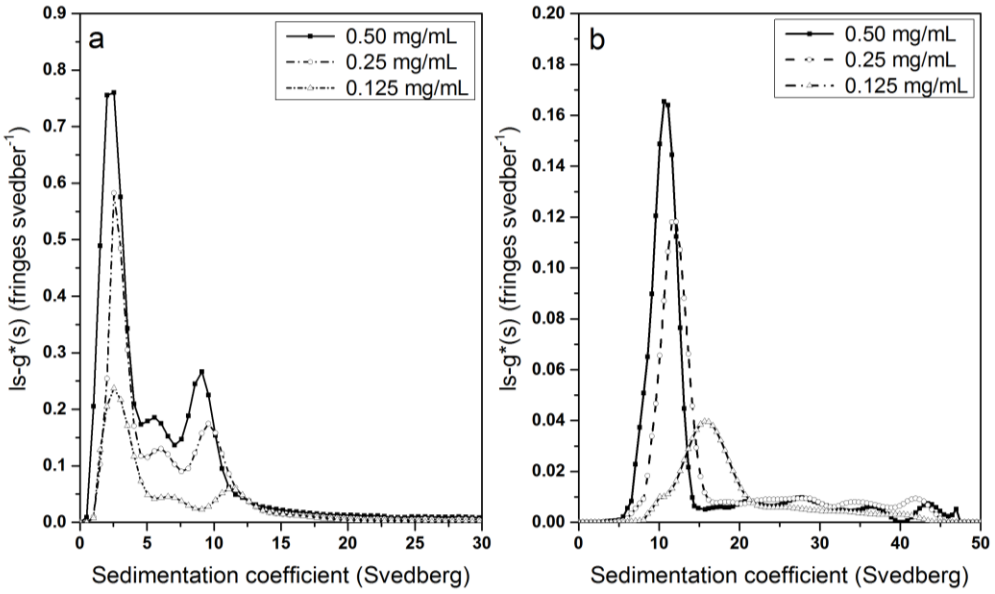


**Figure 7.19:** Apparent sedimentation coefficient distribution profile using least squares g*(s) methods for the mixture of mucin with PGX at different loading concentrations and ionic strength 0.1M; (a) Interference and (b) Absorbance.

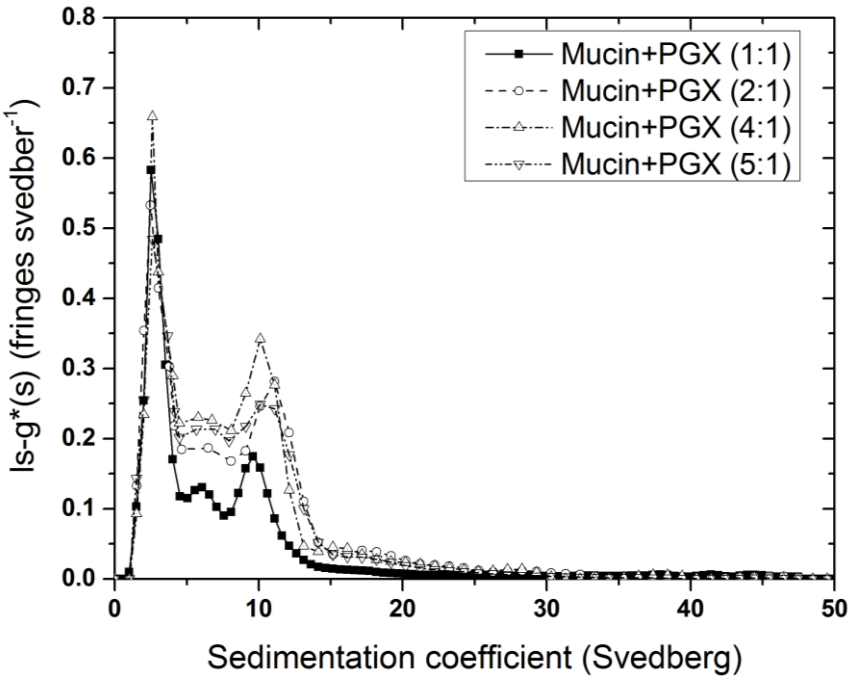


**Figure 7.20:** Apparent sedimentation coefficient distribution profile using least squares g*(s) methods for the mixture of mucin with PGX at loading concentration 0.5 mg $mL^{-1}$ and different ratios (1:1 to 5:1).

# 7.5 DISCUSSION

Three different preparations of mucin samples isolated from pig gastric mucus in aqueous solution were examined in terms of their hydrodynamic properties (e. g. molecular weight and conformation) using analytical ultracentrifugation (AUC) based on sedimentation velocity and equilibrium together with size exclusion chromatography coupled to multi angle laser light scattering (SEC-MALS). Analysis of molecular weight and intrinsic viscosity results provided evidence of bimodal behaviour for mucin samples, which was supported by sedimentation coefficient data in particular for the mucin Oct 13: we suggested that this may represent the smaller breakdown products. The heterogeneity observed here could be explained in terms of proteolysis of some of the proteins cores, although a protease inhibitor was used in the purification stage (Fogg et al., 1996; Jumel et al., 1996).

Molecular weight is an important parameter for the characterisation of mucin glycoproteins. Because of their polydispersity, the value is described as weight average molecular weight, and number of techniques can achieve that. SEC-MALS a technique which has been successfully applied to mucin glycoproteins since Jumel et al., (1997), and the values of molecular weights yielded for all mucin samples in the range of 2-7 x $10^6$ (g $mol^{-1}$). Results were confirmed using modern AUC – sedimentation equilibrium another totally independent method, which determined the weight average molecular weight for the whole distribution – and consistent with those obtained previously (Sheehan and Carlstedt, 1989; Jumel et al., 1996; Fogg et al., 1996). A complementary method was used as a third approach to estimate molecular weight distributions

based on sedimentation coefficient – Extended Fujita recently applied for mucins (Gillis et al., 2013) – results were again in good agreement with those obtained from sedimentation equilibrium and SEC-MALS.

However, the conformation and flexibility of the heterogonous system in solution plays an important role in the structure-function relationship and interactions with other macromolecules (Tombs and Harding, 1998). Although a change in the conformation of mucin was observed using the MHKS plot, the results still suggested a linear random coil conformation, and again consistent with those previously proposed (Harding et al., 1983; Sheehan and Carlstedt, 1984; Sheehan and Carlstedt, 1989; Jumel et al., 1997). Since it has been observed that, different methods biased to their own results (see e.g. Bohdanecky and Petrus, 1991; Patel et al., 2008; Picout et al., 2002). Utilizing different approaches would be more appropriate to determine conformational flexibility of mucin in terms of persistence length, $L_p$ (e. g. Bushin-Bohdanecky and HYDFIT). The persistence length $L_p$ and mass per unit length $M_L$ values yielded utilizing Mulit-HYDFIT appears to be more accurate as it takes into account data sets of both intrinsic viscosities for different molecular weights and sedimentation coefficients for different molecular weights. The Bushin–Bohdanecky analysis however, utilized only the intrinsic viscosity values and also depends on requirement of knowledge of the mass per unit length, $M_L$. Therefore, values of persistence length suggested that, mucins adapted a semi-flexible coil type, and in excellent agreement with a glycoconjugate vaccine (Harding et al., 2012b).

The characterisation of the mucin provided a strong platform to examine the behaviour of mucin mixed with other biopolymers in dilute solution. Peppas

and Buri (1985) had claimed that polyanionic and natural polymers – with hydroxyl or carboxyl groups – are preferable candidates for bioadhesion, due to a mechanism of swelling of the polymer through hydrogen bond interactions with water due to the unionised state of the carboxyl groups at low pH. In this regard, mucin (Nov 13) was mixed with PGX and its individual components separately (KGM, xanthan and alginate) at a concentration of 0.5 mg $mL^{-1}$ and ionic strength 0.1M. Under these conditions, no significant interaction was observed between mucin and the individual components (KGM, xanthan and alginate). At the neutral pH however, the polyanionic polymers were unable to form hydrogen bonds in their fully ionised state in this study. Also, it is known from macroscopic (Lehr et al., 1992) and molecular studies (Anderson, 1991; Fiebrig et al., 1997) mixtures of polyanionic (e.g. xanthan, alginate) with mucin showed no interaction. That can be interpreted in terms of electrostatic repulsion, since the negative charge is employed for both mucin and polyanioins.

On the other hand, the interaction between polycationic polymers (e.g. chitosan) and mucin has been observed using analytical ultracentrifugation, electron microscopy and atomic force microscopy, which may explained by ionic interaction due to the opposite charges (Deacon et al., 1999; Deacon et al., 2000). Furthermore, under the same conditions the mixture of mucin with PGX presented a favourable phenomenon; showing components of PGX interacted at high ionic strength in the presences of mucin. The behaviour seen here for the PGX is different from that in the absence of mucin, which shows components of PGX interacted at low ionic strength and the interaction

disappeared at high ionic strength (Abdelhameed et al., 2010; Harding et al., 2011a; Harding et al., 2012a).

# CHAPTER 8

# CONCLUDING REMARKS AND SUGGESTIONS FOR FUTURE WORK

A comprehensive study has been carried in this thesis on selected marine polysaccharides used for therapeutic purposes – carrageenans and chitosans – in terms of the molecular integrity, size distribution, conformation and their interactions with other biopolymers. This study also showed how useful the biophysical techniques in particular analytical ultracentrifugation (AUC), size exclusion chromatography coupled to multi angle light scattering (SEC-MALS) and viscometry are for the investigation of the structure and interactions of these marine polysaccharides especially when these methods are combined together.

## 8.1 CONCLUDING REMARKS

In *Chapter 1* of this study the potential of marine polysaccharides has been considered in terms of their properties and impact in human healthcare. It was also explained that polysaccharides obtained from different sources of marine organisms such as seaweeds (e.g. carrageenan and alginate) and shellfish (e.g. chitosan) present a huge variety of structures which possess interesting nutraceutical and pharmaceutical behaviour protecting from different diseases (Jiao et al., 2011; Senni et al., 2011), and these are reviewed.

Then in *Chapter 2* we considered the principle and the theory of the methodology employed for characterization the hydrodynamic properties of marine polysaccharides including molecular weight, sedimentation coefficient, intrinsic viscosity, conformational flexibility and interactions with other biopolymers. Analytical ultracentrifugation (AUC) was the main technique used in this PhD study, due to its inherent fractionation ability without the need for columns or membranes (Harding, 2005). Also SEC-MALS and viscometry methods were used as a complementary approach to AUC to establish these biophysical properties in solutions. Methods for shape and flexibility determination for linear polymers in solution were described, such as Wales-van Holde ratio, Mark-Houwink-Kuhn-Sakurada (MHKS), and Multi-HYDFIT.

In *Chapter 3* two samples of lambda carrageenan (GM-λ and TF-λ) with different molecular weight were irradiated for varying times using microwave heating in a high pressure vessel to estimate their hydrodynamic parameters (e. g. molecular weight, sedimentation coefficient, and intrinsic viscosity) and conformational behaviour in aqueous solution. The results obtained from the analytical ultracentrifugation (AUC), viscometry and SEC-MALS have demonstrated that both lambda carrageenan and their preparations (heated for different periods of time) exhibited a homogenous molecular weight distribution with unimodal system confirming the purity of dissolved samples. Further, the 15 s microwave heated samples yielded a slightly higher in sedimentation coefficient value, molecular weight value and intrinsic viscosity

value than that of unheated samples. This may reflect the final dispersion of higher molecular weight material and exhibited good dispersibility without degradation. Heating for an additional 15 second yielded a clear chain separation with a clear reduction in values of sedimentation coefficient, molecular weight and intrinsic viscosity. The Wales-van Holde ratio indicated a more flexible structure ($R$ = 0.4 – 1.0), possibly extended than a random coil, for both lambda carrageenan and their preparations and this was reinforced by Mark-Houwink-Kuhn-Sakurada (MHKS) and conformation zoning. In more detailed both Bushin-Bohdanecky and Yamakawa-Fujii methods were used to identify the conformational flexibility in terms of persistence length ($L_p$) and mass per unit length ($M_L$). The results obtained confirm that both lambda carrageenans adapt a semi-flexible structure. Furthermore, global analysis Multi-HYDFIT a more reliable way of estimating $L_p$ and $M_L$ was used in which consisted with previous proposal of semi-flexible structure by Wales-van Holde ratio and MHKS.

In *Chapter 4*, we now extend our study on lambda carrageenan in relation to other major carrageenans, kappa and iota. The conformational and oligomeric states of three classes of carrageenans (kappa, iota and lambda) were studied in the presence of different solvents (e. g. 0.1 M NaI, 0.1 M PBS, 0.1 M NaCL and DMSO). Initially thermal transition has been studied for the three classes of carrageenans using micro-DSC. Results suggested that kappa and iota carrageenan were the only one that showed thermal transition at all solvents, which confirmed the helix ordered conformation. This ordered conformation is

characterised by a broadening of the transition and a symmetrical melting-curve as reported previously (Rochas and Rinaudo, 1984). For further investigation the hydrodynamic methods - in particular analytical ultracentrifugation (AUC) - were used. The sedimentation coefficient, molecular weight and intrinsic viscosity were measured to provide evidence of single or double helix formation for carrageenans. It can be clearly seen amongst (coil and helix) conformations that there were no signs for double helix formation based on sedimentation coefficient results for iota and lambda carrageenan. Also the molecular weight data obtained showed no significant increase in helix formation compared to coil. Moreover, kappa carrageenan in helix formation showed approximately a doubling of intrinsic viscosity, but lambda and iota did not. This observation was supported by higher molecular weight and sedimentation coefficient values observed in 0.1 M NaI compared to 0.1 M NaCL or DMSO. Thus, these observations provided further evidence of the existence of a dimer (double helix) conformation under those experimental conditions for kappa carrageenan, but not for iota and lambda carrageenan.

In *Chapter 5* chitosan a soluble polycationic derivative of insoluble chitin was considered. A combined hydrodynamic approach namely sedimentation equilibrium, sedimentation velocity, SEC-MALS and viscometry was used for assessing the molecular weight and molecular weight distribution of commercial (“C”) and in-house laboratory (“L”) prepared chitosan samples with different molecular weight and degrees of acetylation. All the methods

provided comparable data with regard molecular weights and these different methods were all in agreement for the six samples studied. Further, the g*(s) profile showed polydisperse distribution in all cases for the apparent sedimentation coefficient distributions and suggested that the samples are unimodal. The conformation analysis using the traditional methods of the combination the sedimentation coefficient and intrinsic viscosity values with molecular weight values, Mark–Houwink–Kuhn–Sakurada (MHKS), suggested a semi-flexible coil conformation for the chitosan samples. The results are consistent with the Wales–van Holde ratio and conformation zoning. Different approaches (e.g. Bushin-Bohdanecky , Yamakawa-Fujii and Multi-HYDFIT) have been applied to estimate the conformational flexibility of chitosan samples in terms of the persistence length $L_p$ based on intrinsic viscosity[η], sedimentation coefficient ($s^o_{20,w}$) and molecular weight ($M_w$). The results obtained proposed a semi-flexible coil conformation in solution ($L_p$ ~7 to 16 nm).

We also demonstrated how the principle of co-sedimentation which has been successfully applied previously to the study of chitosan-mucin glycoprotein interactions - can now be used to study interactions with polyanions such as xanthan and DNA. With the latter this may prove useful for the assay of potential chitosan based materials for the condensation of DNA in gene therapies, particularly if used in conjunction with imaging probes as successfully combined before for the analysis of chitosan mucoadhesive phenomena (Deacon et al., 2000). For this a whole range of appropriate conditions need to be explored – this study has only considered a small subset.

In *Chapter 6* the physical properties of the individual polysaccharides (namely lambda carrageenan, konjac glucomannan and xanthan) were studied to establish their molecular integrity. This was followed by investigating the interaction in the binary mixture of konjac glucomannan and xanthan. From the analytical ultracentrifuge data – in particular sedimentation velocity – a clear interaction was observed between binary mixture of konjac and xanthan. The observations were confirmed by fundamental dilute solution viscosity studies, and are also consistent with previous studies (Foster and Morris, 1994; Dhami, 1996; Harding et al., 2011a). The interaction appeared to be ionic strength sensitive, showing it is electrostatic in nature. However, studies of the sedimentation behaviour of solutions of ternary mixtures containing variable amounts of lambda carrageenan amount ranging from 30% to 5% (C30 to C05) did not provide any evidence for the interaction occurred between the ternary mixtures at both ionic strengths (0.1 M and 0.001 M). In addition, fundamental dilute solution viscosity studies were performed; showing no improvement in intrinsic viscosity values for ternary mixtures compared with predicted values of non-interacting mixture. These results indicated that lambda carrageenan had not interacted with the binary mixture (konjac glucomannan and xanthan) at both ionic strengths scrutinised (0.1M and 0.001M). Furthermore, the behaviour seen here for lambda carrageenan is different from that observed for the ternary mixture - in the presence of alginate - using analytical ultracentrifugation, which confirmed a ternary interaction particularly when the alginate content of the mixture was greater than about 5% (Abdulhameed et al., 2010; Harding et al., 2011a; Harding et al., 2012). Lambda carrageenan offered no significant improvement to the use of alginate in these ternary mixtures.

Finally the hydrodynamic properties (e.g. molecular weight and conformation) for the three different preparations of mucin isolated from pig gastric in aqueous solution were probed using analytical ultracentrifugation and SEC-MALS (*Chapter 7*). It was found that the weight average molecular weights obtained from sedimentation equilibrium were in a perfect agreement with those yielded from SEC-MALS and the complementary Extended Fujita method of *Harding et al.* (Harding et al., 2011b). These results clearly demonstrated the value of combined approaches for the molecular weight distribution analysis of polydisperse materials (Jumel et al., 1996; Fogg et al., 1996). Combination of molecular weight with viscosity data has also been used to estimate the conformational flexibility of mucin samples - these demonstrated a linear random coil conformation, consistent with previous measurements but using refined procedures. Further conformation analysis – using the Multi-HYDFIT method – suggested that some variation in flexibility for different mucin preparations from pig gastric mucus. That was then followed by a study of the interaction in the mixtures of mucin (Nov13) with PGX and its individual components separately (KGM, xanthan and alginate). From the sedimentation velocity profiles, it is evident that there was no interaction observed for the mixture of mucin with individual components of PGX. Mixture of mucin with PGX therefore showed no interaction occurred, whereas interaction occurred among PGX components at high ionic strength (0.1 M). The results clearly indicated that the presence of mucin suppress the electrostatic repulsion effects on the PGX mixture (Abdulhameed et al., 2010; Harding et al., 2011a; Harding et al., 2012).

## 8.2 SUGGESTION FOR FUTURE WORK

There are several interesting follow up areas for this research. For example, the stability and conformation properties of lambda carrageenans application it would be interesting to use different and more controllable irradiation methods such as the new microwave synthesis approach (Kappe and Dallinger, 2006). Although lambda carrageenan appears to offer no alternative to the use of alginate in PGX, both kappa and iota carrageenans could still be explored. These could be investigated using the hydrodynamic methods that have been applied in this thesis. The utility of hydrodynamic methods – including co-sedimentation – to explore DNA interactions with polysaccharides for use in DNA condensation has been clearly demonstrated, but a much wider range of potential condenser polymers could be explored with this methodology. It would also be interesting to investigate these observations using atomic force microscopy (AFM) and isothemal titration calorimetry (ITC). Further, the stability of the interaction products have been observed can be examined at different conditions for instance temperature, time and pH using the biophysical methods applied in this thesis. The field of polysaccharide-ligand interactions to be explored by AUC and hydrodynamics methods is ever growing. Exploring the interactions between polysaccharide/glycoconjugate vaccines and proteins/membrane proteins looks like a particularly fruitful area of research.

# REFERENCES

ABDELHAMEED, A. S., ANG, S., MORRIS, G. A., SMITH, I., LAWSON, C., GAHLER, R., WOOD, S. & HARDING, S. E. 2010. An analytical ultracentrifuge study on ternary mixtures of konjac glucomannan supplemented with sodium alginate and xanthan gum. *Carbohydrate Polymers,* 81**,** 145-148.

ABDUL-HAMID, A. & LUAN, Y. S. 2000. Functional properties of dietary fibre prepared from defatted rice bran. *Food Chemistry,* 68**,** 15-19.

ABU-GHANNAM, N. & COX, S. 2013. Seaweed-based Functional Foods. *In:* HERNANDEZ-LEDESMA, B. & HERRERO, M. (eds.) *Bioactive Compounds from Marine Foods: Plant and Animal Sources.* John Wiley & Sons Ltd.

AHMED, A. B. A., ADEL, M., KARIMI, P. & PEIDAYESH, M. 2014. Chapter Ten - Pharmaceutical, Cosmeceutical, and Traditional Applications of Marine Carbohydrates. *In:* SE-KWON, K. (ed.) *Advances in Food and Nutrition Research.* Academic Press.

ALMUTAIRI, F. M., ADAMS, G. G., KÖK, M. S., LAWSON, C. J., GAHLER, R., WOOD, S., FOSTER, T. J., ROWE, A. J. & HARDING, S. E. 2013. An analytical ultracentrifugation based study on the conformation of lambda carrageenan in aqueous solution. *Carbohydrate Polymers,* 97**,** 203-209.

ALMUTAIRI, F. M., ERTEN, T., ADAMS, G. G., HAYES, M., MCLOUGHLIN, P., KÖK, M. Ş., MACKIE, A. R., ROWE, A. J. & HARDING, S. E. 2015. Hydrodynamic characterisation of chitosan and its interaction with two polyanions: DNA and xanthan. *Carbohydrate Polymers,* 122**,** 359-366.

AMORÓS, D., ORTEGA, A. & GARCÍA DE LA TORRE, J. 2011. Hydrodynamic Properties of Wormlike Macromolecules: Monte Carlo Simulation and Global Analysis of Experimental Data. *Macromolecules,* 44**,** 5788-5797.

ANDERSON, J. W., BAIRD, P., DAVIS JR, R. H., FERRERI, S., KNUDTSON, M., KORAYM, A., WATERS, V. & WILLIAMS, C. L. 2009. Health benefits of dietary fiber. *Nutrition Reviews,* 67**,** 188-205.

ANDERSON, M. T. 1991. *The interaction of mucous glycoproteins with polymeric materials.* Ph.D. thesis, University of Nottingham, UK.

ANDERSON, N. S., CAMPBELL, J. W., HARDING, M. M., REES, D. A. & SAMUEL, J. W. B. 1969. X-ray diffraction studies of polysaccharide sulphates: Double helix models for κ- and ι-carrageenans. *Journal of Molecular Biology,* 45**,** 85-97.

ARVANITOYANNIS, I. S. & VAN HOUWELINGEN-KOUKALIAROGLOU, M. 2005. Functional foods: a survey of health claims, pros and cons, and current legislation. *Critical Reviews in Food Science and Nutrition,* 45**,** 385-404.

ASP, N. G. 2004. Definition, health claims and new challenges. *In:* ASP, N. G., MILLER JONES, J., SCHAAFSMA, G. & VAN DER KAMP, J. W. (eds.) *Dietary Fibre: Bio-active Carbohydrates for Food and Feed.* The Netherlands: Waggeningen Academic Press.

AZEZLI, A. D., BAYRAKTAROGLU, T. & ORHAN, Y. 2007. The use of konjac glucomannan to lower serum thyroid hormones in hyperthyroidism. *Journal of the American College of Nutrition,* 26**,** 663-668.

BANSIL, R. & TURNER, B. S. 2006. Mucin structure, aggregation, physiological functions and biomedical applications. *Current Opinion in Colloid & Interface Science,* 11**,** 164-170.

BEAULIEU, L., THIBODEAU, J., BRYL, P. & CARBONNEAU, M.-É. 2009. Characterization of enzymatic hydrolyzed snow crab (Chionoecetes opilio) by-product fractions: A source of high-valued biomolecules. *Bioresource technology,* 100**,** 3332-3342.

BERTH, G., DAUTZENBERG, H. & PETER, M. G. 1998. Physico-chemical characterization of chitosans varying in degree of acetylation. *Carbohydrate Polymers,* 36**,** 205-216.

BERTH, G., VUKOVIC, J. & LECHNER, M. D. 2008. Physicochemical characterization of carrageenans—A critical reinvestigation. *Journal of Applied Polymer Science,* 110**,** 3508-3524.

BIESALSKI, H.-K., DRAGSTED, L. O., ELMADFA, I., GROSSKLAUS, R., MÜLLER, M., SCHRENK, D., WALTER, P. & WEBER, P. 2009. Bioactive compounds: Definition and assessment of activity. *Nutrition,* 25**,** 1202-1205.

BIXLER, H. & PORSE, H. 2011. A decade of change in the seaweed hydrocolloids industry. *Journal of Applied Phycology,* 23**,** 321-335.

BLACKWOOD, A., SALTER, J., DETTMAR, P. & CHAPLIN, M. 2000. Dietary fibre, physicochemical properties and their relationship to health. *The journal of the Royal Society for the Promotion of Health,* 120**,** 242-247.

BOHDANECKY, M. 1983. New method for estimating the parameters of the wormlike chain model from the intrinsic viscosity of stiff-chain polymers. *Macromolecules,* 16**,** 1483-1492.

BOHDANECKY, M. & PETRUS, V. 1991. Analysis of hydrodynamic data for denatured globular proteins in terms of the wormlike cylinder model. *International Journal of Biological Macromolecules,* 13**,** 231-234.

BONFERONI, M. C., ROSSI, S., TAMAYO, M., PEDRAZ, J. L., DOMINGUEZ-GIL, A. & CARAMELLA, C. 1994. On the employment of λ-carrageenan in a matrix system. II. λ-Carrageenan and hydroxypropylmethylcellulose mixtures. *Journal of Controlled Release,* 30**,** 175-182.

BORDERÍAS, A. J., SÁNCHEZ-ALONSO, I. & PÉREZ-MATEOS, M. 2005. New applications of fibres in foods: Addition to fishery products. *Trends in Food Science & Technology,* 16**,** 458-465.

BORGOGNA, M., BELLICH, B. & CESÀRO, A. 2011. Marine Polysaccharides in Microencapsulation and Application to Aquaculture: "From Sea to Sea". *Marine drugs,* 9**,** 2572-2604.

BROWNLEE, I. A. 2011. The physiological roles of dietary fibre. *Food Hydrocolloids,* 25**,** 238-250.

BRUGNEROTTO, J., DESBRIÈRES, J., ROBERTS, G. & RINAUDO, M. 2001. Characterization of chitosan by steric exclusion chromatography. *Polymer,* 42**,** 09921-09927.

BRUYLANTS, G., WOUTERS, J. & MICHAUX, C. 2005. Differential scanning calorimetry in life science: thermodynamics, stability,

molecular recognition and application in drug design. *Current medicinal chemistry,* 12**,** 2011-2020.

BUCK, C. B., THOMPSON, C. D., ROBERTS, J. N., MÜLLER, M., LOWY, D. R. & SCHILLER, J. T. 2006. Carrageenan is a potent inhibitor of papillomavirus infection. *PLoS pathogens,* 2**,** e69.

BUROVA, T. V., GRINBERG, N. V., GRINBERG, V. Y., USOV, A. I., TOLSTOGUZOV, V. B. & DE KRUIF, C. G. 2007. Conformational changes in ι-and κ-carrageenans induced by complex formation with bovine β-casein. *Biomacromolecules,* 8**,** 368-375.

BURTIN, P. 2003. Nutritional value of seaweeds. *Electronic journal of Environmental, Agricultural and Food chemistry,* 2**,** 498-503.

BUSHIN, S., TSVETKOV, V., LYSENKO, Y. B. & YEMEL'YANOV, V. 1981. The sedimentation-diffusion and viscometric analysis of the conformation properties and molecular rigidity of ladder-like polyphenyl siloxane in solution. *Polymer Science USSR,* 23**,** 2705-2715.

CAMPO, V. L., KAWANO, D. F., SILVA JR, D. B. D. & CARVALHO, I. 2009. Carrageenans: Biological properties, chemical modifications and structural analysis – A review. *Carbohydrate Polymers,* 77**,** 167-180.

CARLSTEDT, I., HERRMANN, A., KARLSSON, H., SHEEHAN, J., FRANSSON, L. & HANSSON, G. C. 1993. Characterization of two different glycosylated domains from the insoluble mucin complex of rat small intestine. *Journal of Biological Chemistry,* 268**,** 18771-18781.

CARLUCCI, M. J., SCOLARO, L. A. & DAMONTE, E. B. 1999. Inhibitory action of natural carrageenans on herpes simplex virus infection of mouse astrocytes. *Chemotherapy,* 45**,** 429-436.

CESCUTTI, P., CAMPA, C., DELBEN, F. & RIZZO, R. 2002. Structure of the oligomers obtained by enzymatic hydrolysis of the glucomannan produced by the plant Amorphophallus konjac. *Carbohydrate Research,* 337**,** 2505-2511.

CHAMP, M., LANGKILDE, A.-M., BROUNS, F., KETTLITZ, B. & COLLET, Y. L. B. 2003. Advances in dietary fibre characterisation. 1. Definition of dietary fibre, physiological relevance, health benefits and analytical aspects. *Nutrition Research Reviews,* 16**,** 71-82.

CHAPLIN, M. 2009. *Water structure and science: Xanthan gum.* [Online]. From http://www1.lsbu.ac.uk/water/hyxan.html. [Accessed 18th August 2014].

CHARRIER, B., LE BAIL, A. & DE REVIERS, B. 2012. Plant Proteus: brown algal morphological plasticity and underlying developmental mechanisms. *Trends in plant science,* 17**,** 468-477.

CHEBA, B. A. 2011. Chitin and chitosan: marine biopoly-mers with unique properties and versatile applications. *Global Journal of***,** 149-153.

CHRONAKIS, I. S., DOUBLIER, J.-L. & PICULELL, L. 2000. Viscoelastic properties for kappa- and iota-carrageenan in aqueous NaI from the liquid-like to the solid-like behaviour. *International Journal of Biological Macromolecules,* 28**,** 1-14.

COLE, J. L., LARY, J. W., P. MOODY, T. & LAUE, T. M. 2008. Analytical Ultracentrifugation: Sedimentation Velocity and Sedimentation Equilibrium. *In:* DR. JOHN, J. C. & DR. H. WILLIAM DETRICH, III (eds.) *Methods in Cell Biology.* Academic Press.

CÖLFEN, H., BERTH, G. & DAUTZENBERG, H. 2001. Hydrodynamic studies on chitosans in aqueous solution. *Carbohydrate Polymers,* 45**,** 373-383.

CÖLFEN, H. & HARDING, S. E. 1997. MSTARA and MSTARI: interactive PC algorithms for simple, model independent evaluation of sedimentation equilibrium data. *European Biophysics Journal,* 25**,** 333-346.

CÖLFEN, H., HARDING, S. E., VÅRUM, K. M. & WINZOR, D. J. 1996. A study by analytical ultracentrifugation on the interaction between lysozyme and extensively deacetylated chitin (chitosan). *Carbohydrate Polymers,* 30**,** 45-53.

COOPER, A., NUTLEY, M. A. & WADOOD, A. 2000. Differential scanning microcalorimetry. *In:* HARDING, S. E. & CHOWDHRY, B. Z. (eds.) *Protein-ligand interactions: Hydrodynamics and calorimetry.* Oxford New York: Oxford University Press, pp, 287-318.

COULTATE, T. P. 2009. *Food: The Chemistry of Its Components*, Royal Society of Chemistry.

COX, S., ABU-GHANNAM, N. & GUPTA, S. 2010. An assessment of the antioxidant and antimicrobial activity of six species of edible Irish seaweeds. *International Food Research Journal***,** 205-220.

CREETH, J. & KNIGHT, C. 1965. On the estimation of the shape of macromolecules from sedimentation and viscosity measurements. *Biochimica et Biophysica Acta (BBA)-Biophysics including Photosynthesis,* 102**,** 549-558.

CREETH, J. M. & HARDING, S. H. 1982. Some observations on a new type of point average molecular weight. *Journal of biochemical and biophysical methods,* 7**,** 25-34.

CUPPO, F. & REYNAERS, H. 2002. Light scattering investigation of association phenomena in saline carrageenan solutions. *Macromolecular Symposia,* 190**,** 65-74.

DAM, J. & SCHUCK, P. 2004. Calculating sedimentation coefficient distributions by direct modeling of sedimentation velocity concentration profiles. *Methods in enzymology,* 384**,** 185-212.

DANLEY, R. L. 2002. New heat flux DSC measurement technique. *Thermochimica Acta,* 395**,** 201-208.

DAVIDSON, R. L. 1980. *Handbook of water-soluble gums and resins,* New York, McGraw-Hill.

DE HOLANDA, H. D. & NETTO, F. M. 2006. Recovery of components from shrimp (Xiphopenaeus kroyeri) processing waste by enzymatic hydrolysis. *Journal of food science,* 71**,** C298-C303.

DE RUITER, G. A. & RUDOLPH, B. 1997. Carrageenan biotechnology. *Trends in Food Science & Technology,* 8**,** 389-395.

DE SOUZA, M. C. R., MARQUES, C. T., DORE, C. M. G., DA SILVA, F. R. F., ROCHA, H. A. O. & LEITE, E. L. 2007. Antioxidant activities of sulfated polysaccharides from brown and red seaweeds. *Journal of Applied Phycology,* 19**,** 153-160.

DEA, I., MORRIS, E. R., REES, D. A., WELSH, E. J., BARNES, H. A. & PRICE, J. 1977. Associations of like and unlike polysaccharides: mechanism and specificity in galactomannans, interacting bacterial polysaccharides, and related systems. *Carbohydrate Research,* 57**,** 249-272.

DEACON, M., MCGURK, S., ROBERTS, C., WILLIAMS, P., TENDLER, S., DAVIES, M., DAVIS, S. & HARDING, S. 2000. Atomic force microscopy of gastric mucin and chitosan mucoadhesive systems. *Biochem. J,* 348**,** 557-563.

DEACON, M. P., DAVIS, S. S., WHITE, R. J., NORDMAN, H., CARLSTEDT, I., ERRINGTON, N., ROWE, A. J. & HARDING, S. E. 1999. Are chitosan–mucin interactions specific to different regions of the stomach? Velocity ultracentrifugation offers a clue. *Carbohydrate Polymers,* 38**,** 235-238.

DHAMI, R. 1996. Interactions of xanthan with locust bean gum, konjac mannan and guar gum. *In:* DHAMI, R. (ed.) *Hydrodynamic studies on xanthan and xylan systems.* Ph.D. Thesis: University of Nottingham; UK [Chapter 8].

DHAMI, R., HARDING, S. E., JONES, T., HUGHES, T., MITCHELL, J. R. & TO, K.-M. 1995. Physico-chemical studies on a commercial food-grade xanthan—I. Characterisation by sedimentation velocity, sedimentation equilibrium and viscometry. *Carbohydrate Polymers,* 27**,** 93-99.

DODD, S., PLACE, G. A., HALL, R. L. & HARDING, S. E. 1998. Hydrodynamic properties of mucins secreted by primary cultures of Guinea-pig tracheal epithelial cells: determination of diffusion coefficients by analytical ultracentrifugation and kinetic analysis of mucus gel hydration and dissolution. *European Biophysics Journal,* 28**,** 38-47.

DRAGET, K. 1996. Associating phenomena in highly acetylated chitosan gels. *Polymer Gels and Networks,* 4**,** 143-151.

DUAN, X.-J., ZHANG, W.-W., LI, X.-M. & WANG, B.-G. 2006. Evaluation of antioxidant property of extract and fractions obtained from a red alga, Polysiphonia urceolata. *Food Chemistry,* 95**,** 37-43.

DUMITRIU, S., MAGNY, P., MONTANE, D., VIDAL, P. & CHORNET, E. 1994. Polyionic hydrogels obtained by complexation between xanthan and chitosan: their properties as supports for enzyme immobilization. *Journal of bioactive and compatible polymers,* 9**,** 184-209.

EINSTEIN, A. 1906. Eine neue Bestimmung der Moleküldimensionen. *Annalen der Physik,* 324**,** 289-306.

ELLEUCH, M., BEDIGIAN, D., ROISEUX, O., BESBES, S., BLECKER, C. & ATTIA, H. 2011. Dietary fibre and fibre-rich by-products of food processing: Characterisation, technological functionality and commercial applications: A review. *Food Chemistry,* 124**,** 411-421.

ERRINGTON, N., HARDING, S., VÅRUM, K. & ILLUM, L. 1993. Hydrodynamic characterization of chitosans varying in degree of acetylation. *International Journal of Biological Macromolecules,* 15**,** 113-117.

ERTEN, T., ADAMS, G. G., FOSTER, T. J. & HARDING, S. E. 2014. Comparative heterogeneity, molecular weights and viscosities of xanthans of different pyruvate and acetate content. *Food Hydrocolloids,* 42**,** 335-341.

FAO 2014. The State of World Fisheries and Aquaculture Rome: Food and Agriculture Organization of the united nation.

FARIAS, W. R. L., VALENTE, A. P., PEREIRA, M. S. & MOURÃO, P. A. S. 2000. Structure and anticoagulant activity of sulfated galactans. Isolation of a unique sulfated galactan from the red algae Botryocladia occidentalis and comparison of its anticoagulant action with that of sulfated galactans from invertebrates. *Journal of Biological Chemistry,* 275**,** 29299-29307.

FAULKNER, D. J. 2000. Marine pharmacology. *Antonie van Leeuwenhoek,* 77**,** 135-145.

FEE, M., ERRINGTON, N., JUMEL, K., ILLUM, L., SMITH, A. & HARDING, S. 2003. Correlation of SEC/MALLS with ultracentrifuge and viscometric data for chitosans. *European Biophysics Journal,* 32**,** 457-464.

FIEBRIG, I., VÅRUM, K. M., HARDING, S. E., DAVIS, S. S. & STOKKE, B. T. 1997. Colloidal gold and colloidal gold labelled wheat germ agglutinin as molecular probes for identification in mucin/chitosan complexes. *Carbohydrate Polymers,* 33**,** 91-99.

FISHMAN, M. L., CHAU, H. K., KOLPAK, F. & BRADY, J. 2001. Solvent effects on the molecular properties of pectins. *Journal of Agricultural and Food Chemistry,* 49**,** 4494-4501.

FOGG, F., HUTTON, D., JUMEL, K., PEARSON, J., HARDING, S. & ALLEN, A. 1996. Characterization of pig colonic mucins. *Biochem. J,* 316**,** 937-942.

FOSTER, T. & MORRIS, E. 1994. Xanthan polytetramer: conformational stability as a barrier to synergistic interaction. *In:* PHILIPS, G., WILLIAMS, P. & WEDLOCK, D. (eds.) *Gums and stabilisers for the food industry 7.* New York: Oxford University Press Inc.

FREIRE, J. J. & GARCIA DE LA TORRE, J. 1992. Sedimentation coefficients of flexible chain polymers. *In:* S.E. HARDING, A. J. R., J.C. HORTON (ed.) *Analytical ultracentrifugation in biochemistry and polymer science.* Cambridge Royal Society of Chemistry (pp. 346-393).

FUJITA, H. 1962. *Mathematical Theory of Sedimentation Analysis,* Academic Press.

FURST, A. 1997. The XL-I analytical ultracentrifuge with Rayleigh interference optics. *European Biophysics Journal,* 25**,** 307-310.

GARCıA-OCHOA, F., SANTOS, V., CASAS, J. & GOMEZ, E. 2000. Xanthan gum: production, recovery, and properties. *Biotechnology advances,* 18**,** 549-579.

GILL, P., MOGHADAM, T. T. & RANJBAR, B. 2010. Differential scanning calorimetry techniques: applications in biology and nanoscience. *Journal of biomolecular techniques: JBT,* 21**,** 167.

GILLIS, R. B., ADAMS, G. G., WOLF, B., BERRY, M., BESONG, T. M. D., CORFIELD, A., KÖK, S. M., SIDEBOTTOM, R., LAFOND, D., ROWE, A. J. & HARDING, S. E. 2013. Molecular weight distribution analysis by ultracentrifugation: Adaptation of a new approach for mucins. *Carbohydrate Polymers,* 93**,** 178-183.

GIROND, S., CRANCE, J., VAN CUYCK-GANDRE, H., RENAUDET, J. & DELOINCE, R. 1991. Antiviral activity of carrageenan on hepatitis A virus replication in cell culture. *Research in virology,* 142**,** 261-270.

GORTARI, M. C. & HOURS, R. A. 2013. Biotechnological processes for chitin recovery out of crustacean waste: A mini-review. *Electronic Journal of Biotechnology,* 16**,** 14-14.

GOYCOOLEA, F. M., MORRIS, E. R. & GIDLEY, M. J. 1995. Screening for synergistic interactions in dilute polysaccharide solutions. *Carbohydrate Polymers,* 28**,** 351-358.

GRALÉN, N. 1944. *Sedimentation and diffusion measurements on cellulose and cellulose derivatives* Sweden: University of Uppsala.

GRASSAUER, A., WEINMUELLNER, R., MEIER, C., PRETSCH, A., PRIESCHL-GRASSAUER, E. & UNGER, H. 2008. Iota-Carrageenan is a potent inhibitor of rhinovirus infection. *Virol J,* 5**,** 422X-5.

GRINBERG, V. Y., GRINBERG, N. V., USOV, A. I., SHUSHARINA, N. P., KHOKHLOV, A. R. & DE KRUIF, K. G. 2001. Thermodynamics of conformational ordering of ι-carrageenan in KCl solutions using high-sensitivity differential scanning calorimetry. *Biomacromolecules,* 2**,** 864-873.

HARDING, S. 2003. Mucoadhesive interactions. *Biochemical Society Transactions,* 31**,** 1036-1041.

HARDING, S. 2013. Polysaccharides: Biophysical Properties. *In:* ROBERTS, G. K. (ed.) *Encyclopedia of Biophysics.* Springer Berlin Heidelberg.

HARDING, S., HORTON, J. & MORGAN, P. 1992. MSTAR: A FORTRAN program for the model independent molecular weight analysis of macromolecules using low speed or high speed sedimentation equilibrium. *In:* HARDING, S. E., ROWE, A. J. & HORTON, J. C. (eds.) *Analytical Ultracentrifugation in Biochemistry and Polymer Science.* Royal Society of Chemistry, Cambridge, UK.

HARDING, S., ROWE, A. & CREETH, J. 1983. Further evidence for a flexible and highly expanded spheroidal model for mucus glycoproteins in solution. *Biochemical Journal,* 209**,** 893.

HARDING, S. E. 1989. The Macrostructure of Mucus Glycoproteins in Solution. *In:* TIPSON, R. S. & DEREK, H. (eds.) *Advances in Carbohydrate Chemistry and Biochemistry.* Academic Press.

HARDING, S. E. 1992. Sedimentation analysis of polysaccharides. *In:* HARDING, S. E., ROWE, A. J. & HORTON, J. C. (eds.) *Analytical*

*ultracentrifugation in biochemistry & polymer science.* Cambridge, UK: Royal Society of Chemistry.

HARDING, S. E. 1997. The intrinsic viscosity of biological macromolecules. Progress in measurement, interpretation and application to structure in dilute solution. *Progress in Biophysics and Molecular Biology,* 68**,** 207-262.

HARDING, S. E. 2005a. Analysis of polysaccharides size, shape and interactions. *In:* SCOTT, D. J., HARDING, S. E. & ROWE, A. J. (eds.) *Analytical ultracentrifugation techniques and methods.* Cambridge, UK: Royal Society of Chemistry.

HARDING, S. E. 2005b. Challenges for the modern analytical ultracentrifuge analysis of polysaccharides. *Carbohydrate Research,* 340**,** 811-826.

HARDING, S. E. 2006. Trends in muco-adhesive analysis. *Trends in Food Science & Technology,* 17**,** 255-262.

HARDING, S. E. 2012. *Viscometry, Analytical Ultracentrifugation and Light Scattering Probes for Carbohydrate Stability,* Cambridge UK, Royal Society of Chemistry.

HARDING, S. E., ABDELHAMEED, A. S., MORRIS, G. A., ADAMS, G., LALOUX, O., CERNY, L., BONNIER, B., DUVIVIER, P., CONRATH, K. & LENFANT, C. 2012b. Solution properties of capsular polysaccharides from Streptococcus pneumoniae. *Carbohydrate Polymers,* 90**,** 237-242.

HARDING, S. E., ALMUTAIRI, F., ADAMS, G. G., MORRIS, G., LAWSON, C. J., GAHLER, R. J. & WOOD, S. 2012a. Dilute Solution Viscometry Studies on a Therapeutic Mixture of Non-digestible Carbohydrates. *International Journal of Biotechnology for Wellness Industries,* 1**,** 107-114.

HARDING, S. E., DAY, K., DHAMI, R. & LOWE, P. M. 1997. Further observations on the size, shape and hydration of kappa-carrageenan in dilute solution. *Carbohydrate Polymers,* 32**,** 81-87.

HARDING, S. E., SCHUCK, P., ABDELHAMEED, A. S., ADAMS, G., KÖK, M. S. & MORRIS, G. A. 2011b. Extended Fujita approach to the molecular weight distribution of polysaccharides and other polymeric systems. *Methods,* 54**,** 136-144.

HARDING, S. E., SMITH, I. H., LAWSON, C. J., GAHLER, R. J. & WOOD, S. 2011a. Studies on macromolecular interactions in ternary mixtures of konjac glucomannan, xanthan gum and sodium alginate. *Carbohydrate Polymers,* 83**,** 329-338.

HARDING, S. E., VÅRUM, K., STOKKE, B. R. T. & SMIDSRØD, O. 1991. Molecular weight determination of polysaccharides. *Advances in carbohydrate analysis,* 1**,** 63-144.

HAUG, A., LARSEN, B. R. & SMIDSROD, O. 1967. Studies on the sequence of uronic acid residues in alginic acid. *Acta Chem Scand,* 21**,** 691-704.

HEINZE, T., NIKOLAJSKI, M., DAUS, S., BESONG, T. M. D., MICHAELIS, N., BERLIN, P., MORRIS, G. A., ROWE, A. J. & HARDING, S. E. 2011. Protein-like Oligomerization of Carbohydrates. *Angewandte Chemie International Edition,* 50**,** 8602-8604.

HEJAZI, R. & AMIJI, M. 2003. Chitosan-based gastrointestinal delivery systems. *Journal of Controlled Release,* 89**,** 151-165.

HELANDER, I. M., NURMIAHO-LASSILA, E. L., AHVENAINEN, R., RHOADES, J. & ROLLER, S. 2001. Chitosan disrupts the barrier properties of the outer membrane of Gram-negative bacteria. *International Journal of Food Microbiology,* 71**,** 235-244.

HEU, M.-S., KIM, J.-S. & SHAHIDI, F. 2003. Components and nutritional quality of shrimp processing by-products. *Food Chemistry,* 82**,** 235-242.

HIRANO, S. 1996. Chitin biotechnology applications. *Biotechnology annual review,* 2**,** 237-258.

HJERDE, T., KRISTIANSEN, T. S., STOKKE, B. T., SMIDSRØD, O. & CHRISTENSEN, B. E. 1994. Conformation dependent depolymerisation kinetics of polysaccharides studied by viscosity measurements. *Carbohydrate Polymers,* 24**,** 265-275.

HOEFLER, A. 2001. Carrageenan: chemistry, functionality, and applications. *Oxford***,** pp: 1-14.

HÖHNE, G., HEMMINGER, W. & FLAMMERSHEIM, H.-J. 2003. *Differential scanning calorimetry,* Springer Science & Business Media.

HOKPUTSA, S., JUMEL, K., ALEXANDER, C. & HARDING, S. E. 2003. A comparison of molecular mass determination of hyaluronic acid using

SEC/MALLS and sedimentation equilibrium. *European Biophysics Journal,* 32**,** 450-456.

HOLDT, S. L. & KRAAN, S. 2011. Bioactive compounds in seaweed: functional food applications and legislation. *Journal of Applied Phycology,* 23**,** 543-597.

HOPMAN, W., HOUBEN, P., SPETH, P. & LAMERS, C. 1988. Glucomannan prevents postprandial hypoglycaemia in patients with previous gastric surgery. *Gut,* 29**,** 930-934.

HORTON, J., HARDING, S., MITCHELL, J. & MORTON-HOLMES, D. 1991b. Thermodynamic non-ideality of dilute solutions of sodium alginate studied by sedimentation equilibrium ultracentrifugation. *Food Hydrocolloids,* 5**,** 125-127.

HORTON, J. C., HARDING, S. E. & MITCHELL, J. R. 1991a. Gel permeation chromatography - Multi-angle laser light scattering characterization of the molecular mass distribution of 'Pronova' sodium alginate. *Biochemical Society Transactions,* 19**,** 510-511.

HU, F. B. & WILLETT, W. C. 2002. Optimal diets for prevention of coronary heart disease. *JAMA,* 288**,** 2569-2578.

HU, Y., DU, Y., YANG, J., TANG, Y., LI, J. & WANG, X. 2007. Self-aggregation and antibacterial activity of N-acylated chitosan. *Polymer,* 48**,** 3098-3106.

HUGERTH, A., CARAM-LELHAM, N. & SUNDELÖF, L.-O. 1997. The effect of charge density and conformation on the polyelectrolyte complex formation between carrageenan and chitosan. *Carbohydrate Polymers,* 34**,** 149-156.

HUGGINS, M. L. 1942. The viscosity of dilute solutions of long-chain molecules. IV. Dependence on concentration. *Journal of the American Chemical Society,* 64**,** 2716-2718.

HWANG, J. & KOKINI, J. L. 1991. Structure and rheological function of side branches of carbohydrate polymers. *Journal of texture studies,* 22**,** 123-167.

IGLAUER, S., WU, Y., SHULER, P., TANG, Y. & GODDARD III, W. A. 2011. Dilute iota- and kappa-Carrageenan solutions with high

viscosities in high salinity brines. *Journal of Petroleum Science and Engineering,* 75**,** 304-311.

IL'INA, A. V. & VARLAMOV, V. P. 2005. Chitosan-based polyelectrolyte complexes: A review. *Applied Biochemistry and Microbiology,* 41**,** 5-11.

IMESON, A., PHILLIPS, G. & WILLIAMS, P. 2009. Carrageenan and furcellaran. *Handbook of hydrocolloids***,** 164-185.

JACKSON, C.-J. C. & PALIYATH, G. 2011. Functional Foods and Nutraceuticals. *Functional Foods, Nutraceuticals, and Degenerative Disease Prevention.* Wiley-Blackwell.

JANG, M. K., KONG, B. G., JEONG, Y. I., LEE, C. H. & NAH, J. W. 2004. Physicochemical characterization of α-chitin, β-chitin, and γ-chitin separated from natural resources. *Journal of Polymer Science Part A: Polymer Chemistry,* 42**,** 3423-3432.

JAYAKUMAR, R., CHENNAZHI, K., MUZZARELLI, R., TAMURA, H., NAIR, S. & SELVAMURUGAN, N. 2010. Chitosan conjugated DNA nanoparticles in gene therapy. *Carbohydrate Polymers,* 79**,** 1-8.

JAYAKUMAR, R., NWE, N., TOKURA, S. & TAMURA, H. 2007. Sulfated chitin and chitosan as novel biomaterials. *International Journal of Biological Macromolecules,* 40**,** 175-181.

JENKINS, D. J., KENDALL, C. W., AXELSEN, M., AUGUSTIN, L. S. & VUKSAN, V. 2000. Viscous and nonviscous fibres, nonabsorbable and low glycaemic index carbohydrates, blood lipids and coronary heart disease. *Current opinion in lipidology,* 11**,** 49-56.

JIAO, G., YU, G., ZHANG, J. & EWART, H. 2011. Chemical Structures and Bioactivities of Sulfated Polysaccharides from Marine Algae. *Marine drugs,* 9**,** 196-223.

JIMÉNEZ-ESCRIG, A. & SÁNCHEZ-MUNIZ, F. 2000. Dietary fibre from edible seaweeds: Chemical structure, physicochemical properties and effects on cholesterol metabolism. *Nutrition Research,* 20**,** 585-598.

JUMEL, K., BROWNE, P. & KENNEDY, J. F. 1992. The use of low angle laser light scattering with gel permeation chromatography for the molecular weight determination of biomolecules. *In:* S.E. HARDING,

D.B. SATELLE & BLOOMFIELD, V. A. (eds.) *Laser light scattering in biochemistry.* Cambridge Royal Society of Chemistry, pp. 275–293.

JUMEL, K., FIEBRIG, I. & HARDING, S. E. 1996. Rapid size distribution and purity analysis of gastric mucus glycoproteins by size exclusion chromatography/multi angle laser light scattering. *International Journal of Biological Macromolecules,* 18**,** 133-139.

JUMEL, K., FOGG, F. J., HUTTON, D. A., PEARSON, J., ALLEN, A. & HARDING, S. E. 1997. A polydisperse linear random coil model for the quaternary structure of pig colonic mucin. *European Biophysics Journal,* 25**,** 477-480.

KAPPE, C. O. & DALLINGER, D. 2006. The impact of microwave synthesis on drug discovery. *Nat Rev Drug Discov,* 5**,** 51-63.

KATO, Y., ONISHI, H. & MACHIDA, Y. 2005. Contribution of chitosan and its derivatives to cancer chemotherapy. *in vivo,* 19**,** 301-310.

KATSURAYA, K., OKUYAMA, K., HATANAKA, K., OSHIMA, R., SATO, T. & MATSUZAKI, K. 2003. Constitution of konjac glucomannan: chemical analysis and 13C NMR spectroscopy. *Carbohydrate Polymers,* 53**,** 183-189.

KELLY, R., GUDO, E., MITCHELL, J. & HARDING, S. 1994. Some observations on the nature of heated mixtures of bovine serum albumin with an alginate and a pectin. *Carbohydrate Polymers,* 23**,** 115-120.

KENDALL, C. W., ESFAHANI, A. & JENKINS, D. J. 2010. The link between dietary fibre and human health. *Food Hydrocolloids,* 24**,** 42-48.

KIM, S.-K. & WIJESEKARA, I. 2010. Development and biological activities of marine-derived bioactive peptides: A review. *Journal of Functional Foods,* 2**,** 1-9.

KING, A. H. 1983. Brown seaweed extracts (alginates). *In:* GLICKSMAN, M. (ed.) *Food hydrocolloids.* Boca Raton, FL: CRC Press. pp.115-188.

KÖK, M. S., ABDELHAMEED, A. S., ANG, S., MORRIS, G. A. & HARDING, S. E. 2009. A novel global hydrodynamic analysis of the molecular flexibility of the dietary fibre polysaccharide konjac glucomannan. *Food Hydrocolloids,* 23**,** 1910-1917.

KOSTANSKI, L. K., KELLER, D. M. & HAMIELEC, A. E. 2004. Size-exclusion chromatography—a review of calibration methodologies. *Journal of biochemical and biophysical methods,* 58**,** 159-186.

KRAEMER, E. O. 1938. Molecular Weights of Celluloses and Cellulose Derivates. *Industrial & Engineering Chemistry,* 30**,** 1200-1203.

LAHAYE, M. 1991. Marine algae as sources of fibres: Determination of soluble and insoluble dietary fibre contents in some 'sea vegetables'. *Journal of the Science of Food and Agriculture,* 54**,** 587-594.

LANGENDORFF, V., CUVELIER, G., LAUNAY, B., MICHON, C., PARKER, A. & DE KRUIF, C. G. 1999. Casein micelle/iota carrageenan interactions in milk: Influence of temperature. *Food Hydrocolloids,* 13**,** 211-218.

LANGENDORFF, V., CUVELIER, G., MICHON, C., LAUNAY, B., PARKER, A. & DE KRUIF, C. G. 2000. Effects of carrageenan type on the behaviour of carrageenan/milk mixtures. *Food Hydrocolloids,* 14**,** 273-280.

LAUE, T. 2004. Analytical ultracentrifugation: a powerful 'new'technology in drug discovery. *Drug Discovery Today: Technologies,* 1**,** 309-315.

LAUE, T. & STAFFORD III, W. 1999. Modern applications of analytical ultracentrifugation. *Annual review of biophysics and biomolecular structure,* 28**,** 75-100.

LAURIENZO, P. 2010. Marine polysaccharides in pharmaceutical applications: an overview. *Marine drugs,* 8**,** 2435-2465.

LE QUESTEL, J.-Y., CROS, S., MACKIE, W. & PÉREZ, S. 1995. Computer modelling of sulfated carbohydrates: applications to carrageenans. *International Journal of Biological Macromolecules,* 17**,** 161-175.

LEE, K. Y., PARK, W. H. & HA, W. S. 1997. Polyelectrolyte complexes of sodium alginate with chitosan or its derivatives for microcapsules. *Journal of Applied Polymer Science,* 63**,** 425-432.

LEHR, C.-M., BOUWSTRA, J. A., SCHACHT, E. H. & JUNGINGER, H. E. 1992. In vitro evaluation of mucoadhesive properties of chitosan and some other natural polymers. *International Journal of Pharmaceutics,* 78**,** 43-48.

LEÓN, A. E., RIBOTTA, P. D., AUSAR, S. F., FERNÁNDEZ, C., LANDA, C. A. & BELTRAMO, D. M. 2000. Interactions of different carrageenan isoforms and flour components in breadmaking. *Journal of Agricultural and Food Chemistry,* 48**,** 2634-2638.

LI, L., NI, R., SHAO, Y. & MAO, S. 2014. Carrageenan and its applications in drug delivery. *Carbohydrate Polymers,* 103**,** 1-11.

MABEAU, S. & FLEURENCE, J. 1993. Seaweed in food products: biochemical and nutritional aspects. *Trends in Food Science & Technology,* 4**,** 103-107.

MACARTAIN, P., GILL, C. I. R., BROOKS, M., CAMPBELL, R. & ROWLAND, I. R. 2007. Nutritional Value of Edible Seaweeds. *Nutrition Reviews,* 65**,** 535-543.

MÄCHTLE, W. & BÖRGER, L. 2006. *Analytical ultracentrifugation of polymers and nanoparticles,* Springer.

MAEDA, M., SHIMAHARA, H. & SUGIYAMA, N. 1980. Detailed examination of the branched structure of konjac glucomannan. *Agricultural and biological chemistry,* 44**,** 245-252.

MARCHETTI, M., PISANI, S., PIETROPAOLO, V., SEGANTI, L., NICOLETTI, R. & ORSI, N. 1995. Inhibition of herpes simplex virus infection by negatively charged and neutral carbohydrate polymers. *Journal of chemotherapy,* 7**,** 90-96.

MARGARITIS, A. & ZAJIC, J. E. 1978. Mixing, mass transfer, and scale-up of polysaccharide fermentations. *Biotechnology and Bioengineering,* 20**,** 939-1001.

MARTÍNEZ-RUVALCABA, A., CHORNET, E. & RODRIGUE, D. 2007. Viscoelastic properties of dispersed chitosan/xanthan hydrogels. *Carbohydrate Polymers,* 67**,** 586-595.

MATSUKAWA, R., DUBINSKY, Z., KISHIMOTO, E., MASAKI, K., MASUDA, Y., TAKEUCHI, T., CHIHARA, M., YAMAMOTO, Y., NIKI, E. & KARUBE, I. 1997. A comparison of screening methods for antioxidant activity in seaweeds. *Journal of Applied Phycology,* 9**,** 29-35.

MAYAKRISHNAN, V., KANNAPPAN, P., ABDULLAH, N. & AHMED, A. B. A. 2013. Cardioprotective activity of polysaccharides derived from

marine algae: An overview. *Trends in Food Science & Technology,* 30**,** 98-104.

MCGUCKIN, M. A., LINDÉN, S. K., SUTTON, P. & FLORIN, T. H. 2011. Mucin dynamics and enteric pathogens. *Nature Reviews Microbiology,* 9**,** 265-278.

MEMBER, M. W. N. & MORRIS, E. R. 1995. Solubility, solution rheology and salt-induced gelation of welan polysaccharide in organic solvents. *Carbohydrate Polymers,* 27**,** 23-36.

MORITAKA, H., TAKAHASHI, M. & KUBOTA, K. 2007. Effects of cooling rate and sodium chloride on polysaccharide gelation. *Food science and technology research,* 13**,** 345-350.

MORRIS, E. R. 1990. Comparison of the properties and function of alginates and carragenan. *In:* GLYN O. PHILLIPS, DAVID J. WEDLOCK & WILLIAMS, P. A. (eds.) *Gum and stabilizers for the food industry 5.* Oxford: Pergamon Press.

MORRIS, E. R., REES, D. A. & ROBINSON, G. 1980. Cation-specific aggregation of carrageenan helices: Domain model of polymer gel structure. *Journal of Molecular Biology,* 138**,** 349-362.

MORRIS, G. 2001. *Hydrodynamic Investigation of Polysaccharides and their Interactions with Casein.* PhD, The University of Nottingham.

MORRIS, G. A., ADAMS, G. G. & HARDING, S. E. 2014. On hydrodynamic methods for the analysis of the sizes and shapes of polysaccharides in dilute solution: A short review. *Food Hydrocolloids*.

MORRIS, G. A., CASTILE, J., SMITH, A., ADAMS, G. G. & HARDING, S. E. 2009. Macromolecular conformation of chitosan in dilute solution: A new global hydrodynamic approach. *Carbohydrate Polymers,* 76**,** 616-621.

MORRIS, G. A., FOSTER, T. J. & HARDING, S. E. 2000. The effect of the degree of esterification on the hydrodynamic properties of citrus pectin. *Food Hydrocolloids,* 14**,** 227-235.

MORRIS, G. A. & HARDING, S. E. 2009. Polysaccharides, Microbial. *In:* SCHAECHTER, M. (ed.) *Encyclopedia of Microbiology 3rd ed.* Amsterdam: Elsevier.482-494.

MORRIS, G. A., KÖK, S. M., HARDING, S. E. & ADAMS, G. G. 2010. Polysaccharide drug delivery systems based on pectin and chitosan. *Biotechnology and genetic engineering reviews,* 27**,** 257-284.

MORRIS, G. A., PATEL, T. R., PICOUT, D. R., ROSS-MURPHY, S. B., ORTEGA, A., GARCIA DE LA TORRE, J. & HARDING, S. E. 2008. Global hydrodynamic analysis of the molecular flexibility of galactomannans. *Carbohydrate Polymers,* 72**,** 356-360.

MUZZARELLI, R. A. A., AND MUZZARELLI, C. 2009. Chitin and chitosan hydrogels. *In:* PHILLIPS, G. O., & WILLIAMS, P. A. (ed.) *Handbook of hydrocolloids.* 2nd ed. Cambridge, UK: Woodhead Publishing Ltd.

NAKASHIMA, H., KIDO, Y., KOBAYASHI, N., MOTOKI, Y., NEUSHUL, M. & YAMAMOTO, N. 1987. Purification and characterization of an avian myeloblastosis and human immunodeficiency virus reverse transcriptase inhibitor, sulfated polysaccharides extracted from sea algae. *Antimicrobial Agents and Chemotherapy,* 31**,** 1524-1528.

NIEBEL, Y., BUSCHMANN, M. D., LAVERTU, M. & DE CRESCENZO, G. 2014. Combined Analysis of Polycation/ODN Polyplexes by Analytical Ultracentrifugation and Dynamic Light Scattering Reveals their Size, Refractive Index Increment, Stoichiometry, Porosity, and Molecular Weight. *Biomacromolecules,* 15**,** 940-947.

NIGRELLI, R. F., STEMPIEN JR, M. F., RUGGIERI, G. D., LIGUORI, V. R. & CECIL, J. T. Substances of potential biomedical importance from marine organisms. Federation proceedings, 1966. 1197-1205.

NO, H., MEYERS, S., PRINYAWIWATKUL, W. & XU, Z. 2007. Applications of chitosan for improvement of quality and shelf life of foods: a review. *Journal of food science,* 72**,** R87-R100.

NODA, H., AMANO, H., ARASHIMA, K. & NISIZAWA, K. 1990. Antitumor activity of marine algae. *Hydrobiologia,* 204**,** 577-584.

ORTEGA, A. & GARCÍA DE LA TORRE, J. 2007. Equivalent radii and ratios of radii from solution properties as indicators of macromolecular conformation, shape, and flexibility. *Biomacromolecules,* 8**,** 2464-2475.

ORTIZ, J., ROMERO, N., ROBERT, P., ARAYA, J., LOPEZ-HERNÁNDEZ, J., BOZZO, C., NAVARRETE, E., OSORIO, A. & RIOS, A. 2006. Dietary fiber, amino acid, fatty acid and tocopherol contents of the

edible seaweeds Ulva lactuca and Durvillaea antarctica. *Food Chemistry,* 99**,** 98-104.

PATEL, T. R., HARDING, S. E., EBRINGEROVA, A., DESZCZYNSKI, M., HROMADKOVA, Z., TOGOLA, A., PAULSEN, B. S., MORRIS, G. A. & ROWE, A. J. 2007. Weak Self-Association in a Carbohydrate System. *Biophysical Journal,* 93**,** 741-749.

PATEL, T. R., MORRIS, G. A., EBRINGEROVÁ, A., VODENIČAROVÁ, M., VELEBNÝ, V., ORTEGA, A., GARCIA DE LA TORRE, J. & HARDING, S. E. 2008. Global conformation analysis of irradiated xyloglucans. *Carbohydrate Polymers,* 74**,** 845-851.

PAVLOV, G., HARDING, S. & ROWE, A. 1999. Normalized scaling relations as a natural classification of linear macromolecules according to size. *Analytical Ultracentrifugation V.* Springer.

PAVLOV, G. M., ROWE, A. J. & HARDING, S. E. 1997. Conformation zoning of large molecules using the analytical ultracentrifuge. *TrAC Trends in Analytical Chemistry,* 16**,** 401-405.

PEPPAS, N. A. & BURI, P. A. 1985. Surface, interfacial and molecular aspects of polymer bioadhesion on soft tissues. *Journal of Controlled Release,* 2**,** 257-275.

PÉREZ, S., KOUWIJZER, M., MAZEAU, K. & ENGELSEN, S. B. 1996. Modeling polysaccharides: Present status and challenges. *Journal of Molecular Graphics,* 14**,** 307-321.

PERSIN, Z., STANA-KLEINSCHEK, K., FOSTER, T. J., VAN DAM, J. E., BOERIU, C. G. & NAVARD, P. 2011. Challenges and opportunities in polysaccharides research and technology: The EPNOE views for the next decade in the areas of materials, food and health care. *Carbohydrate Polymers,* 84**,** 22-32.

PICOUT, D. R., ROSS-MURPHY, S. B., JUMEL, K. & HARDING, S. E. 2002. Pressure cell assisted solution characterization of polysaccharides. 2. Locust bean gum and tara gum. *Biomacromolecules,* 3**,** 761-767.

PICULELL, L. 1995. Gelling carrageenans. *Food polysaccharides and their applications***,** 205-244.

PINHEIRO, A. C., BOURBON, A. I., ROCHA, C., RIBEIRO, C., MAIA, J. M., GONÇALVES, M. P., TEIXEIRA, J. A. & VICENTE, A. A. 2011. Rheological characterization of κ-carrageenan/galactomannan and xanthan/galactomannan gels: Comparison of galactomannans from non-traditional sources with conventional galactomannans. *Carbohydrate Polymers,* 83**,** 392-399.

POMPONI, S. A. 1999. The bioprocess - Technological potential of the sea. *Journal of Biotechnology,* 70**,** 5-13.

PONGJANYAKUL, T. & PUTTIPIPATKHACHORN, S. 2007. Sodium alginate-magnesium aluminum silicate composite gels: Characterization of flow behavior, microviscosity, and drug diffusivity. *AAPS PharmSciTech,* 8**,** E158-E165.

PRAJAPATI, V. D., MAHERIYA, P. M., JANI, G. K. & SOLANKI, H. K. 2014. Carrageenan: A natural seaweed polysaccharide and its applications. *Carbohydrate Polymers,* 105**,** 97-112.

PRIVALOV, P. L. & POTEKHIN, S. A. 1986. Scanning microcalorimetry in studying temperature-induced changes in proteins. *Methods in enzymology,* 131**,** 4-51.

PUTTIPIPATKHACHORN, S., PONGJANYAKUL, T. & PRIPREM, A. 2005. Molecular interaction in alginate beads reinforced with sodium starch glycolate or magnesium aluminum silicate, and their physical characteristics. *International Journal of Pharmaceutics,* 293**,** 51-62.

RALSTON, G. B. 1993. *Introduction to analytical ultracentrifugation,* California, USA, Beckman Instruments.

RATCLIFFE, I., WILLIAMS, P. A., VIEBKE, C. & MEADOWS, J. 2005. Physicochemical characterization of konjac glucomannan. *Biomacromolecules,* 6**,** 1977-1986.

RAVI KUMAR, M. N. 2000. A review of chitin and chitosan applications. *Reactive and Functional Polymers,* 46**,** 1-27.

RICHARDSON, R. K. & GOYCOOLEA, F. M. 1994. Rheological measurement of κ-carrageenan during gelation. *Carbohydrate Polymers,* 24**,** 223-225.

RINAUDO, M. 2006. Chitin and chitosan: properties and applications. *Progress in polymer science,* 31**,** 603-632.

RINAUDO, M. 2008. Main properties and current applications of some polysaccharides as biomaterials. *Polymer International,* 57**,** 397-430.

RINAUDO, M., MILAS, M. & DUNG, P. L. 1993. Characterization of chitosan. Influence of ionic strength and degree of acetylation on chain expansion. *International Journal of Biological Macromolecules,* 15**,** 281-285.

ROCHAS, C. & RINAUDO, M. 1982. Calorimetric determination of the conformational transition of kappa carrageenan. *Carbohydrate Research,* 105**,** 227-236.

ROCHAS, C. & RINAUDO, M. 1984. Mechanism of gel formation in κ-carrageenan. *Biopolymers,* 23**,** 735-745.

RØDDE, R. H., EINBU, A. & VÅRUM, K. M. 2008. A seasonal study of the chemical composition and chitin quality of shrimp shells obtained from northern shrimp (Pandalus borealis). *Carbohydrate Polymers,* 71**,** 388-393.

ROLLINGS, J. E. 1992. Use of on-line laser light scattering coupled to chromatographic separations for the determination of molecular weight, branching, size and shape distributions of polysaccharides. *In:* S.E. HARDING, D.B. SATELLE & BLOOMFIELD, V. A. (eds.) *Laser light scattering in biochemistry. Royal Society of Chemistry, Cambridge, UK. pp. 275–293.*

ROWE, A. 1977. The concentration dependence of transport processes: a general description applicable to the sedimentation, translational diffusion, and viscosity coefficients of macromolecular solutes. *Biopolymers,* 16**,** 2595-2611.

ROWE, A. J. 1992. The concentration dependence of sedimentation. *In:* HARDING, S. E., ROWE, A. J. & HORTON, J. C. (eds.) *Analytical ultracentrifugation in biochemistry and polymer science.* Cambridge: Royal Society of Chemistry, pp. 394–406.

SÆTHER, H. V., HOLME, H. K., MAURSTAD, G., SMIDSRØD, O. & STOKKE, B. T. 2008. Polyelectrolyte complex formation using alginate and chitosan. *Carbohydrate Polymers,* 74**,** 813-821.

SAGHEER, F. A. A., AL-SUGHAYER, M. A., MUSLIM, S. & ELSABEE, M. Z. 2009. Extraction and characterization of chitin and chitosan from marine sources in Arabian Gulf. *Carbohydrate Polymers*, 77**,** 410-419.

SCHACHMAN, H. K. 1959. *Ultracentrifugation in biochemistry*, Academic Press.

SCHUCK, P. 2000. Size-distribution analysis of macromolecules by sedimentation velocity ultracentrifugation and lamm equation modeling. *Biophysical Journal,* 78**,** 1606-1619.

SCHUCK, P., GILLIS, R. B., BESONG, T. M., ALMUTAIRI, F., ADAMS, G. G., ROWE, A. J. & HARDING, S. E. 2014. SEDFIT–MSTAR: molecular weight and molecular weight distribution analysis of polymers by sedimentation equilibrium in the ultracentrifuge. *Analyst,* 139**,** 79-92.

SCHUSTER, T. M. & TOEDT, J. M. 1996. New revolutions in the evolution of analytical ultracentrifugation. *Current Opinion in Structural Biology,* 6**,** 650-658.

SCOTT, D. J. & SCHUCK, P. 2005. A Brief Introduction to the Analytical Ultracentrifugation of Proteins for Beginners. *In:* SCOTT, D. J., HARDING, S. E. & ROWE, A. J. (eds.) *Analytical Ultracentrifugation: Techniques and Methods.* Cambridge, UK: Royal Society of Chemistry.

SENNI, K., PEREIRA, J., GUENICHE, F., DELBARRE-LADRAT, C., SINQUIN, C., RATISKOL, J., GODEAU, G., FISCHER, A.-M., HELLEY, D. & COLLIEC-JOUAULT, S. 2011. Marine polysaccharides: A source of bioactive molecules for cell therapy and tissue engineering. *Marine drugs,* 9**,** 1664-1681.

SHAHIDI, F. & ABUZAYTOUN, R. 2005. Chitin and Chitodan and Co-products: Chemistry, Producation, Applications and Health Effects. *In:* TAYLOR, S. (ed.) *Advances in Food and Nutrition Research.* Academic Press.

SHATWELL, K. P., SUTHERLAND, I. W., ROSS-MURPHY, S. B. & DEA, I. C. M. 1991. Influence of the acetyl substituent on the interaction of xanthan with plant polysaccharides — III. Xanthan-konjac mannan systems. *Carbohydrate Polymers,* 14**,** 131-147.

SHCHIPUNOV, Y., SARIN, S., KIM, I. & HA, C.-S. 2010. Hydrogels formed through regulated self-organization of gradually charging chitosan in solution of xanthan. *Green Chemistry,* 12**,** 1187-1195.

SHEEHAN, J. & CARLSTEDT, I. 1984. Hydrodynamic properties of human cervical-mucus glycoproteins in 6M-guanidinium chloride. *Biochem. J,* 217**,** 93-101.

SHEEHAN, J. K. & CARSTEDT, I. 1989. Models for the macromolecular structure of mucin glycoproteins. *In:* HARDING, S. E. & ROWE, A. J. (eds.) *Dynamic properies of biomolecular assemblies.* Cambridge: The Royal Society of Chemistry. pp. 256-275.

SHELSO, G. L. 1990. Commercialisation of new synergistic application of carrageenan. *In:* PHILLIPS, G. O., WEDLOCK, D. J. & WILLIAMS, P. A. (eds.) *Gum and Stabilisers for the Food Industry 5.* New York: Oxford University Press Inc.

SHEPHERD, R., READER, S. & FALSHAW, A. 1997. Chitosan functional properties. *Glycoconjugate Journal,* 14**,** 535-542.

SLAVIN, J. L. 2005. Dietary fiber and body weight. *Nutrition,* 21**,** 411-418.

SLOOTMAEKERS, D., MANDEL, M. & REYNAERS, H. 1991b. Dynamic light scattering by κ- and λ-carrageenan solutions. *International Journal of Biological Macromolecules,* 13**,** 17-25.

SLOOTMAEKERS, D., VAN DIJK, J. A. P. P., VARKEVISSER, F. A., BLOYS VAN TRESLONG, C. J. & REYNAERS, H. 1991a. Molecular characterisation of κ- and λ-carrageenan by gel permeation chromatography, light scattering, sedimentation analysis and osmometry. *Biophysical Chemistry,* 41**,** 51-59.

SMIDSRØD, O. 1974. Molecular basis for some physical properties of alginates in the gel state. *Faraday discussions of the Chemical Society,* 57**,** 263-274.

SMIDSRØD, O., ANDRESEN, I.-L., GRASDALEN, H., LARSEN, B. & PAINTER, T. 1980. Evidence for a salt-promoted "freeze-out" of linkage conformations in carrageenans as a prerequisite for gel-formation. *Carbohydrate Research,* 80**,** C11-C16.

SMIDSRØD, O. & GRASDALEN, H. 1984. Polyelectrolytes from seaweeds. *Hydrobiologia,* 116**,** 19-28.

SMITH, I. H., LAWSON, C. J., HARDING, S. E., GAHLER, R. J., LYON, M. R. & WOOD, S. 2014. Viscosity development during aqueous dispersion and dissolution: A comparison of PGX® with other dietary supplements and individual polysaccharides. *Food Hydrocolloids,* 38**,** 152-162.

STAFFORD III, W. F. 1992. Boundary analysis in sedimentation transport experiments: a procedure for obtaining sedimentation coefficient distributions using the time derivative of the concentration profile. *Analytical Biochemistry,* 203**,** 295-301.

STOKKE, B. T., ELGSAETER, A., SKJRAK-BRJEK, G. & SMIDSRØD, O. 1987. The molecular size and shape of xanthan, xylinan, bronchial mucin, alginate, and amylose as revealed by electron microscopy. *Carbohydrate Research,* 160**,** 13-28.

STUDIER, F. W. 1965. Sedimentation studies of the size and shape of DNA. *Journal of Molecular Biology,* 11**,** 373-390.

SYMES, K. 1980. The relationship between the covalent structure of the Xanthomonas polysaccharide (Xanthan) and its function as a thickening, suspending and gelling agent. *Food Chemistry,* 6**,** 63-76.

SYNOWIECKI, J. & AL-KHATEEB, N. A. 2003. Production, properties, and some new applications of chitin and its derivatives.

SZARC VEL SZIC, K., NDLOVU, M. N., HAEGEMAN, G. & VANDEN BERGHE, W. 2010. Nature or nurture: Let food be your epigenetic medicine in chronic inflammatory disorders. *Biochemical Pharmacology,* 80**,** 1816-1832.

TAKEMASA, M. & NISHINARI, K. 2004. The effect of the linear charge density of carrageenan on the ion binding investigated by differential scanning calorimetry, dc conductivity, and kHz dielectric relaxation. *Colloids and Surfaces B: Biointerfaces,* 38**,** 231-240.

TAN, S. P., O'SULLIVAN, L., LUZ PRIETO, M., MCLOUGHLIN, P., LAWLOR, P. G., HUGHES, H. & GARDINER, G. E. 2013. Seaweed Antimicrobials: Isolation, Characterization, and Potential Use in Functional Foods. *In:* HERNANDEZ-LEDESMA, B. & HERRERO, M. (eds.) *Bioactive Compounds from Marine Foods.* John Wiley & Sons Ltd.

TANFORD, C. 1961. *Physical chemistry of macromolecules,* New York, Wiley.

TAPIA, C., ESCOBAR, Z., COSTA, E., SAPAG-HAGAR, J., VALENZUELA, F., BASUALTO, C., NELLA GAI, M. A. & YAZDANI-PEDRAM, M. 2004. Comparative studies on polyelectrolyte complexes and mixtures of chitosan–alginate and chitosan–carrageenan as prolonged diltiazem clorhydrate release systems. *European Journal of Pharmaceutics and Biopharmaceutics,* 57**,** 65-75.

THEISEN, A., JOHANN, C., DEACON, M. & HARDING, S. E. 2000. *Refractive increment data-book: for polymer and biomolecular scientists,* Nottingham, UK, Nottingham University Press.

THERKELSEN, G. H. 1995. Carrageenan. *In:* WHISTLER, R. L. A. B., J.N. (ed.) *Industrial Gum. Polysaccharides and their Derivatives (pp. 145-180).* Inc. San Diego: Academic Press.

TOMBS, M. P. & HARDING, S. E. 1998. An Introduction to Polysaccharide Biotechnology. Gunpowder Square, London: Taylor and Francis Ltd.

TØNNESEN, H. H. & KARLSEN, J. 2002. Alginate in drug delivery systems. *Drug development and industrial pharmacy,* 28**,** 621-630.

VAN DE VELDE, F., KNUTSEN, S. H., USOV, A. I., ROLLEMA, H. S. & CEREZO, A. S. 2002. 1H and 13C high resolution NMR spectroscopy of carrageenans: application in research and industry. *Trends in Food Science & Technology,* 13**,** 73-92.

VAN HOLDE, K. 1985. *Physical Biochemistry,* Prentice-Hall, New Jersey.

VAN HOLDE, K. E. 2002. A hypothesis concerning diffusion-limited protein–ligand interactions. *Biophysical Chemistry,* 101–102**,** 249-254.

VANNESTE, K., MANDEL, M., PAOLETTI, S. & REYNAERS, H. 1994. Molecularity of the Salt-Induced Conformational Transition of .iota.-Carrageenan. *Macromolecules,* 27**,** 7496-7498.

VANNESTE, K., SLOOTMAEKERS, D. & REYNAERS, H. 1996. Light scattering studies of the dilute solution behaviour of κ-, ι-and λ-carrageenan. *Food Hydrocolloids,* 10**,** 99-107.

VARUM, K. M. & SMIDSRØD, O. 2004. Structure-property relationship in chitosans. *In:* DUMITRIU, S. (ed.) *Polysaccharides: Structural*

*Diversity and Functional Versatility (pp 625-642).* New York: Macel Dekker, Inc.

VAUGELADE, P., HOEBLER, C., BERNARD, F., GUILLON, F., LAHAYE, M., DUEE, P.-H. & DARCY-VRILLON, B. 2000. Non-starch polysaccharides extracted from seaweed can modulate intestinal absorption of glucose and insulin response in the pig. *Reproduction nutrition development,* 40**,** 33-48.

VENUGOPAL, V. 2009. *Marine products for healthcare: functional and bioactive nutraceutical compounds from the ocean,* CRC press.

VENUGOPAL, V. 2011. *Marine polysaccharides: Food applications,* CRC Press.

VIEBKE, C., BORGSTRÖM, J., CARLSSON, I., PICULELL, L. & WILLIAMS, P. 1998. A differential scanning calorimetry study of κ-carrageenan in the NACl/NaI/CsI/CsCl systems and analysis by Poisson-Boltzmann calculations. *Macromolecules,* 31**,** 1833-1841.

VIEBKE, C., BORGSTRÖM, J. & PICULELL, L. 1995. Characterisation of kappa- and iota-carrageenan coils and helices by MALLS/GPC. *Carbohydrate Polymers,* 27**,** 145-154.

VIEBKE, C. & WILLIAMS, P. A. 2000. Determination of molecular mass distribution of κ-carrageenan and xanthan using asymmetrical flow field-flow fractionation. *Food Hydrocolloids,* 14**,** 265-270.

VOLD, I. M. N. 2004. *Periodate oxidised chitosans: Structure and solution properties.,* PhD Dissertation, Norwegian University of Science and Technology, Trondheim, Norway.

VREEMAN, H., SNOEREN, T. & PAYENS, T. 1980. Physicochemical investigation of k-carrageenan in the random state. *Biopolymers,* 19**,** 1357-1374.

VUKSAN, V., JENKINS, D., SPADAFORA, P., SIEVENPIPER, J. L., OWEN, R., VIDGEN, E., BRIGHENTI, F., JOSSE, R., LEITER, L. A. & BRUCE-THOMPSON, C. 1999. Konjac-mannan (glucomannan) improves glycemia and other associated risk factors for coronary heart disease in type 2 diabetes. A randomized controlled metabolic trial. *Diabetes care,* 22**,** 913-919.

VUKSAN, V., SIEVENPIPER, J., OWEN, R., SWILLEY, J., SPADAFORA, P., JENKINS, D., VIDGEN, E., BRIGHENTI, F., JOSSE, R. & LEITER, L. 2000. Beneficial effects of viscous dietary fiber from Konjac-mannan in subjects with the insulin resistance syndrome: results of a controlled metabolic trial. *Diabetes care,* 23**,** 9-14.

WALES, M. & VAN HOLDE, K. 1954. The concentration dependence of the sedimentation constants of flexible macromolecules. *Journal of Polymer Science,* 14**,** 81-86.

WANG, K. & HE, Z. 2002. Alginate–konjac glucomannan–chitosan beads as controlled release matrix. *International Journal of Pharmaceutics,* 244**,** 117-126.

WEINBRECK, F., NIEUWENHUIJSE, H., ROBIJN, G. W. & DE KRUIF, C. G. 2004. Complexation of whey proteins with carrageenan. *Journal of Agricultural and Food Chemistry,* 52**,** 3550-3555.

WEN, J., ARAKAWA, T. & PHILO, J. S. 1996. Size-Exclusion Chromatography with On-Line Light-Scattering, Absorbance, and Refractive Index Detectors for Studying Proteins and Their Interactions. *Analytical Biochemistry,* 240**,** 155-166.

WEN, X., WANG, T., WANG, Z., LI, L. & ZHAO, C. 2008. Preparation of konjac glucomannan hydrogels as DNA-controlled release matrix. *International Journal of Biological Macromolecules,* 42**,** 256-263.

WIJESEKARA, I., PANGESTUTI, R. & KIM, S.-K. 2011. Biological activities and potential health benefits of sulfated polysaccharides derived from marine algae. *Carbohydrate Polymers,* 84**,** 14-21.

WIJESINGHE, W. & JEON, Y.-J. 2012. Biological activities and potential industrial applications of fucose rich sulfated polysaccharides and fucoidans isolated from brown seaweeds: A review. *Carbohydrate Polymers,* 88**,** 13-20.

WILLIAMS, M. A., FOSTER, T. J., MARTIN, D. R., NORTON, I. T., YOSHIMURA, M. & NISHINARI, K. 2000. A molecular description of the gelation mechanism of konjac mannan. *Biomacromolecules,* 1**,** 440-450.

WILLIAMS, P., CLEGG, S., LANGDON, M., NISHINARI, K. & PICULELL, L. 1993. Investigation of the gelation mechanism in. kappa.-

carrageenan/konjac mannan mixtures using differential scanning calorimetry and electron spin resonance spectroscopy. *Macromolecules,* 26**,** 5441-5446.

WITTGREN, B., BORGSTRÖM, J., PICULELL, L. & WAHLUND, K. G. 1998. Conformational change and aggregation of κ-carrageenan studied by flow field-flow fractionation and multiangle light scattering. *Biopolymers,* 45**,** 85-96.

WYATT, P. J. 1992. Combined differential light scattering with various liquid chromatography separation techniques. *In:* S.E. HARDING, D. B. S., V.A. BLOOMFIELD (ed.) *Laser light scattering in biochemistry,*. Cambridge, UK (pp. 35-58): The Royal Society of Chemistry.

WYATT, P. J. 1993. Light scattering and the absolute characterization of macromolecules. *Analytica chimica acta,* 272**,** 1-40.

WYATT, P. J. 2013. Multiangle Light Scattering from Separated Samples (MALS with SEC or FFF). *In:* ROBERTS, G. K. (ed.) *Encyclopedia of Biophysics.* Springer Berlin Heidelberg.

XIA, W., LIU, P., ZHANG, J. & CHEN, J. 2011. Biological activities of chitosan and chitooligosaccharides. *Food Hydrocolloids,* 25**,** 170-179.

YAMAKAWA, H. & FUJII, M. 1973. Translational friction coefficient of wormlike chains. *Macromolecules,* 6**,** pp. 407-415.

YE, H., WANG, K., ZHOU, C., LIU, J. & ZENG, X. 2008. Purification, antitumor and antioxidant activities in vitro of polysaccharides from the brown seaweed Sargassum pallidum. *Food Chemistry,* 111**,** 428-432.

ZHOU, G., SUN, Y., XIN, H., ZHANG, Y., LI, Z. & XU, Z. 2004. In vivo antitumor and immunomodulation activities of different molecular weight lambda-carrageenans from Chondrus ocellatus. *Pharmacological Research,* 50**,** 47-53.

ZUCCA, N., ERRIU, G., ONNIS, S. & LONGONI, A. 2004. An analytical expression of the output of a power-compensated DSC in a wide temperature range. *Thermochimica Acta,* 413**,** 117-125.

# APPENDIX

PUBLICATION (I) An analytical ultracentrifugation based study on the conformation of lambda carrageenan in aqueous solution.

ALMUTAIRI FM, ADAMS GG, KÖK MS, LAWSON CJ, GAHLER R, WOOD S, FOSTER TJ, ROWE AJ and HARDING SE, 2013. Carbohydrate Polymers. 97(1), 203-9

PUBLICATION (II) SEDFIT-MSTAR: Molecular weight and molecular weight distribution analysis of polymers by sedimentation equilibrium in the ultracentrifuge.

SCHUCK P, GILLIS RB, BESONG D, ALMUTAIRI F, ADAMS GG, ROWE AJ and HARDING SE, 2014. Analyst. 139, 79-92

PUBLICATION (III) Hydrodynamic characterisation of chitosan and its interaction with two polyanions: DNA and xanthan.

ALMUTAIRI, F. M., ERTEN, T., ADAMS, G. G., HAYES, M., MCLOUGHLIN, P., KÖK, M. Ş., MACKIE, A. R., ROWE, A. J. & HARDING, S. E., 2015. Carbohydrate Polymers122**,** 359-366